Field Testing, Modelling and Analysis of Ferroresonance in a High Voltage Power System

by

DAVID A. N. JACOBSON

A Thesis
Submitted to the Faculty of Graduate Studies
in Partial Fulfillment of the Requirements
for the Degree of

DOCTOR OF PHILOSOPHY

Department of Electrical and Computer Engineering
The University of Manitoba
Winnipeg, Manitoba, Canada

THE UNIVERSITY OF MANITOBA

FACULTY OF GRADUATE STUDIES

*****

COPYRIGHT PERMISSION PAGE

Field Testing, Modelling and Analysis of Ferroresonance in a High Voltage Power System

BY

David A.N. Jacobson

A Thesis/Practicum submitted to the Faculty of Graduate Studies of The University of Manitoba in partial fulfillment of the requirements of the degree of Doctor of Philosophy

Abstract

Catastrophic equipment failures continue to occur today due to ferroresonance even though this phenomenon has been extensively studied over the past ninety years. This thesis is concerned with the tasks of defining where ferroresonance problems can exist in a high voltage power system, of determining methods for displaying safety margins between nonferroresonant and ferroresonant operating regions and improving upon existing ferroresonance simulation techniques.

Several different ferroresonant circuits have been modelled and compared with field measurements taken on the Manitoba Hydro 230-kV power system or compared with laboratory measurements including: a de-energized transformer connected to the grading capacitance of an open circuit breaker, a transformer-terminated double-circuit transmission line and a coupling capacitor voltage transformer. In a high voltage power system, the most prevalent ferroresonance circuit occurs between a de-energized transformer and the grading capacitor of an open circuit breaker.

Experimental work has shown that losses in a practical transformer are much larger during ferroresonance oscillation modes than predicted by conventional modelling techniques. A simple switched eddy-current loss resistor is found able to model the losses during subharmonic and fundamental frequency ferroresonance in a laboratory transformer.

A major contribution of this work is a new method of visualizing the margin between non-ferroresonant and ferroresonant states in a transformer/grading capacitor circuit has been developed. A general set of averaged equations is derived that permit the analysis of an n^{th} order polynomial approximation of the magnetization curve. The location of the saddle points and slope of the stable manifold through the saddle points can be determined for a particular transformer under study. The Limacon of Pascal is found to be a good approximation to the geometric shape of the basin of attraction of the period-1 ferroresonant attractor and can be calculated using the saddle point location and slope of the stable manifold. The critical parameters resulting in a crossing of the separatrix can then be found by iteratively solving the Limacon equations. The new method will assist utility engineers in quickly assessing the potential risk of ferroresonance in their power system.

Acknowledgments

I would like to thank the support of Manitoba Hydro, in providing some financial funding and allowing me the time to pursue this research.

I am grateful for the patience and support shown by my Manitoba Hydro supervisor, Ron Mazur, and my department manager, Clarence Thio, over the past several years.

My academic supervisor, Dr. Robert Menzies, deserves special mention in that he was willing to take a chance with a part-time Ph.D. student. He provided a lot of encouragement to continue with the work.

Collaborations with Dr. Peter Lehn (Department of Electrical and Computer Engineering, University of Toronto) and Dr. David Swatek (Manitoba Hydro) were especially beneficial in my maintaining focus and direction.

Maria Magalhaes' assistance with performing laboratory experiments on measuring distribution transformer losses during ferroresonance was greatly appreciated. Maria completed her undergraduate thesis at the University of Manitoba under my supervision in May, 2000.

Useful discussions with Dr. Luis Marti (Ontario Hydro), concerning frequency dependent line modelling and the application of the EMTP Type-92 nonlinear inductor, were helpful in developing an accurate model of the Silver transformer.

Dedication

This thesis is dedicated to my wife, Marlis, and to my children. Natasha, Kristjan and Stefan. Without their encouragement and support, this work would never have been possible.

Contents

List of Figures

List of Tables

Chapter 1

Introduction

1.1 MOTIVATION

The Dorsey 230-kV Converter Station is located just north of Winnipeg in the southern portion of the province of Manitoba. This station can be considered the backbone of the Manitoba Hydro (MH) system as 70% of the province's total power generation enters this station and is distributed to load in southern Manitoba or exported to neighbouring utilities.

It was identified in MH planning studies several years ago that twenty-five breakers and current transformers should be replaced and five breakers upgraded in the Dorsey Station. The reasons included wear and tear on existing breakers and lack of available spare parts. However, mainly the existing 30-kA short circuit interrupting duty of these breakers would not be sufficient following proposed system upgrades. The new breakers are required to have a 63.5-kA interrupting rating at -55° Celsius. Also, the breakers should be able to clear short line faults at up to 90% of the short-circuit current rating.

As a result of these specifications, the manufacturer proposed installing multi-head breakers with two breaks/phase and 1500 pF of grading capacitance across each break. In addition, the low-temperature high-current interrupting rating required a mixing of carbon tetrafluoride (CF_4) with the normal sulfur hexafluoride (SF_6) gas. Following all proposed replacements and upgrades, the maximum total grading capacitance of all parallel breakers will increase from 2000 pF to 7500 pF, following a *jumbo* bus outage.

The Dorsey Station is constructed in a standard breaker-and-a-third configuration as shown in Fig. 1.1. However, there are four main buses instead of two. The long bus or *jumbo* bus is roughly 500 m long while the short bus is 50 m. All nine ac filters, four station service transformers and wound potential transformers (PTs) of interest are also shown in Fig. 1.1.

On May 20, 1995, jumbo bus A2 was scheduled to be removed from service to

accommodate the replacement of some of the circuit breakers and current transformers. The manual disconnects of three breakers were previously open and the motor operated disconnect of the station service transformer (SST2) was also open. The shaded boxes in Fig. 1.1 indicate the open breakers with grading capacitors (i.e. 5061 pF total) connected to the de-energized bus.

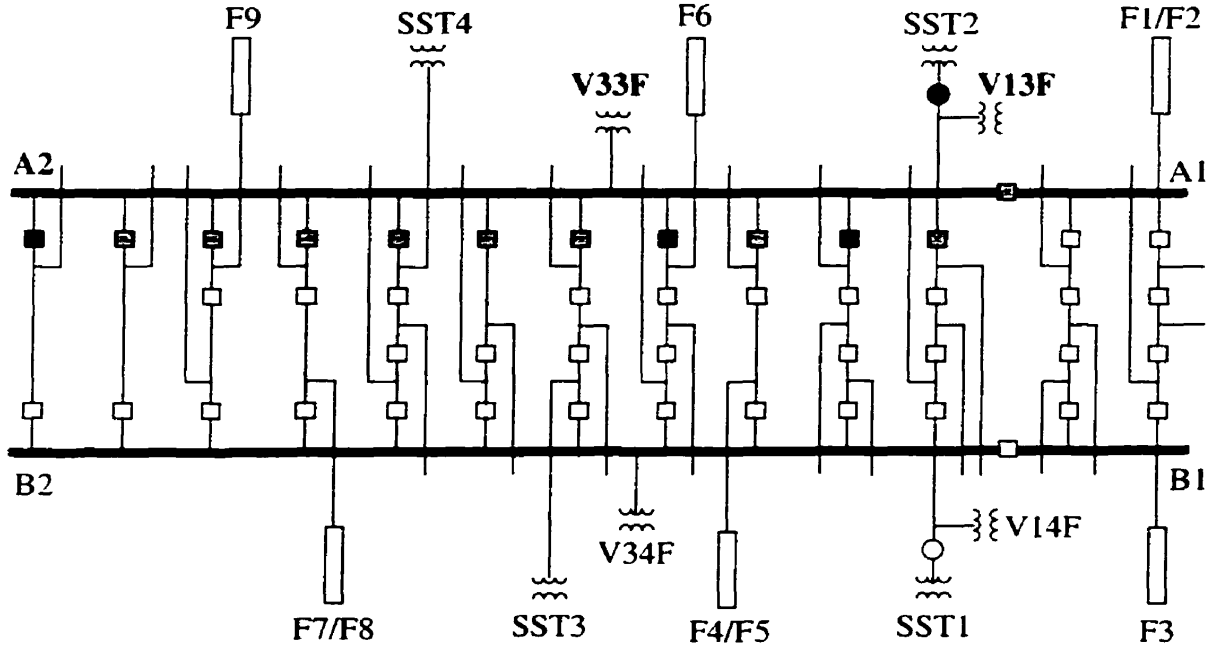

Fig. 1.1 Dorsey bus configuration prior to explosion of potential transformer.

Approximately thirty minutes following the bus de-energization, phase A of wound PT V13F failed catastrophically. A photograph taken shortly after the explosion is shown in Fig. 1.2.

Personnel were in the yard at the time of the explosion, starting to open the circuit breaker manual disconnects. The failure of phase A of potential transformer V13F resulted in shards of broken porcelain scattering up to 30 m away from the site of the explosion. This disturbance prompted a detailed study to be undertaken, to determine the cause of the failure and to recommend immediate solutions.

Fig. 1.2 Catastrophic failure of V13F due to ferroresonance.

1.2 HISTORICAL BACKGROUND/ ONGOING RESEARCH[1]

Boucherot [A2] originally coined the word *ferroresonance* in 1920 to describe the phenomenon of two stable fundamental frequency operating points coexisting in a series resistor, nonlinear inductor, capacitor circuit. The first published work, a 1907 paper by Bethenod [A1], simply described the phenomenon as transformer resonance. Today, the term ferroresonance is firmly established in the power system engineer's vocabulary and is used to not only describe the jump to a higher current fundamental frequency state but also bifurcations to subharmonic, quasi-periodic and even chaotic oscillations in any circuit containing a nonlinear inductor.

Graphical or experimental methods were used predominantly in the 1920s and 1930s to analyze the circuit as the field of nonlinear dynamics was in its infancy. Poincaré (1854-

1. A comprehensive annotated bibliography of ferroresonance papers is included in Appendix A. References to these papers use the notation [A1] to refer to the first paper in Appendix A, for example. References without the leading *A* are not directly related to ferroresonance and are summarized at the end of each chapter.

1912) is generally credited with developing the qualitative or topological theory of differential equations while he was studying problems in celestial mechanics near the end of the nineteenth century. In the same period, Lyapunov (1857-1918) developed his theories pertaining to the stability of differential equations. Work proceeded in the early part of the twentieth century along two separate paths: topological ideas were developed by Birkhoff (1884-1944) and others, and practical analytical approaches were pursued mainly by Russian mathematicians such as Krylov, Bogoliubov and Mitropolsky.

A milestone year in ferroresonance research occurred in 1950, where three important books were published. Rüdenberg [A9] uses the graphical method to display multiple operating points and to show the effect of parameter variations. Clarke [A10] uses sequence component calculations to verify laboratory measurements of the unbalanced operation of transformers. Peterson [A11] investigated grounded potential transformers in ungrounded systems using a laboratory model. Depending on the system parameters, subharmonic oscillation of one-half the system frequency with a small beat frequency could be excited. Such an oscillation is now labelled as being *quasi-periodic*, which is defined as motion resulting from two different frequencies in which the ratio of the frequencies cannot be expressed as a ratio of integers. The abnormal oscillations obtained by Peterson required shocks to be applied such as circuit energizing or fault removal. In some cases, quasi-static variation of the source voltage could excite the oscillations.

The coupling of nonlinear dynamics with ferroresonance began in 1964 with the pioneering work of Hayashi [A19]. Topological and analytical methods are applied to both Duffing's and van der Pol's equations. Duffing's equation closely represents the behavior of a series ferroresonant circuit. The first detailed topological portraits of forced oscillators, using techniques first put forward by Poincaré, are presented. The main emphasis of the work focuses on harmonic and subharmonic oscillations, however, quasi-periodic oscillations are briefly investigated and are referred to by Hayashi as *almost periodic oscillations*.

Little use was made of Hayashi's work until the 1970s. Y. Ueda [A65] extended the investigations made by Hayashi on Duffing's equation. He discovered an oscillation occurs at high values of applied voltage which he terms as a *randomly transitional oscillation* although he prefers to think of it as turbulence in an electric circuit. D. Ruelle, who had already coined the phrase *strange attractor* with F. Takens in 1971 [2], met Ueda in 1978 and named the strange attractor, discovered by Ueda, the Japanese attractor.

The study of nonlinear dynamics has become highly diversified since Hayashi's work was

first published. Specialized literature now exists in such diverse areas as chaos theory, catastrophe theory, bifurcation theory, iterated mapping techniques etc., which are generally only accessible to pure mathematicians. Books that bridge the gap between theory and applications to the physical sciences are necessary before wide spread use of new ideas can be made. Hilborn [3] creates an engaging overview of chaos and nonlinear dynamics. Bifurcation theory is becoming a standard tool for studying the behavior of state space attractors as system parameters are varied. Hilborn recommends reading the books by Thompson and Stewart [4] and Guckenheimer and Holmes [5] in order to learn more about the theory of bifurcations. Another book by Parker and Chua [6] is important because it describes the algorithms required to create, for example, bifurcation diagrams and Poincaré maps; examples of modern nonlinear dynamics tools.

The majority of publications devoted to ferroresonance prior to 1990 made little connection between nonlinear dynamics methods and ferroresonance, primarily because of the lack of publications bridging the gap between theory and practice. Experimental approaches, as in the work performed by Hopkinson [A21] in 1965, were the main tool used to define acceptable system parameters that would avoid ferroresonance. Actually, the ratio of phase-to-ground capacitance (X_C) to magnetizing reactance (X_m) defined by Hopkinson is still used by distribution engineers today [A70]. Through experimentation, Hopkinson determined that if the X_C/X_m ratio was larger than forty, no ferroresonance was expected to occur. Simulation studies began to replace transient network analyzer (TNA) studies in the 1970s and 1980s following pioneering work in digital computer solution methods by Dommel [1].

Swift [A28], in his 1969 paper, stimulated interest in nonlinear dynamics applications to ferroresonant circuits by analyzing a parallel ferroresonant circuit using describing function theory. In 1975, Germond [A41] applied Galerkin's method of harmonic balance to a variety of ferroresonance circuits. Chua [A59] used piecewise-linear analysis in 1982 to demonstrate for the first time that chaos can occur in a real ferroresonant circuit. Janssens [A79] extends the harmonic balance method in 1990 to directly calculate the stability zones of different ferroresonant oscillations. Also in 1990, Kieny [A78], [A84] applied bifurcation theory to a practical ferroresonant circuit for the first time.

The 1990s has seen an explosion of papers applying nonlinear dynamics techniques to ferroresonant circuits. Kieny is pursuing perturbation methods [A96], Floquet theory [A83] and continuation methods [A90]. Mork/Stuehm [A102] have developed five-legged transformer models for the EMTP and have analyzed unbalanced operation using

bifurcation diagrams. Mozaffari/Soudack have created basin of attraction plots [A136], bifurcation diagrams, and have calculated Lyapunov exponents [A109] for a chaotic attractor. Chakravarthy/Nayer have analyzed the method of slowly varying amplitudes [A112], Melnikov's method [A115], and sine circle maps [A129]. Janssens/van Craenenbroeck have calculated stability domains for three-phase circuits using bifurcation theory and Floquet theory [A117],[A121]. Naidu/de Souza present bifurcation diagrams for several circuits calculated using a continuation method [A128], [A137].

Other areas of power systems have seen the benefits of applying nonlinear dynamics techniques. Deane/Hamill [7] describe several examples of subharmonic, quasi-periodic and chaotic behavior in power electronic circuits mainly by using experimental bifurcation diagrams. Also included in their paper is a discussion of ferroresonance. Bifurcation behavior of the power system swing equations have been analyzed by Tan *et al.* [8]. The Galerkin method of harmonic balance is used by Vaiman/Sobajic [9] to calculate power system oscillations in a simple twenty-four bus power system model. Subsynchronous resonance oscillations are analyzed by Mitani *et al.* [10] using bifurcation theory.

Ferroresonance research is ongoing. Mork/Morched/Walling [A126] recommend efforts be put forward to developing more accurate transformer models. Improvements in transformer core representations and saturation characteristics need to be accurately determined at high operating voltages. The majority of nonlinear dynamics methods have looked at low order state space models. Naidu/de Souza are investigating how the methodology needs to be adjusted to handle larger networks [A137]. Janssens/van Craenenbroeck are planning on extending their stability domain calculation method to include a more detailed transformer model [A121].

1.3 RESEARCH OBJECTIVES

The main objective of this thesis is to attempt to answer the following question:

> *Given an operating point in a parameter space, what margin exists between the operating point and the nearest ferroresonant state?*

The catastrophic failure of a wound potential transformer at Dorsey has made this more than an academic question but rather an important safety issue for personnel that must be addressed.

Time-domain simulation using detailed transformer and system models is the most accurate method for determining the probability of ferroresonance aside from full scale

laboratory testing. Hundreds of simulations are required to get a sufficient feel for the effect of parameter variations. Each simulation however, is no better than throwing a dart. The resulting scatter diagram does not give any information about the behavior of untested cases.

Direct calculation of the stability domains, as proposed by Janssens/van Craenenbroeck [A79] [A117], is a better technique. The only drawback is the stability domain boundaries represent quasi-static bifurcations. Network switching events may cause bifurcations to occur at different parameters than predicted by the quasi-static approach. As well, low-order state-space models and/or simplified transformer models are generally used to make the method analytically tractable. The proposed work will identify the differences between the time-domain and direct stability domain boundary calculation methods. An alternative method that bridges the gap between the brute-force time-domain and existing direct stability domain boundary calculation methods will be developed.

Transformer models have developed to a high degree of sophistication in time-domain simulation programs. Recent research efforts have focussed on improving the representation of the transformer at high frequencies. Neves/Dommel [11] give an example where the additional modelling detail does not improve the representation of ferroresonance. Several investigators of ferroresonance have pointed to the need for improvements in the modelling of low frequency behavior. Janssens [A62], [A79] sees the need for better theoretical modelling of hysteresis and eddy-current losses during the transient periods which contain subharmonics and harmonics. Brierly/Morched [A91] indicate EMTP studies are limited due to the accuracy of available models and available information on saturation characteristics. Walling [A97], [A101] has performed detailed laboratory studies of transformers with silicon-steel and amorphous-metal core transformers. He has observed that ferroresonance susceptibility is directly related to iron-core loss. In a discussion to a paper written by Short *et al.* [A100], Walling makes the comment that field tests are always less severe than those predicted by digital simulation. The nonlinear behavior of the iron-core losses is extremely difficult to model and is critical to ferroresonance prediction. Kunde et al. [A124] make similar observations in their investigation of Haefely Trench potential transformers. Their field tests showed that actual transformers damped transient ferroresonance faster than calculations predicted. They hypothesize that additional non-measurable losses occur in the transformer. Laboratory investigations are proposed that will measure transformer losses during various modes of ferroresonance. An improved iron-core loss model will be developed and tested by comparing laboratory tests with digital time-domain simulations.

1.4 OUTLINE OF THE THESIS

Ferroresonance analysis techniques are first developed. Beginning from the earliest known method of graphical analysis, several important classical nonlinear dynamics techniques are then described culminating with a description of modern bifurcation analysis. All analytical techniques which have been developed tend to view ferroresonance from a quasi-static point of view. In other words, spontaneous jumps to new operating states will occur as parameters are slowly varied.

The method of averaging is extended to demonstrate the influence initial conditions have on the fundamental frequency or period-1 stability domains. A simple third-order polynomial approximation to the magnetizing curve is analyzed to demonstrate the concept. By making use of the fact that the Limacon of Pascal is a good geometric approximation of the separatrix between no ferroresonance and period-1 ferroresonance, a greatly improved prediction of the jump to period-1 ferroresonance is possible.

Based on a comprehensive literature review, three components in a high voltage (i.e. greater than 66 kV) power system are vulnerable to ferroresonance. They are unloaded transformers connected in series with the grading capacitance of open circuit breakers, capacitor voltage transformers and transformer-terminated transmission lines. Capacitor voltage transformers have built-in ferroresonance suppression circuitry to eliminate any concerns and therefore they are only briefly studied in Appendix A [A143].

Two transformer/grading-capacitor examples are chosen for detailed study. Complete simulation models are developed and are validated against field recordings. The model is reduced as far as possible in order to derive a minimum set of state equations, which may be analyzed using an analytical technique. A set of equations are derived that permit the analysis of a general n^{th} order polynomial approximation of the magnetization curve.

Modelling of transformer losses in digital simulation packages does not appear to be adequate to accurately represent field cases of ferroresonance. Specific examples from field tests are recreated in a scaled-down laboratory environment. Losses are recorded for several different modes of ferroresonance and an improved iron-core loss model is proposed.

Finally, a transformer-terminated double-circuit transmission line example of ferroresonance is investigated through field tests and digital simulation. Further improvements in modelling techniques are realized.

1.5 REFERENCES

[1] Dommel, H.W.,"Digital Computer Solution of Electromagnetic Transients in Single- and Multiphase Networks", *IEEE Trans. on Power Apparatus and Systems*, Vol. PAS-88, No. 4, pp. 388-398, April 1969.

[2] Ruelle, D., and Takens, F.,"On the Nature of Turbulence", *Communic. Math. Phys.*, vol. 20, 167-192; vol. 23, 343-344, 1971.

[3] Hilborn, R. C., *Chaos and Nonlinear Dynamics: An Introduction for Scientists and Engineers*, Oxford University Press: New York, 1994.

[4] Thompson, J.M.T., and Stewart, H.B., *Nonlinear Dynamics and Chaos*, Wiley: New York, 1986.

[5] Guckenheimer, J., and Holmes, P., *Nonlinear Oscillations, Dynamical Systems, and Bifurcations of Vector Fields*, 3rd ed., Springer-Verlag: New York, 1990.

[6] Parker, T.S., and Chua, L.O., *Practical Numerical Algorithms for Chaotic Systems*, Springer-Verlag: New York, 1989.

[7] Deane, J.H.B., and Hamill, D.C.,"Instability, Subharmonics, and Chaos in Power Electronic Systems", *IEEE Trans. on Power Electronics*, Vol. 5, No. 3, pp. 260-268, July 1990.

[8] Tan, C-W., Varghese, M., Varaiya, P., Wu, F.F.,"Bifurcation, Chaos, and Voltage Collapse in Power Systems", *Proceedings of the IEEE*, Vol. 83, No. 11, pp. 1484-1496, November 1995.

[9] Vaiman, M.Y., and Sobajic, D.J.,"A Novel Approach to Compute Characteristics of Sustained Interarea Oscillations", *IEEE Power Engineering Review: Power Eng. Letters*, pp. 52-54, January 1998.

[10] Mitani, Y., Tsuji, K., Varghese, M., Wu, F.F., Varaiya, P.,"Bifurcations Associated with Subsynchronous Resonance", *IEEE Trans. on Power Systems*, Vol. 13, No. 1 pp. 139-144, February 1998.

[11] Neves, W.L.A., Dommel, H.W.,"Transformer Core Modelling", *IPST '95 - International Conference on Power Systems Transients*, pp. 125-130, Sept. 1995.

Chapter 2

Ferroresonance Analysis Methods

The true method of foreseeing the future of mathematics is to study its history and its actual state.

—H. Poincaré 1908

2.1 INTRODUCTION

The purpose for analyzing ferroresonance using methods other than experimentation or brute-force time-domain simulation has varied. Rüdenberg's graphical approach is the earliest method, which was used to explain the existence of multiple periodic steady-states co-existing with the same set of parameters.

An active research area is in developing efficient methods that may be used to compute the steady-state solution. One popular method being used is a hybrid time and frequency domain methodology as described in a recent survey paper [1]. Computing the periodic steady state in a system with both linear and nonlinear components is useful in general harmonic power flow programs, for initializing Electromagnetic Transient Type Programs (EMTP) or for the systematic extraction of all periodic solutions as a parameter is varied.

Predicting when spontaneous jumps to dangerous operating conditions will occur has been another active area of ferroresonance research. Various techniques have been used, such as: describing functions [A28], Floquet theory [A121], the Galerkin-method of harmonic balance [A41] and the method of averaging [A19] to directly calculate critical parameters, which result in a transition to a new periodic steady-state.

Various techniques of analysis will be discussed in this chapter, ranging from classic methods such as Rüdenberg's graphical approach, Swift's describing function method, the harmonic balance method, and the method of averaging to modern methods relying on bifurcation theory. Poincaré's approach of foreseeing the future by studying the history and the actual present state will be applied to the study of ferroresonance analysis methods.

2.2 GRAPHICAL METHOD

The graphical method displays operating points as intersections of load lines. Simple linear resonance will be used as an example of the application of this method. Following Rüdenberg[1] [A9], the method will be extended to explain the existence of multiple operating points corresponding to ferroresonant states.

2.2.1 Linear Resonance

A system is said to be in ***resonance*** when its natural frequency is reinforced by a source of the same frequency.

Natural frequency voltages (and currents) appear immediately after a disturbance (e.g. following a capacitor energization or the removal of a fault). If the source is not of the same frequency as the natural frequency of the system, the oscillations will damp due to the system's inherent resistive losses. The oscillations are referred to as transient voltages and currents in this case. Once all transient oscillations have decayed to zero the system is in ***steady state***.

A linear time-invariant system excited by a sinusoidal periodic function of frequency (ω) will have a unique sinusoidal steady state at frequency (ω) [*Fundamental theorem of the sinusoidal steady state* [2]]. A function is said to be ***periodic*** if it is defined for all time and repeats itself after a given period. Periodic functions can be expanded into a Fourier series or sum of pure sinusoids. The frequency of each sinusoid is an integer multiple or ***harmonic*** of the excitation frequency. A system is in ***harmonic resonance*** when its natural frequency is a harmonic and is reinforced by a source of the same frequency.

Superposition is an important principle of linear systems that may be used to great advantage when studying electrical transients and linear resonance. The principle states that:

> *in any linear system if a stimulus S_1 produces a response R_1, and a stimulus S_2 produces a response R_2, then S_1 and S_2 applied simultaneously will evoke a response R_1+R_2 [A81].*

Following a disturbance, the source or stimulus can be a voltage or current source

---

1. The method is normally referred to as Rüdenberg's. however. Odessey and Weber [A5] in an earlier paper, describe the method as being introduced by Stark in 1917 and refined by Margand (1921). Rüdenberg (1923) and Rouelle (1934).

composed of:

- fundamental frequency (i.e. 60 Hz),
- natural frequencies or transients,
- harmonics.

In electrical power systems, linear resonance can be described by studying two important circuits, namely the series and parallel resistance-inductance-capacitance (*RLC*) circuits. The basic circuit configurations are shown in Fig. 2.1. Superposition has been utilized to represent only the sources of harmonics in the two circuits. Transients and the normal fundamental frequency excitation have been ignored.

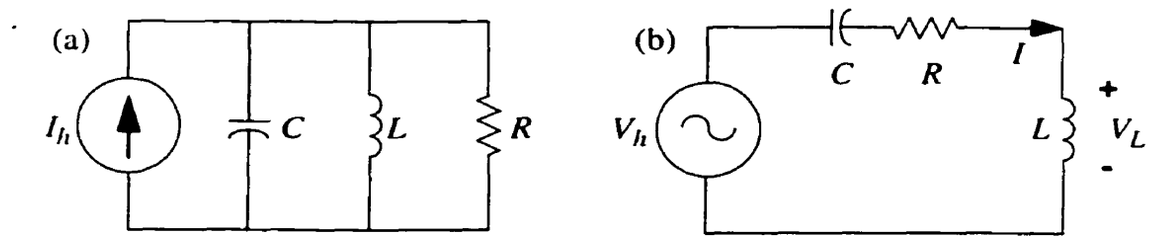

Fig. 2.1 *RLC* resonant circuit examples, (a) parallel *RLC* circuit, (b) series *RLC* circuit.

The parallel resonant case has the most potential to cause problems such as excessive harmonic voltage and current distortion. The reason is that sources of harmonic current (e.g. adjustable speed drives, switch-mode power supplies, saturating transformers) are more prevalent than sources of harmonic voltage (arc furnaces, generators). Harmonic current sources cause a large steady-state harmonic voltage to develop if the parallel combination of inductance and capacitance is resonant at the same frequency as the source. The harmonic voltage causes large circulating harmonic currents to flow between the capacitor and inductor.

Very high voltages and currents can result across the elements of a series or parallel *RLC* circuit when it is excited at or near its natural frequency. A common method used to display linear resonance information is to calculate an impedance vs. frequency plot [5] or a voltage vs. frequency plot.

As an example, (2-1) represents the steady-state rms inductor voltage as a function of frequency in the series *RLC* circuit.

$$|V_L| = \frac{V_h}{\sqrt{\left[\left(\frac{R}{\omega L}\right)^2 + \left(1 - \frac{1.}{\omega^2 LC}\right)^2\right]}} \tag{2-1}$$

The natural frequency of oscillation (ω_n) is calculated using (2-2). Sustained resonance results when the source frequency is equal to the natural frequency of the circuit.

$$\omega_n = \frac{1}{\sqrt{LC}} \tag{2-2}$$

The following component values are chosen to demonstrate the linear resonance phenomonon:

- resistance (R): 612.9 Ω,
- capacitance (C): 15530 pF,
- inductance (L): 2500.0 H,
- source voltage (V_h): 0.34 pu.

Equation 2-1 is plotted in Fig. 2.2. At the natural resonant frequency of the circuit (i.e. 25.54 Hz using (2-2)), voltages in excess of 6.0 pu can be expected across the inductor.

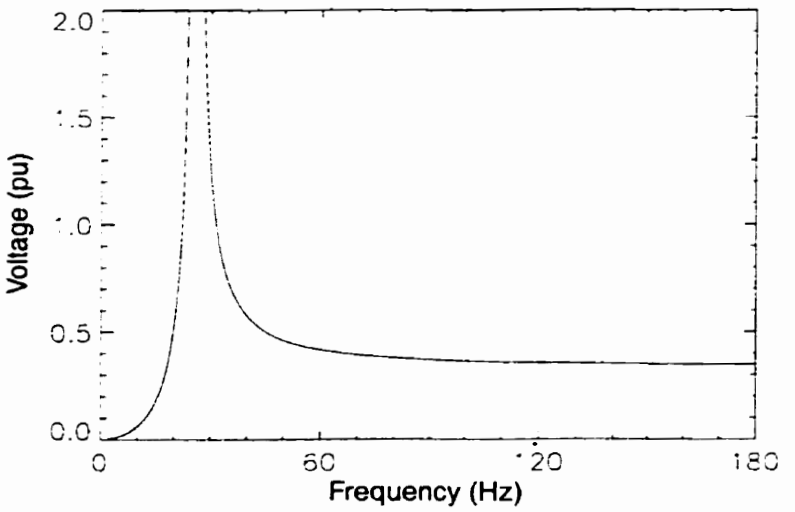

Fig. 2.2 Linear frequency response of a series *RLC* circuit.

Another way of illustrating the steady-state inductor voltage and current at particular operating frequencies is by plotting the relation given by (2-3) [A9].

$$V_L = \sqrt{[|V_h|^2 - (I \cdot R)^2]} + \frac{I}{\omega C} = \omega L I \tag{2-3}$$

A graphical solution is found at the intersection of the straight line and ellipse.

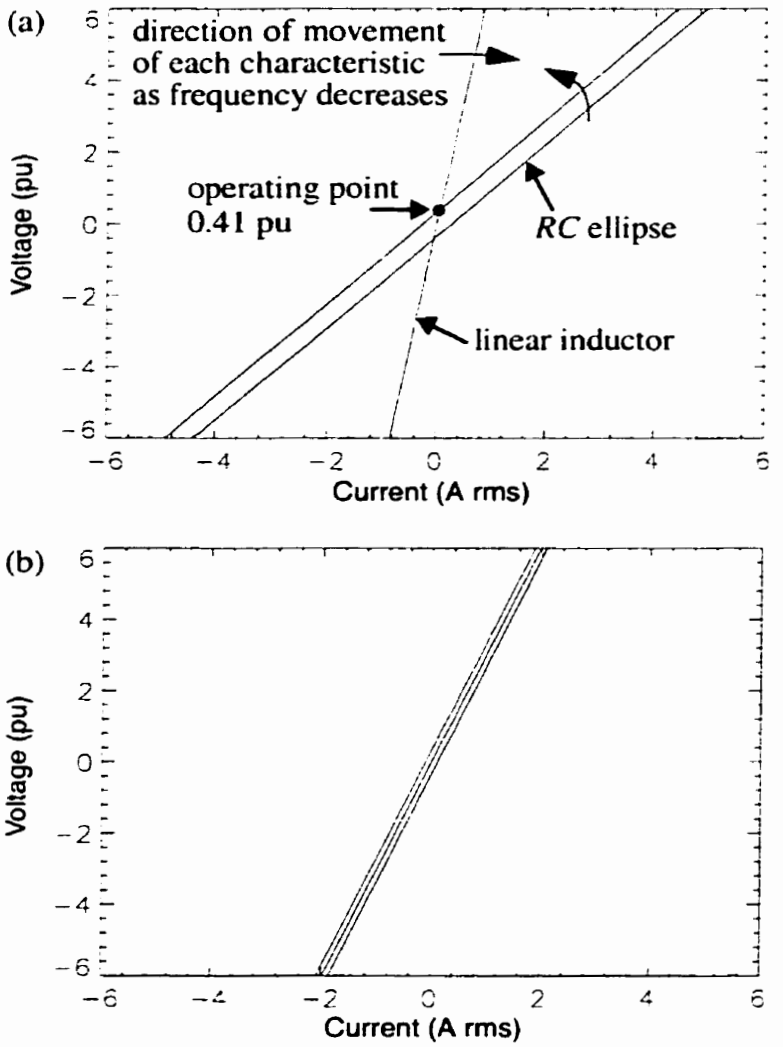

Fig. 2.3 Graphical analysis of series *RLC* circuit with linear inductor, (a) 60 Hz operation, (b) 25.54 Hz operation or operation at resonance.

As linear resonance is approached, Fig. 2.3 illustrates a rotation of the two load lines. Starting from 60 Hz, the ellipse rotates counterclockwise towards 25.54 Hz while the inductor's load line rotates clockwise. At resonance, the impedance of the capacitor and inductor cancel leaving only the resistance to limit the voltage and current in the circuit.

2.2.2 Ferroresonance

If the linear inductor in Fig. 2.1b is replaced by a nonlinear inductor, the circuit shown in Fig. 2.4 results. Several different steady-state conditions can co-exist in this type of nonlinear circuit. The basic frequency of these oscillations could be the network frequency (fundamental frequency ferroresonance) or fractions of the network frequency (subharmonic ferroresonance). Small parameter variations or disturbances can cause *jumps* from one state to another. The graphical method of analysis [A9] will be used to show the existence of multiple fundamental frequency states.

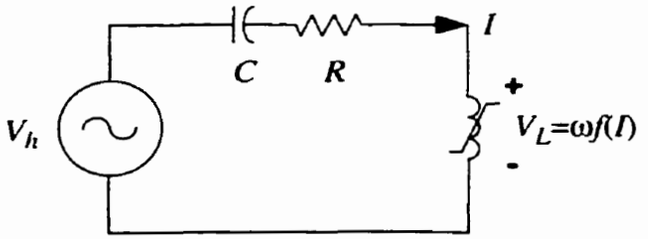

Fig. 2.4 Series *RLC* ferroresonant circuit example.

Equation 2-4 describes the top half of an ellipse [A9].

$$V_L = \sqrt{[|V_h|^2-(I \cdot R)^2]} + \frac{I}{\omega C} \tag{2-4}$$

V_L is also a nonlinear function of current [A9].

$$V_L = \omega \cdot f(I) \tag{2-5}$$

The intersection of (2-4) and (2-5), plotted in Fig. 2.5, indicates three possible 60 Hz steady-state operating points for positive values of voltage and current. Points (a) and (c) are stable operating points while point (b) is unstable. Stability of the operating points can be determined mathematically using small signal techniques.

Ferroresonance is only similar to linear resonance in that large steady-state voltages and currents can be experienced. That is where the similarity ends, however. The ferroresonant circuit does not experience a form of linear resonance where the natural frequency of the circuit is sustained by a source with the same frequency. Concepts such as superposition, which are applicable to linear circuits, are not applicable to a ferroresonant circuit.

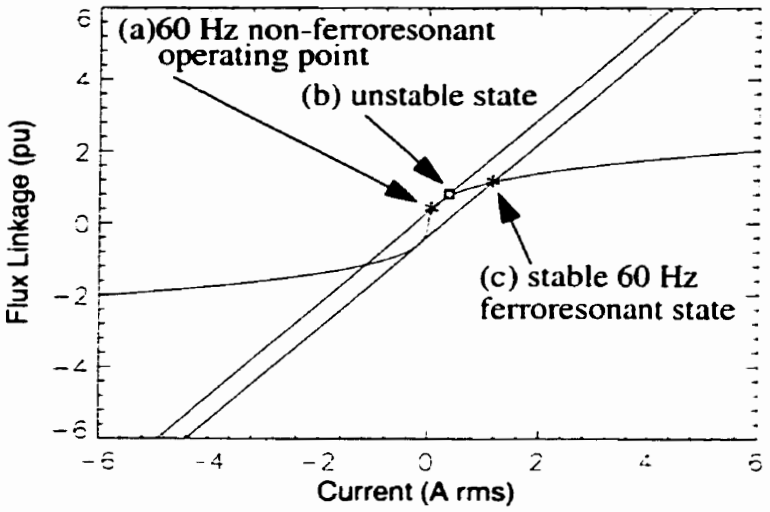

Fig. 2.5 Graphical analysis of series *RLC* circuit with a nonlinear inductor.

Rüdenberg's graphical approach is limited to describing the existence of ferroresonant states that have a dominant fundamental frequency component. Ferroresonant oscillations can be periodic and have dominant subharmonic components, quasi-periodic or even chaotic. These oscillations cannot be predicted by a graphical analysis. Other techniques of analysis will be discussed in the following sections of this chapter.

2.3 HARMONIC BALANCE METHOD

Several analytical methods for finding the periodic steady state of a nonlinear differential equation are described by Hayashi [A19]. The methods include: perturbation, iteration, averaging and the method of harmonic balance. All methods assume the nonlinearity is small compared with the linear portion of the differential equation. The averaging method further assumes that the amplitude and phase of the oscillation vary slowly with time. Hayashi considers the method of harmonic balance to be the widest used and applicable to cases when the nonlinearity becomes large. A simple numerical example will be used to illustrate the method later in this section.

Given the simple circuit shown in Fig. 2.6, which could represent an unloaded transformer or nonlinear inductor in series with a capacitor, a nonlinear differential equation for flux linkage (in per unit) is desired. The unloaded transformer is represented by a magnetizing branch in parallel with a linear resistor that models the total iron-core losses. This model assumes the winding resistance and leakage inductance are negligable. The voltage source in series with a capacitor (C) is equivalent to a strong network connected to an open circuit breaker with parallel grading capacitor (C_g). Between the grading capacitor and unloaded transformer, an equivalent capacitor-to-ground (C_b) is included that represents the total stray capacitance.

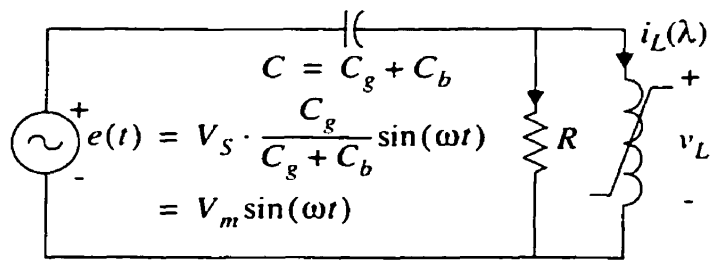

Fig. 2.6 Ferroresonant circuit for illustrating the harmonic balance method.

Before the nonlinear differential equation is derived, it is instructive to examine the two-term polynomial relation that can be used to represent the magnetizing characteristic of the nonlinear iron-core. In the following equation, the input flux linkage (λ_{pu}) is in per unit and the output current (i_{Lpu}) is in per unit. Instantaneous quantities are assumed in the relation.

$$i_{Lpu}(\lambda_{pu}) = a_1 \lambda_{pu} + a_n \lambda_{pu}^{\,n} \tag{2-6}$$

The units of a_1 and a_n are in amperes/volt-seconds if real values are used. However, they

are dimensionless if per unit values are used. Fig. 2.7 shows the per unit versus the actual flux linkage-magnetizing current relation. Working with per unit values is much easier when trying to match an actual flux-current relation.

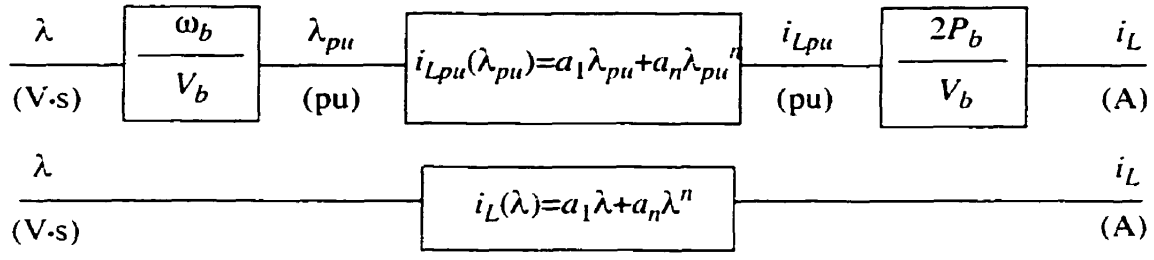

Fig. 2.7 Comparison between per unit and real-valued magnetizing curve two-term polynomial relation.

An example of two flux linkage-magnetizing current relations is shown in Fig. 2.8. The third-order polynomial is a contrived example chosen to simplify the mathematics and will be used in the remainder of this chapter to illustrate the nonlinear dynamics methods. A comparison with a linear inductor is made to show that the problem under investigation is not weakly nonlinear (i.e. almost linear).

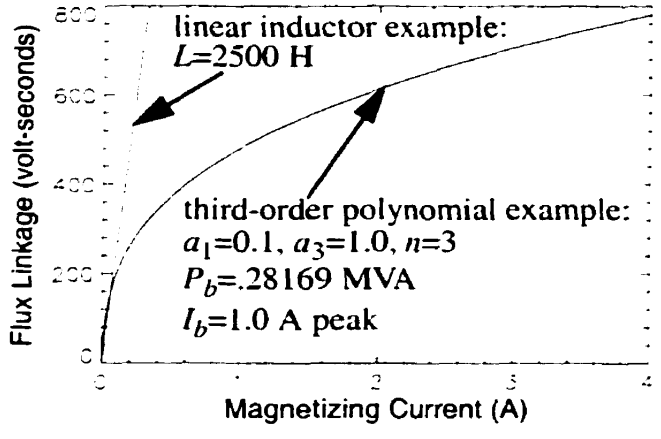

Fig. 2.8 Comparison of an actual wound potential transformer magnetizing curve with a third order polynomial approximation.

Using real values of voltage, current and flux linkage, the following equation is derived:

$$e(t) = \frac{1}{C}\int(i_L \cdot dt) + \frac{1}{RC}\int\frac{d\lambda}{dt}dt + \frac{d\lambda}{dt}. \qquad (2\text{-}7)$$

If the equation is rewritten in Laplace form, the following non per-unitized equation

results,

$$s^2\Lambda(s) + \frac{s\Lambda(s)}{RC} + \frac{a_1\Lambda(s) + a_3\Lambda^3(s)}{C} = s(E(s)), \tag{2-8}$$

which can also be written as,

$$\ddot{\lambda} + \frac{\dot{\lambda}}{RC} + \frac{a_1\lambda + a_3\lambda^3}{C} = \omega V_m \cos(\omega t). \tag{2-9}$$

Now let $e_{pu}=e/V_b$, $i_{Lpu}=i_L/I_b$, $\lambda_{pu}=\lambda/\Lambda_b$ and substitute into (2-7).

$$V_b e_{pu}(t) = \frac{I_b}{C}\int(i_{Lpu}\cdot dt) + \frac{\Lambda_b}{RC}\int\frac{d\lambda_{pu}}{dt}dt + \Lambda_b\frac{d\lambda_{pu}}{dt} \tag{2-10}$$

Rewrite (2-10) in Laplace form, dividing both sides by Λ_b and substituting (2-6) for $i_{Lpu}(\lambda_{pu})$.

$$\frac{V_b}{\Lambda_b}E_{pu}(s) = \frac{I_b\cdot(a_1\Lambda_{pu}(s) + a_3\Lambda_{pu}{}^3(s))}{s(C\cdot\Lambda_b)} + \frac{\Lambda_{pu}(s)}{RC} + s\Lambda_{pu} \tag{2-11}$$

Multiply (2-11) by s and expand Λ_b as V_b/ω_b.

$$s^2\Lambda_{pu}(s) + \frac{s\Lambda_{pu}(s)}{RC} + \frac{\omega_b(a_1\Lambda_{pu}(s) + a_3\Lambda_{pu}{}^3(s))\cdot I_b}{C\cdot V_b} = \omega_b(sE_{pu}(s)) \tag{2-12}$$

Finally, (2-12) can be rewritten and simplified by letting $\lambda_{pu}=\lambda$:

$$\ddot{\lambda} + \frac{\dot{\lambda}}{RC} + \frac{\omega_b(a_1\lambda + a_3\lambda^3)I_b}{CV_b} = \omega_b\omega\frac{V_m}{V_b}\cos(\omega t) \tag{2-13}$$

In order to illustrate the harmonic balance method, (2-13) is further simplified by making variable substitutions.

$$\ddot{\phi} + k\dot{\phi} + C_1\phi + C_3\phi^3 = G\cos(\omega t), \text{ where} \tag{2-14}$$

$$k = \frac{1}{RC},\ C_1 = \frac{a_1\omega_b I_b}{CV_b},\ C_3 = \frac{a_3\omega_b I_b}{CV_b}, \text{ and } G = \frac{\omega_b\omega V_m}{V_b} \tag{2-15}$$

Equation 2-14 is also known as Duffing's[2] equation. A higher-order nonlinearity (i.e. 9th-15th) approximates an actual saturation curve more closely; however, because (2-14) is of

the same form as Duffing's equation, the results can be compared with historical work performed by Hayashi [A19].

A first-order solution to (2-14) can be assumed to be of the form:

$$\lambda(t) = a\cos(\omega t) + b\sin(\omega t). \tag{2-16}$$

The basic procedure of harmonic balance is to substitute (2-16) into (2-14) and equate terms of $\cos(\omega t)$ and $\sin(\omega t)$. Since this is a first-order approximation, third harmonic coefficients are ignored. After equating terms, the following equations result:

$$a\left((\omega^2 - C_1) - \frac{3C_3}{4}(a^2 + b^2)\right) - k\omega b = -G. \tag{2-17}$$

$$-b\left((\omega^2 - C_1) - \frac{3C_3}{4}(a^2 + b^2)\right) - k\omega a = 0. \tag{2-18}$$

Marti and Soudack [A87] refer to this as Ritz's method of harmonic balance. Hayashi [A19] credits van der Pol in developing the technique.

Solutions may be found if we square and add the two previous equations and convert the rectangular coordinates (a,b) to polar coordinates (r,θ).

$$r^2\left(\left(\omega^2 - C_1 - \frac{3C_3 r^2}{4}\right)^2 + k^2\omega^2\right) = G^2 \tag{2-19}$$

Equation 2-19 can be rewritten as a cubic polynomial in r^2. Real roots of the polynomial correspond to possible equilibrium points or solutions to the original differential equation. The solutions for $r^2=a^2+b^2$ can be substituted back into (2-18) and (2-17), and solutions for (a,b) can then be found.

A particular example, using the following parameters, will illustrate the procedure:

- resistance (R): 4.76E7 Ω,
- capacitance (C): 15530.0 pF,
- source voltage (V_m): $0.34V_b$ volts peak,
- saturation curve: a_1=0.1, a_3=1.0, n=3,

---

2. G. Duffing introduced a nonlinear oscillator in 1918 with a cubic spring stiffness term to describe the hardening spring effect observed in many mechanical problems.

- Voltage base (V_b): 187794.2 volts peak,
- Frequency (ω_b): 376.991 rad/s.

Three solutions were found for (a,b): {(-.436,.002),(-.872,.008),(1.309,.02)}.

The harmonic balance method analytically determines approximate periodic solutions to the nonlinear differential equation. The stability of each solution needs to be determined by considering the behavior of the system to small perturbations.

In order to determine the stability of the solutions, (2-14) can be linearized in order to derive the variational equation. The classical linearization technique is to assume a small variation (ξ) about a known solution (λ_0) and solve the linearization equation:

$$F(\xi) = F(\phi_0 + \xi) - F(\lambda_0). \tag{2-20}$$

Solving (2-20) for the steady-state solution results in the following *first variational equation*:

$$F(\xi) = \ddot{\xi} + k\dot{\xi} + (C_1 + 3C_3\lambda_0^2)\xi = 0. \tag{2-21}$$

The stability of the solution can be determined by following Hayashi [A19] who makes use of a variable transformation (i.e. (2-22)), which converts (2-21) into Mathieu's equation (2-23).

$$\xi = e^{\left(-\frac{k}{2}\right)t}\eta \tag{2-22}$$

$$\ddot{\eta} + [\theta_0 + 2\theta_1\cos(2\omega t - \varepsilon)]\eta = 0 \tag{2-23}$$

The variables θ_0 and θ_1, in (2-34), can be determined by equating terms from the transformed variational equation.

$$\theta_0 = -\frac{k^2}{4} + C_1 + \frac{3C_3r^2}{2} \tag{2-24}$$

$$\theta_1 = \frac{3C_3r^2}{4} \tag{2-25}$$

Equation 2-23 can be rewritten in state variable form ($dX/dt=A(t)X$) as shown in (2-26).

$$\begin{bmatrix} \dot{\eta}_1 \\ \dot{\eta}_2 \end{bmatrix} = \begin{bmatrix} 0 & 1 \\ -\{\theta_0 + 2\theta_1 \cos(2\omega t - \varepsilon)\} & 0 \end{bmatrix} \begin{bmatrix} \eta_1 \\ \eta_2 \end{bmatrix} \tag{2-26}$$

The matrix $A(t)$ is periodic with period T. Floquet[3]'s theorem [15]-[18], states that such a system has at least one non-trivial solution ($\Phi(t)$) with the property:

$$\Phi(t+T) = M\Phi(t). \tag{2-27}$$

M is a nonsingular constant matrix corresponding to the eigenvalues of $\Phi^{-1}(0)\Phi(T)$. The eigenvalues are also known as the characteristic multipliers or Floquet multipliers of the original differential equation. The characteristic exponents or Floquet exponents are defined by:

$$M = e^{\mu T}. \tag{2-28}$$

In order for the solution of the original differential equation to be stable, the solution of the variational equation must approach zero as time approaches infinity. The characteristic multipliers must therefore approach zero, which requires the characteristic exponents to have negative real parts. Combining (2-28) and (2-22) results in the following stability condition:

$$-\frac{k}{2} \pm u < 0. \tag{2-29}$$

This technique is difficult to use as the fundamental solutions $\Phi(t)$ are, in general, unknown. However, Mathieu's equation, which is a special case of the more general Hill's equation, has been studied extensively by Hayashi [A19]. One technique which may be used to determine u is outlined below. Using Floquet's theory, a solution to (2-23) is assumed to have the form:

$$\eta = e^{\mu t}\sin(n\omega t + \sigma). \tag{2-30}$$

Equation 2-30 is then inserted into (2-23) and coefficients of $\sin(n\omega t)$ and $\cos(n\omega t)$ are equated. The following two equations result:

$$2un\omega\sin(\sigma) + (\theta_0 + u^2 - n^2\omega^2)\cos(\sigma) - \theta_1\cos(\sigma) = 0, \tag{2-31}$$

---

3. Gaston Floquet (1847-1920) was a French mathematician who studied the properties of differential equations with periodic coefficients.

$$2un\omega\cos(\sigma)-(\theta_0 + u^2 - n^2\omega^2)\sin(\sigma) - \theta_1\sin(\sigma) = 0. \quad (2\text{-}32)$$

These two equations can be simplified in order to find an equation for the characteristic exponent as a function of the input parameters.

$$u^2 = -(\theta_0 + n^2\omega^2) \pm \sqrt{4n^2\omega^2\theta_0 + \theta_1^2} \quad (2\text{-}33)$$

Equation 2-33 may be combined with (2-29) and a generalized stability condition determined.

$$\frac{k^4}{16} + \frac{k^2}{2}(\theta_0 + n^2\omega^2) + (\theta_0 - n^2\omega^2)^2 > \theta_1^2 \quad (2\text{-}34)$$

After substituting parameter values, as mentioned previously, and the calculated solutions resulting from the harmonic balance method into (2-34) through (2-25), the stability of each solution can be determined. The inequality is violated for the case (a,b): {(-.872,.008)} but holds true for the other two solutions. When n=1, the inequality ascertains the stability against buildup of an unstable oscillation in which the fundamental-frequency component predominates over higher harmonics. If a higher order solution had been assumed instead of (2-16), then n would take on values corresponding to each harmonic. For stability to be ensured, the inequality would have to hold true for all values of n simultaneously.

2.3.1 Galerkin's Method

As more precision is required, the preceding method can become difficult to use. A numerical technique based on Galerkin's method was first proposed to be used on the ferroresonant circuit by Germond [A41]. Janssens *et al.* [A75], [A79], [A117], Kieny *et al.* [A90] and van Craenenbroeck *et al.* [A148] have also used Galerkin's method.

Galerkin's method transforms the problem into the frequency domain. First the circuit is split into a linear and nonlinear network as shown in Fig. 2.9. Multiple nonlinearities can be studied if the Thévenin equivalent of the linear network is well-defined (i.e. if it does not contain any element which is coupled to some variable outside of the network).

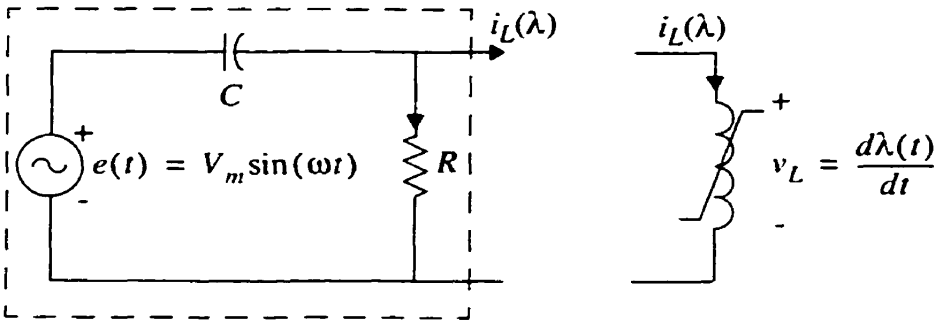

Fig. 2.9 Equivalent circuit model for illustrating the Galerkin harmonic balance method.

The flux linkage in the nonlinear inductor is represented by a limited Fourier series given by (2-35).

$$\lambda(t) = \Lambda_0 + \sum_{k=1}^{n} (\Lambda_{k,c}\cos(k\omega t) + \Lambda_{k,s}\sin(k\omega t)) \tag{2-35}$$

The Fourier coefficients, $\Lambda_{k,c}$ and $\Lambda_{k,s}$ are defined by:

$$\Lambda_{k,c} = \frac{2}{T}\int_0^T \lambda(t)\cos(k\omega t)dt\,, \tag{2-36}$$

$$\Lambda_{k,s} = \frac{2}{T}\int_0^T \lambda(t)\sin(k\omega t)dt\,. \tag{2-37}$$

The linear portion of the circuit reduces to the following equation in the frequency domain:

$$jk\omega\Lambda_k = E_k - Z_k I_k\,. \tag{2-38}$$

The relation between current and flux linkage is nonlinear and can be represented by (2-6).

The method begins by guessing at an initial approximation of the flux linkage waveform. The current waveform is then calculated using (2-6) and the Fourier transform is calculated in order to derive the Fourier coefficients. The unknown Fourier coefficients of flux linkage (Λ_k) and current (I_k) are replaced in (2-38). The residual vector is defined as:

$$F_k(\Lambda_k, E_k) = jk\omega\Lambda_k - E_k + Z_k I_k = 0.0\,,\ k=1,2,...n \tag{2-39}$$

The $(2n+1)$ residual vector equations are solved using the Newton-Raphson method for the unknown vector of Fourier components of flux linkage (Λ_k) at a fixed parameter (E_k).

If the residual vector has continuous first partial derivatives, then the differential can be determined at any point along the solution and is defined as,

$$\frac{\partial F(\Lambda, E)}{\partial \Lambda} d\Lambda + \frac{\partial F(\Lambda, E)}{\partial E} dE = 0.0 , \tag{2-40}$$

which after dividing by dE and rearranging may be rewritten as,

$$\frac{\partial F}{\partial \Lambda} \cdot \frac{d\Lambda}{dE} = -\frac{\partial F}{\partial E} . \tag{2-41}$$

When the matrix $\frac{\partial F}{\partial \Lambda}$ becomes singular, the slope of the tangent to the curve (Λ(E)) becomes infinite [A90] (i.e. see Fig. 2.17). Janssens takes advantage of this fact when determining stability domain boundaries [A79].

The next section will discuss the describing function method.

2.4 DESCRIBING FUNCTION METHOD

Swift [A28] was the first to apply this method to a ferroresonant circuit. The method has also been used by Kumar *et al.* ([A36], [A39], [A86]), Hirst and Baràkat ([A52], [A54]), Prusty *et al.* [A47] and Masson [A58]. All researchers limited their investigation to transformers with 3^{rd}, 5^{th} or 7^{th} order polynomial nonlinearities. Prusty was able to obtain a closed form analytical solution for a 5^{th} order polynomial. Hirst and Baràkat extended the analysis to three-phase circuits by including a Newton-Raphson iteration scheme. Previously only single-phase circuits were analyzed and the jump to period-1 or period-3 ferroresonance determined. Higher order nonlinearities are difficult to solve analytically because it is difficult to isolate the complex roots [A47].

The analysis method is reasonable for capacitor voltage transformers (CVTs) [A86] but is not recommended for high voltage power transformers where 11^{th} order polynomials [A136] are typical. Although, most CVTs tend to have subharmonic responses that result from perturbations in the circuit. Swift's method is most appropriate for spontaneous jumps resulting from slow parameter variations.

The method is a form of harmonic balance in that the form of solution must be known *apriori* and assumed to be a truncated Fourier series. Normally, only one or two terms are retained.

The series or parallel ferroresonant circuit can be represented by the block diagram given

in Fig. 2.10. The flux linkage signal ($\Lambda(s)$) input to the nonlinear block (N_L) has been per-unitized.

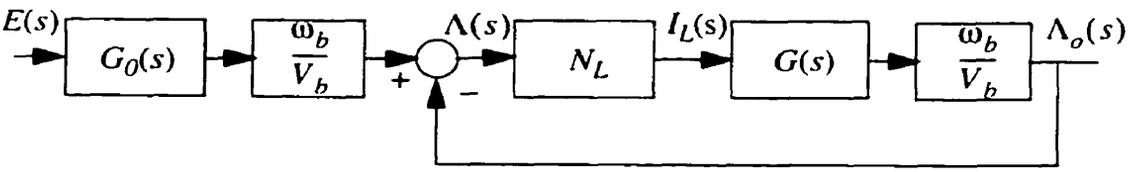

Fig. 2.10 Block diagram representation of circuit for use with describing function method.

For a series *RLC* circuit as depicted in Fig. 2.6, the expression for $G(s)$ can be derived to be:

$$G(s) = \frac{R}{s(1 + sRC)}. \tag{2-42}$$

The saturation nonlinearity (N_L) is defined by a polynomial relation:

$$i_L(\lambda) = a_1\lambda + a_n\lambda^n. \tag{2-43}$$

The dual input describing function (didf) is determined by exciting the nonlinear element (N_L) with two sinusoidal inputs and calculating the harmonic content of the output. The ratio of the fundamental harmonic of the output to the input is defined as the dual input describing function.

Swift [A28] assumed the following relation to represent a small perturbation from the operating steady state:

$$\lambda(t) = \lambda_m \cos(\omega t + \alpha) + \mu\cos(\omega t). \tag{2-44}$$

For a subharmonic state, the perturbation frequency may be changed to $\omega/3$ as suggested by Kumar *et al.* [A86]. The didf is then the ratio of the output subharmonic to the input subharmonic. All higher harmonics are neglected in the analysis.

The closed loop frequency response is determined from,

$$\frac{\Lambda_o(j\omega)}{\Lambda(j\omega)} = \frac{N_L G(j\omega)}{1 + N_L G(j\omega)}. \tag{2-45}$$

When $G(j\omega)=-1/N_L$ then the output will exhibit sustained oscillations. The intersection of

the two functions can be determined graphically in the complex plane or analytically if the nonlinearity is limited to a fifth order polynomial [A47].

Following the method outlined by Swift [A28], the dual input describing function (N_L) can be found by substituting (2-44) into (2-43). Since $\mu << \lambda_m$, higher order terms of μ can be ignored. Also, only fundamental frequency terms are retained. Assuming a third order polynomial representation of the magnetizing characteristic, the following equation results for i_L.

$$i_L(t) = a\lambda_m\cos(\omega t + \alpha) + a\mu\cos(\omega t) + \frac{3b\lambda_m^3}{4}\cos(\omega t + \alpha) + \frac{3b\lambda_m^2\mu}{2}\cos(\omega t) + \frac{3b\lambda_m^2\mu}{4}\cos(\omega t + 2\alpha) \tag{2-46}$$

As far as the increment μ is concerned, the effective gain of the describing function is,

$$N_L = \frac{a\mu + 3b\lambda_m^2\mu/2 + 3b\lambda_m^2\mu/4e^{j(2\alpha)}}{\mu}. \tag{2-47}$$

which may be simplified to,

$$N_L = a + \frac{3b\lambda_m^2}{4}(2 + e^{j(2\alpha)}). \tag{2-48}$$

The incremental describing function is plotted as $-1/(N_L(\lambda_m,\alpha))$ in Fig. 2.11 for λ_m={-.436, -.873, 1.309}. Also plotted in Fig. 2.11 is $G(j\omega)$ for the case where ω is 377 rad/second.

In linear control analysis (N_L=1), the Nyquist stability criterion states that the feedback system is stable if the Nyquist contour, mapped into the $G(s)$ plane, does not encircle the (-1,0) point. West *et al.* [8] define the region of instability as the point where the curve ($-1/N_L$) cuts the response locus of the linear system. Therefore, referring to Fig. 2.11, the middle circle is unstable while the outer two circles are stable. The three circles correspond to particular solutions found using the harmonic balance method for a particular input voltage.

Slowly increasing the source voltage will result in the outer-left and middle circles approaching the point G(j377). Spontaneous jumps to period-1 ferroresonance will occur at the critical value of flux linkage where the three functions intersect. Similarly, slowly

reducing the source voltage will result in the middle and outer-right circles converging. Through experimentation, the two critical values of flux linkage where a jump will occur are λ_m={-0.67, 1.15}. Fig. 2.11b shows the case where λ_m=-0.67. The information contained in Fig. 2.11 is comparable with the bifurcation diagram shown in Fig. 2.17.

The jump to period-1 ferroresonance will not occur if G(j377) is outside of the nonlinearity envelope, defined by dashed lines in Fig. 2.11. Kumar et al. [A36], [A86] analyzes the susceptibility of several circuits to ferroresonance by comparing the locus of $G(j\omega)$ with the nonlinearity envelope.

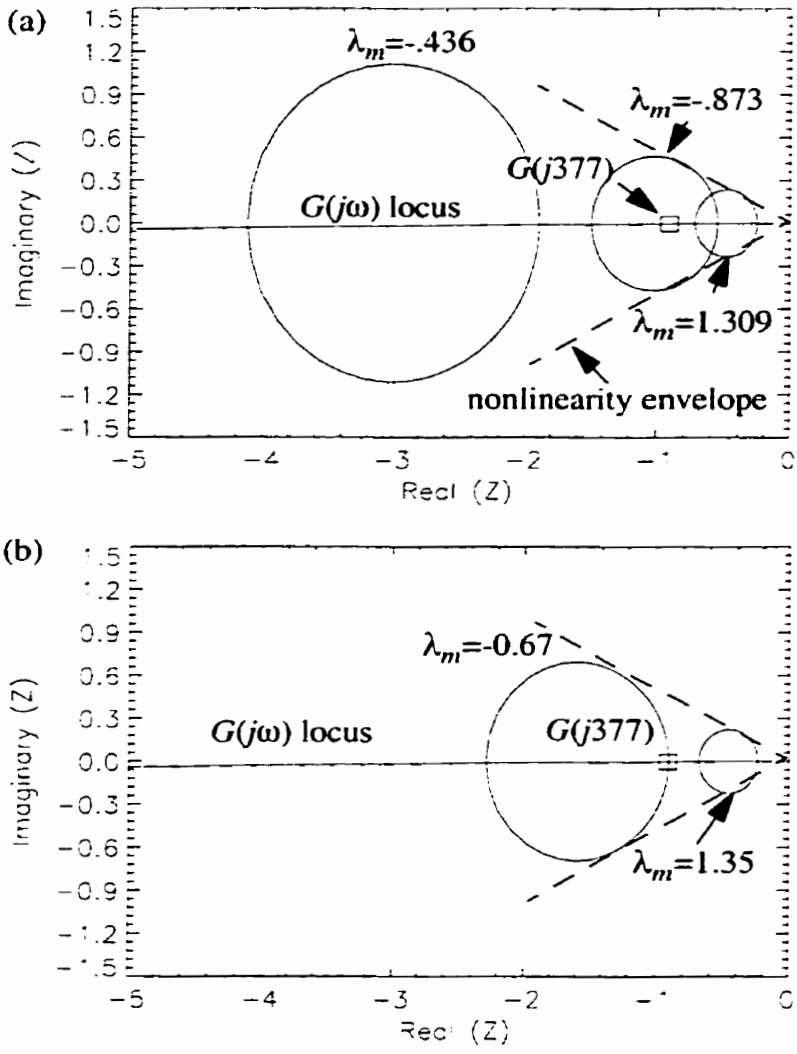

Fig. 2.11 Incremental describing function stability analysis showing, (a) steady-state operation at V_s=1.04 pu, (b) critical flux linkage at V_s=1.23 pu.

The method suffers from several inaccuracies resulting from the assumed form of flux

linkage (2-44) and truncations required in creating the describing function. If an analytical expression can't be found for determining points of intersection, then a graphical approach must be taken, which results in further inaccuracies. The method is inconvenient to use for more complicated circuits or for higher order nonlinearities. Hysteresis would be very difficult to accurately include in the development of the describing function. Because of the small perturbation assumption, the method attempts to predict spontaneous jumps resulting from slow parameter variations.

The next section will discuss the method of averaging.

2.5 AVERAGING METHOD

The method of averaging is useful for visualizing the nature of solutions near equilibrium points for weakly nonlinear problems. The method was originally conceived by Krylov, Bogoliubov and Mitropolsky and is therefore sometimes referred to as the KBM method [14]. Another popular name is the SVA or slowly varying amplitude method [A129].

The method begins by assuming that a solution to the differential equation, given by (2-14), can be written in the following form:

$$\lambda(t) = a(t)\cos(\omega t) + b(t)\sin(\omega t) \tag{2-49}$$

where a and b are slowly-varying amplitudes compared with $\cos(\omega t)$ and $\sin(\omega t)$. The averaging method is applicable not only to the study of periodic oscillations but also transient oscillations where the amplitude and phase vary slowly over time.

The method proceeds as in the harmonic balance method. The solution is substituted into the differential equation and coefficients of sin and cos are equated. Second order derivatives of a and b, terms in $\cos(3\omega t)$ and $\sin(3\omega t)$ and terms kda/dt and kdb/dt are neglected.

After equating terms and solving for the first derivative of a and b, the following averaged equations result.

$$\dot{a} = A(a,b) = \frac{-b}{2\omega}\left((\omega^2 - C_1) - \frac{3C_3}{4}(a^2 + b^2)\right) - \frac{ka}{2} \tag{2-50}$$

$$\dot{b} = B(a,b) = \frac{a}{2\omega}\left((\omega^2 - C_1) - \frac{3C_3}{4}(a^2 + b^2)\right) - \frac{kb}{2} + \frac{G}{2\omega} \tag{2-51}$$

A typical portrait in the *a-b* phase plane or van der Pol[4] plane, using the parameters given in Section 2.3, is shown in Fig. 2.12.

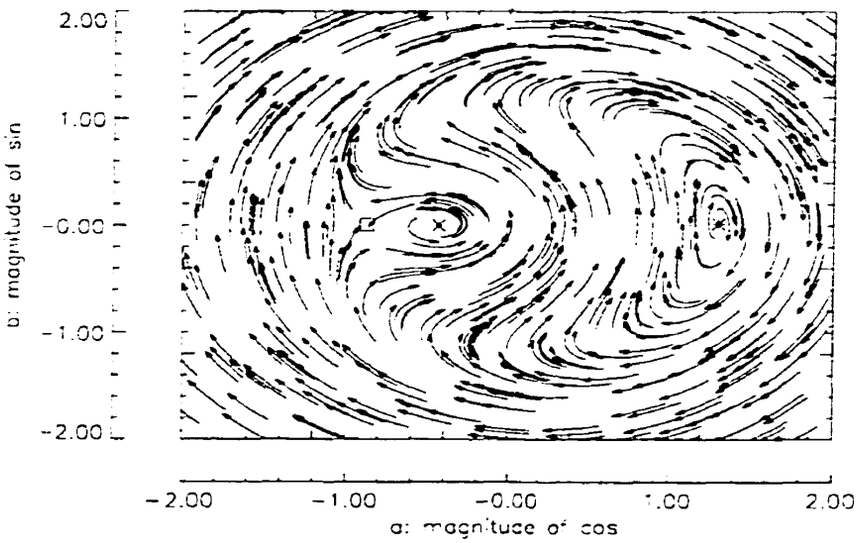

Fig. 2.12 Paths in the van der Pol plane for a ferroresonant circuit.

The fixed points calculated previously using the harmonic balance method are also displayed. The stability of each is immediately apparent by examining the behavior of the velocity field in a small neighbourhood around the fixed points. Stable fixed points are denoted by asterisks and the unstable fixed point is denoted by a box.

The velocity field is drawn using a standard library procedure that comes with PV-WAVE. Two 600 element arrays are created associated with the derivatives along the *a* and *b* axis (i.e. (2-50) and (2-51)). Normally, the procedure will draw an arrow in the direction of the field and proportional to the strength of the field at each location. Since only visualization of the stability of each of the fixed points is desired, the calculated derivatives are normalized.

The averaging technique has transformed a nonautonomous differential equation into an autonomous differential equation. Limit cycles are replaced by fixed points. The stability of the fixed points can be determined by performing a Taylor expansion in a small neighbourhood around the fixed points.

---

4. Named after Balthasar van der Pol (1889-1959), a Dutch physicist who studied the dynamics of electronic oscillators in the 1920s.

$$\begin{bmatrix} \dot{\xi}_1 \\ \dot{\xi}_2 \end{bmatrix} = \begin{bmatrix} \frac{\partial}{\partial a}A(a_i, b_i) & \frac{\partial}{\partial b}A(a_i, b_i) \\ \frac{\partial}{\partial a}B(a_i, b_i) & \frac{\partial}{\partial b}B(a_i, b_i) \end{bmatrix} \begin{bmatrix} \xi_1 \\ \xi_2 \end{bmatrix} \tag{2-52}$$

The fixed points are stable if the trace of the Jacobian is negative and the determinant of the Jacobian is positive or more simply, the eigenvalues have negative real parts.

Evaluating the partial derivatives in (2-52) results in the following Jacobian:

$$\begin{bmatrix} A_1 & A_2 \\ B_1 & B_2 \end{bmatrix} = \begin{bmatrix} -\frac{k}{2} + \frac{3C_3 a_i b_i}{4\omega} & -\left(\frac{\omega^2 - C_1}{2\omega}\right) + \frac{3C_3}{8\omega} \cdot a_i^2 + \frac{9C_3}{8\omega} \cdot b_i^2 \\ \left(\frac{\omega^2 - C_1}{2\omega}\right) - \frac{3C_3}{8\omega} \cdot b_i^2 - \frac{9C_3}{8\omega} \cdot a_i^2 & -\frac{k}{2} - \frac{3C_3 a_i b_i}{4\omega} \end{bmatrix} . \tag{2-53}$$

The **trace** (i.e. sum of the principle diagonal elements) is equal to $-k$ and will always be negative since the ferroresonant circuit only has positive damping. The determinant of the Jacobian will determine the stability. Table 2.1 summarizes the calculations made to determine the stability and classification of the fixed points in the van der Pol plane.

Table 2.1 Fixed Point Classification

fixed point (a_i, b_i)	trace (A_1+B_2)	determinant $(A_1B_2-A_2B_1)$	eigenvalues	eigenvectors	classification
1.30891, 0.01807	-1.35276	23984.20	-.676 ±j154.9	$\begin{bmatrix} -0.302j \\ 0.953 \end{bmatrix}, \begin{bmatrix} 0.302j \\ 0.953 \end{bmatrix}$	stable focus
-.43673, 0.002012	-1.35276	14356.40	-.676 ±j119.8	$\begin{bmatrix} 0.775 \\ -0.632j \end{bmatrix}, \begin{bmatrix} 0.775 \\ 0.632j \end{bmatrix}$	stable focus
-.87229, 0.008026	-1.35276	-8980.75	-95.445, 94.093	$\begin{bmatrix} 0.620 \\ 0.784 \end{bmatrix}, \begin{bmatrix} -0.606 \\ 0.796 \end{bmatrix}$	unstable saddle point

The calculations confirm the conclusions drawn from observing the behavior in the van der Pol plane.

2.6 MODERN NONLINEAR DYNAMICS METHODS

The study of the dynamical behavior of nonlinear systems is called ***nonlinear dynamics***. Classical nonlinear dynamics methods, such as the graphical and analytical analysis of the previous sections, have been used to show the existence of multiple operating states in a nonlinear inductor circuit. However, the highly complex dynamic nature of this phenomenon has only been hinted at.

Recently, new nonlinear dynamics methods have been applied to the analysis of ferroresonance [A136], [A125], [A103], [A102]. Concepts such as attractors, Poincaré[5] sections, bifurcations and basins of attraction provide a framework for discussion and analysis of the ferroresonance phenomenon. These ideas and their applications are discussed next.

2.6.1 Characterization of Attractors

An ***attractor*** is a description of the final operating state of a dynamic system. The attractor is most clearly illustrated by plotting the trajectory of the system response in state-space. Attractors can be characterized as being single points, periodic orbits or complex ribbons (chaotic attractor) folding through state-space.

Hilborn [9] defines motion as being ***quasi-periodic*** if it is composed of two different frequencies in which the ratio of the frequencies cannot be expressed as a ratio of integers. Hence, the ratio is *irrational* or the frequencies are *incommensurate*.

An example of an attractor with a rational ratio of frequencies is shown in Fig. 2.13. The two oscillation frequencies in the example are 50 Hz (i.e. around major radius of torus) and 50/22 Hz around the minor radius. In the absence of all losses, the motion repeats itself, hence the Poincaré section consists of a finite number of points and the behavior is referred to as ***frequency-locked***. If the frequencies were incommensurate, the motion never exactly repeats itself and the Poincaré section would eventually fill a closed curve.

---

5. Henri Poincaré (1854-1912), known as the founder of geometric dynamics, worked on problems in celestial mechanics during the 1890s.

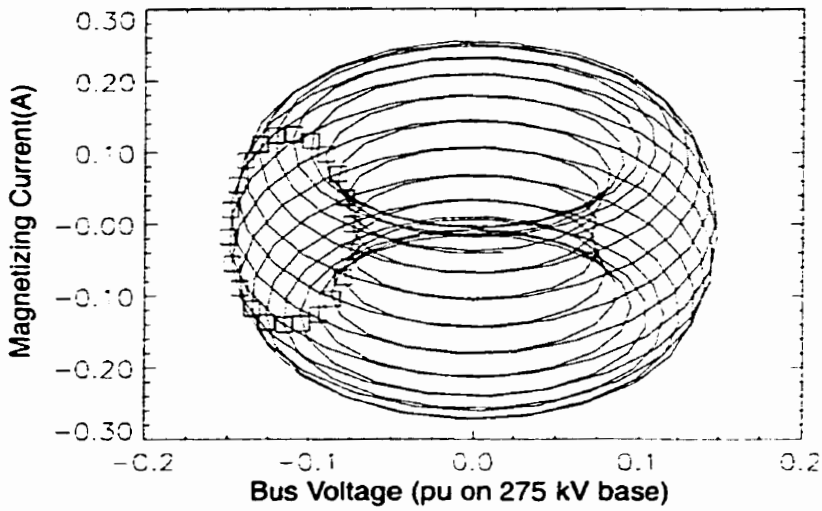

Fig. 2.13 Frequency-locked behavior [A129].

Poincaré sections are a useful method of displaying or characterizing the attractor. In this thesis, ***Poincaré sections*** refer to slices across the time axis of a two dimensional attractor (e.g. flux linkage vs. voltage). The sections are calculated by sampling the state variables once per drive cycle at a fixed phase angle. The aggregate of all slices (i.e. Poincaré sections covering 0 to 360 degrees) is the full attractor.

It is possible in some cases to mathematically derive a ***Poincaré map*** (also called ***iterated map*** or ***first return map***) [17]. The advantage to studying a Poincaré map is similar to that found for the method of averaging. The dimensionality of the original problem is reduced by one. Rather than studying limit cycles resulting from a two-dimensional nonautonomous d.e., the transformation allows one to study fixed points of a two-dimensional autonomous differential equation.

The ratio of the natural period of the dynamic system to the period of the drive or source is equal to the number of points in the Poincaré section. A single point indicates the frequency of the attractor is the same as the sampling frequency and is referred to as *period-1* or fundamental frequency ferroresonance.

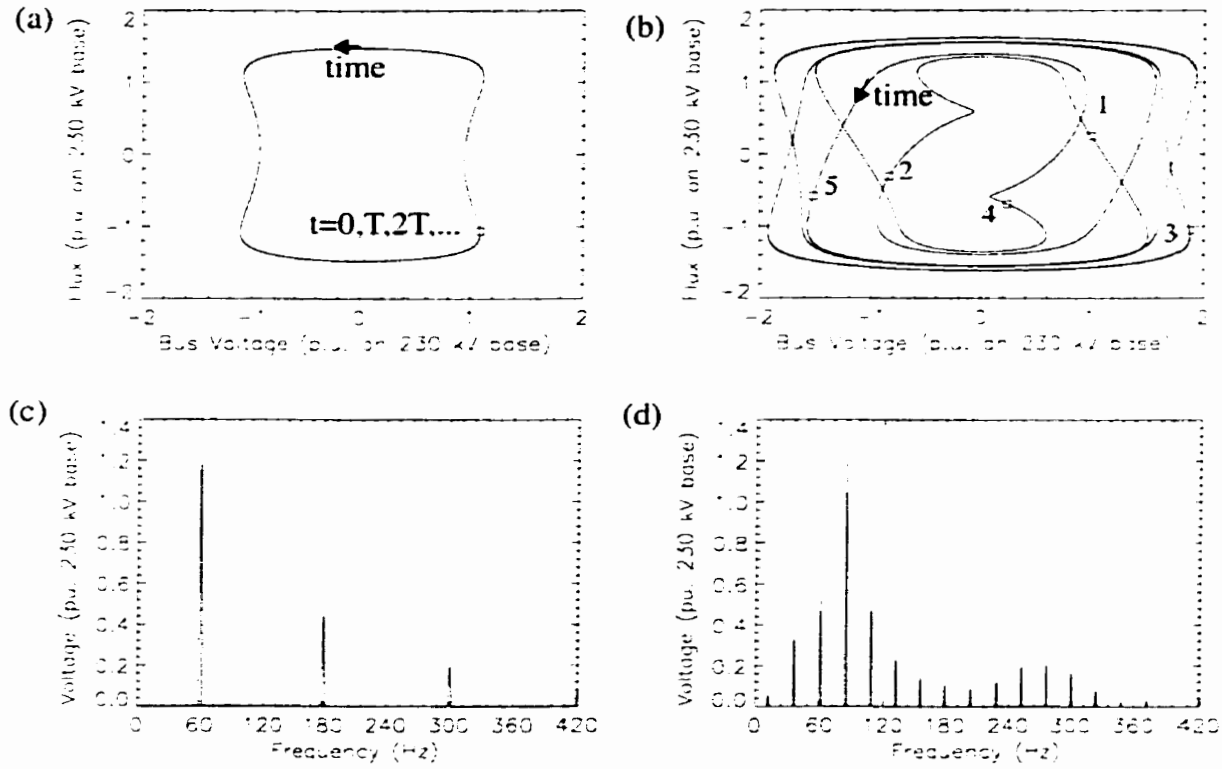

Fig. 2.14 Characterization of two different periodic attractors, (a) state space trajectory of period-1 attractor using parameters: V_s=1.00 pu, C_g=7250 pF, C_b=10450 pF, (b) state space trajectory of period-5 attractor using parameters: V_s=1.18 pu, C_g=7250 pF, C_b=10450 pF, (c) spectrum of capacitor voltage for period-1 attractor, (d) spectrum of capacitor voltage for period-5 attractor.

A discrete Fourier transform (DFT) of the time series can also be used for characterization. Two examples of periodic orbits are given in Fig. 2.14. The lowest frequency of a period-5 attractor, for example, is (60/5) or 12 Hz. The frequency spacing can correspond to integer or odd multiples of the lowest frequency depending on the signal's symmetry.

An example of a chaotic response in an actual power system ferroresonant circuit has never been reported in the literature. Simulations at unrealistically high source voltages [A136], [A125] have been able to force chaotic responses. To this author's knowledge, Mork *et al.* [A102] were the first to excite a chaotic response in a laboratory setup. In their experiment, a 5-legged core, 12.5 kV distribution transformer was found to exhibit chaotic and periodic responses if energized from one or two phases. The resulting response depended greatly on the value of capacitance connected to the unenergized phases. Walling *et al.* [A101] also has demonstrated chaotic type responses in similar experiments.

However, the analysis of their system is more complicated because a nonlinear metal oxide varistor appears to be influencing the final state.

There are many useful introductory texts describing chaotic vibrations and methods of quantifying chaos. Two very readable texts by Moon [10] and Hilborn [9] are recommended.

When discussing chaotic attractors, the concept of fractal dimension has been used to characterize the attractor. There are many definitions of a fractal and many types of fractal dimension measures. A comprehensive discussion of all such concepts is beyond the scope of this thesis and the author refers the reader to [9] and [10] for a detailed introduction.

Using fractal dimension to compare simulations with laboratory work has been shown to be questionable by Mork [11]. Moon [10] also questions the practical use of fractal dimension. He suggests using a combination of Poincaré sections, Fourier spectra, Lyaponov[6] exponents or fractal dimension measurement before pronouncing a system chaotic.

What is a fractal? A ***fractal*** is a subset of a set of points in an n-dimensional space having the properties of self-similarity and noninteger fractal dimension less than n. Geometrical figures are ***self-similar*** if the structure of the figure remains the same on different scales.

Before a definition of fractal dimension is given, one must first consider the topological or Euclidean dimension (D_E). For example, the topological dimension of natural objects can be envisaged. A point has dimension D_E=0, a line has D_E=1, a surface has D_E=2 and a volume has D_E=3. The simplest class of fractal dimension is one based on morphology. An example is the Hausdorf mesh or box counting dimension (D_{HM}). The box counting dimension is defined by (2-54).

$$D_{HM} = \lim_{r \to 0} \frac{\log(N_r)}{\log\left(\frac{1}{r}\right)} \tag{2-54}$$

The number of boxes containing a portion of the image is defined by the number N_r. The size of the square box is defined by the variable r. As the size of the measuring element approaches 0, the box counting dimension approaches a fixed value characterizing the

6. Alexander Michailowitsch Lyapunov (1857-1918)

complexity or morphology of the image. Values of D_{HM} between one and two are expected. A value of 1 would indicate a simple straight line (i.e. D_E=1) and a value of 2 would indicate a space filling curve. The ***fractal dimension***, in this case, indicates the extent to which the set of points fills a two dimensional space.

Practically, the box counting dimension cannot be calculated as described above. The resolution of the given image will dictate appropriate yardstick lengths. Too large or too small a yardstick will cause the resulting estimate of the box counting dimension to saturate [9].

If a state space attractor is suspected to be chaotic, normally a Poincaré section is taken to reduce the dimensionality by one (e.g. time dependence is removed). A particular fractal dimension measuring technique (i.e. such as box counting) is used to determine if the dimension of the Poincaré section is noninteger. In this case, the attractor is called a ***strange attractor***. However, further tests are required to determine if the system is truly chaotic. Some features of a chaotic system include:

- sensitivity to initial conditions
- spectrum of waveform is distributed due to random or aperiodic time behaviour

Lyapunov exponents measure quantitatively the divergence of nearby trajectories. A positive exponent indicates diverging trajectories while a negative exponent indicates converging trajectories. A bifurcation takes place when a Lyapunov exponent equals zero. Quivy/Kieny [A83] use Lyapunov exponents to determine when a bifurcation takes place as a parameter is varied. Mozaffari/Soudack [A109] calculate Lyapunov exponents in order to confirm an attractor is chaotic.

2.6.2 Nonlinear Frequency Response

Another way of visualizing the difference between linear resonance and ferroresonance is to plot the nonlinear frequency response. The nonlinear frequency response (i.e. curve *f* in Fig. 2.15) was calculated using (2-19).

Also shown in Fig. 2.15 are two subharmonic ferroresonant states: a flux linkage wave oscillating with one-third the source frequency (*f*/3) calculated using (3-32) and a flux linkage wave with one-half the source frequency (*f*/2) calculated by solving (3-20)-(3-22).

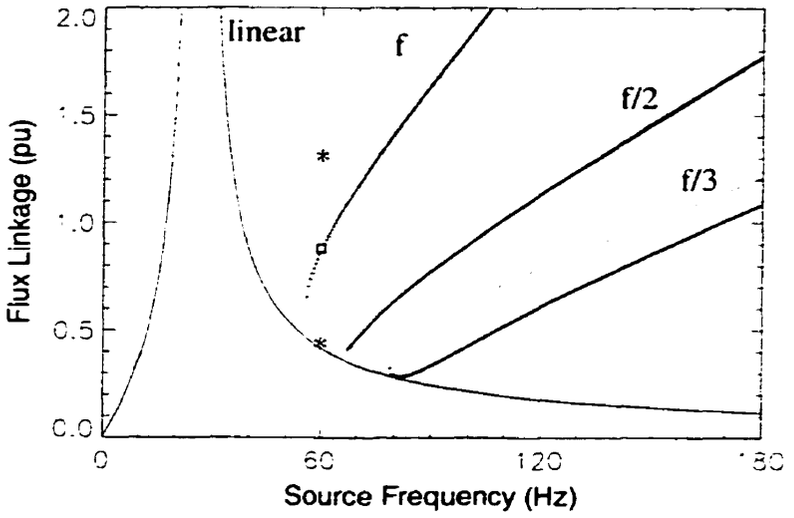

Fig. 2.15 Nonlinear frequency response of the circuit given in Fig. 2.6 with circuit parameters: C_g=5080 pF, C_b=10450 pF, V_s=1.04 pu, R=4.76e7 Ω.

If the nonlinear fundamental frequency response is compared with the overlaid linear frequency response, calculated using (2-55), a noticeable bending to the right is observed.

$$|\lambda| = \frac{E}{\sqrt{\left[\left(\frac{1}{RC}\right)^2 + \left(\omega - \frac{1}{\omega LC}\right)^2\right]}} \tag{2-55}$$

The effect of this bending is the generation of multiple operating points at 60 Hz, for example. Such a characteristic is typical of a *hard spring*, where the coefficient of the nonlinear restoring force (b in (2-43)) is positive [15].

This *bending* has been predicted by Wrate *et al.* [6]-[7] using so-called nonlinear frequency scans. The authors model a current source with a time-dependent frequency. The frequency of the source is slowly ramped near resonance points to determine the effects of nonlinearities. The authors have discovered that the frequency shift is dependent on the magnitude of current injection and on the direction of the frequency ramp. The response of the system to an increasing frequency is different from the response to a decreasing frequency. Drawbacks of the method include long simulation times and uncertainty in how to use the information.

Wrate's method was modified in order to calculate a brute-force nonlinear frequency response and compare it with the analytically calculated one. A voltage source with time-varying frequency was setup in the same way as a frequency modulated signal. In this

case, the derivative of the angle varies linearly with the modulating signal, $x(t)$, as shown by (2-56).

$$\frac{d\theta(t)}{dt} = 2\pi(f_c + x(t)) = \omega_i(t) \tag{2-56}$$

An example of a linearly varying wave is a triangle wave varying between 20 Hz and 200 Hz with a period of 20 seconds. The carrier frequency (f_c) is equal to the average of the minimum and maximum frequencies or 110 Hz.

The voltage source shown in Fig. 2.6, which has constant frequency, is replaced by one with a time varying frequency by using the integral of (2-56). A revised differential equation, given by (2-57), results.

$$\ddot{\lambda} + k\dot{\lambda} + C_1\lambda + C_3\lambda^3 = \frac{\omega_b\omega_i(t)V_m}{V_b}\cos(\theta(t)) \tag{2-57}$$

If the flux linkage ($\lambda(t)$) and instantaneous frequency ($\omega_i(t)$) waveforms are sampled at a constant phase angle (i.e. $\theta(t)$=0.0), a brute-force nonlinear frequency scan can be plotted. The results for a particular set of parameters is given in Fig. 2.16b. Bifurcations at 110 Hz for increasing frequency and 45 Hz for decreasing frequency are clearly seen. The Poincaré sampled response also shows variation in the relative phase of the flux linkage waveform while the calculated steady-state response only represents the magnitude.

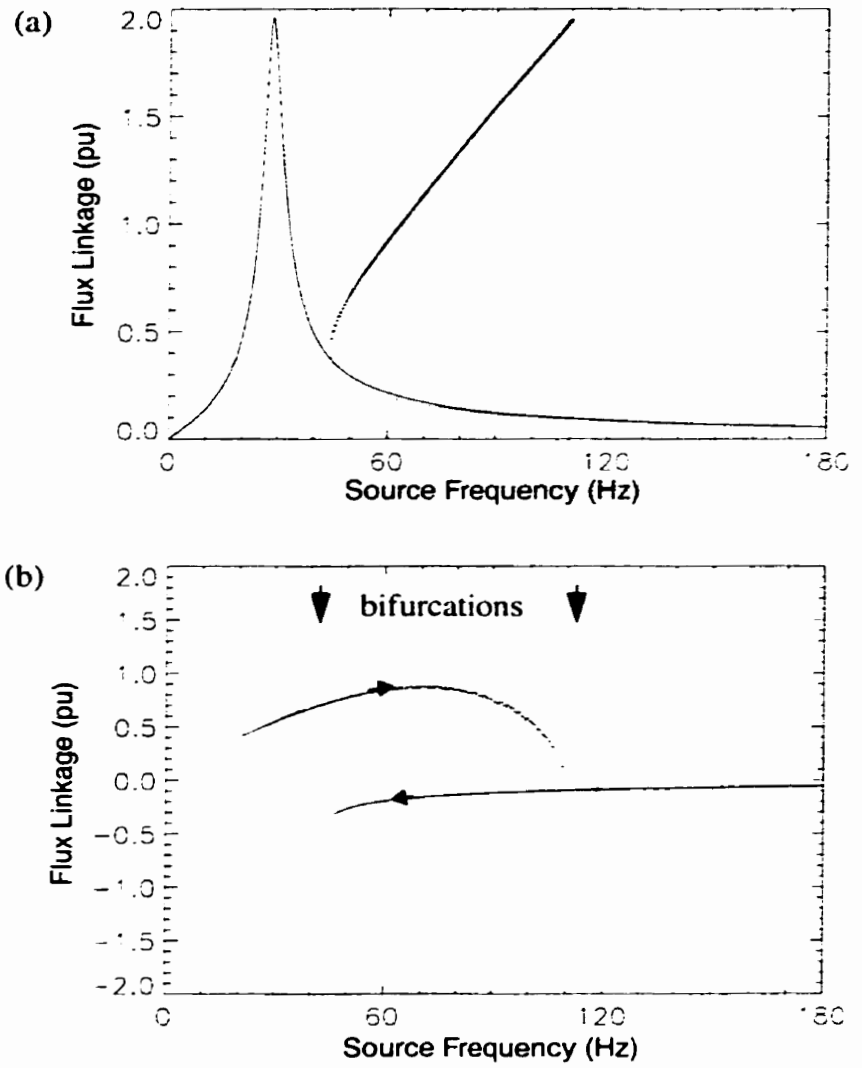

Fig. 2.16 Nonlinear frequency response comparison, (a) linear vs. nonlinear scans, (b) Poincaré sampled flux linkage wave with parameters: C_g=2000 pF, C_b=10450 pF, V_s=1.04 pu, R=.25e7 Ω. Initial conditions at 20 Hz were a=.389604 and b=.0807575.

2.6.3 Bifurcations and Basin of Attraction Concepts

A ***bifurcation*** is the abrupt change in the qualitative nature of the system's final operating state as a system parameter is quasi-statically varied. A ***bifurcation diagram***[7] records the locations of all bifurcation points over a range of parameter values. Two main techniques exist for the calculation of a bifurcation diagram. One is based on the principle of continuation and the other is based on experimentation or time-domain simulation and is

7. A practical example of a brute-force bifurcation diagram for a wound potential transformer is given in Section 4.7.

sometimes referred to as a brute-force bifurcation diagram [17].

Several continuation methods are described by Seidel [13]. The pseudo arclength continuation method has been used by several researchers of ferroresonance [A90], [A96], [A128]. One author has pointed out that existing continuation software such as AUTO can only examine single valued saturation curves [A134]. The continuation method begins from a known solution and traces solutions as a parameter is varied.

Bifurcation diagrams have been generated using commercial simulation packages such as EMTDC [A125] or EMTP [A102]. Poincaré samples are taken as a parameter is slowly varied. The circuit is simulated using a time-domain method. An attempt to mirror the continuation technique is made.

Experimental bifurcation diagrams have been presented by Deane [A103]. His experiments and simulations show hysteretic behavior as parameters are slowly varied (i.e. increasing parameters behave differently from decreasing parameters).

An example of a bifurcation diagram can be found analytically by solving (2-19) as a bifurcation parameter (e.g. source voltage) is varied. Fig. 2.17 illustrates a typical bifurcation diagram for an assumed fundamental frequency solution.

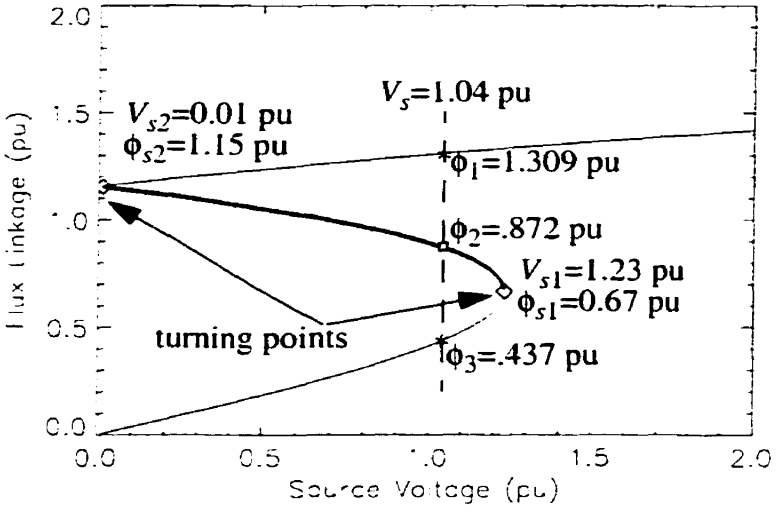

Fig. 2.17 Bifurcation diagram of ferroresonant circuit with parameters: C_g=5080 pF, C_b=10450 pF, V_s=1.04 pu.

The turning points or bifurcation points can be determined by several methods. Since we have an equation that relates source voltage to flux linkage, (2-58) can be used to identify

turning points.

$$\frac{dG^2}{dr^2} = 3\left(\frac{3C_3}{4}\right)^2 (r^2)^2 - 4(\omega^2 - C_1)\left(\frac{3C_3}{4}\right) r^2 + k^2\omega^2 + (\omega^2 - C_1)^2 = 0 \qquad (2\text{-}58)$$

The two solutions for r^2 are substituted back into (2-19) in order for G^2 to be calculated. The coordinates of the turning points calculated using this method are shown in Fig. 2.17. The critical values of flux linkage are in agreement with the numbers calculated using the dual input describing function method.

As the bifurcation parameter is slowly increased, a jump in flux linkage occurs at the first turning point. Similarly, as the bifurcation parameter is slowly decreased from a high value, a jump decrease in flux linkage occurs at the second turning point. The result is a hysteretic type pattern. The type of bifurcation just illustrated is referred to as a ***jump resonance*** [A28] or a ***cyclic fold*** or ***saddle-node*** bifurcation [16]. At the turning point, one eigenvalue is attempting movement into the right-half of the complex plane. The determinant of the Jacobian (2-53) is zero at the bifurcation point.

Two other types of local bifurcations exist for cycles. ***Period doubling*** (***flip***, ***pitchfork*** or ***subharmonic***) bifurcations refer to the emergence of a periodic orbit of period twice as long as the period of the original and has been shown to be a route to chaos [4]. A ***Hopf***[8] ***bifurcation*** refers to the emergence of a limit cycle from a fixed point and results when two eigenvalues attempt to enter the right-half plane. Quasi-periodic oscillations result from a Hopf bifurcation.

The bifurcations are sometimes further classified as being catastrophic or subtle. A ***catastrophic*** (or ***subcritical***) bifurcation occurs when the fixed point suddenly appears, disappears or jumps discontinuously to a new location. The cyclic fold bifurcation is catastrophic. A ***subtle*** (or ***supercritical***) bifurcation occurs when the fixed point changes smoothly as a parameter is varied.

Explaining the theory of bifurcations in detail is beyond the scope of this thesis. The interested reader is referred to texts by Thompson and Stewart [12], and Guckenheimer and Holmes [16].

The turning points shown in Fig. 2.17 can be calculated as a function of two parameters

---

8. In 1942, mathematician E. Hopf, extended the two-dimensional work of Poincaré and Russian mathematician Andonov to higher dimensional state spaces.

(e.g. grading capacitance and source voltage). A projection of the lower turning point on the grading capacitance-source voltage parameter plane is shown in Fig. 2.18. The curve indicates the parameter values required to achieve a spontaneous jump to a ferroresonant condition. An ***exchange of stability*** occurs at the bifurcation points being projected on the C_g-V_s parameter plane. Instead of bifurcation points, the diagram now shows ***bifurcation lines***. The region to the right of the curve indicates the ***stability domain*** of the period-1 mode of ferroresonance. The bifurcation line, therefore, is also referred to as a period-1 ***stability domain boundary***.

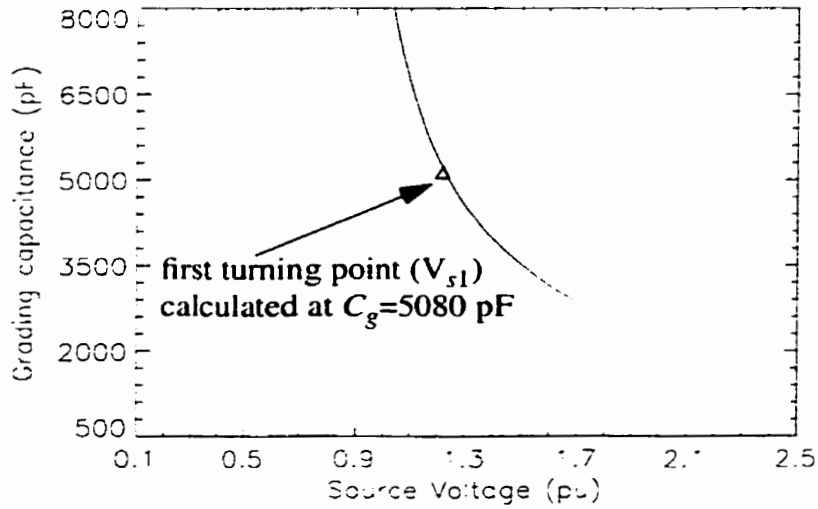

Fig. 2.18 Projection of fold on the C_g-V_s plane with stray capacitance fixed at 10450 pF.

The ***basin of attraction*** is the set of initial conditions leading to a particular attractor. Given a particular set of system parameters, a pair of initial conditions can be chosen on the two-dimensional phase plane and the final trajectory calculated. At the coordinates of the initial conditions chosen, a symbol representing the final attractor is placed. Mozaffari/ Soudack show examples of basins of attraction for unbalanced energizing of an unloaded transformer [A136].

The van der Pol diagram shown in Fig. 2.12 is meant to graphically indicate the stability of fixed points; however, it can also be used to illustrate the concept of a basin of attraction. For the set of parameters chosen, there are two stable spiral attractors indicated by asterisks. Two regions or basins of initial conditions exist in Fig. 2.12 such that the trajectories will converge onto a specific attractor. The curve separating the two basins is called the ***separatrix***.

The separatrix may be sketched from the velocity field, or it may be computed by time-

domain simulation of (2-50) and (2-51) for decreasing time. If the simulation approach is used, the system states must be initialized to correspond to the unstable fixed point plus a small deviation along the stable eigenvector associated with this point [17]. The slope through the stable (η_s) and unstable eigenvectors (η_u) is calculated using the values given in Table 2.1. The separatrix is also known as the ***stable manifold***. In Fig. 2.19, the stable manifold is comprised of the union of the two stable half manifolds (i.e. W^{s+} and W^{s-}).

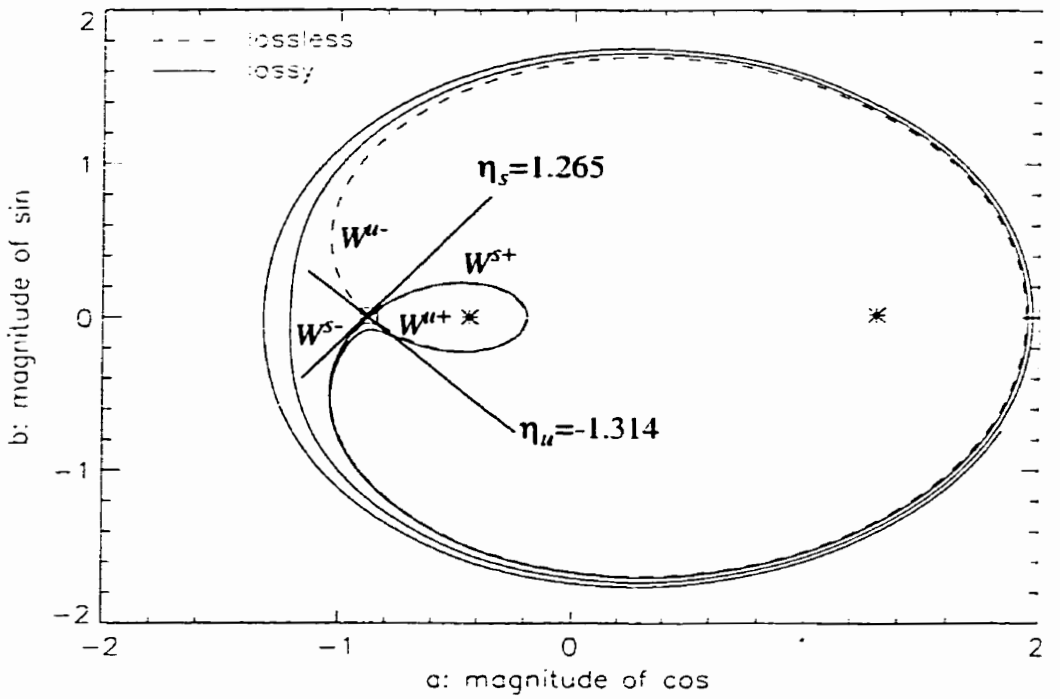

Fig. 2.19 Basin of attraction of fundamental frequency attractors derived from reverse time equations.

Guckenheimer and Holmes further classifies the separatrix in the lossless case as a double saddle loop and as a ***homoclinic orbit*** since the orbit connects the saddle point to itself. When losses are included, the unstable half manifolds approach the stable fixed points in both forward and reverse time.

The next chapter will investigate the influence of subharmonics on the basins of attraction and determine a method for displaying margins to ferroresonance on a two-dimension parameter plane.

2.7 SUMMARY

An overview of the most prevalent techniques of ferroresonance analysis have been given in this chapter. The treatment of each topic was brief in order that the main ideas would not be overshadowed by details. This chapter has provided the opportunity to define terminology, which is becoming relevant in the study of ferroresonance.

2.8 REFERENCES

[1] Martinez-Velasco, J.A.,"Computational Methods for EMTP Steady-State Initialization", *International Conference on Power System Transients, IPST'99*, Budapest, Hungary, pp. 69-74, June 20-24, 1999.

[2] Chua, L.O., Desoer, C.A., Kuh, E.S.,*Linear and Nonlinear Circuits*, New York:McGraw Hill,1987.

[3] Dommel, H.W.,"EMTP Reference Manual: EMTP Theory Book", Sec.6.6.3, August 1986.

[4] Lee, B., and Ajjarapu, V.,"Period-Doubling Route to Chaos in an Electrical Power System", *IEE Proceedings-C*, Vol. 140, No. 6, November 1993.

[5] Dugan, R.C., McGranaghan, M.F., and Beaty, H.W.,"*Electrical Power System Quality*, McGraw Hill: New York,1996.

[6] Wrate, G.T., Mork, B.A., Mustaphi, K.K., and Dellwo, S.P.,"Using the Electromagnetic Transient Program for Frequency Scans", *Proceedings of the 1994 Minnesota Power Conference*, Minneapolis, MN., pp. 65-76, October 1994.

[7] Wrate, G.T., Mork, B.A., and Mustaphi, K.K.,"A New Method to Determine Frequency Characteristics of a Power System Including Nonlinear Effects", *IPST '97*, pp. 11-16, June 1997.

[8] West, J.C., Douce, J.L., and Livesley, R.K.,"The Dual-Input Describing Function and its use in the Analysis of Nonlinear Feedback Systems", *Proc. IEE*, Vol. 103B, pp.463-473, 1956.

[9] Hilborn, R. C., *Chaos and Nonlinear Dynamics: An Introduction for Scientists and Engineers*, Oxford University Press: New York, 1994.

[10] Moon, F. C., *Chaotic Vibrations: An Introduction for Applied Scientists and Engineers*, John Wiley & Sons: New York, 1987.

[11] Mork, B. A., *Ferroresonance and Chaos - Observation and Simulation of Ferroresonance in a Five-Legged Core Distribution Transformer*, Ph.D. Thesis, North Dakota State University, May 1992.

[12] Thompson, J.M.T., and Stewart, H.B., *Nonlinear Dynamics and Chaos*, Wiley:

New York, 1986.

[13] Seydel, R., *From Equilibrium to Chaos: Practical Bifurcation and Stability Analysis*, Elsevier: New York, 1988.

[14] Minorsky, N., *Nonlinear Oscillations*, Van Nostran: New York, 1962.

[15] Jordan, D.W., and Smith, P., *Nonlinear Ordinary Differential Equations: Second Edition*, Oxford Press: New York, 1987.

[16] Guckenheimer, J., and Holmes, P., *Nonlinear Oscillations, Dynamical Systems, and Bifurcations of Vector Fields*, 3rd ed., Springer-Verlag: New York, 1990.

[17] Parker, T.S., and Chua, L.O., *Practical Numerical Algorithms for Chaotic Systems*, Springer-Verlag: New York, 1989.

[18] Grimshaw, R., *Nonlinear Ordinary Differential Equations*, Blackwell Scientific: Oxford, 1990.

Chapter 3

Stability Domain Boundaries

3.1 INTRODUCTION

The most important question that can be asked about a ferroresonant circuit is:

> *Given an operating point in a parameter space, what margin exists between the operating point and the nearest ferroresonant state?*

Mapping regions of existence of all possible types of steady-state oscillations has traditionally been done by two quasi-static or slowly-varying techniques. Hayashi [A19] extends the method of averaging to calculate stability domain boundaries on a two-dimensional parameter plane. Janssens *et al.* [A79] derives a set of frequency domain equations using the Galerkin-method of harmonic balance from which the stability domain boundaries can be calculated.

The future of displaying margins to ferroresonance lies in coupling the basin of attraction with the quasi-static boundary. The basin of attraction can be used to improve upon the prediction of ferroresonance as simply a jump phenomenon, since it accounts for the initial conditions. Premature transition into a ferroresonance state can result depending on the particular initial conditions. The method of averaging, because it considers oscillations in the transient state, will be extended to demonstrate the influence initial conditions have on the period-1 stability domain boundary.

A slight modification will be made to the assumed transformer losses in this chapter. The simplified model given in Fig. 2.6, used to derive the equations in the foregoing analysis, assumed negligible series winding resistance and included the iron-core losses of two parallel wound potential transformers. This assumption makes the convergence of the full nonlinear differential equation slow. By decreasing the core loss resistance to 11.9 MΩ, faster convergence is achieved without sacrificing accuracy. The losses are higher than a potential transformer but lower than a 10 MVA station service transformer.

3.2 INITIAL CONDITION MAPPING

Depending on the particular ferroresonant circuit, the initial conditions may not realistically cover the entire phase plane. For example, for the case where a wound potential transformer is being de-energized, the initial conditions are prescribed at the instant the circuit breaker opens. Therefore, only two initial conditions are possible in a single-phase model assuming the breaker opens exactly at a current zero.

Assuming the stray capacitance dominates the impedance of the three parallel elements, the flux linkage will be zero and the rate-of-change of flux linkage will be maximum and equal to the source voltage (V_s) at the instant the circuit breaker opens. The instantaneous initial conditions, however, are not mapped onto the van der Pol plane.

A Poincaré sampled $d\lambda/dt$ vs. λ plane can be thought of as a subset of the van der Pol plane. An example is given in Fig. 3.1. The flux linkage and $d\lambda/dt$ waveforms are synchronously sampled once each period of the forcing function (i.e. $\sin(\omega t)$). The sampled points can be laid on top of the van der Pol diagram given in Fig. 2.12 and an improved trajectory (i.e. compared with straight line segments) sketched using the velocity field lines.

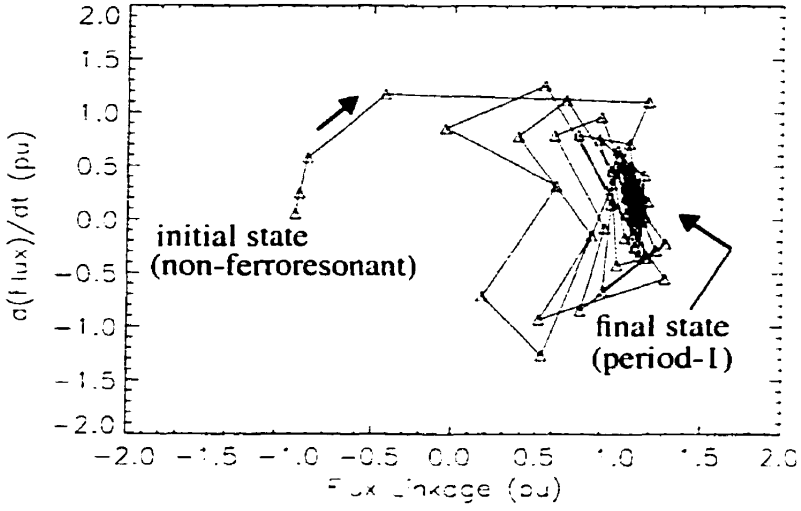

Fig. 3.1 Poincaré sampled trajectory of the transition to a period-1 attractor using the parameters: C_g: 2000 pF and V_s: 0.90 pu.

By selecting sampling to occur at ωt=0, the $d\lambda/dt$ term in the initial state is zero and the final state corresponds to the fixed point calculated by the harmonic balance method. For the case of a wound potential transformer being de-energized, the initial flux linkage in the nonlinear inductor at the time of the first Poincaré sample is equal to the integral of the

source voltage (i.e. $-V_s/\omega$ or $-V_s/V_b$ in pu). Referring to Fig. 3.2a, this initial condition lies on the a-axis near the separatrix. An increase in source voltage magnitude will cause a leftward shift of the initial condition, resulting in the period-1 attractor while a small decrease in voltage will result in the nonferroresonant state.

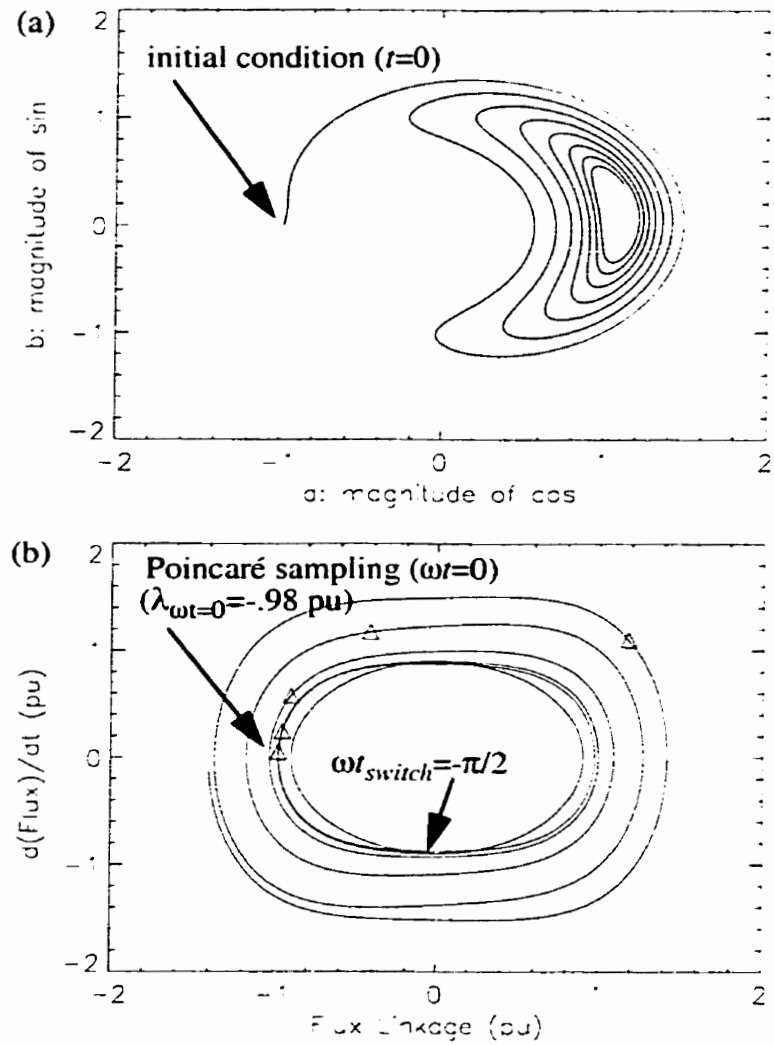

Fig. 3.2 Initial condition mapping comparison of (a) averaged equations in the van der Pol plane with parameters: C_g: 2000 pF, V_s: 0.98 pu and (b) complete nonlinear equation in the phase plane with parameters: C_g: 2000 pF, V_s: 0.90 pu.

Alternatively, the mapping can be calculated analytically by realizing the period-1 solution assumed by the averaging method in (2-49) forces the following relation between the phase plane limit cycles and the fixed points (a,b) in the van der Pol plane:

$$\begin{bmatrix} \lambda(t) \\ \dot{\lambda}(t) \end{bmatrix} = \begin{bmatrix} \cos(\omega t) & \sin(\omega t) \\ -\omega\sin(\omega t) & \omega\cos(\omega t) \end{bmatrix} \begin{bmatrix} a \\ b \end{bmatrix}. \tag{3-1}$$

The limit cycle will map to a fixed point in the van der Pol plane via the following relation:

$$\begin{bmatrix} a \\ b \end{bmatrix} = \frac{1}{\omega} \begin{bmatrix} \omega\cos(\omega t) & -\sin(\omega t) \\ \omega\sin(\omega t) & \cos(\omega t) \end{bmatrix} \begin{bmatrix} \lambda(t) \\ \dot{\lambda}(t) \end{bmatrix}. \tag{3-2}$$

Using the relation given by (3-2), the limit cycles shown in Fig. 3.2b are mapped to the *a*-*b* plane with the results displayed in Fig. 3.3a.

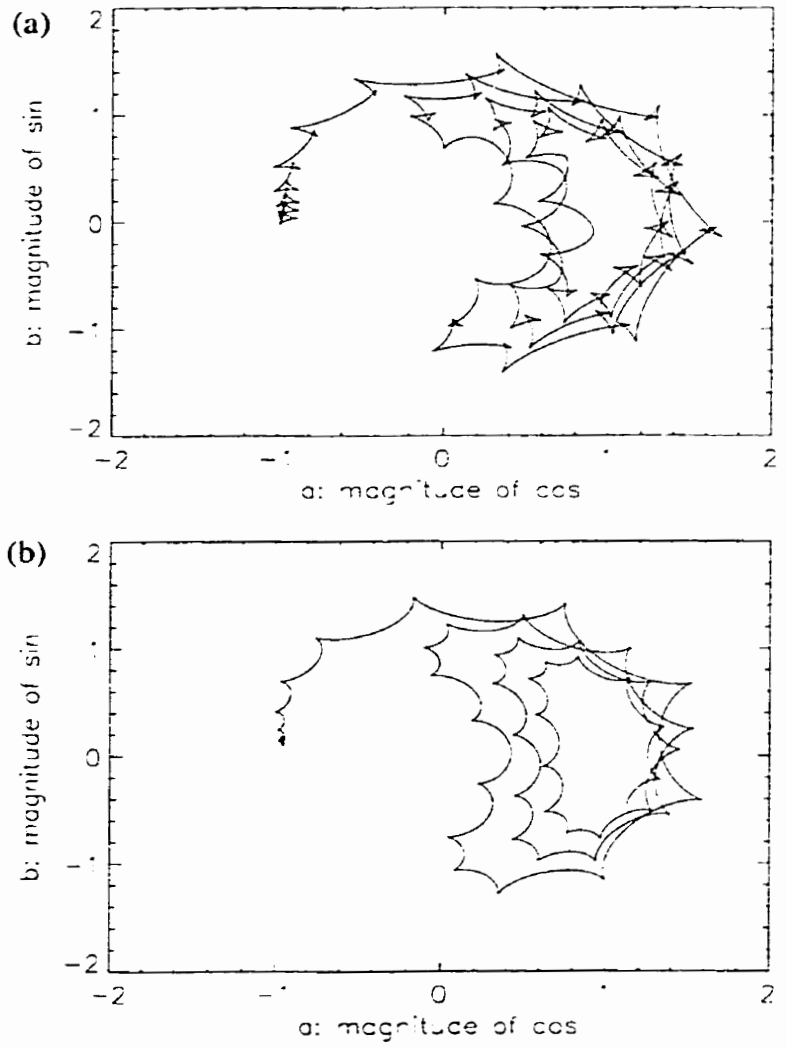

Fig. 3.3 Mapped trajectories in van der Pol plane using the parameters: C_g: 2000 pF, V_s: 0.98 pu, (a) with no filtering of transients, (b) using a sliding window FFT to extract the 60 Hz component.

The cusping in the trajectory can be smoothed by using a sliding window fast Fourier transformation (FFT) to extract the 60 Hz magnitude and phase from the instantaneous flux linkage and derivative of flux linkage components. The cusping is not totally removed because the FFT is a steady-state transformation and only provides approximate results during transients. The cusping in the unfiltered trajectory (i.e. Fig. 3.3a) is a feature of the actual system and is a result of higher order harmonics present in the flux linkage waveform.

The next section will describe an analytical approximation to the period-1 separatrix.

3.3 ANALYTICAL PERIOD-1 SEPARATRIX

The location of the separatrix is affected by variations in the source voltage as are the initial conditions. Consequently an iterative approach would be required to determine at what voltage level the initial conditions leave the basin of attraction of the nonferroresonant state. Each iteration would require simulation of the system equations.

To circumvent this complexity, a closed form solution is sought for describing the separatrix as some function of the system parameters. The analysis is simplified by assuming the system to be conservative (i.e. $k=0$ in (2-50) and (2-51)).

The separatrix has thus far been determined by reverse time integration from the saddle point. In the conservative case, however, its general shape likens that of the geometrical figure known as the Limacon of Pascal[1]. Fig. 3.4 compares the shape of the double saddle loop separatrix to the Limacon of Pascal.

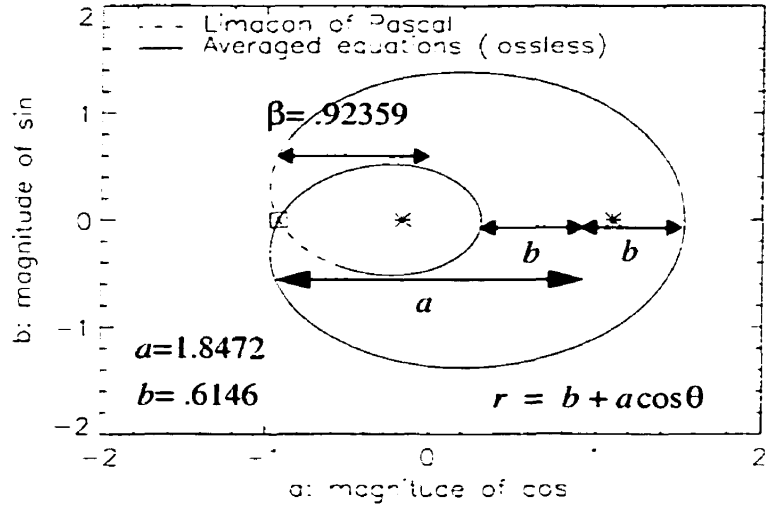

Fig. 3.4 Period-1 basin of attraction shape comparison between the lossless case calculated from the averaged set of equations using the parameters: C_g: 2000 pF, V_s: 0.924 pu and the Limacon of Pascal.

Standard mathematical tables lists the equation for the Limacon of Pascal in polar coordinates as:

$$r = b + a\cos\theta . \tag{3-3}$$

1. Étienne Pascal (1588-1651), the father of Blaise Pascal the famous mathematician, is credited as the discoverer of the curve known as the Limacon of Pascal. Limacon comes from the Latin word *limax* which means snail. Roberval, a French geometer, named the curve in 1650.

The double loop shape is guaranteed if a is greater than b.

Making the substitution, $x_1=r\cos(\theta)$ and $x_2=r\sin(\theta)$, in (3-3) results in the following two equations:

$$x_1 = \frac{a}{2} + b\cos(\theta) + \frac{a}{2}\cos(2\theta), \tag{3-4}$$

$$x_2 = b\sin(\theta) + \frac{a}{2}\sin(2\theta). \tag{3-5}$$

The shift required in x_1 for the two curves to match is $-a/2$.

This likeness to the Limacon of Pascal identifies the following class of functions as candidates for the solution of the separatrix. For convenience, the variable substitutions $\alpha=b$ and $\beta=a/2$ are made in (3-4) and (3-5).

$$a(\theta) = \alpha\cos\theta + \beta\cos 2\theta \tag{3-6}$$

$$b(\theta) = \alpha\sin\theta + \beta\sin 2\theta \tag{3-7}$$

These general functions are then substituted into the lossless reverse time differential equations, derived from (2-50) and (2-51). Solving for the constants α and β yields the following two equations:

$$\beta = \sqrt[3]{-\frac{2G}{3C_3} + \sqrt{\left(\frac{4(C_1-\omega^2)}{9C_3}\right)^3 + \left(\frac{2G}{3C_3}\right)^2}} + \sqrt[3]{-\frac{2G}{3C_3} - \sqrt{\left(\frac{4(C_1-\omega^2)}{9C_3}\right)^3 + \left(\frac{2G}{3C_3}\right)^2}}, \tag{3-8}$$

$$\alpha = \sqrt{\frac{8G}{3C_3\beta}}. \tag{3-9}$$

With the above values of α and β, (3-6) and (3-7) are used to plot the exact separatrix for the conservative system. Fig. 3.5 compares the exact lossless separatrix from theory with the separatrix for the dissipative system. It may be seen that the lossless separatrix yields a slightly conservative estimate for the basin of attraction of the nonferroresonant operating point. Also, shown in Fig. 3.5 is an improved estimate of the Limacon which considers the location of the saddle point in the lossy case.

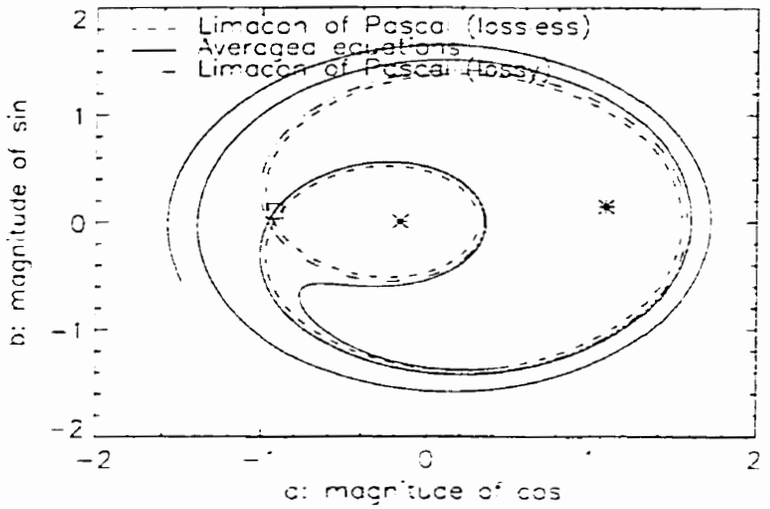

Fig. 3.5 Comparison of period-1 basin of attraction shape when losses are included using the parameters: C_s: 2000 pF, V_s: 0.924 pu.

The exact location of the separatrix for the lossy case can be calculated given the location of the saddle point (a_i,b_i) and the slope of the stable manifold (n_s) through the saddle point. Three equations in three unknowns (α, β, θ) are setup:

$$a_i = \alpha\cos\theta + \beta\cos 2\theta, \tag{3-10}$$

$$b_i = \alpha\sin\theta + \beta\sin 2\theta, \tag{3-11}$$

$$\frac{1}{n_s} = \frac{-\alpha\sin\theta - 2\beta\sin 2\theta}{\alpha\cos\theta + 2\beta\cos 2\theta}. \tag{3-12}$$

After some manipulations, an equation in θ can be derived.

$$0. = \left(\frac{2.a_i}{n_s} + b_i\right)\tan\theta^3 - \left(2.a_i + \frac{b_i}{n_s}\right)\tan\theta^2 + 3b_i\tan\theta + \frac{b_i}{n_s} \tag{3-13}$$

After solving (3-13) for θ, the new Limacon of Pascal constants can be calculated using,

$$\beta = -a_i + \frac{b_i}{\tan\theta}, \tag{3-14}$$

$$\alpha = \frac{a_i - \beta\cos 2\theta}{\cos\theta}. \tag{3-15}$$

The influence of subharmonics on the basins of attraction and stability domain boundaries will be discussed in the following section.

3.4 SUBHARMONIC OSCILLATIONS

The method of averaging will be used to derive crude basins of attraction for subharmonic oscillations in this section. Also, the equations necessary to determine the stability domain boundaries using the Newton Raphson method are derived. Existence of subharmonic fixed points tends to influence the shape of the period-1 basin of attraction. The accuracy of the double loop period-1 basin of attraction shape is compared with the exact basin of attraction, which considers the presence of multiple attractors.

3.4.1 Period-2 Ferroresonance

Hayashi [A19] assumed a period-2 subharmonic solution to the differential equation, given by (2-14), to be of the following form:

$$\lambda(t) = c + a(t)\cos\left(\frac{\omega t}{2}\right) + b(t)\sin\left(\frac{\omega t}{2}\right) + \zeta\cos(\omega t). \tag{3-16}$$

The approximation is valid if the nonlinearity is small or the sinusoidal flux linkage approximation is reasonable; however, Hayashi maintains that the approximation is valid even when the departure from linearity is large. The assumed form of the period-2 solution includes a constant dc offset term (c). Even with a symmetrical nonlinearity and symmetric source, it is possible to excite an asymmetric period-2 oscillation if the damping coefficient (k) is low enough.

The coefficient of the $\cos(\omega t)$ term can be calculated by rewriting (2-14) assuming the system is conservative and linear.

$$\ddot{\lambda} + \omega_1^2\lambda = K_c\omega^2\cos(\omega t) \tag{3-17}$$

By using the method of undetermined coefficients, the solution to the linear differential equation is found to be:

$$\lambda(t) = a\cos(\omega_1 t) + b\sin(\omega_1 t) + \frac{K_c\omega^2}{\omega_1^2 - \omega^2}\cos(\omega t). \tag{3-18}$$

The coefficient (ζ) is equated to the coefficient of the particular solution in(3-19). In addition, simplifications are made assuming a period-n solution (i.e. $\omega_1=\omega/n$) and by expanding the forcing term.

$$\zeta = \frac{K_c\omega^2}{\omega_1^2 - \omega^2} = \frac{G}{\left(\frac{\omega}{n}\right)^2 - \omega^2} = \frac{\omega_b}{\omega}\frac{V_m n^2}{V_b(1-n^2)} \tag{3-19}$$

The assumed solution given by (3-16) is substituted into the original nonlinear differential (2-14) and coefficients of sin and cos are equated. Second order derivatives of a and b, higher-order terms in cos and sin and terms *kda/dt* and *kdb/dt* are neglected.

After equating terms and solving for the first derivative of a and b, the following averaged equations result:

$$\dot{a} = \frac{1}{\omega}\left(bL - 3C_3bc\zeta - \frac{k\omega a}{2}\right) = A(a, b, c), \tag{3-20}$$

$$\dot{b} = \frac{-1}{\omega}\left(aL + 3C_3ac\zeta + \frac{k\omega b}{2}\right) = B(a, b, c), \tag{3-21}$$

$$0 = C_1c + C_3\left(c^3 + \frac{3c}{2}\cdot(a^2 + b^2 + \zeta^2) + \frac{3\zeta}{4}\cdot(a^2 - b^2)\right) = C(a, b, c), \tag{3-22}$$

where L is given by,

$$L = C_1 - \frac{\omega^2}{4} + \frac{3C_3}{4}(a^2 + b^2 + 4c^2 + 2\zeta^2). \tag{3-23}$$

The system of equations can be solved for the fixed points by combining (3-20) and (3-21) and solving two nonlinear simultaneous equations for r and c. An equation for the angle can be found using a similar technique as described in the next section for the period-3 solution. However, determining the correct phase becomes difficult. The technique chosen for calculating fixed points is to solve (3-20)-(3-22) simultaneously using a Newton-Raphson method. The actual algorithm used is a modified Powell hybrid algorithm, which is a variation of the Newton-Raphson method. The subroutine is available in several popular mathematical software packages such as IMSL, MINPACK and PV-WAVE.

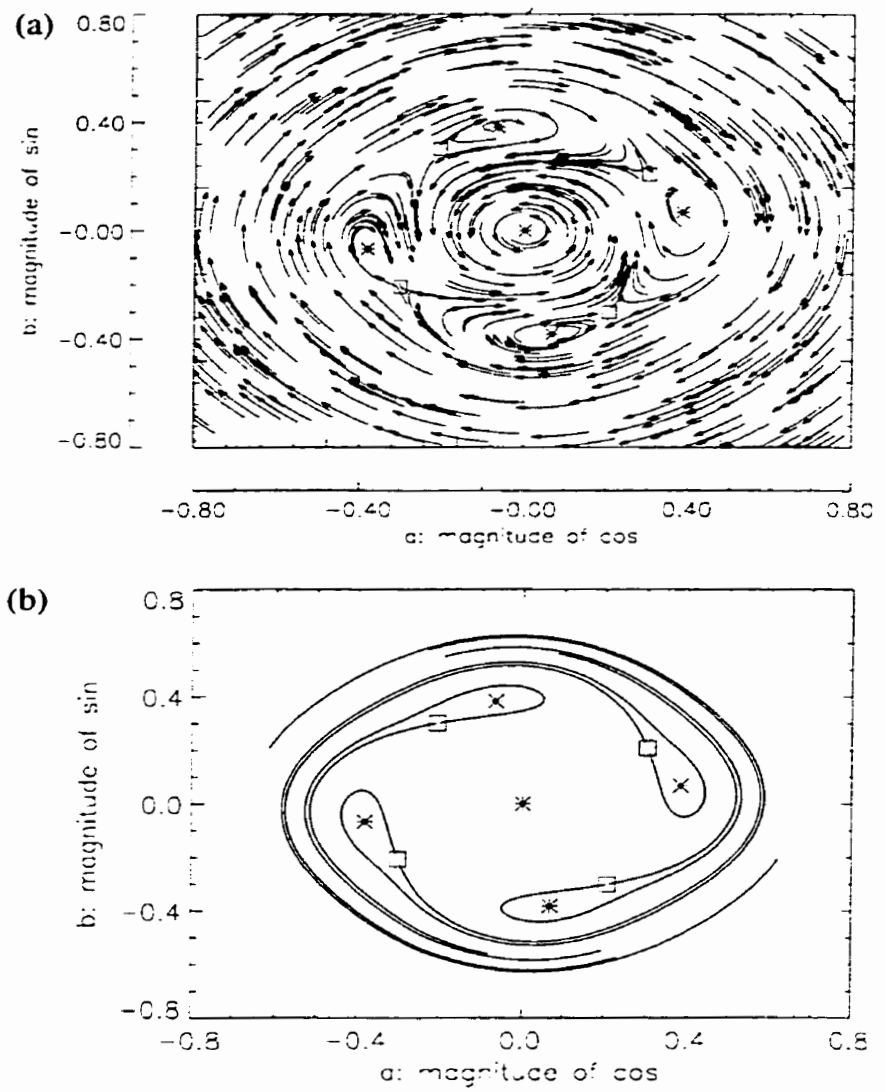

Fig. 3.6 Period-2 example of (a) van der Pol diagram and (b) separatrix calculated by reverse time integration of averaged equations using V_s=.55 pu, C_g=3000 pF, C_b=10450 pF, R=11.9 MΩ

The fixed points are summarized in Table 3.1. Also included are eigenvalues, slope through the saddle points and stability classification.

Table 3.1 Period-2 Fixed Point Summary using V_s=.55 pu, C_g=3000 pF, C_b=10450 pF.

Singular Point	a_i	b_i	c_i	eigenvalues	η_s,η_u	type
1	.301022	.206882	.017224	-36.6503, 0.00000 30.4025, 0.00000	-3.71845 -0.555351	saddle
2	-.206882	.301022	-.017224	-36.6503, 0.00000 30.4025, 0.00000	0.268929 1.80066	saddle
3	-.301022	-.206882	.017224	-36.6503, 0.00000 30.4025, 0.00000	-3.71845 -0.555351	saddle
4	.206882	-.301022	-.017224	-36.6503, 0.00000 30.4025, 0.00000	0.268929 1.80066	saddle
5	.382316	.0671704	.0471738	-3.12393, ±j35.6813		focus
6	.0671704	-.382316	-.0471738	-3.12393, ±j35.6813		focus
7	-.382316	-.0671704	.0471738	-3.12393, ±j35.6813		focus
8	-.0671704	.382316	-.0471738	-3.12393, ±j35.6813		focus
9	0.000000	0.000000	0.000000	-3.12393, ±j38.7682		focus

There are four possible stable period-2 solutions. The options for displaying the results on a one dimensional bifurcation diagram are varied. The most appropriate way is to calculate the modulus of the flux linkage, using (3-24), in order that the relative magnitudes of the different oscillations can be compared.

$$\|\lambda_i\| = \sqrt{c_i^2 + \sum(a^2{}_i + b_i^2) + \zeta^2} \tag{3-24}$$

The results are displayed in Fig. 3.7.

It should be noted that the period-2 solution is an **isola** or isolated set of fixed points. Specific initial conditions can excite a period-2 response, however, a slowly-varying source voltage will not produce a bifurcation to a period-2 state.

Fig. 3.8 shows a brute-force bifurcation diagram for a slowly ramped (i.e. 1.9 pu increase in 20 seconds, 50 μs time-step) source voltage. The bifurcation to period-1 is clearly seen, however, the period-2 solution is not excited. The absolute value of the Poincaré sampled flux linkage waveform is displayed in Fig. 3.8.

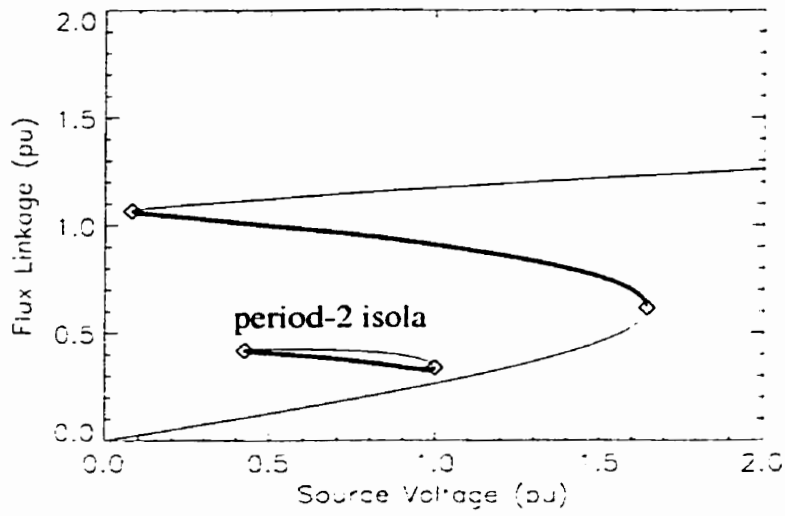

Fig. 3.7 Bifurcation diagram showing period-1 and period-2 amplitude characteristics using C_g=3000 pF and C_b=10450 pF.

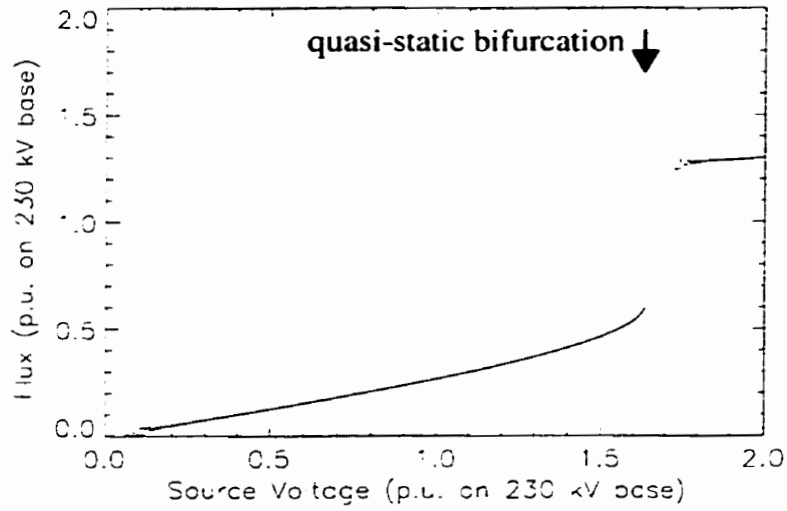

Fig. 3.8 Quasi-static bifurcation diagram created by simulating a source where the magnitude increases slowly and linearly using the parameters C_g=3000 pF and C_b=10450 pF.

Stability of the fixed points are determined by calculating eigenvalues of the Jacobian:

$$\begin{bmatrix} \frac{\partial A}{\partial a} & \frac{\partial A}{\partial b} & \frac{\partial A}{\partial c} \\ \frac{\partial B}{\partial a} & \frac{\partial B}{\partial b} & \frac{\partial B}{\partial c} \\ \frac{\partial C}{\partial a} & \frac{\partial C}{\partial b} & \frac{\partial C}{\partial c} \end{bmatrix}_{a_i b_i c_i} =$$

$$\begin{bmatrix} \frac{-1}{2}\left(k-\frac{3C_3}{\omega}(a_i b_i)\right) & \frac{1}{\omega}\left(E+3C_3\left(\frac{b_i^2}{2}-c_i\zeta\right)\right) & \frac{3C_3 b_i}{\omega}(2c_i-\zeta) \\ \frac{-1}{\omega}\left(E+3C_3\left(\frac{a_i^2}{2}+c_i\zeta\right)\right) & \frac{-1}{2}\left(k+\frac{3C_3}{\omega}(a_i b_i)\right) & \frac{-3C_3 a_i}{\omega}(2c_i+\zeta) \\ \frac{3C_3 a_i}{2}(2c_i+\zeta) & \frac{3C_3 b_i}{2}(2c_i-\zeta) & C_1+C_3\left(3c_i^2+\frac{3}{2}(\zeta^2+r_i^2)\right) \end{bmatrix} \quad (3\text{-}25)$$

The period-2 stability domain boundary is calculated by solving four nonlinear algebraic equations simultaneously (i.e. (3-20)-(3-22) and the determinant of the Jacobian (3-25) equals zero).

3.4.2 Period-3 Ferroresonance

Hayashi [A19] and Jordan [1] have assumed a period-3 subharmonic solution to the differential equation, given by (2-14), to be of the following form:

$$\lambda(t) = a(t)\cos\left(\frac{\omega t}{3}\right) + b(t)\sin\left(\frac{\omega t}{3}\right) + \zeta\cos(\omega t)\,. \quad (3\text{-}26)$$

The assumed solution given by (3-26) is substituted into the original nonlinear differential equation (2-14) and coefficients of sin and cos are equated. Second order derivatives of a and b, higher-order terms in cos and sin and terms kda/dt and kdb/dt are neglected.

After equating terms and solving for the first derivative of a and b, the following averaged equations result:

$$\dot{a} = \frac{3b}{2\omega}\left(C_1-\frac{\omega^2}{9}+\frac{3C_3}{4}(a^2+b^2+2\zeta^2-2a\zeta)\right)-\frac{ka}{2} = A(a,b)\,. \quad (3\text{-}27)$$

$$\dot{b} = \frac{3a}{2\omega}\left(\frac{\omega^2}{9} - C_1 - \frac{3C_3}{4}(a^2 + b^2 + 2\zeta^2 + a\zeta)\right) - \frac{kb}{2} + \frac{9C_3 b^2 \zeta}{8\omega} = B(a, b) \,. \quad (3\text{-}28)$$

The two equations can be plotted in the a-b phase plane showing the velocity field or the separatrix calculated by reverse time integration from the saddle points. The results are shown in Fig. 3.9.

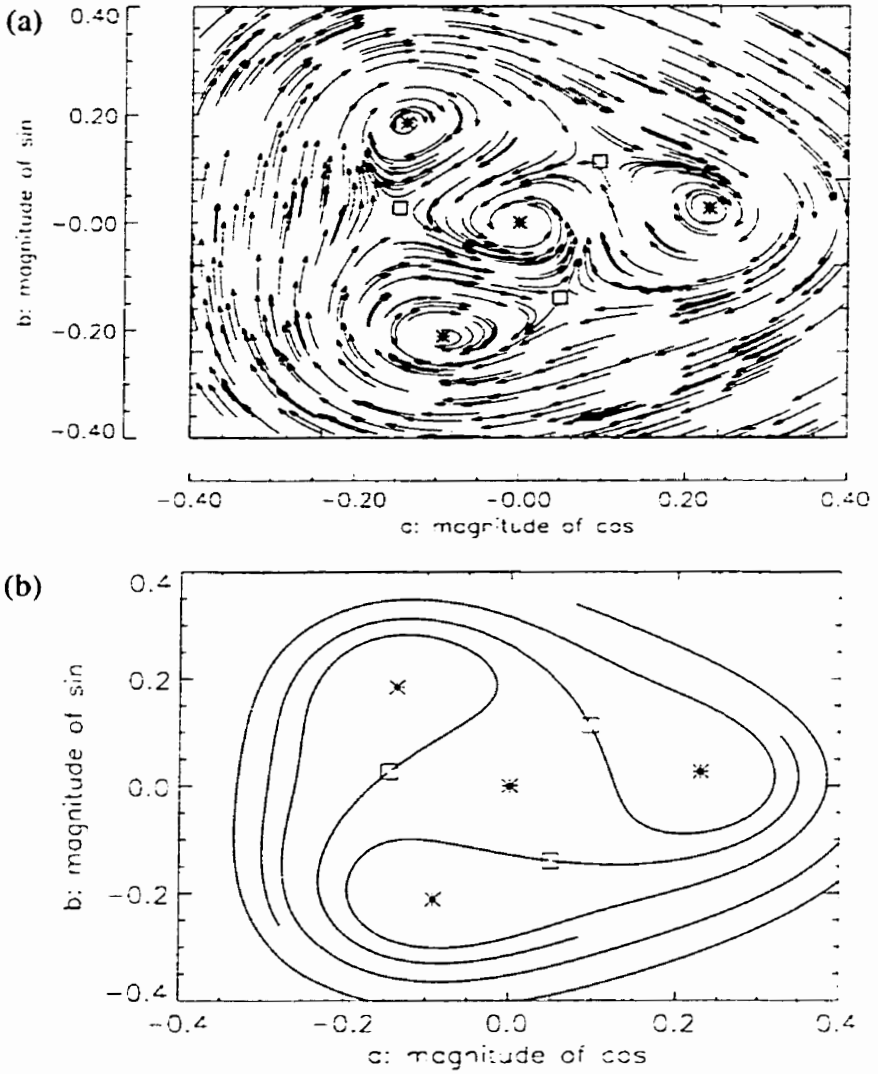

Fig. 3.9 Period-3 example of (a) van der Pol diagram and (b) separatrix calculated by reverse time integration of averaged equations using V_s=.2 pu, C_g=7000 pF, C_b=10450 pF.

Also plotted in Fig. 3.9, are the stable and unstable fixed points. In order to solve for the fixed points, the harmonic balance method may be used as described in Section 2.3 or the Newton-Raphson method can be applied to the averaged equations and solved where the

first derivatives are zero. The disadvantage of the Newton-Raphson method is reasonable initial guesses to the final solutions must be provided, otherwise convergence is not guaranteed.

Proceeding with the harmonic balance method, the following equations are derived:

$$aL - \frac{k\omega b}{3} = \frac{-3C_3\zeta(b^2 - a^2)}{4}, \tag{3-29}$$

$$-bL - \frac{k\omega a}{3} = \frac{3C_3\zeta(2ab)}{4}, \tag{3-30}$$

where L is given by,

$$L = \frac{\omega^2}{9} - C_1 - \frac{3C_3}{4}(a^2 + b^2 + 2\zeta^2). \tag{3-31}$$

In order to solve for $r^2=a^2+b^2$, square and add (3-29) and (3-30). The following quadratic amplitude relation results for r^2:

$$\frac{9}{16}C_3^2(r^2)^2 + \left[\frac{3}{2}C_3\left(C_1 - \frac{\omega^2}{9}\right) + \frac{27C_3^2\zeta^2}{16}\right]r^2 + \left(C_1 - \frac{\omega^2}{9} + \frac{3C_3\zeta^2}{2}\right)^2 + \left(\frac{k\omega}{3}\right)^2 = 0. \tag{3-32}$$

To complete the conversion to polar coordinates, the angle (θ) must be determined. The first step in solving for the angle is eliminating L from (3-29) and (3-30). To achieve this multiply (3-29) by b, multiply (3-30) by a and add the results. After substituting $a^2=r^2-b^2$ into the sum and simplifying, (3-33) results.

$$0 = b^3 - \frac{3br^2}{4} - \frac{k\omega r^2}{9C_3\zeta} \tag{3-33}$$

Into this equation, the polar coordinate conversion ($b=r\sin(\theta)$) is substituted, resulting in the following angle relation:

$$\sin(3\theta) = \frac{32k\omega C_1}{9C_3Gr}. \tag{3-34}$$

Similarly, if k is eliminated then a relation for $\cos(3\theta)$ can be developed.

$$\cos(3\theta) = \frac{4E}{3C_3\zeta r} \tag{3-35}$$

If the assumption is made that a solution exists in the first quadrant, only (3-35) gives the correct sign. The remaining solutions can be found by rotating by ±120 degrees.

A new bifurcation diagram is shown in Fig. 3.10 that overlays the amplitude relations for the period-3 (3-32) and period-2 subharmonics and period-1 harmonic (2-19).

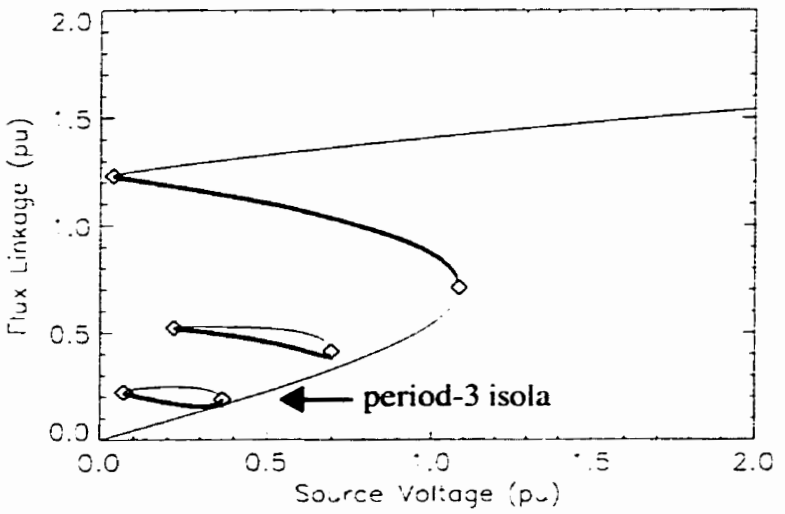

Fig. 3.10 Bifurcation diagram showing period-1, period-2 and period-3 amplitude characteristics using C_g=7000 pF, C_b=10450 pF.

Stability of the fixed points are determined by calculating eigenvalues of the Jacobian given by (3-36).

$$\begin{bmatrix} \frac{\partial A}{\partial a} & \frac{\partial A}{\partial b} \\ \frac{\partial B}{\partial a} & \frac{\partial B}{\partial b} \end{bmatrix}_{a,b,} = \tag{3-36}$$

$$\begin{bmatrix} \frac{9C_3}{4\omega}\cdot(a_i b_i - b_i\zeta) - \frac{k}{2} & \frac{3}{2\omega}\left(C_1 - \frac{\omega^2}{9}\right) + \frac{9C_3}{8\omega}\cdot(a_i^2 + 3b_i^2 + 2\zeta^2 - 2a_i\zeta) \\ \frac{-3}{2\omega}\left(C_1 - \frac{\omega^2}{9}\right) - \frac{9C_3}{8\omega}\cdot(b_i^2 + 3a_i^2 + 2\zeta^2 + 2a_i\zeta) & \frac{-9C_3}{4\omega}\cdot(a_i b_i - b_i\zeta) - \frac{k}{2} \end{bmatrix}$$

The limits of existence of the period-3 solution or period-3 stability domain boundary can be calculated using a Newton-Raphson technique. A set of three nonlinear algebraic equations in three unknowns (a, b, V_s) can be formed from (3-28), (3-27) and from equating the determinant of the Jacobian (3-36) to zero.

3.4.3 Influence of Subharmonics on P-1 Stability Domain Boundaries

Detailed basins of attraction can be calculated by simulating the complete nonlinear differential equation in reverse time [A19]. If the reverse time equations are initialized near the unstable saddle point along the stable eigenvector, the Poincaré map will trace out discrete values that lie on the stable manifold or separatrix. If the Poincaré map is iterated from a succession of initial values over a short section of the stable manifold near the saddle point, then the complete separatrix takes shape. An example of a detailed basin of attraction is shown in Fig. 3.11.

The period-1 saddle point is initialized at (a, b)=(-0.98125, 0.13245) with a slope along the stable eigenvector of 2.2392. From (3-1), the a and b coordinates calculated using the harmonic balance method are equivalent to the per-unitized $\lambda(0)$ and $d\lambda(0)/dt$ coordinates.

In order to use the previously calculated period-2 fixed points given in Table 3.1, the relation between the assumed solution for flux linkage and derivative of flux linkage must be examined.

$$\begin{bmatrix}\lambda(t)\\ \dot{\lambda}(t)\end{bmatrix} = \begin{bmatrix}\cos\left(\frac{\omega t}{2}\right) & \sin\left(\frac{\omega t}{2}\right)\\ -\frac{\omega}{2}\sin\left(\frac{\omega t}{2}\right) & \frac{\omega}{2}\cos\left(\frac{\omega t}{2}\right)\end{bmatrix}\begin{bmatrix}a\\ b\end{bmatrix} + \begin{bmatrix}1 & \cos(\omega t)\\ 0 & -\omega\sin(\omega t)\end{bmatrix}\begin{bmatrix}c\\ \zeta\end{bmatrix} \tag{3-37}$$

If the derivative of flux linkage is per-unitized by dividing by ω, the period-2 fixed points are then mapped to the state plane by (3-38).

$$\begin{bmatrix}\lambda(0)\\ \dot{\lambda}(0)\end{bmatrix} = \begin{bmatrix}a + c + \zeta\\ \frac{b}{2}\end{bmatrix} \tag{3-38}$$

The slope through the saddle point calculated in Table 3.1 is in reference to the projection on the a-b plane and can't be mapped to the state plane. Detailed calculations can be made to determine the slope, however, for the purpose of illustrating the method, the approximate slope in the state plane is one-fifth the slope listed in Table 3.1.

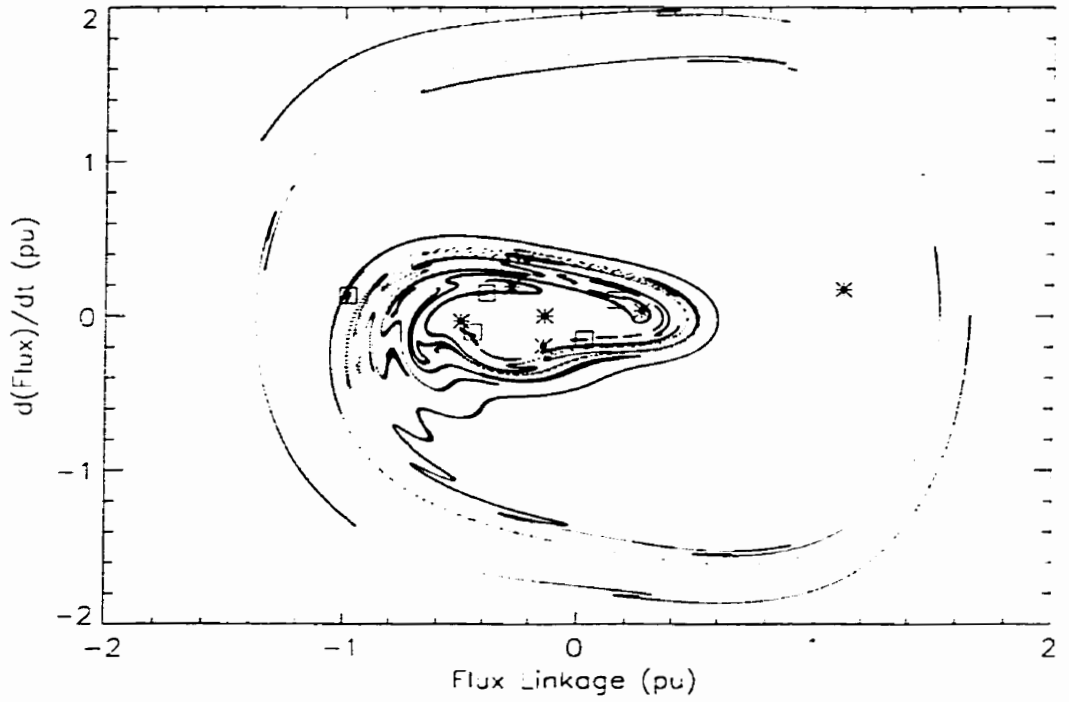

Fig. 3.11 Detailed basins of attraction for period-1 and period-2 attractors. (C_g: 3000 pF, C_b: 10450 pF, V_s: 0.55 pu).

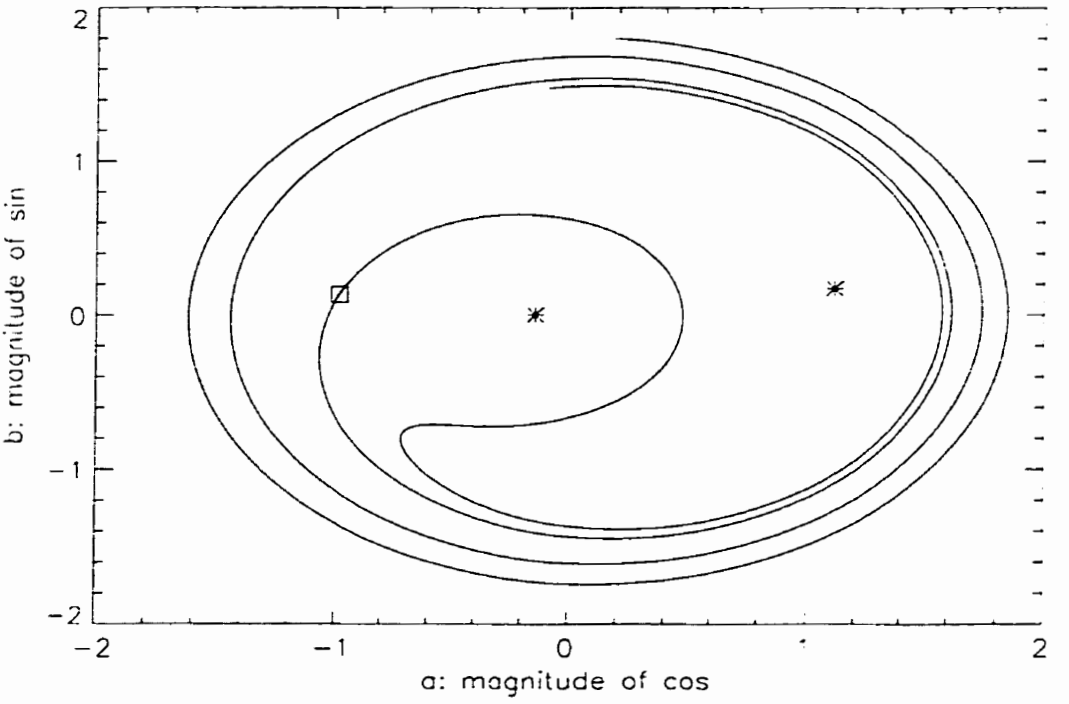

Fig. 3.12 Approximate basins of attraction for period-1 attractor using the parameters C_g: 3000 pF, C_b: 10450 pF, V_s: 0.55 pu.

When subharmonic attractors are considered, the basin boundaries become extremely complex as first demonstrated by Hayashi [A19]. Fig. 3.11 and Fig. 3.12 compare detailed basins of attractions with the period-1 approximation calculated using the method of averaging. The complexity of the subharmonic basins is apparent in Fig. 3.11 even with a limited set of mapped points.

The subharmonic basins of attraction are enclosed within the non-ferroresonant period-1 basin. There may be other attractors within the period-1 basin; however, they were not investigated.

For the chosen nonlinear differential equation under study in this chapter, the period-1 separatrix calculated using the method of averaging is a reasonable approximation to the detailed separatrix—especially, near the saddle point. The period-2 separatrix is very different from the calculated one shown previously in Fig. 3.6b. However, the stability domain boundary for the subharmonic attractor determined by the method of averaging defines the limits of existence reasonably accurately.

3.5 DISPLAYING MARGINS TO FERRORESONANCE

The best way of displaying margins to ferroresonance is by creating parameter plane maps or two-dimensional bifurcation diagrams. The relevant range of the system parameters under study can be placed on such a diagram. Using one of several methods, the probability of a particular oscillation occurring can be determined. Brute-force, Newton-Raphson and a new direct method, which considers the shape of the basin of attraction, will be discussed.

3.5.1 Brute-Force Method

The brute-force method consists of repeated time-domain simulations followed by frequency-domain analysis of the final steady-state to determine the attractor's periodicity. Fig. 3.13 is the result of 7260 individual 1.5 second time-domain simulations. Different shading is applied depending on the periodicity of the final state. Each simulation begins with a discrete set of system parameters and a short-circuited grading capacitor. A consistent set of initial conditions is applied by opening the circuit breaker at a current zero crossing.

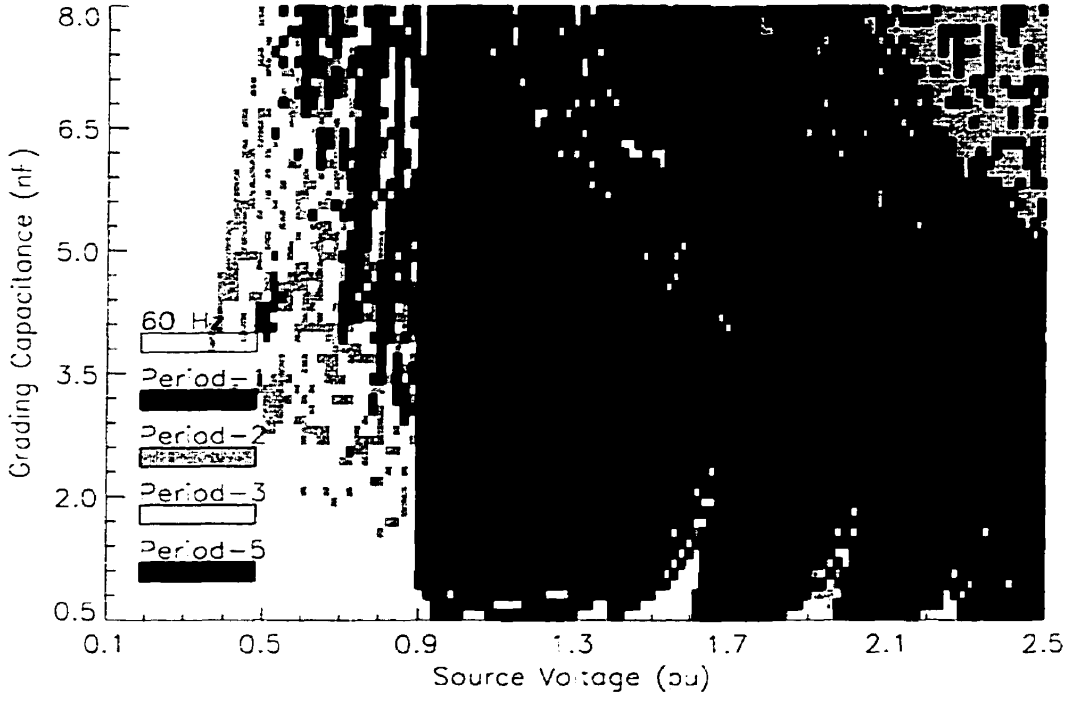

Fig. 3.13 Brute-force two-dimensional bifurcation diagram on the grading-capacitance/ source-voltage parameter plane with stray capacitance fixed at 10450 pF.

The brute-force method is accurate but suffers from a computational disadvantage because several thousand time-domain simulations are required before a sufficiently detailed parameter plane map is produced. The method may not find all of the possible responses, however, it will find isolated responses where a quasi-static technique cannot. One of the main tasks is to accurately define the parameters that result in a jump to period-1 ferroresonance.

For values of grading capacitance less than 2000 pF, the brute-force stability domain boundary shows the possibility of non-ferroresonant modes existing at source voltages higher than 0.9 pu. By examining Fig. 3.13, this behavior can be predicted from the reverse time integration of the dissipative system equations. The basin of attraction for the two fundamental frequency oscillation modes spiral out in the *a-b* phase plane. If the initial source voltage is high enough, there is a finite probability that the initial conditions will lie in either the non-ferroresonant or period-1 ferroresonant basin.

The purpose of this analysis is to create a screening tool that can be used to quickly evaluate a set of parameters for the possibility of period-1 ferroresonance being excited. As the source voltage is increased, only the first transition of the basin boundary should be considered. By ignoring subsequent transitions, a more cautious assessment of the system is achieved.

3.5.2 Newton-Raphson Method

The stability domain boundaries can be numerically calculated using the Newton-Raphson (NR) method. An example is displayed in Fig. 3.14. The stability boundary of each attractor is calculated first at a grading capacitance of 8000 pF as described in Section 3.4. The grading capacitance is then decreased slowly in small steps. New limits for each subharmonic are calculated using the previously calculated values as initial guesses for the NR method. The NR method is computationally superior to the brute-force method.

The NR approach analyzes each possible attractor separately and superposes the results on the same parameter plane in order to show the position of all stability domain boundaries. As pointed out by Hayashi [A19], this method suffers from a serious drawback in that it is inapplicable if a number of steady-state responses are expected for the same set of parameters. For example, at a grading capacitance of 6500 pF and 0.3 pu source voltage, both period-2 and period-3 responses are expected. The results from brute-force integration shows only the non-ferroresonant oscillation occurs at these parameters for the given set of initial conditions.

3.5.3 Limacon of Pascal Method

The Limacon of Pascal method attempts to combine the computational advantages of the Newton-Raphson method with the inclusion of initial condition information in order that the accuracy of the brute-force method is approached. As described in Section 3.3, two cases are considered: lossless and lossy separatrixes.

The initial conditions lie on the boundary between nonferroresonance and period-1 ferroresonance in the lossless case when,

$$\frac{-V_s}{V_b} = \alpha \cdot \cos\theta_1 + \beta \cdot \cos 2\theta_1 . \tag{3-39}$$

where α and β are functions of G, which is in turn a function of the system voltage and grading capacitance. The critical angle (θ_1) lies between zero and π and is calculated by finding the zero of (3-7). Equation 3-39 implicitly defines the critical system voltage at which period-1 ferroresonance first occurs, as a function of the system parameters. Solving for this critical system voltage as a function of the grading capacitance yields a modified stability boundary, as depicted in Fig. 3.14.

The above procedure outlines a technique that may be applied to the more general boundary crossing case. For the specific transition in question, the simple function $\beta(V_s,C_g)$-V_s=0.0 can be solved for V_s. The only valid solution is V_s=0.9236 pu for any value of C_g between 500 pF and 8000 pF.

Using (3-14) and 2000 pF of grading capacitance, the exact location of the separatrix where a crossover occurs is at V_s=0.96 pu as compared to 0.9236 pu, which was calculated assuming no losses. The improvement in estimate becomes more important as the losses increase. This estimate is close to the Poincaré sampled initial condition of 0.967 pu calculated in Section 3.2.

Using either the lossless or lossy separatrix calculation method, the calculated stability domain boundary is found to be nearly grading capacitance invariant within the range 500 pF to 8000 pF. This feature is also strongly evident in the brute-force diagram given in Fig. 3.13. For grading capacitance less than 2500 pF, the error between the brute-force boundary and the calculated boundary is attributed to the time difference between the switching instant in the state plane to the time when the first Poincaré sample is taken.

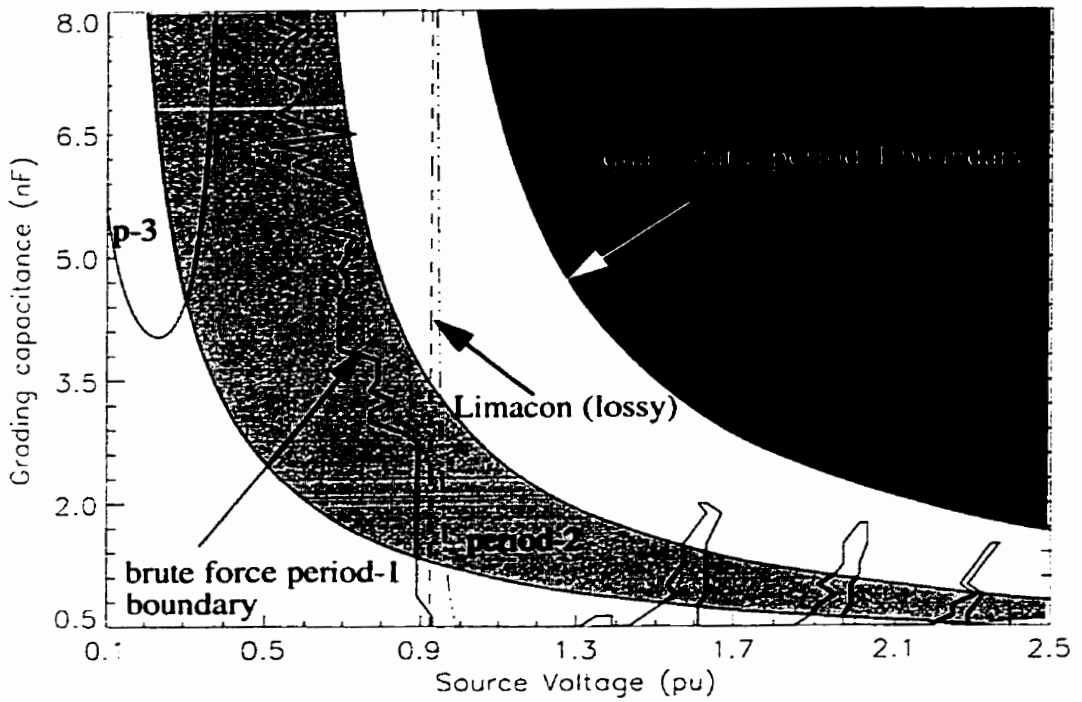

Fig. 3.14 Calculated stability domain boundaries on grading-capacitance/source-voltage parameter plane with stray capacitance fixed at 10450 pF.

As C_g increases, a period-2 ferroresonance mode develops as shown in Fig. 3.13. The presence of subharmonics tends to shift the brute-force period-1 boundary to the left. As shown in Fig. 3.15, the period-1 separatrix crosses the negative flux-linkage axis a number of times before the final predicted crossing near the saddle point.

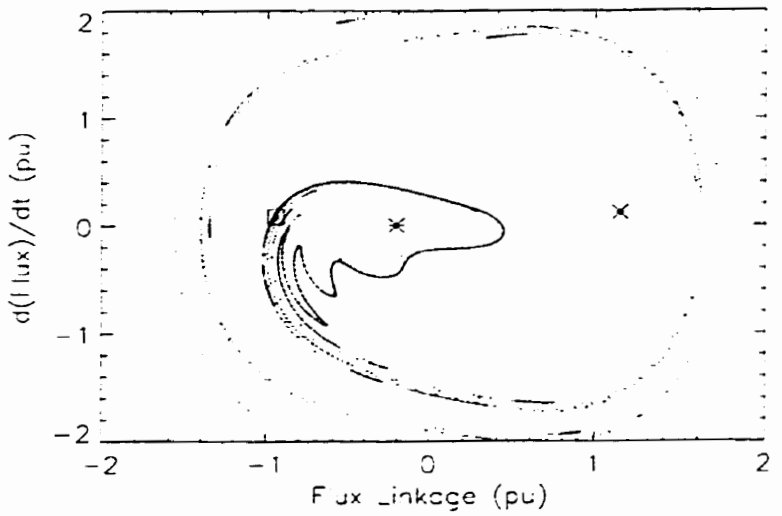

Fig. 3.15 Detailed basins of attraction for period-1 attractor using the parameters C_g: 3000 pF, C_b: 10450 pF, V_s: 0.80 pu.

These multiple crossings result in the premature transition to period-1 ferroresonance indicated in Fig. 3.14. The Limacon method cannot be adjusted to take into account the distortion in the period-1 basin of attraction, which occurs as a result of the location of the period-2 fixed points. Additional margin is required on the parameter plane in these areas to account for the uncertainty.

The region bounded by the axis and the union of the subharmonic boundaries and Limacon boundary gives a reasonable indication of a set of safe parameters. As the parameters approach the calculated boundary, more detailed simulations using the complete nonlinear differential equation must be used.

3.6 SUMMARY

A brute-force two-dimensional bifurcation diagram is an ideal tool for displaying margins between ferroresonant and non-ferroresonant states. However, an extensive number of long duration time-domain simulations are required in the calculation of such a diagram.

Direct calculation of the stability domains can be achieved quickly by using the Galerkin method of harmonic balance or by the method of averaging. The difference in the stability domain boundary calculated by the quasi-static (i.e. direct) and brute-force technique is attributed to the initial conditions at the time of the perturbation. Different final operating states are possible depending on which basin of attraction the initial conditions lie in.

The Limacon of Pascal is a good approximation to the geometric shape of the basin of attraction of the period-1 ferroresonant attractor and can be used to analytically calculate a better approximation of the stability domain boundary. The initial conditions that depend on the time a transformer is de-energized can result in a jump to period-1 ferroresonance that is not predicted by quasi-static methods.

Near the period-2 subharmonic stability domain, multiple crossings of the separatrix on the negative flux-linkage axis result in early transitions to period-1 ferroresonance. Additional margin in the parameter plane is required in regions where there is uncertainty in the shape of the basin of attraction.

A step has been made in this chapter in satisfying the objective of determining margins to ferroresonance given an operating point in a parameter space. Regions of nonferroresonance are identified in a two dimensional parameter plane by combining the subharmonic and fundamental frequency stability domains calculated by the method of averaging and the period-1 stability domain boundary that considers initial conditions. Future work should investigate higher order saturation nonlinearities and their influence on the location of stability domain boundaries and their influence on the shape of the period-1 basin of attraction.

3.7 REFERENCES

[1] Jordan, D.W., and Smith, P., *Nonlinear Ordinary Differential Equations: Second Edition*, Oxford Press: New York, 1987.

Chapter 4

Transformer/Grading-Capacitor

4.1 INTRODUCTION

In a high voltage (i.e. greater than 66 kV) power system, the most prevalent ferroresonant circuit occurs between an unloaded transformer and the grading capacitor of an open circuit breaker. Two examples are considered in this chapter. The wound potential-transformer/circuit-breaker grading-capacitance ferroresonant event described in Chapter 1 is further investigated. Also, the possibility of ferroresonance occuring in larger station service transformers is investigated. A detailed three-phase EMTP model is developed and schemes for mitigating ferroresonance are evaluated. The three-phase model is reduced to an equivalent single-phase circuit and a polynomial curve is used to replace the piecewise-linear representation of the magnetization curve. Time-domain simulations of the circuit show regions of existence of non-ferroresonant states, subharmonic ferroresonance and period-1 ferroresonance. A two-dimensional bifurcation diagram is shown to be an ideal visualization tool for this ferroresonant circuit. Stability domain boundaries are directly calculated and compared with brute-force simulations. The equations developed in Chapter 3 are reformulated to allow a general n^{th} order polynomial approximation of the saturation curve to be studied.

4.2 LITERATURE REVIEW

Wound potential transformers (PTs) have been connected in several configurations that have resulted in ferroresonance.

Grounded PTs connected in ungrounded systems have been known to ferroresonate following a voltage disturbance such as energizing the PT or removal of a temporary fault [A11], [A16], [A62], [A69], [A104], [A117], [A121] and [A126]. Other terms such as *neutral inversion* and *neutral instability* have also been used to describe the phenomenon when it was first discovered [A16]. General experimental studies of this circuit have been performed by Peterson [A11]. In these studies, the oscillation modes which have been

excited include: unbalanced fundamental (UF), quasi-periodic-1/2 (QP-1/2), quasi-periodic-2, and harmonic-3. The most common modes are UF and QP-1/2 and have been investigated and observed by others [A104], [A117].

The PT is normally installed for ground fault detection in an ungrounded distribution system. The secondary of the PT is quite often connected in broken delta and the voltage across the break in the delta winding is used to indicate the presence of a fault and to operate relays. During ferroresonance, false signals can be detected across the open delta. A typical solution to this problem is to add resistance to the secondary burden [A11]. However, in some cases the required resistor may lead to excessive current flow in the PT and subsequent thermal failure if allowed to persist. Crane and Walsh recommend the replacement of PTs with capacitor voltage transformers (CVTs) in this case [A69].

Three-phase models are required to simulate a grounded PT connected in an ungrounded system [A117]. The majority of transformer models which have been used to simulate the phenomenon are composed of three single-phase transformers with a normal saturation curve and linear core loss model. Attempts at more detailed models have been made by Janssens [A62]. Experimental approaches are considered to be the best way to investigate ferroresonance and determine appropriate mitigation schemes for this circuit [A104].

A recent publication has indicated unbalanced operation of a high voltage (115 kV) PT can result in ferroresonance [A132]. The situation is somewhat unique as single-phase midspan openers were used to de-energize a PT. Normally, a three-phase disconnect is used at transmission level voltages. The PT was damaged during this procedure which led to its catastrophic failure following subsequent re-energization.

Several authors have found ferroresonance can occur between a PT and the grading capacitance of nearby open circuit breakers [A50], [A56], [A60], [A66], [A71], [A74], [A75], [A79], [A85], [A90], [A93], [A124] and [A127]. All cases described situations which occurred on grounded transmission systems with voltages between 138 kV and 400 kV. Depending on the parameters involved both period-1 and period-3 ferroresonance oscillations have been recorded [A50], [A60]. Janssens has used the harmonic balance method to calculate zones of existence for period-2, period-5 and period-7 subharmonics as well [A79]. Solutions to the ferroresonance problem for this circuit have included: placing a larger capacitor in parallel with the PT [A66], installing resistors in the broken delta (if such a winding exists), installing switched loading resistors ([A66],[A93]), replacing PTs

with CCVTs ([A56], [A74], [A124]), replacing existing PTs with higher loss units [A90], and installing a saturated inductor/resistor in the secondary [A79].

Single-phase modelling of the PT/grading-capacitor combination has been shown to adequately reproduce field measurements. Several problems with the PT model have been noted, however. Janssens has found numerical problems can occur with a piecewise-linear saturation curve and has implemented a curve based on a parabolic spline [A79]. Most researchers, who use a continuous saturation curve to avoid numerical problems, have chosen a polynomial representation [A137], [A136], [A129], [A121].

Selecting an appropriate model for PT losses is difficult. The most common model is a linear resistor connected in parallel with the magnetization characteristic representing the total measured iron-core losses at base system frequency. This model is sufficiently accurate for prediction of period-1 ferroresonance [8]. Although, field tests show additional damping occurs compared to model predictions [A124]. In strongly saturated states, supplementary losses can occur due to eddy-currents flowing in deflector screens and the tank of the PT or are occurring because of corona losses [A79]. Subharmonic states are sensitive to hysteresis losses [A134]. The particular model chosen to represent hysteresis or the ratio between hysteresis and eddy-current losses will influence the region of existence of subharmonic states.

A wound 220 kV PT failed catastrophically after its circuit was de-energized and left coupled to a parallel energized 380 kV line [A120]. Subharmonic oscillations (period-3) were observed. The addition of damping resistors or the replacement with SF_6 PTs with gapped cores were recommended. More will be said about transformer-terminated double-circuit lines in a later chapter.

4.3 EMTP MODEL DEVELOPMENT

EMTP (ElectroMagnetic Transients Program) is a general-purpose program used for simulation of transient phenomena in power systems [1]. The network is represented as a circuit with only current sources and conductances (i.e trapezoidal integration is used to transform inductors and capacitors into their companion circuits). The network is solved by LU factorization of the resulting conductance matrix. The current version of the program works well for most problems. However. for analyzing specific problems such as ferroresonance, other methods may be more appropriate. A Runge Kutta solution method is discussed later in the chapter.

The EMTP model used in the investigation of the May 20, 1995 Dorsey disturbance is shown in Fig. 4.1 [11]. Details of the incident were mentioned in Chapter 1.

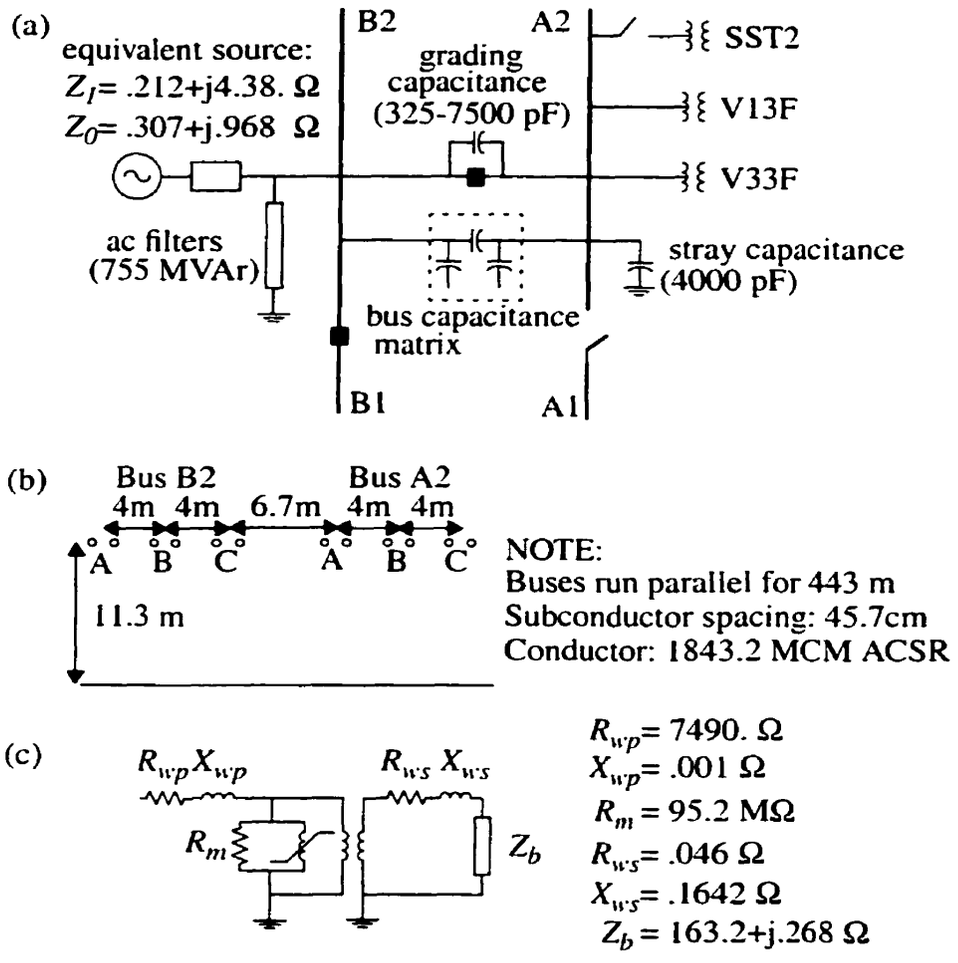

Fig. 4.1 EMTP model of the May 20, 1995, Dorsey disturbance showing (a) main circuit components, (b) model of buswork and (c) model of potential transformer.

4.3.1 Equivalent Source

The short circuit strength at Dorsey does not influence the onset of ferroresonance because the impedance is not of the same order as the saturated potential transformer impedance. A strong 12000 MVA equivalent impedance was used in all simulations.

4.3.2 Filters

The exact number of ac filters at Dorsey will not influence the onset of ferroresonance. Detailed models of each ac filter branch were included in the model, however, to assess the effectiveness of mitigating ferroresonance by switching a filter onto the de-energized bus.

4.3.3 Bus Capacitance

An accurate model of the bus capacitance is required to simulate ferroresonant conditions reliably. A value can be estimated if the induced voltage on the de-energized busbar is measured and the grading capacitor value is known. The system cannot be in ferroresonance for an accurate estimate to be made.

When bus A2 is de-energized, it remains capacitively coupled to the parallel bus B2. A first order model of the capacitive coupling between conductors was created using the data given in Fig. 4.1b. The capacitance matrix calculated by EMTP for the system of equivalent phase conductors is shown in Fig. 4.2. The length of the *jumbo* bus is 0.443 km

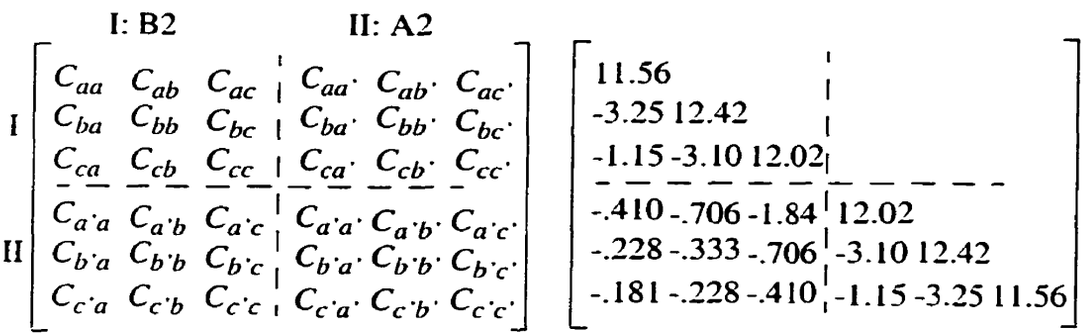

a) capacitance matrix b) EMTP calculation (nF/km)

Fig. 4.2 Capacitance matrix of Dorsey bus conductors.

The equivalent positive sequence bus capacitance to ground value can be roughly calculated if the bus is assumed balanced. The equivalent phase-to-ground capacitance (C_g) is 5.316 nF and the mutual capacitance (C_m) is 1.108 nF. By using (6-9), the positive

sequence capacitance is 6424 pF. However, this amount is too low to match field measurements of the steady-state coupled voltage under non-ferroresonant conditions. An additional value of 4000 pF to ground was added to account for equipment stray capacitance. Table 4.1 summarizes the stray capacitance calculations. Typical values of stray capacitance are taken from [9]-[10].

Table 4.1 Stray Capacitance Determination

Element	Typical Value (pF)	Number	Total (pF)
Live tank CB (open)	100	9	900
Outdoor PT	360-680	2	720-1360
Disconnect (closed)	90	8	720
Disconnect (open)	60	3	180
Outdoor CT	300	0	0
CVT	8000-12000	0	0
lightning arrester	100	0	0
support insulators	10	38	380
Total Stray ±15%			2900-3540 ±500 pF

4.3.4 Grading Capacitors

Grading capacitors are necessary for obtaining the proper voltage distribution across each break of a multi-break circuit breaker as well as improving the short line fault transient recovery voltage (TRV). The total amount of grading capacitance on the Dorsey bus has increased as circuit breakers have been upgraded to a 63 kA standard interrupting rating. The magnitude of grading capacitance is a critical parameter for determining the probability and severity of ferroresonance.

A total of 12 circuit breakers (see Fig. 1.1 for the bus layout) can be connected to bus A2 following an outage. Seven breakers are SF_6/CF_4. Each has 2 breaks per phase with a 1500

pF capacitor across each break. Five breakers are minimum oil with 4 breaks per phase. Four of these five breakers are equipped with a 1350 pF capacitor across each outside break and 1250 pF across the inside breaks. The fifth breaker has 1350 pF across each break.

At the time of the bus de-energization, the disconnects on three circuit breakers were open leaving a total of 5061 pF connecting bus B2 with bus A2. The maximum grading capacitance of all 12 breakers is 6885.5 pF. Typical tolerances in grading capacitor values are ±2%. Therefore, considering possible circuit breaker upgrades, the maximum circuit breaker grading capacitance operating range is between 325 and 7500 pF.

4.3.5 Potential Transformers

The two wound potential transformers involved in the ferroresonant disturbance (V13F and V33F) are both 4 kVA, 138000 Volt grounded wye-115V/69V grounded wye voltage transformers. Critical parameters for the wound PT include core losses, winding resistance and exciting current.

The losses measured in an excitation test are the iron-core losses, which are due to the cyclic changes in flux. The iron-core losses are composed of both hysteresis ($P_{hysteresis}$) and eddy-current ($P_{eddycurrent}$) losses.

$$P_{iron-core} = P_{hysteresis} + P_{eddycurrent} \tag{4-1}$$

In the original derivation of the hysteresis loss formula (4-2) by Dr. Steinmetz in 1892 [2], the exponent a was computed to be 1.6 and the losses were found to be proportional to frequency. The proportionality constant, k_h, depends on the core material and size of the core.

The hysteresis losses represent the work done in re-orienting the magnetic moments of the material as the magnetizing curve is traversed. Recent work has shown that for modern grain-oriented steels the exponent a can vary between 1.5 and 2.5 [3].

$$P_{hysteresis} = k_h \cdot B^a \cdot f \tag{4-2}$$

Eddy-current losses are proportional to flux density (B) squared, frequency squared and to the square of the lamination thickness (t) [4]. The eddy-current losses represent the losses

in the core caused by circulating currents in the laminations, where k_e is a constant that depends on the core material and size.

$$P_{eddycurrent} = k_e \cdot t^2 \cdot B^2 \cdot f^2 \tag{4-3}$$

A constant resistance may be chosen to model the average power losses in the iron-core as shown in (4-4).

$$P_{iron-core} = \frac{V_{rms}^{\ 2}}{R_m} = \frac{(\omega \cdot \lambda)^2}{2 \cdot R_m} = \frac{2 \cdot \pi^2}{R_m} \cdot \lambda^2 \cdot f^2 \tag{4-4}$$

The approximation is valid if one considers that typically hysteresis losses are only one-third the eddy-current losses [7] and the frequency does not vary much from the base 60 Hz frequency. Dick and Watson [8] have suggested that hysteresis may be safely neglected in cases of high-current ferroresonance. Detailed study of subharmonic ferroresonance may warrant the use of more accurate hysteresis models [3]. A value of 200 watts (no-load loss) per phase at nominal voltage (115 V) was used for each PT. The corresponding value for R_m reflected to the primary is 95.2 MΩ.

In regions of high saturation, the value of resistance (R_m) is no longer constant but is greatly reduced thus increasing the effective iron-core losses [A79]. The change is due to the magnetic properties of the core and to supplementary losses. By ignoring these additional losses, an additional safety margin is ensured in a mitigation scheme.

The leakage inductance of the primary winding is assumed to be negligible and is set at 0.001 ohms. The remaining component values are listed in Fig. 4.1c. A burden of 75 VA is assumed to be the normal PT loading. The R and X values for the PT burden (Z_b) were taken from CSA standard C13-M83.

Manufacturer's data was used to model the PT saturation characteristic. The fully saturated (air-core) inductance was not available. A value of 62 H was assumed as it produced a ferroresonant state that matched field recordings. The magnetization curve used in the EMTP model and a 15^{th} order polynomial approximation is shown in Fig. 4.3.

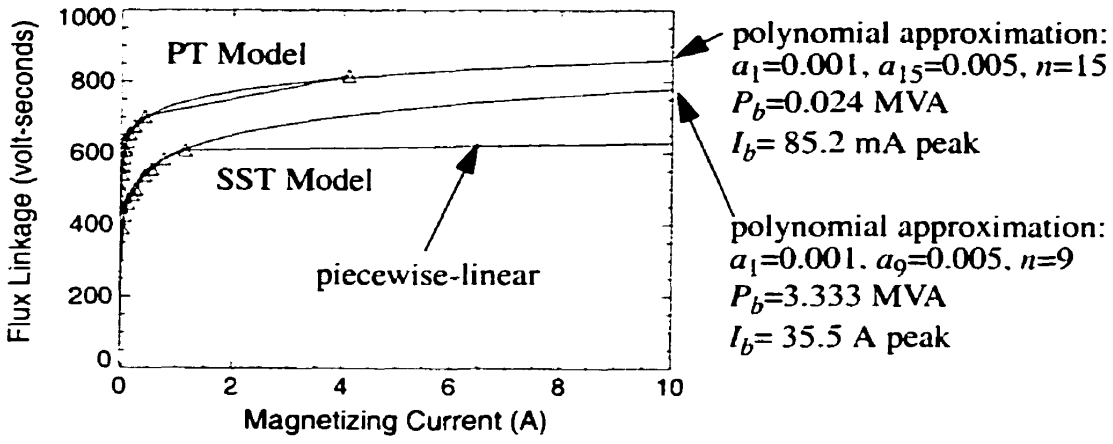

Fig. 4.3 Comparison of polynomial and piecewise-linear magnetization curves for the potential transformer and station service transformer.

4.3.6 Station Service Transformer

The station service transformer (SST) is a 10 MVA, 230 kV grounded wye - 4.16 kV wye transformer. The secondary is grounded through a 2.4 ohm neutral resistor rated at 2400 volts and 1000 amps for 10 seconds. The positive sequence impedance is 12.2%. Iron-core losses are 17 kW at nominal voltage. Manufacturer's data was used to model the saturation characteristic. The fully saturated (air-core) inductance was calculated by the manufacturer to be 884 ohms (2.34 H). The air-core inductance was used to calculate an extrapolated point on the magnetization curve shown in Fig. 4.3 in the EMTP model. Also shown in Fig. 4.3 is a 9^{th} order polynomial approximation.

The station service transformer is constructed as a three-phase device. However, the core configuration and zero sequence short circuit test data was not available. Therefore, a simplified single-phase representation was used as a first order approximation. The single-phase representation assumes the positive and zero sequence impedances are the same and that there is no coupling between phases.

4.4 DUPLICATING FIELD MEASUREMENTS

An oscillogram was located which shows the A2 Bus voltage for the Dorsey ferroresonant event of 95/05/20 at 22:04, after the last breaker cleared the bus. The trace is included in Fig. 4.4 for reference. The oscillogram shows phase A and B experienced chaotic transient oscillations for the first 700 ms before settling into a steady-state fundamental frequency ferroresonant state. Phase C did not experience ferroresonance.

The particular chaotic pattern shown in the oscillograph is almost impossible to duplicate. It is a function of the breaker opening times, pre-switch voltage and the exact values of all parameters in each phase. Benchmark tests showed for example that by varying the time step either all phases could jump into the final ferroresonant state immediately or any phase or combination of phases could remain at low voltage. A typical EMTP simulation[1] is shown at the bottom of Fig. 4.4.

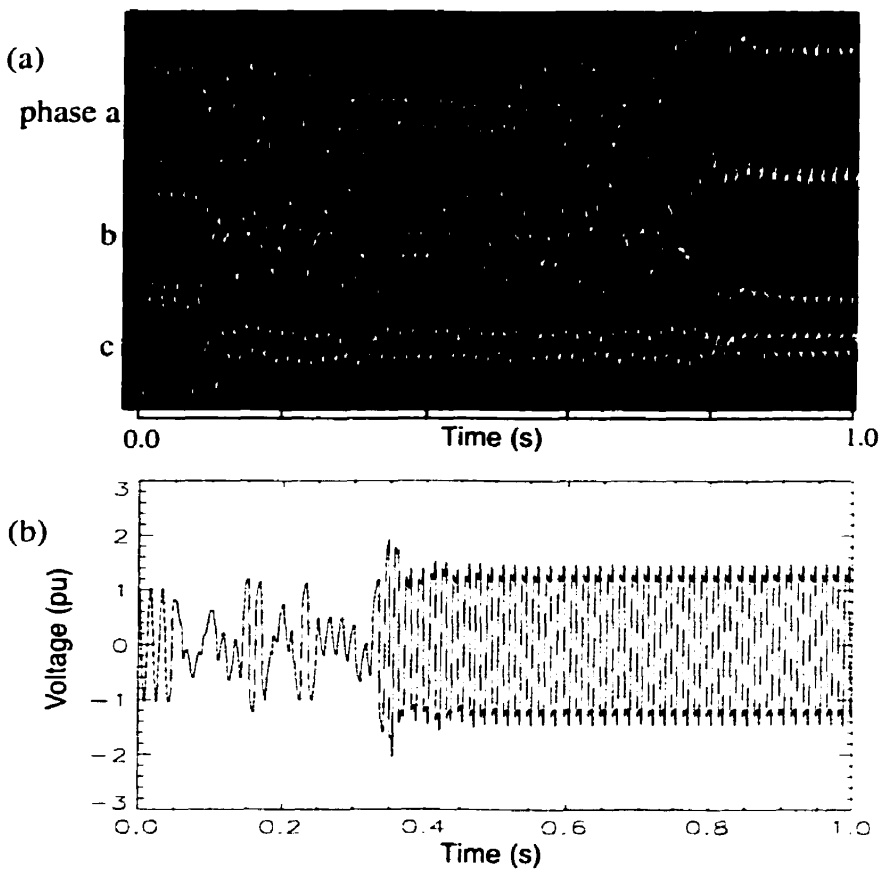

Fig. 4.4 Comparison of (a) field recording with (b) EMTP simulation.

1. A listing of the EMTP data file for this case is included in Appendix B.1.

4.5 EMTP FERRORESONANCE STUDY

Analysis of the benchmarked EMTP model has confirmed that the wound PTs failed due to ferroresonance. An estimated 50 per unit current flowed through the primary winding of the PT, which led to its thermal failure.

Mitigation is required to damp or detune the ferroresonance if bus A2 or B2 is isolated automatically by bus protection. Several mitigating options were investigated [11].

- station service transformer (SST) damping resistor
- potential transformer (PT) damping resistor
- 230 kV bus reactor
- 230 kV bus-connected filter
- 230 kV bus capacitor
- switching of SST and PTs using motor-operated disconnect
- replacement of PT with capacitor voltage transformer (CVT)
- bus surge arrester
- three-phase grounding switch
- PT ferroresonant suppression circuit

The only feasible short term solution to the ferroresonance problem that is secure and reliable is the installation of permanently connected damping resistors on the secondary of the SST. A longer term solution is the replacement of the wound PTs with CVTs.

The SST alone does not damp or detune the ferroresonance when the bus is isolated through circuit breaker grading capacitance values above 1500 pF. The lower knee point of the SST saturation characteristic limits the overvoltage on the bus, and thereby limits the magnitude of the magnetizing current of the wound PTs. However, the bus is in sustained ferroresonance and the magnetizing current of both the SST and PT contain large triplen[2] harmonic components. The power dissipation in each device is approximately 40% above rated values at the worst case grading capacitance (7460 pF).

A wye connected loading resistor of 200 ohms per phase (nominally 28.8 kW/phase) connected permanently to the 4.16 kV secondary of the SST will damp the ferroresonance

2. Triplen harmonics is a term used to refer to the odd multiples of the third harmonic.

in both the PTs and SST and not cause either device to be overloaded following unfaulted bus isolation.

4.6 STATE VARIABLE MODELLING

As was previously mentioned, the exact replication of a chaotic system transient is next to impossible. Small variations in system parameters or in the nature of the disturbance can lead to a completely different final state. In order to gain necessary insight into the ferroresonance circuit, a simplified single-phase equivalent state variable model was constructed. This model has the flexibility needed to perform systematic evaluations such as bifurcation analysis.

A single-phase positive sequence representation is justified for the potential transformers because they are constructed as three single-phase grounded-wye grounded-wye units in a grounded system. The grading capacitance and stray capacitance is relatively balanced between phases.

4.6.1 Derivation of Equations

The essential features of the detailed EMTP model are retained and are shown in Fig. 4.5.

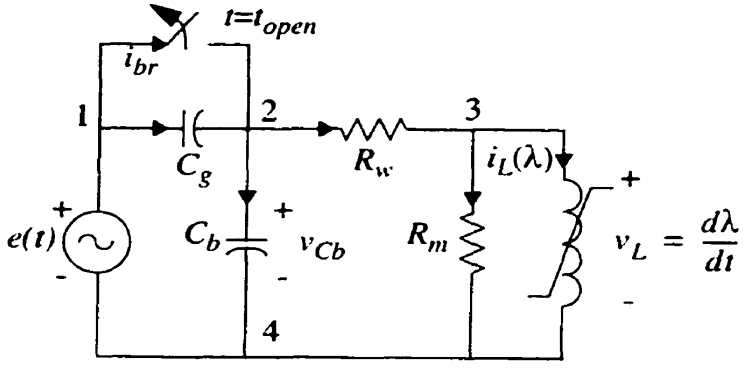

Fig. 4.5 Single-phase circuit model used to derive state equations.

The equations describing the dynamics of the circuit may be derived. The most systematic way of deriving the equations for the above circuit is to use elementary graph theory [5]. The circuit can be redrawn, as shown in Fig. 4.6, as a graph showing the normal tree as a solid line and the cotree branches as dashed lines.

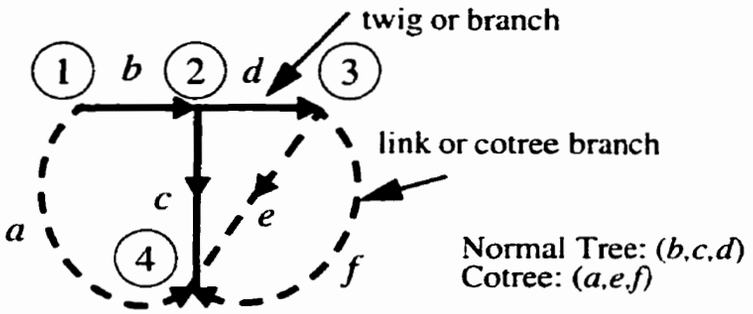

Fig. 4.6 Digraph of single-phase circuit given in Fig. 4.5.

The fundamental loops can be determined by retaining one link of the cotree and the complete normal tree: $\{(a,b,c), (c,d,e), (c,d,f)\}$. Only the loops containing an inductor are retained (c,d,f). Kirchhoff's Voltage Law is then used to write the equations for this loop:

$$0 = v_d + v_f - v_c \ . \tag{4-5}$$

Similarly, fundamental cutsets are created by retaining one branch of the normal tree and all links of the cotree: $\{(a,b), (a,c,e,f), (d,e,f)\}$. All cutsets containing capacitors are retained and then Kirchhoff's Current Law is used to write the equations at each node. Current entering a node is assumed positive.

$$0 = i_a + i_c + i_e + i_f \tag{4-6}$$

The next step is to substitute the device characteristics into the above equations and solve in terms of the variables $\{v_{Cb}, \lambda, i_L(\lambda)\}$. The end result is a second order nonautonomous (time dependent) system with state variables capacitor voltage (v_{Cb}) and transformer flux linkage (λ).

Equation 4-5 may be rewritten as:

$$0 = \left(i_L(\lambda) + \frac{1}{R_m} \cdot \frac{d\lambda}{dt}\right) \cdot R_w + \frac{d\lambda}{dt} - v_{Cb} \ , \tag{4-7}$$

or rearranging and solving for the first derivative of flux linkage,

$$\frac{d\lambda}{dt} = -\frac{R_m \cdot R_w}{R_m + R_w} \cdot i_L(\lambda) + \frac{R_m}{R_m + R_w} \cdot v_{Cb} \ . \tag{4-8}$$

Equation 4-6 may be rewritten as,

$$0 = -C_g \cdot \frac{d(v_S - v_{Cb})}{dt} + C_b \cdot \frac{dv_{Cb}}{dt} + \frac{v_{Cb} - R_w \cdot i_L(\lambda)}{R_m + R_w} + i_L(\lambda), \tag{4-9}$$

or rearranging and solving for the first derivative of bus voltage,

$$\frac{dv_{Cb}}{dt} = \frac{-(v_{Cb} + R_m \cdot i_L(\lambda))}{(R_m + R_w) \cdot (C_g + C_b)} + \frac{C_g}{C_g + C_b} \cdot \frac{de}{dt} . \tag{4-10}$$

The nonlinear inductor is represented as a continuous curve of the form given by (4-11)[A109] rather than a piecewise-linear representation used by EMTP. The continuous curve does away with the necessity of using interpolation between each straight line segment.

$$i_L(\lambda) = a_1 \cdot \lambda + a_n \cdot \lambda^n \tag{4-11}$$

If current and flux linkage are per-unitized, the constants a_1=.1, a_{15}=.06 and n=15 provide a reasonable approximation to the nonlinear saturation characteristic (Fig. 4.3). The SST characteristic up to the kneepoint can be well represented if a_1=.001, a_9=.005 and n=9. Beyond the kneepoint, the magnetization curve is unknown except that the slope should asymptotically approach the air-core inductance. The per unit flux contained by the iron-core under full saturation (λ_s) can be obtained by linearly extrapolating the highly saturated values back to the flux linkage axis. Dick and Watson [8] have made some measurements and determined that λ_s lies in the range 1.18 to 1.345 times the nominal flux linkage. It is expected that the true magnetization curve will lie somewhere between the polynomial and piecewise-linear approximations. More experimental work in transformer core modelling during ferroresonance would be of benefit.

A set of initial state equations can be derived with the circuit breaker closed. Equation 4-8 remains unchanged, however, (4-10) can be simplified to:

$$v_{Cb} = e = V_s \cdot \cos(\omega t) . \tag{4-12}$$

The transition from the initial to the final set of state equations occurs at a current zero assuming no current chopping takes place in the circuit breaker. The exact time step where a current zero occurs is found by detecting a change in sign of the breaker current given by (4-13).

$$i_{br} = C_b \cdot \frac{dv_{Cb}}{dt} + \frac{1}{R_m} \cdot \frac{d\lambda}{dt} + i_L(\lambda) \tag{4-13}$$

4.6.2 Solution Method

The set of first-order differential equations ((4-8) and (4-10)) were solved using a fourth order Runge-Kutta numerical integration technique. An adaptive time step feature was tested but was found to cause unreasonably long simulation times. A fixed time step of 50 μs was found to be a good compromise between accuracy and cpu time.

The fourth order Runge-Kutta method employs the following recurrence formula [6].

$$x_{i+1} = x_i + (k_1 + 2 \cdot k_2 + 2 \cdot k_3 + k_4)/6 . \tag{4-14}$$

The k-values are computed from the differential equation at various points in the time step. As we have a set of coupled first order equations, the k values must be calculated successively before the final recurrence formula is used. If the autonomous differential equations were not coupled, the following set of equations would be used to evaluate the k-values:

$$k_1 = \Delta t \cdot f(x_i), \tag{4-15}$$

$$k_2 = \Delta t \cdot f(x_i + k_1/2), \tag{4-16}$$

$$k_3 = \Delta t \cdot f(x_i + k_2/2), \tag{4-17}$$

$$k_4 = \Delta t \cdot f(x_i + k_3). \tag{4-18}$$

Comparisons were made between the detailed EMTP model and the simple single-phase model and were found to be in good agreement.

4.7 NONLINEAR DYNAMICS ANALYSIS

Systematic analysis of a practical circuit requires the mapping of the final operating state as parameters are varied as in the traditional bifurcation diagram, yet each operating state must be derived from a rest state or pre-switched state as in a basin of attraction. Thus a hybrid approach is taken by combining the traditional bifurcation and basin of attraction concepts.

4.7.1 Brute-Force Method

A kick-initiated rather than a slow parameter varying approach is taken in the generation of bifurcation diagrams. The slow parameter varying approach exhibits hysteretic mode transitions depending on whether the bifurcation parameter is being increased or decreased [A102]. The kick-initiated approach gives the best indication of the parameters necessary to jump to a ferroresonant mode for a particular set of initial conditions. Also, isolated sets of solutions can be found.

The *kick* applied to the circuit shown in Fig. 4.5 is initiated by opening the circuit breaker at the first current zero after time t_{open}=.04 seconds. After two seconds, the transients are assumed to have decayed leaving only the final attractor. A Poincaré section is then taken for the next thirty cycles, thus recording the essential features of the attractor (i.e. the periodicity).

As an example, a bifurcation diagram is shown in Fig. 4.7 for the case of two parallel PTs with 10450 pF of bus capacitance and 5080 pF of grading capacitance. As the source voltage is varied incrementally between two extremes, the character of the bifurcation diagram changes greatly. Classic period doubling bifurcations begin at 6.7 pu source voltage. At low values of source voltage, transitional chaos dominates. Several co-existing attractors are competing to determine which will be the system's final state.

The region of transitional chaos is the most interesting from a practical point of view. An alternative way of visualizing the dynamics in this region is to construct a two-dimensional (2d) bifurcation diagram. Two system parameters are selected to be varied and the final state of the system determined. A symbol is used to represent the final attractor's periodicity. For the ferroresonant circuit under study, the source voltage and grading capacitance may vary the most during normal system operation. Other parameters will remain fixed, however there may be some uncertainty in their values which would lead to an n-dimensional bifurcation diagram.

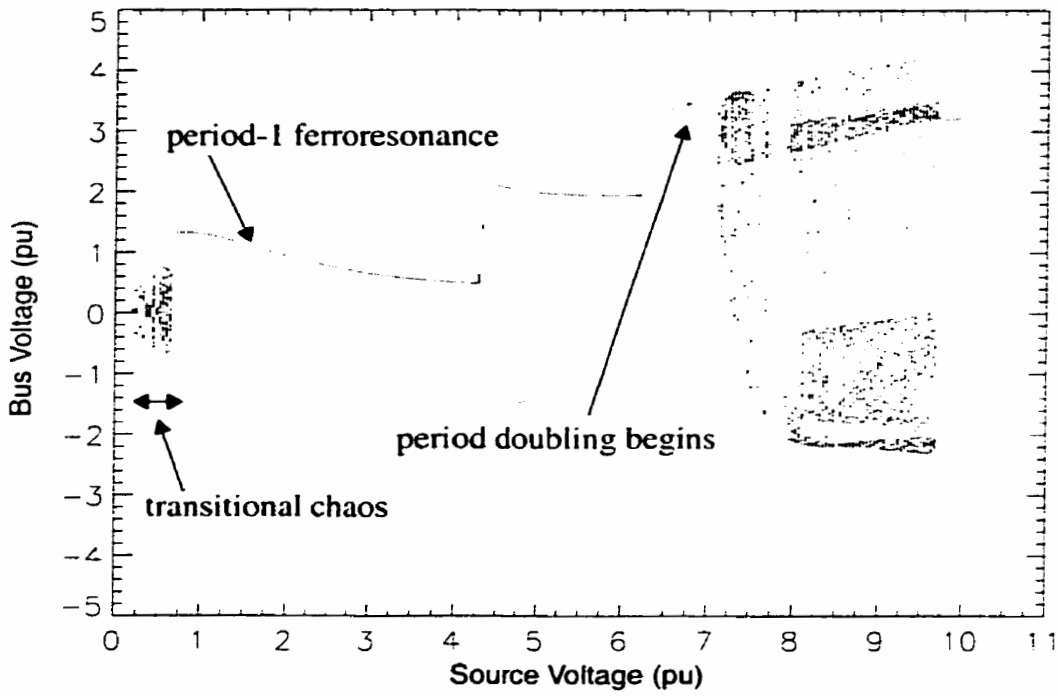

Fig. 4.7 Bifurcation diagram for the case of two potential transformers with C_g=5080 pF and C_b=10450 pF.

Two cases are shown to illustrate the improved visualization that can be realized by a 2d bifurcation diagram. The first case (Fig. 4.8) maps the ferroresonant regions of two parallel PTs. A parallel SST is added in the second case (Fig. 4.9). Examples of the state-space trajectories of two attractors were shown previously in Fig. 2.14.

The states marked unknown in Fig. 4.8 are still indeterminate after 2.5 seconds due to the low damping of this circuit.

The main effect of including the SST is an increase in the steady-state losses occurs, which causes the first transition to fundamental frequency (period-1) ferroresonance to shift to a higher grading capacitance value. The transitional chaos region is not as complex as for the two PT case as fewer subharmonic states are sustained.

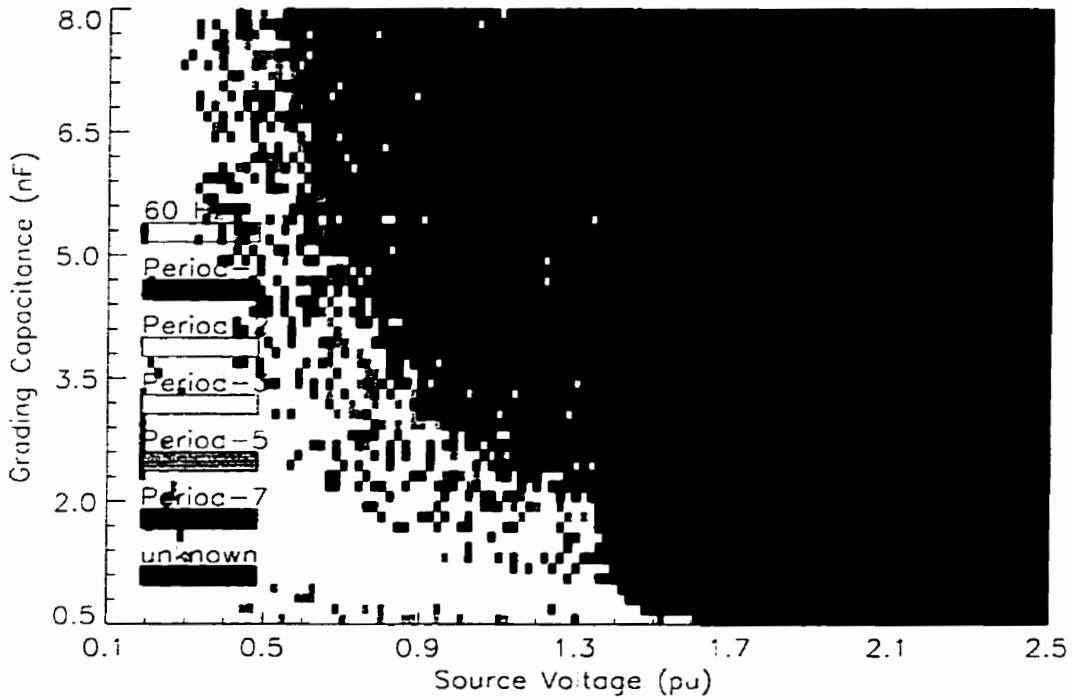

Fig. 4.8 Brute-force two dimensional bifurcation diagram of two parallel PTs.

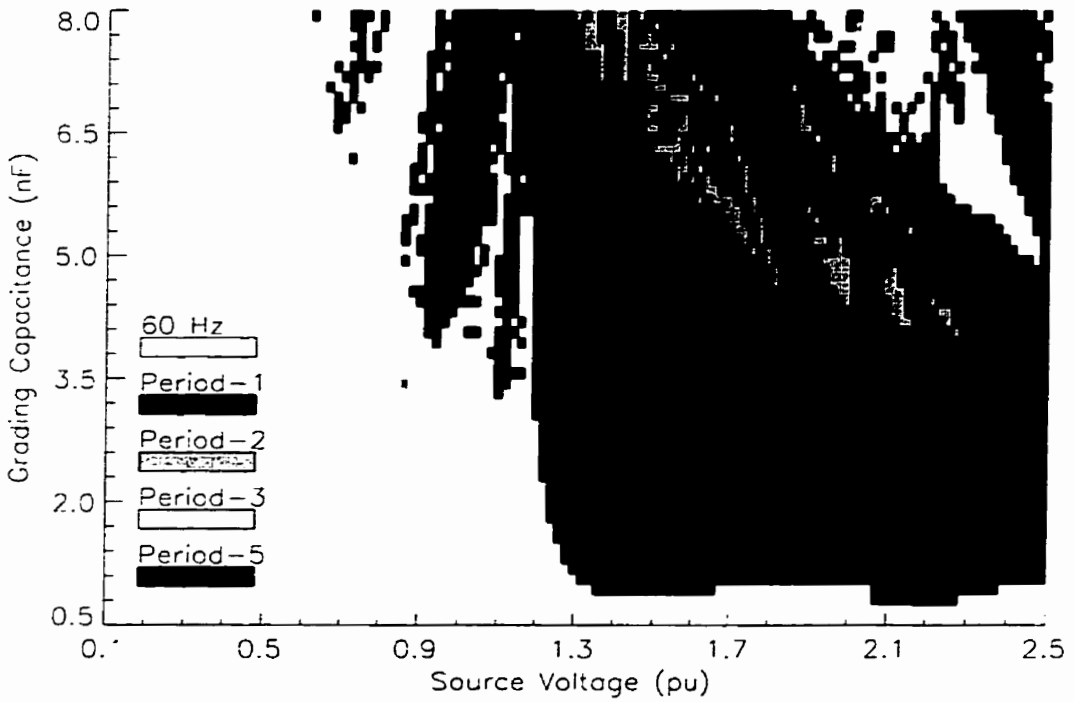

Fig. 4.9 Brute force two-dimensional bifurcation diagram of the parallel combination of two potential transformers and a station service transformer.

One possible *safe* operating zone can be identified in Fig. 4.9. If the source voltage is kept below 1.1 pu and the grading capacitance is kept below 4000 pF, the risk of ferroresonance is minimized. The maximum grading capacitance in the circuit could be as high as 7500 pF, which requires mitigation. Inclusion of permanently connected 200 ohm/phase damping resistors on the secondary of the SST extends the safe operating zone such that the entire plane in Fig. 4.9 is non-ferroresonant.

4.7.2 Higher-Order Period-1 Stability Domain Boundary Calculation

In order to locate fixed points precisely, higher-order approximations to the final solution need to be considered. Higher-order approximations allow precise computation of basins of attraction or bifurcation diagrams. A popular numerical technique based on Galerkin's method of harmonic balance has been used by several researchers [A41], [A75], [A90]. One major disadvantage of this method is initial conditions are not considered; therefore, optimistic estimates of the parameters necessary to produce a bifurcation to ferroresonance are often produced.

The question arises, "How well does a first-order approximation represent the behaviour of the complete nonlinear system?". In Chapter 2, the slowly varying averaging (SVA) method was introduced and was used to calculate an improved period-1 ferroresonance stability domain boundary in Chapter 3. In order to retain the two-dimensional visualization afforded by the van der Pol plane, the SVA method is limited to a first-order approximation to the final solution. Mathematically speaking, it is possible to think of higher-order approximations and multi-dimensional van der Pol spaces. The resulting equations would be too cumbersome to be of practical use as a screening tool.

In order to illustrate the ferroresonance analysis methods in Chapter 2 and 3, a third-order polynomial approximation to the true saturation curve was used. Actual transformers are better represented by at least a 9^{th} order polynomial. In this section, the averaged equations will be modified to allow a general n^{th} order polynomial relation to be used. Comparisons will be made with the brute-force bifurcation diagrams shown in Fig. 4.8 and Fig. 4.9.

The differential equation to be solved (4-19) is similar to the original equation (2-14), which was solved in Chapter 2.

$$\ddot{\lambda} + k\dot{\lambda} + C_1\lambda + C_3\lambda^n = G\cos(\omega t) \tag{4-19}$$

A first order solution to (4-20) can be assumed to be of the form:

$$\lambda(t) = a(t)\cos(\omega t) + b(t)\sin(\omega t) = r(t)\cos(\omega t + \theta). \tag{4-20}$$

The method of harmonic balance requires the assumed solution (4-20) to be substituted into (4-19) and the coefficients of sin and cos equated. Before that step is taken, the first and second derivatives of flux linkage are calculated and an expression for flux linkage to the power of n developed:

$$\dot{\lambda}(t) = (\dot{a} + b\omega)\cos(\omega t) + (\dot{b} - a\omega)\sin(\omega t), \tag{4-21}$$

$$\ddot{\lambda}(t) = (2\dot{b}\omega - a\omega^2)\cos(\omega t) + (-2\dot{a}\omega - b\omega^2)\sin(\omega t), \tag{4-22}$$

$$\lambda^n(t) = (a(t)\cos(\omega t) + b(t)\sin(\omega t))^n = r^n(t)\cos(\omega t + \theta)^n. \tag{4-23}$$

It is convenient to represent the n^{th} order expression in polar form. Let $\alpha=\omega t+\theta$, and represent cosine in exponential form:

$$\cos(\alpha)^n = \left(\frac{e^{j\alpha}}{2} + \frac{e^{-j\alpha}}{2}\right)^n = (x + y)^n. \tag{4-24}$$

The polynomial can be expanded using the binomial series expansion [12]:

$$(x + y)^n = x^n + nx^{n-1}y + \frac{n(n-1)}{2!}x^{n-2}y^2 + \frac{n(n-1)(n-2)}{3!}x^{n-3}y^3 + \ldots \tag{4-25}$$

For example, with n=5 the following series expansion results:

$$(x + y)^5 = x^5 + 5x^4y + 10x^3y^2 + 10x^2y^3 + 5xy^4 + y^5. \tag{4-26}$$

After substituting for x and y, the terms can be grouped in the following manner:

$$\cos(\alpha)^5 = d_1\left(\frac{e^{j\alpha}}{2} + \frac{e^{-j\alpha}}{2}\right) + d_3\left(\frac{e^{j3\alpha}}{2} + \frac{e^{-j3\alpha}}{2}\right) + d_5\left(\frac{e^{j5\alpha}}{2} + \frac{e^{-j5\alpha}}{2}\right). \tag{4-27}$$

By inspection, d_1=10/16, d_3=5/16 and d_5=1/16.

The coefficients of the binomial expansion can also be written in combinatorial notation:

$$(x+y)^n = \binom{n}{0}^n + \binom{n}{1}x^{n-1}y + \binom{n}{2}x^{n-2}y^2 + \binom{n}{3}x^{n-3}y^3 + \ldots \tag{4-28}$$

For a first-order approximation, the coefficient d_1 needs to be determined. From the binomial expansion, it is evident that the coefficient of the middle two terms needs to be retained. Therefore, d_1 can be written as,

$$d_1 = \left(\frac{1}{2}\right)^{n-1}\binom{n}{(n-1)/2}. \tag{4-29}$$

By using (4-29), (4-23) can be rewritten as,

$$\lambda^n(t) \equiv r^n d_1 \cos(\omega t + \theta) = (a^2+b^2)^{\frac{n-1}{2}} d_1(a\cos(\omega t) + b\sin(\omega t)). \tag{4-30}$$

Now (4-30), (4-22) and (4-21) can be substituted into (4-19) and coefficients of sine and cosine equated. Second order derivatives of a and b, terms in $\cos(3\omega t)$ and $\sin(3\omega t)$ and terms kda/dt and kdb/dt are neglected. After equating terms and solving for the first derivative of a and b, the following averaged equations result:

$$\dot{a} = A(a,b) = \frac{-b}{2\omega}\left((\omega^2 - C_1) - C_3(a^2+b^2)^{\frac{n-1}{2}} d_1\right) - \frac{ka}{2}, \tag{4-31}$$

$$\dot{b} = B(a,b) = \frac{a}{2\omega}\left((\omega^2 - C_1) - C_3(a^2+b^2)^{\frac{n-1}{2}} d_1\right) - \frac{kb}{2} + \frac{G}{2\omega}. \tag{4-32}$$

Squaring and adding (4-31) and (4-32) and substituting $R=a^2+b^2$ results in the following amplitude equation:

$$G^2 = ((\omega^2 - C_1)^2 + k^2\omega^2)R - 2C_3 d_1(\omega^2 - C_1)R^{\frac{n+1}{2}} + C_3^2 d_1^2 R^n. \tag{4-33}$$

Real values of R that satisfy (4-33) are substituted into (4-31) and (4-32) in order to determine equilibrium points. Stability of the equilibrium points is determined by calculating the eigenvalues of the Jacobian,

$$\begin{bmatrix} \dot{\xi}_1 \\ \dot{\xi}_2 \end{bmatrix} = \begin{bmatrix} \frac{\partial}{\partial a}A(a_i, b_i) & \frac{\partial}{\partial b}A(a_i, b_i) \\ \frac{\partial}{\partial a}B(a_i, b_i) & \frac{\partial}{\partial b}B(a_i, b_i) \end{bmatrix} \begin{bmatrix} \xi_1 \\ \xi_2 \end{bmatrix}, \tag{4-34}$$

where,

$$\frac{\partial}{\partial a}A(a, b) = -\frac{k}{2} + \frac{C_3 a_i b_i d_1 (n-1) R^{\frac{n-3}{2}}}{2\omega}, \tag{4-35}$$

$$\frac{\partial}{\partial b}A(a, b) = -\left(\frac{\omega^2 - C_1}{2\omega}\right) + \frac{C_3 d_1 (a_i^2 + n b_i^2) R^{\frac{n-3}{2}}}{2\omega}, \tag{4-36}$$

$$\frac{\partial}{\partial a}B(a, b) = \left(\frac{\omega^2 - C_1}{2\omega}\right) - \frac{C_3 d_1 (b_i^2 + n a_i^2) R^{\frac{n-3}{2}}}{2\omega}, \tag{4-37}$$

$$\frac{\partial}{\partial b}B(a, b) = -\frac{k}{2} - \frac{C_3 a_i b_i d_1 (n-1) R^{\frac{n-3}{2}}}{2\omega}. \tag{4-38}$$

The lossy Limacon technique determines the parameter values that result in crossing of the separatrix, using only the calculated location of the unstable fixed point and slope through the fixed point. Given a general n^{th} order polynomial representation of the saturation curve, (4-31)-(4-38) can be used to determine the unstable fixed point and slope through the fixed point as a function of the network parameters. The parameter values that result in crossing of the separatrix is found using (3-39).

4.7.3 Direct Calculation of the Stability Domains

The general set of equations just derived is used to develop specific sets of equation corresponding to the 15^{th} order potential transformer example and a 9^{th} order station service example. In general, the parameters match those used to create the brute-force bifurcation diagrams shown in Fig. 4.8 and Fig. 4.9. The only exceptions are that the winding resistance is neglected and the station service transformer example does not include parallel potential transformers.

The period-1 turning points are calculated using the Newton-Raphson method and are projected on the grading capacitance-source voltage parameter plane. Alternatively, (4-33) could be solved for critical points as described in Section 2.6.3. The Newton method is initialized by first solving for the set of unstable fixed points as a function of source voltage. The two extreme unstable fixed points are used as initial guesses in a Newton-Raphson search for turning points. As the order of the polynomial increases, it becomes more difficult to isolate the real solutions of (4-33). Laguerre's method (PV-WAVE function ZROOTS based on a routine in *Numerical Recipes in C: The Art of Scientific Computing*, Cambridge Press, 1988) failed to converge for a 15^{th} order polynomial and a companion matrix method (PV-WAVE:IMSL function ZEROPOLY) is used instead.

The Limacon of Pascal method is used to calculate the parameters that result in a crossing of the lossy separatrix.

Fig. 4.10 and Fig. 4.11 show the calculated period-1 stability domain boundaries of the 15^{th} order potential transformer example and the 9^{th} order station service transformer example. An assessment of the risk of period-1 ferroresonance is also indicated.

Any parameter values to the right of the Limacon boundary and above the left hand side projected turning point will experience period-1 ferroresonance. Parameter values in the white region below the left hand side projected turning point will not experience ferroresonance.

By displaying the projection of the upper and lower period-1 turning points (i.e. see Fig. 2.17), calculation of the subharmonic stability domains can be avoided. The shaded area indicated as medium risk may experience subharmonic ferroresonance or period-1 ferroresonance. The risk increases for low loss systems such as the potential transformer example as Fig. 4.8 and Fig. 4.9 clearly demonstrate. The increased amount of subharmonics distorts the assumed double-loop shape of the period-1 basin of attraction resulting in a leftward shift in the transition to period-1 ferroresonance. Improved modelling of losses may assist in producing more accurate stability domain boundaries.

One major advantage the direct calculation method has over the brute-force method is computational speed. For example, it takes roughly 48 hours of computation time to produce Fig. 4.9 compared with 5 minutes needed to produce Fig. 4.11.

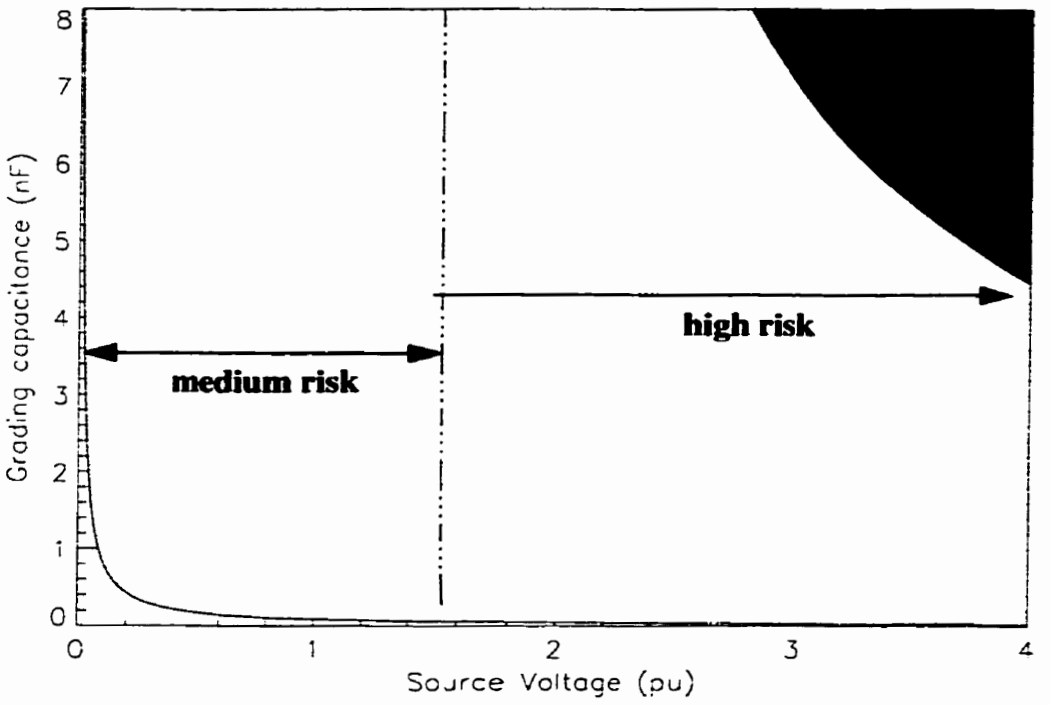

Fig. 4.10 Calculated period-1 stability domain boundaries of two PT example.

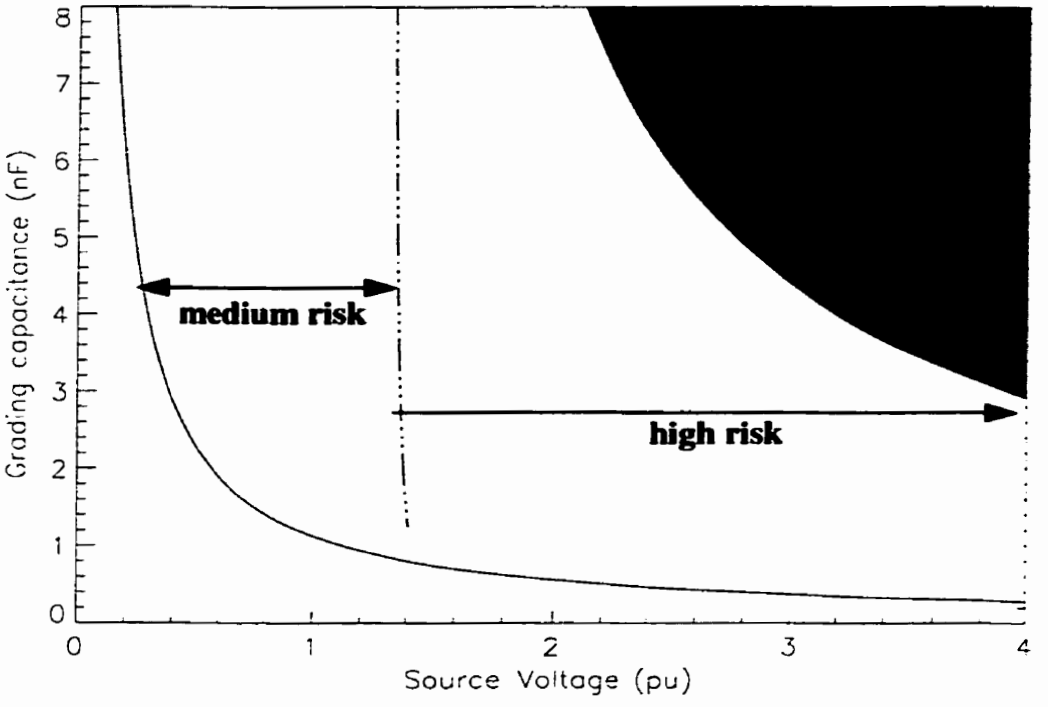

Fig. 4.11 Calculated period-1 stability domain boundaries of SST example.

4.8 SUMMARY

Digital simulation has been used to study ferroresonance in a 230 kV circuit. The study has shown that there are sufficient losses in a station service transformer to prevent ferroresonance up to a grading capacitance value of 4000 pF. Due to circuit breaker upgrades, the maximum grading capacitance could reach 7500 pF, which requires some form of mitigation. A 200 ohm/phase damping resistor installed on the secondary of the SST eliminates ferroresonance for faulted and unfaulted bus clearing. The resistor increases the effective core losses of the SST by a factor of six. If the SST is unavailable, ferroresonance will develop in wound potential transformers even at minimum grading capacitance. Wound potential transformers are to be replaced by capacitor voltage transformers.

A two-dimensional (2d) bifurcation diagram is an ideal tool for visualizing the behavior of a ferroresonant circuit. The margin of safety between ferroresonant and non-ferroresonant states can clearly be seen. A kick-initiated approach should be used in the generation of bifurcation diagrams since it mirrors true system initial conditions.

One major disadvantage of the brute-force method is computation time. Direct calculation of the stability domains reduces the computation time from days to minutes. A general set of equations was derived to permit the analysis of n^{th} order polynomial approximations of the saturation curve. Comparisons of the brute-force 2d bifurcation calculations with direct calculation of the stability domain boundaries was made. Some of the coarse features of the brute-force calculated bifurcation diagram can be reproduced via direct methods. The stability domain boundary calculated using the Limacon of Pascal approach is more accurate compared with the quasi-static boundary.

This chapter has shown the need for further study into kick or transient induced ferroresonance as opposed to conventional quasi-static approaches. Ferroresonance can be induced quasi-statically by slowly varying a system parameter until a spontaneous jump to a new operating point occurs. A transient can induce a jump to a new operating mode at lower values of source voltage, for example, compared with the quasi-static approach.

Conventional transformer models have been used with success to model the jump to a period-1 ferroresonant mode. Based on the literature, there is some uncertainty as to how well a conventional model will predict subharmonic states. Hysteresis models and

modified core loss models may provide better quantitative prediction of subharmonic states. Further laboratory and simulation work investigating losses as a function of the type of ferroresonance oscillation mode would be beneficial.

4.9 REFERENCES

[1] Dommel, H.W., *Electromagnetic Transients Program Reference Manual: EMTP Theory Book*, Bonneville Power Administration: Portland, August, 1986.

[2] Steinmetz, C.P.,"On the Law of Hysteresis", *AIEE Transactions*, No. 9, pp. 3-51, 1892.

[3] de León, F., and Semlyen, A., "A Simple Representation of Dynamic Hysteresis Losses in Power Transformers", *IEEE Trans. on Power Delivery*, Vol. 10, No. 1, pp.315-321, January 1995.

[4] Slemon, G.R., and Straughen, A., *Electric Machines*, Addison-Wesley Publishing: Reading, Mass., pp. 22-27, 1980.

[5] Chua, L.O., Desoer, C.A., Kuh, E.S.,*Linear and Nonlinear Circuits*, New York:McGraw Hill, pp. 695-739, 1987.

[6] James, M.L., Smith, G.M., and Wolford, J.C., *Applied Numerical Methods for Digital Computation*, Harper & Row: New York, pp. 447-460, 1985.

[7] Swift, G.W.,"Power Transformer Core Behavior Under Transient Conditions", *IEEE Trans. on Power Apparatus and Systems*, Vol. PAS-90, No.5, pp. 2206-2210, Sept./Oct. 1971.

[8] Dick, E.P. and Watson, W.,"Transformer Models for Transient Studies Based on Field Measurements", *IEEE Trans. on Power Apparatus and Systems*, Vol. PAS-100, No. 1, pp. 409-419, January 1981.

[9] *Application Guide for Transient Recovery Voltage for AC High Voltage Circuit Breakers Rated on a Symmetrical Basis*, ANSI/IEEE C37-011-1979

[10] Greenwood, A., *Electrical Transients in Power Systems*, John Wiley & Sons: New York, 1991.

[11] Jacobson, D., and Swatek, D.,"Analysis of the Dorsey Ferroresonant Incident (95 05 20",*Manitoba Hydro Technical Memorandum*, TM 95-15, November 25, 1995.

[12] Beyer, W.H., *CRC Standard Mathematical Tables: 27th Edition*, CRC Press: Florida, pp. 295, 1984.

Chapter 5

Experimental Measurement and Modelling of Transformer Losses

5.1 INTRODUCTION

In Chapter 4, a practical example of ferroresonance was studied where the key circuit elements involved were an unloaded transformer and circuit breaker grading capacitance. The need for improved modelling of losses during fundamental and subharmonic ferroresonance was recommended in order to enable more accurate predictions.

In this Chapter, laboratory experiments[1] are performed on a distribution transformer in order to improve the understanding of losses during different modes of ferroresonance. A general and robust methodology for modelling the nonlinear lossy characteristics of the transformer's iron-core is required for accurate modelling of ferroresonance in high voltage transformers.

5.2 LITERATURE REVIEW

Losses in the iron-core are often referred to as the no-load losses. Load losses or copper losses occur in the transformer winding only when the transformer is loaded. The no-load losses can be categorized into five components: hysteresis losses in the core laminations; eddy-current losses in the core laminations; I^2R losses due to no-load exciting current; stray eddy-current losses in the tank, core clamps, bolts, and other core components; and dielectric losses [2]. Kennedy [2] assumes 99% of the no-load losses are comprised of hysteresis and eddy-current losses. Beckley [4] considers an anomalous loss component arising from the detail of the domain and grain structure of the steel to be significant. Swift defines the anomalous losses as the discrepancy between a classical calculation of eddy current loss and measurements of the frequency-dependent losses [3]. Janssens *et al.* [A79] note that there are supplementary losses occurring in strongly saturated states, such as eddy-current losses in the deflector screens and transformer tank and corona losses.

---

1. Acknowledgement is given to M. Magalhaes for performing the lab experiments, under my supervision, as part of her B.Sc. thesis [9].

In general, it is common practice to say that $P_{iron\text{-}core}=Af+Bf^2$ is not a bad approximation to the no-load losses, where A is a constant corresponding to hysteresis effects (i.e. influenced by metallurgical effects such as impurities, crystal damage, surface roughness etc.) and B is a constant corresponding to eddy-current effects (i.e. influenced by thickness and resistivity of the metal) [4].

Historically, the hysteresis losses have been assumed to be 1/3 the eddy current losses for modern transformers constructed using grain-oriented silicon-steel sheets [3]. Earlier work suggested using a ratio of 2/3 for grain-oriented and 3.0 for nonoriented steel [1]. Janssens *et al.* [A79] assumed a 50:50 split between eddy-current and hysteresis losses in their work.

Various types of hysteresis models have been proposed such as: the Stoner-Wolhfarth model, the Jiles-Atherton model, the Globus model, and the Preisach model [5]. de León *et al.* [6] state that detailed macroscopic models are not required by power system engineers. The model should be sufficient to predict the losses in transient and steady-state conditions as well as accurately representing the basic magnetization curve.

Measurements of iron-core losses have been performed by Swift [3]. Swift assumed hysteresis loss is only about one-third of the eddy-current loss. He performed 20 Hz and 60 Hz tests on a 10 kVA distribution transformer and concluded that a single linear resistor representing all core loss as eddy-current loss is sufficiently accurate.

The majority of papers discussing the modelling of losses during ferroresonance have taken Swift's approach and assumed a single linear resistor is adequate to represent all iron-core loss. However, observations made by Walling [A100] and Kunde et al. [A124] indicate that field tests show actual transformers damp transient ferroresonance faster than calculations predict. Kunde hypothesizes that additional non-measurable losses (i.e. using standard test methods) occur in the transformer.

Janssens *et al.* [A79] have used an iterative approach to adapt the value of eddy-current loss and hysteresis loss. An attempt is made to reproduce the correct losses as a function of the amplitude and shape of the oscillation. Measurements of a 245 kV gas-insulated potential transformer show the equivalent iron-core loss conductance can increase to four times its nominal value in strongly saturated states.

Based on a review of the literature, two models of iron-core losses should be investigated: a single linear resistor representing all iron-core loss as eddy-current loss; and an iron-core loss model that has 25% hysteresis losses and 75% eddy-current losses.

5.3 SYSTEM DESCRIPTION

Since the May 20, 1995, destruction of wound potential transformer V13F, all wound potential transformers of concern at the Dorsey Station have been replaced with capacitor voltage transformers. A plan is in place to enhance the reliability of the station by adding a third bus and several new bus tie breakers and disconnects. By October 2003, the Dorsey station single line diagram will be modified as indicated in Fig. 5.1.

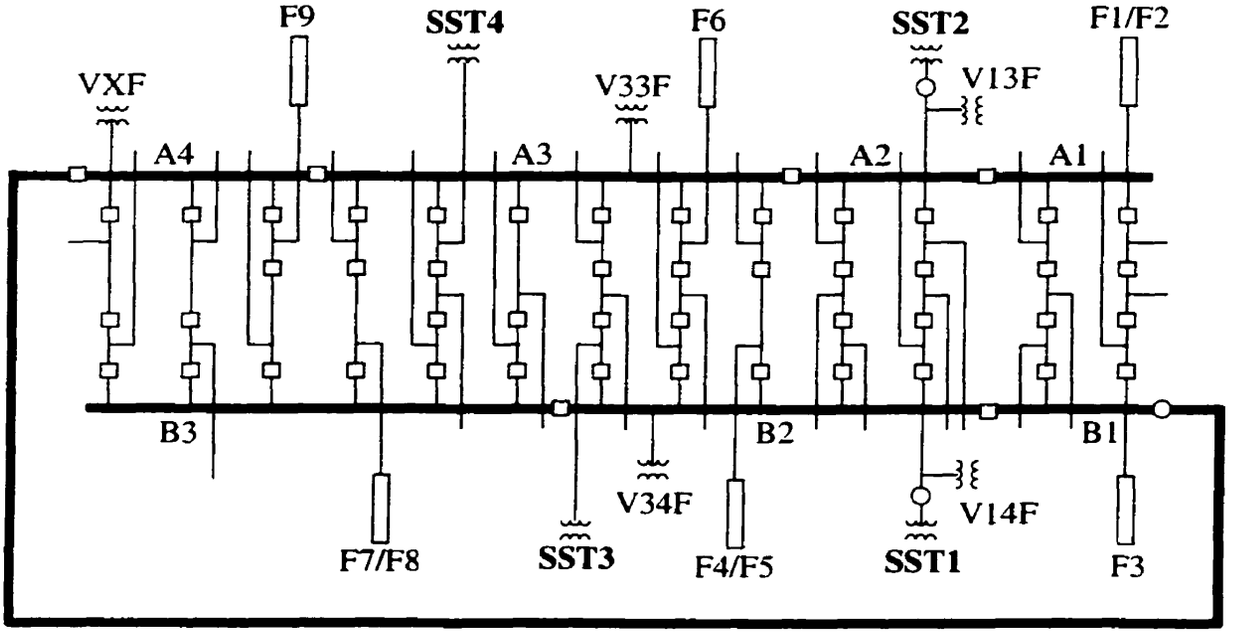

Fig. 5.1 Dorsey bus enhancement project.

Permanently connected 200 ohm loading resistors are installed on the 4.16 kV secondary bus of station service transformers SST1 and SST2. Because of the bus configuration change, there may be an opportunity for removing the loading resistors if the potential for period-1 ferroresonance is eliminated.

Table 5.1 estimates possible combinations of stray and grading capacitance in which the station service transformers may operate. The same information is also illustrated in Fig. 5.2

Table 5.1 Stray Capacitance and Grading Capacitance Variations

Element	Grading Capacitance (pF)	Stray Capacitance (pF)
i. SST1--normal clearing	3973.5	29785-34285
ii. SST2--normal clearing	3000	15505-20045
iii. SST3/4--normal clearing	649	3124-8264
iv. SST1--breaker fail	5473.5	51145-55935
v. SST2--breaker fail	3750	28875-33705
vi. SST2--breaker fail	5811	31563-41103
vii. SST3--breaker fail	3223.5	32554-42234
viii. SST4--breaker fail	3561	19452-24592
ix. SST2--existing configuration	6885.5	10258-15138

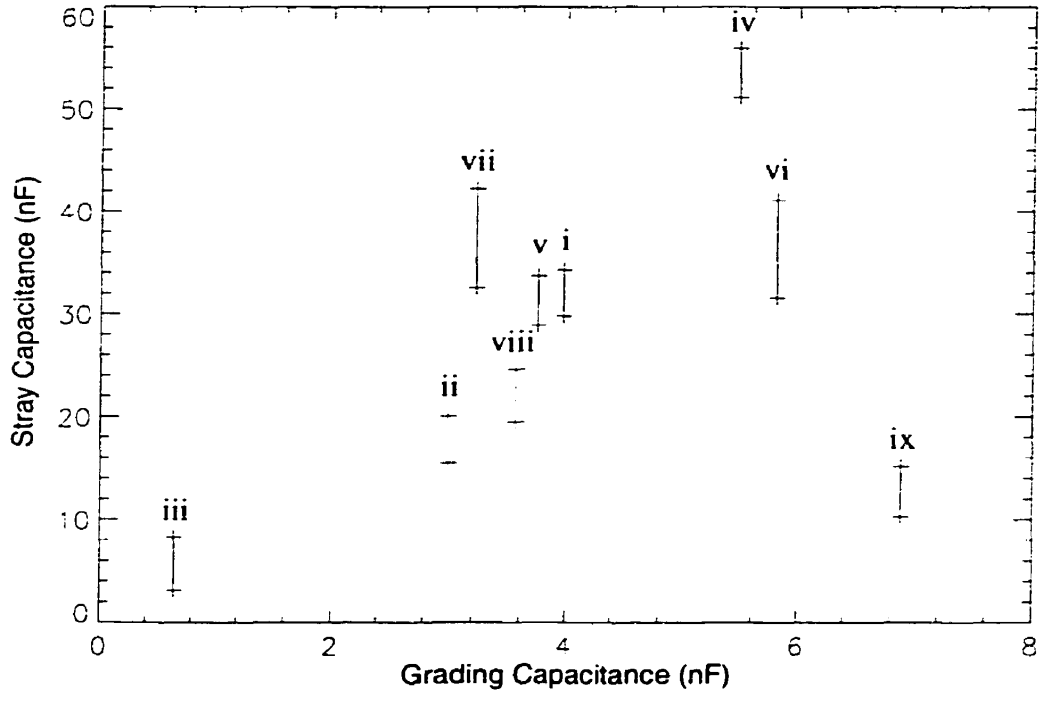

Fig. 5.2 Dorsey station service transformer stray and grading capacitance operating environment.

A single-phase scaled model of the Dorsey station is desired to be setup in the laboratory. The method chosen is to first select a transformer and then calculate appropriate values of capacitance by maintaining the same ratio of capacitive impedance to magnetizing impedance (i.e. X_c/X_m) in the laboratory model as exists in the field model.

The station service transformer model parameters are described in Section 4.3. The magnetizing reactance of the station service transformer is 5.92 MΩ. A limited number of distribution transformers were available for selection. The one chosen has a dual 115 volt secondary winding and 2.3 kV primary winding. The magnetizing reactance of the distribution transformer is 250.3 ohms. A detailed discussion of transformer tests can be found later in this chapter.

Using the aforementioned values of magnetizing reactance, the capacitance plot shown in Fig. 5.2 is scaled to an equivalent range appropriate for the laboratory distribution transformer. Six combinations of grading capacitance and stray capacitance are selected for ferroresonance testing and are displayed on Fig. 5.3. The capacitors were selected based on off-the-shelf sizes available in the laboratory. Results from ferroresonance tests will be discussed in Section 5.5.2.

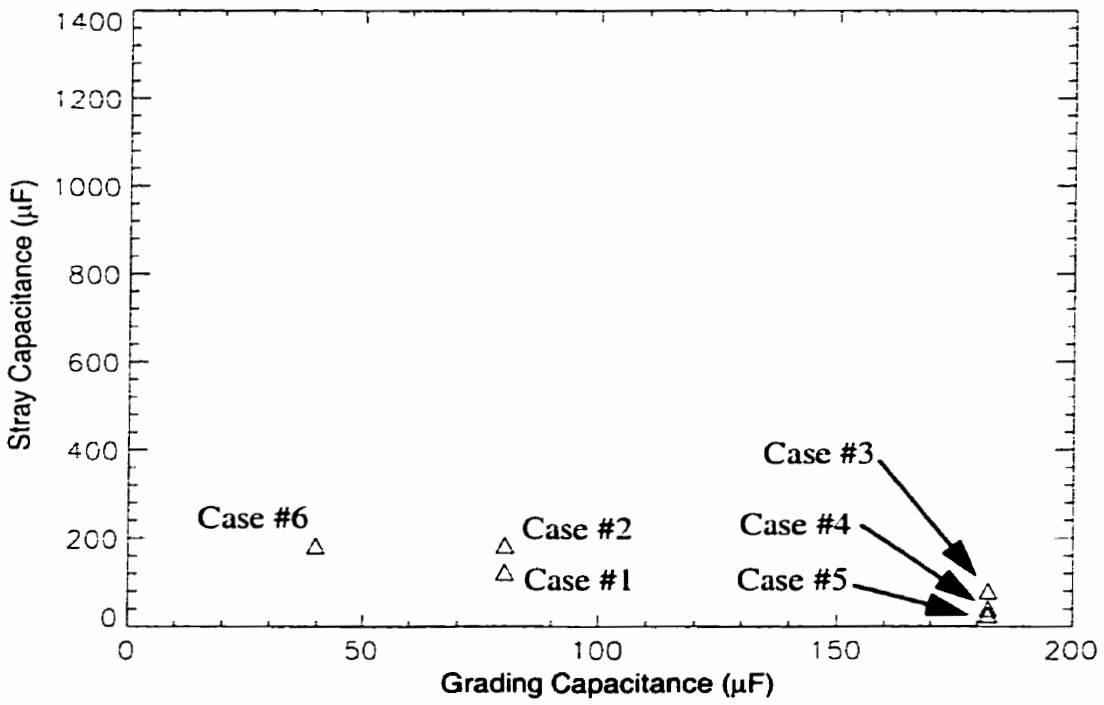

Fig. 5.3 Scaled laboratory values of stray and grading capacitance.

A single-line diagram representing the studied system is given in Fig. 5.4. The distribution transformer was energized from the 115 volt side because an appropriate high voltage source was not available.

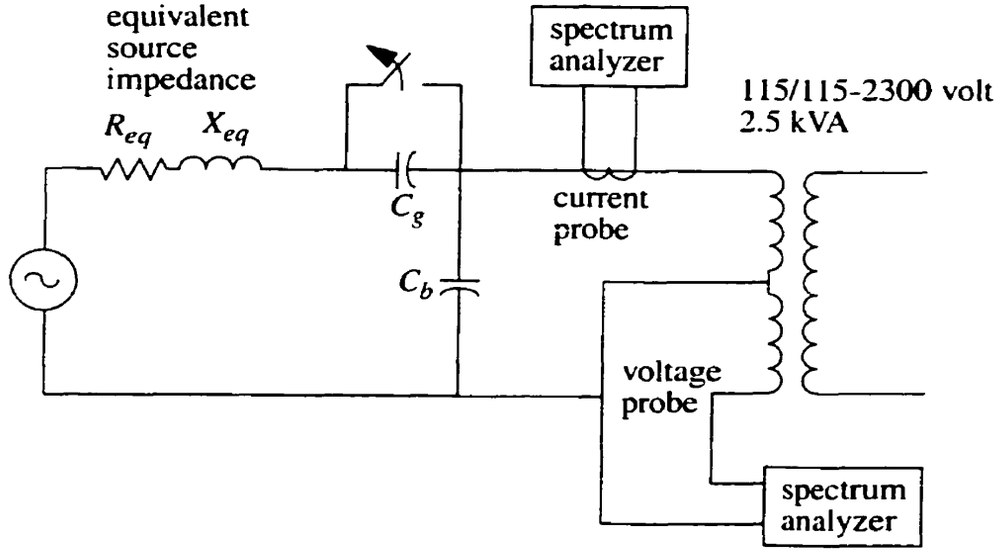

Fig. 5.4 Laboratory model representing a high voltage ferroresonant circuit.

5.4 MEASUREMENT OF PARAMETERS

Tests are performed to determine values to use for the equivalent source impedance, grading capacitance, stray capacitance and distribution transformer.

The equivalent source impedance is determined by first measuring the source voltage with no load (V_{NL}) connected followed by recording the voltage and current with a resistive (V_R and I_R) and a capacitive load connected (V_C and I_C). The following two equations can be solved for the unknowns (R_{eq} and X_{eq}).

$$0 = (V_R + R_{eq}I_R)^2 + (X_{eq}I_R)^2 - V_{NL}^2 \tag{5-1}$$

$$0 = (X_{eq}I_C - V_C)^2 + (R_{eq}I_C)^2 - V_{NL}^2 \tag{5-2}$$

The no-load voltage in the laboratory at the time of the test was 120.45 volts. Connecting a 6.0 Ohm resistor to the source resulted in a voltage (V_R) of 118.69 volts and current (I_R) of 18.78 amperes. A 182.3 μF capacitor connected to the source resulted in a measured voltage (V_C) of 120.82 volts and current (I_C) of 8.09 amperes. Solving (5-1) and (5-2) results in a value of 93.55 mΩ for R_{eq} and 46.03 mΩ for X_{eq}. These values were modified after digital simulations to account for contact resistance, capacitor losses and to match

recordings of ferroresonant modes. The final value chosen for R_{eq} is 272.96 mΩ and 79.65 mΩ for X_{eq}.

Electrolytic capacitors are used in the laboratory experiments. Rather than rely on nameplate values, which can be up to 15% lower than the actual capacitance, each can is energized and the measured voltage and current are used to calculate the impedance.

5.4.1 Transformer Measurements

Standard open-circuit and short-circuit tests were performed on the distribution transformer in order to determine parameters to use in the digital model. The digital model used to represent the distribution transformer is assumed identical to the wound potential transformer shown in Fig. 4.1c.

The measured iron-core losses at 115 volt rated voltage is 28.6 watts. Total leakage inductance is found by shorting the 2300 volt winding while maintaining rated current. Assuming an equal split in leakage inductance between the high and low side windings results in a X_{ws} of 26.5 mΩ and a X_{wp} of 10.59 Ω. The total measured winding resistance is 68.13 mΩ and is assumed to split in roughly a 70:30 ratio between the low and high side (i.e. R_{ws} is 48.6 mΩ and R_{wp} of 7.814 Ω).

Two methods are used to determine the magnetization characteristic of the transformer. The first method uses a variable input voltage to drive the transformer into saturation and the exciting current and flux linkage are recorded. Flux linkage is calculated by integrating the voltage across the open-circuit 115 volt secondary winding. The second method records the flux linkage and inrush current that result following energization of the transformer. In order to be as accurate as possible, the voltage across the open-circuit low voltage winding is measured because it is assumed this winding is located closest to the iron-core and therefore has the best coupling with the flux in the iron [7]. Alternative methods based on direct current excitation have also been proposed in [8] but were not investigated.

Fig. 5.5 compares experimental measurements with the following polynomial approximation.

$$i_L(\lambda) = 0.02 \cdot \lambda + 0.026 \cdot \lambda^{19} \tag{5-3}$$

Because the transformer under test is tanked, there is some inherent stray capacitance-to-ground present due to the transformer bushing. The stray capacitance lowers the true value

of exciting current, which would result if the core is tested while the transformer is detanked assuming the bushing capacitance is much larger than the stray capacitance-to-ground of the winding. Some authors propose using a dual frequency test (i.e. 60 Hz and 180 Hz) to determine the actual stray capacitance [12].

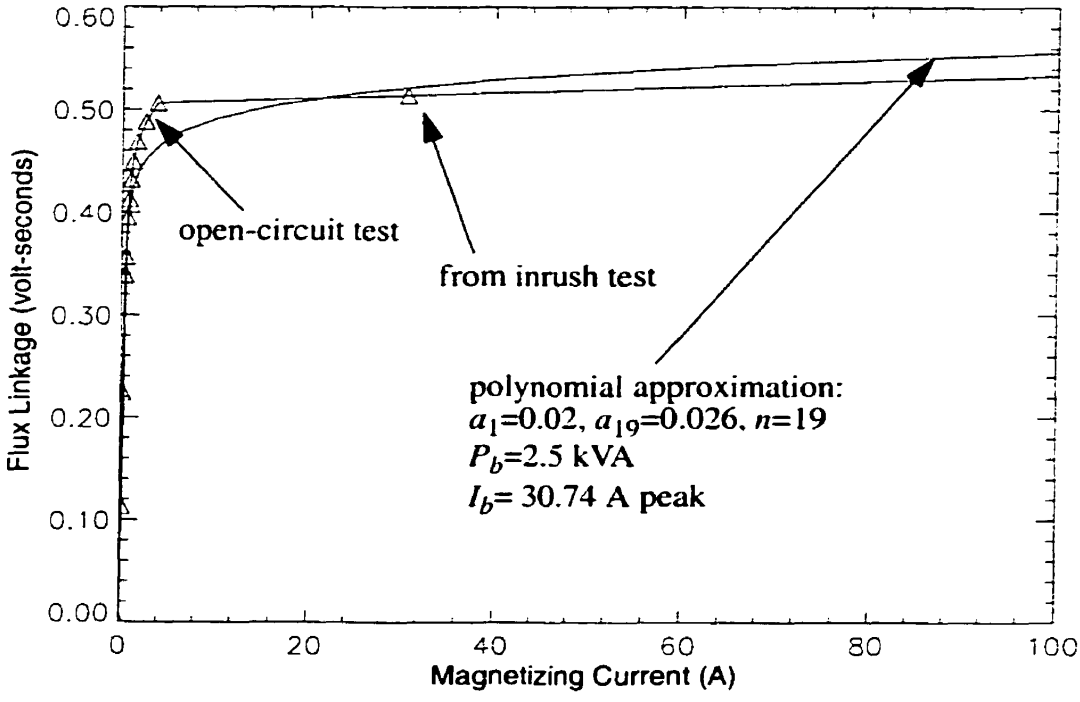

Fig. 5.5 Magnetization characteristic of 2.5 kVA distribution transformer.

5.5 COMPARISON WITH EXPERIMENTAL RESULTS

Two digital models of the iron-core loss behaviour are compared with laboratory experiments. As mentioned in Section 5.2, there are two main types of iron-core loss models. The first type uses a single-valued magnetization characteristic and a linear resistor to model the total iron-core losses. A constant linear resistance model is reasonable if hysteresis losses are considered negligible. The second type uses a nonlinear inductor with hysteresis. A linear eddy-current loss resistor is included, which represents 75% of the total iron-core losses.

Two measures of real or active power losses are used. The first measure represents the average power and is calculated by integrating the instantaneous power (i.e. $v(t)i(t)$) over one period (T). In most situations, steady-state behaviour in the positive and negative half-cycle are identical, thus even order harmonics are eliminated and average power can be calculated over a half-cycle. However, depending on the mode of ferroresonance, there is

some possibility of even harmonics, therefore integration over the full period is performed.

$$P_{average} = \frac{1}{T}\int_0^T v(t)i(t)dt \tag{5-4}$$

The presence of harmonics leads to a second measure of power, harmonic power (P_H). In the limit, the sum of the fundamental active power plus the total harmonic power is equal to the average power given by (5-4).

$$P_H = \sum_{h \neq 1} V_h I_h \cos(\theta_h) \tag{5-5}$$

5.5.1 Variable Voltage and Frequency Tests

Variable voltage and variable frequency tests are performed to enable a better understanding of transformer losses.

Fig. 5.6 compares test results and simulation results of the open-circuit variable voltage test. Both the normal saturation and hysteresis models capture the quadratic relation between iron-core losses and voltage up to 120 volts. After 120 volts, additional harmonics are being generated in the distribution transformer, which tends to decrease the measured average power.

The variable frequency test is performed by injecting current into the transformer at a specific frequency. A constant peak volts/Hz ratio of 2.25 is maintained by adjusting the magnitude of the injected current. In other words, an attempt is made to hold the core flux constant. Fig. 5.7 compares lab measurements with simulation results. Since the core is being excited with a peak voltage of 135 volts at 60 Hz (i.e. 95.45 volts rms), the equivalent hysteresis losses is 25% of 20 watts or 5 watts. As the frequency is decreased to 0 Hz, the eddy-current losses decrease quadratically to zero and the hysteresis losses decrease linearly to zero (i.e. see (4-2) and (4-3)). The lab measurements show this trend and the hysteresis model is best able to match the lab measurements. Errors between the hysteresis and eddy-current models are maximum in the 20 to 40 Hz range. At 30 Hz, the eddy-current model losses are 20% smaller than the combined hysteresis/eddy-current model losses.

Either model is adequate to reproduce measurements up to rated voltage and rated frequency. At this point, preference is given to the hysteresis model as low frequency behaviour is modelled more accurately.

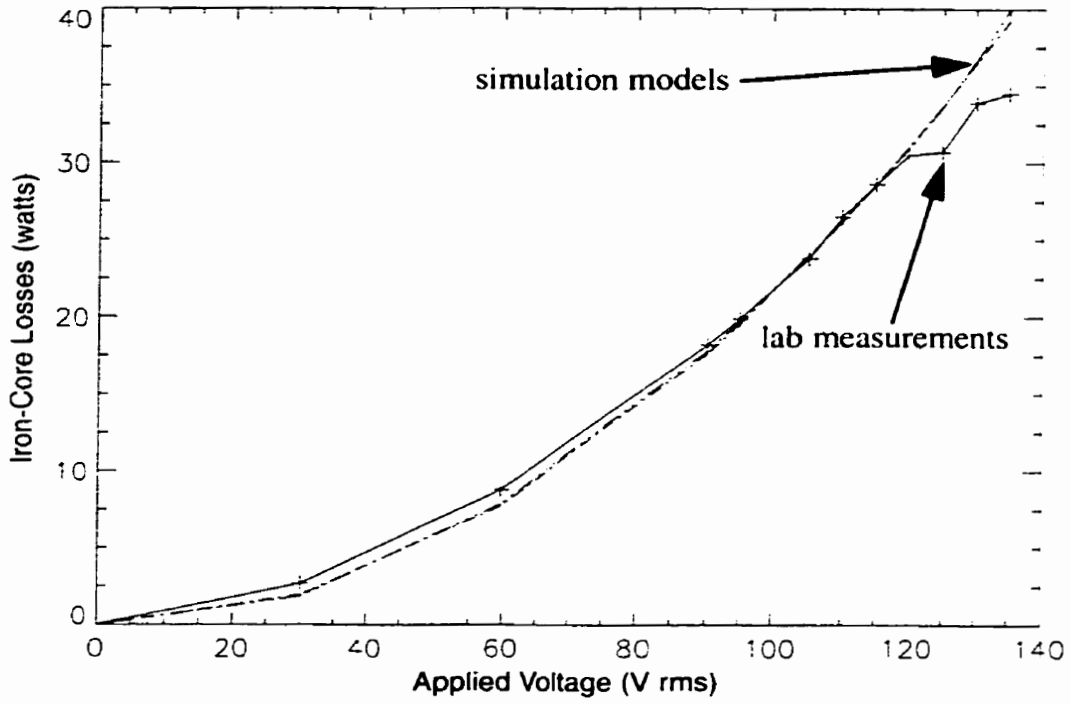

Fig. 5.6 Variable voltage open-circuit test.

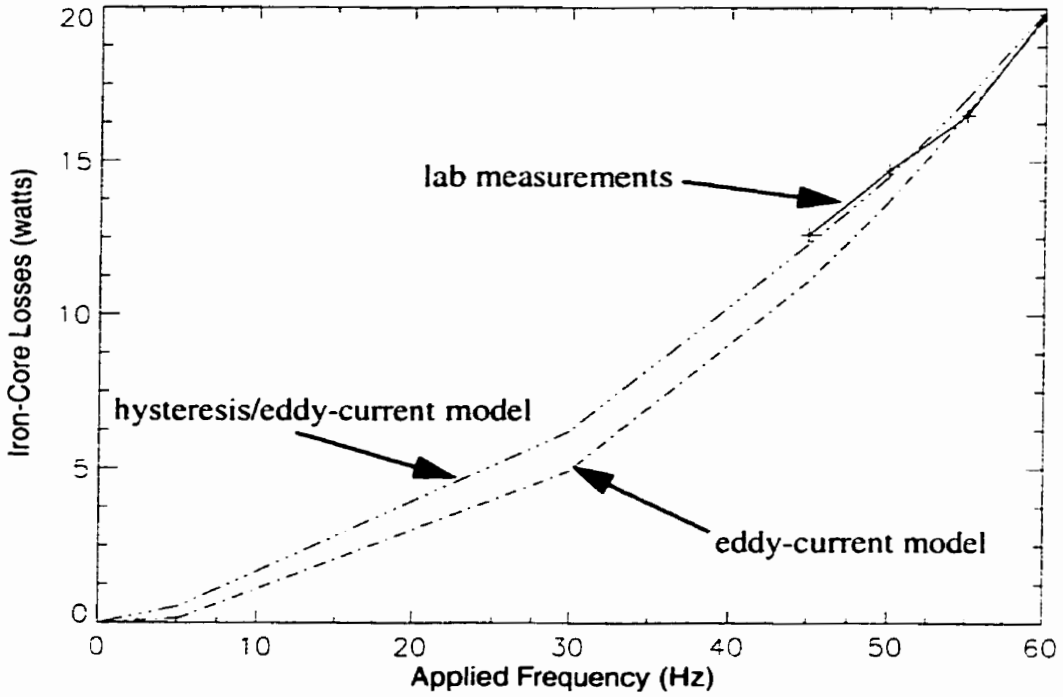

Fig. 5.7 Variable frequency open-circuit test performed while maintaining a constant 2.25 volts/Hz ratio.

5.5.2 Ferroresonance Tests

The circuit configuration used in the ferroresonance tests is shown in Fig. 5.4. Six combinations of grading capacitance and stray capacitance are tested. Five produced period-1 ferroresonance and one produced period-3 ferroresonance.

The hysteresis model is not robust. In some cases, no ferroresonance occurred where period-1 ferroresonance is expected. The simulated exciting current was too high in the hysteresis model. During extreme saturation, the slope of the magnetizing characteristic plays a large role in determining peak values of magnetizing current and bus voltage. Control over the slope in the EMTP hysteresis model is not possible. In addition, voltage oscillations were observed in the hysteresis model, which are not present in the laboratory measurements. Harmonic power produced during period-1 ferroresonance is also much higher in the hysteresis model compared with the normal saturation model. Only the single-valued magnetizing characteristic model matched the experimental results and therefore will be discussed further in this section.

Table 5.2 and Table 5.3 compare experimentally measured and simulated power losses for each tested combination of grading capacitance and stray capacitance. The results match closely for cases #4 and #6. A comparison between the experimental measurements and EMTP simulated[2] voltage and current waveforms for these two cases is presented in Fig. 5.8 and Fig. 5.9.

One notable difference between measurements and simulations is the large discrepancy in the 5^{th} harmonic power component. The simplified equivalent model of the external network is only meant to match the 60 Hz behaviour of the network. Based on the measurements, the impedance of the network and grading/stray capacitance is resonant near the fifth harmonic resulting in an increased fifth harmonic power flow. No attempt was made to modify the network model to match measurements. Detailed modelling can be achieved by analyzing the transients that result from capacitor switching, for example [10].

---

2. A listing of the EMTP data file for this case is included in Appendix B.2.

Table 5.2 Experimental Power Losses

Loss	#1: C_g/C_b 79.9/122.4	#2: C_g/C_b 79.9/183.3	#3: C_g/C_b 182.3/79.9	#4: C_g/C_b 182.3/39.7	#5: C_g/C_b 182.3/26.5	#6: C_g/C_b 39.7/182.3
P_1	250.0	270.0	445.0	420.0	422.0	15.05
P_3	-27.5	-25.0	-65.0	-60.0	-77.0	0
P_5	-30.0	-27.5	-100.0	-100.0	-111.0	0
P_7	-22.5	-25.0	-50.0	-40.0	-50.0	0
P_9	-10.0	-12.5	-35.0	-30.0	-33.0	0
P_{11}	-5.0	-10.0	-15.0	-15.0	-15.0	0
P_{13}	-5.0	-5.00	-10.0	-7.5	-5.0	0
P_{15}	-1.0	-1.50	-2.50	-2.5	-1.0	0
P_H	-101.0	-106.5	-277.50	-255.0	-292.0	0.0
P_1+P_H	150.0	163.5	167.50	165.0	130.0	15.05

Table 5.3 Simulated Power Losses

Loss	#1: C_g/C_b 79.9/122.4	#2: C_g/C_b 79.9/183.3	#3: C_g/C_b 182.3/79.9	#4: C_g/C_b 182.3/39.7	#5: C_g/C_b 182.3/26.5	#6: C_g/C_b 39.7/182.3
P_1	241.3	251.2	410.6	411.0	413.1	15.2
P_3	-8.5	-13.1	-59.9	-59.6	-59.4	0
P_5	-7.1	-10.5	-48.3	-47.1	-48.2	0
P_7	-5.6	-7.5	-35.4	-33.3	-35.6	0
P_9	-4.0	-4.7	-23.6	-21.0	-24.0	0
P_{11}	-2.7	-2.5	-14.3	-11.8	-14.9	0
P_{13}	-1.8	-1.2	-8.0	-5.9	-8.5	0
P_{15}	-1.1	-0.5	-4.1	-2.8	-4.4	0
P_{17}	-0.6	-0.2	-2.0	-1.3	-2.1	0
P_{19}	-0.4	-0.1	-0.9	-0.7	-0.8	0
P_H	-31.9	-40.2	-196.6	-183.50	-197.8	0.0
P_1+P_H	209.4	211.0	214.0	227.5	215.3	15.2
$P_{average}$	200.0	203.4	214.4	214.2	214.4	15.2

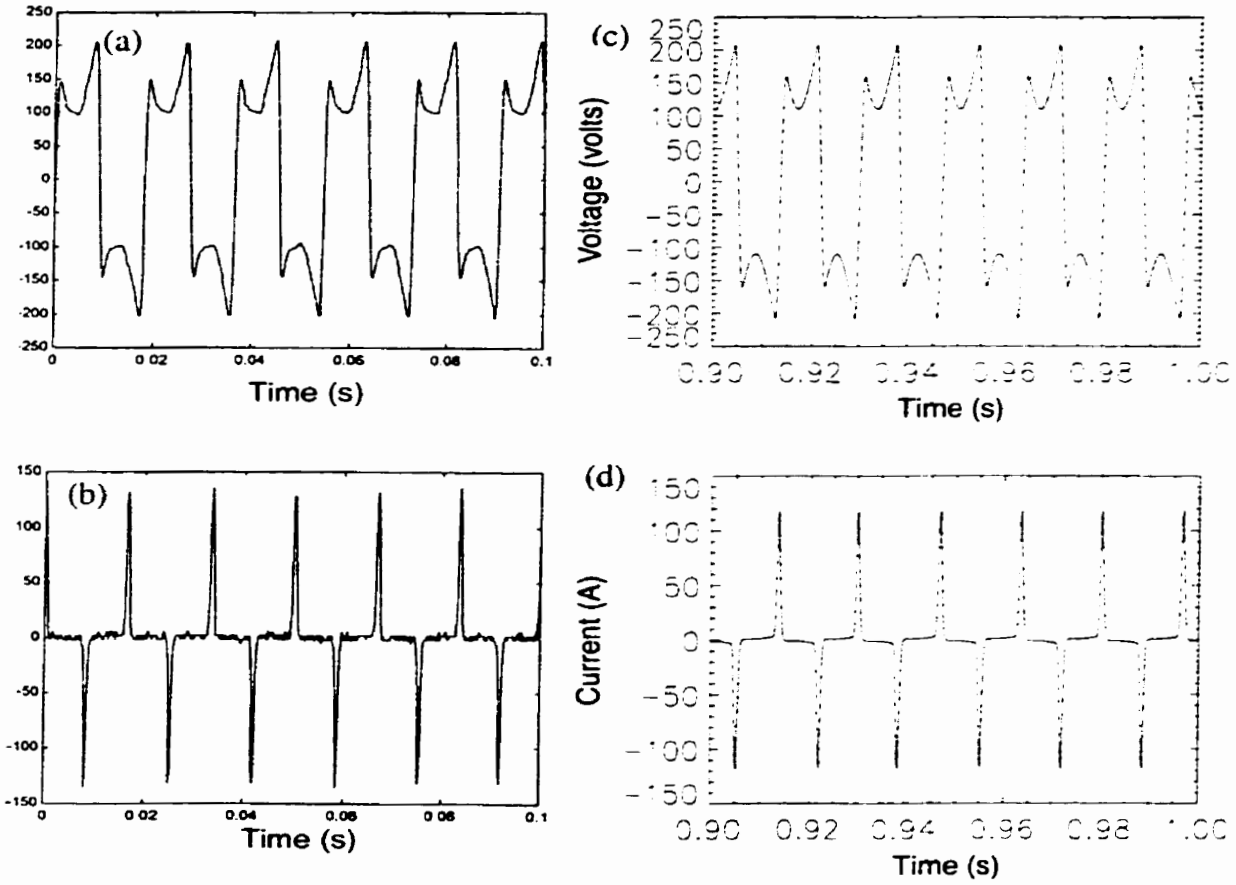

Fig. 5.8 Comparison of period-1 ferroresonance with C_s=182.3 μF and C_b=39.7 μF showing (a) experimental voltage [9], (b) experimental current [9], (c) simulated voltage, (d) simulated current.

The subharmonic case is difficult to produce in the lab as well as in simulations. The grading capacitor was switched in and out of the circuit several times before the correct set of initial conditions resulted in a period-3 attractor. The phase of the simulated voltage appears to be 180 degrees out-of-phase with the measured voltage. Multiple subharmonic attractors are expected that have the same magnitude but varying phase[3]. In addition, the iron-core loss model required adjustment. The next section discusses the iron-core loss model changes in more detail.

3. Section 3.4 describes the calculation of subharmonic oscillations in detail.

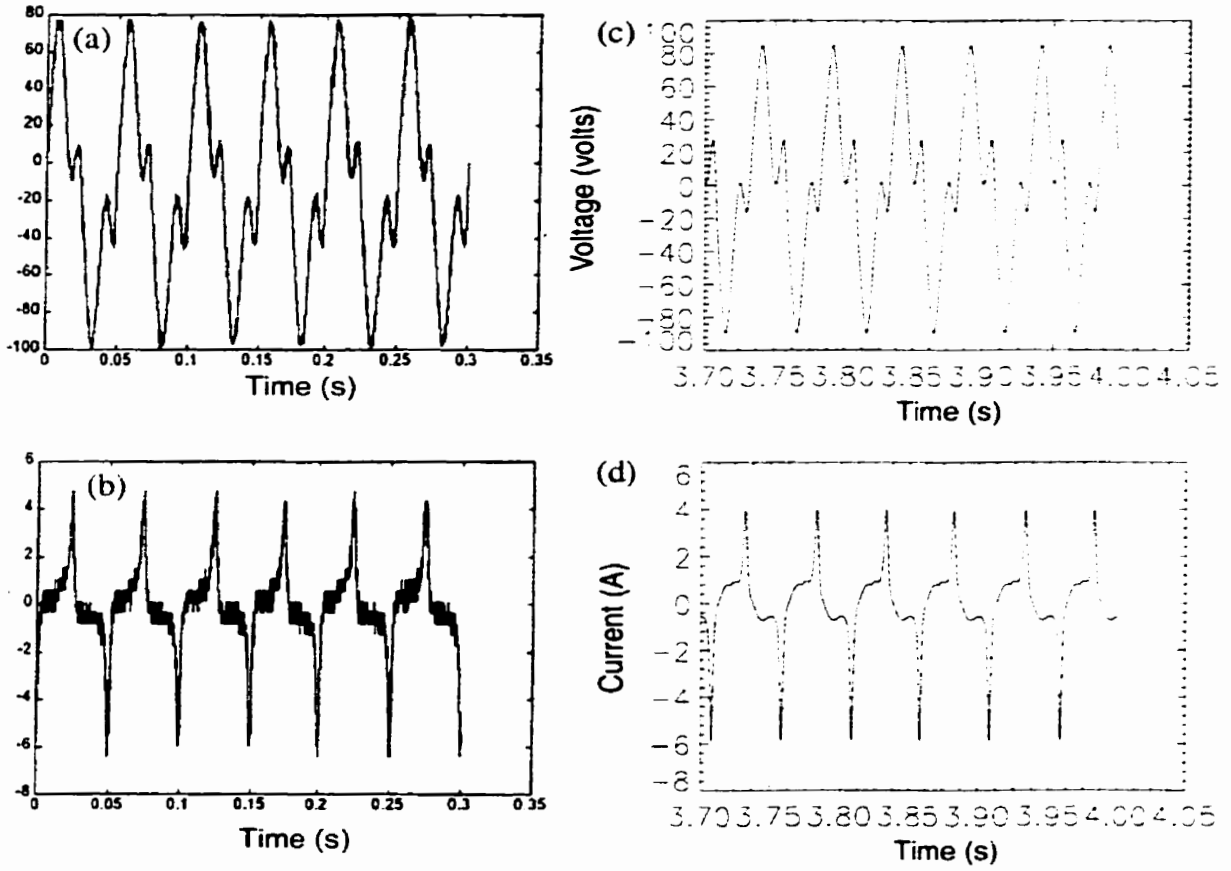

Fig. 5.9 Comparison of subharmonic ferroresonance with C_s=39.7 μF and C_b=182.3 μF showing (a) experimental voltage [9], (b) experimental current [9], (c) simulated voltage, (d) simulated current.

5.5.3 Modified Transformer Iron-Core Loss Model

In order to match power measurements, the iron-core loss model requires modification. Table 5.4 compares the results of six different loss models.

In order to match the measured 60 Hz power losses during ferroresonance, the eddy-current loss resistor must be reduced by a factor of five (i.e. case (e) in Table 5.4). Increasing the series winding resistance by 0.23 ohms (i.e. case (f) in Table 5.4) also enables the 60 Hz power losses to be matched; however, the harmonic losses double in size. Because the transformer behaves like a harmonic current source, any additional series resistance will result in higher harmonic power losses. Since these additional harmonic power losses are not observed, it is concluded that the switched eddy-current loss resistor model is the best representation of the loss behaviour of the distribution transformer during period-1 ferroresonance.

Table 5.4 Modified Transformer Loss Models for Case 4

Loss	(a) base P_{ec}=28.6	(b) 2xP_{ec}	(c) 3xP_{ec}	(d) 4xP_{ec}	(e) *** 5xP_{ec}	(f) add 0.23 Ω to R_w
P_1	232.0	298.0	338.5	370.0	411.0	408.5
P_3	-79.2	-59.3	-58.9	-62.2	-59.6	-129.0
P_5	-61.4	-48.4	-48.0	-48.8	-47.1	-98.3
P_7	-42.4	-36.1	-35.8	-34.3	-33.3	-65.9
P_9	-26.4	-24.4	-24.4	-21.8	-21.0	-38.7
P_{11}	-15.0	-15.0	-15.3	-12.7	-11.8	-20.2
P_{13}	-7.9	-8.5	-8.8	-6.9	-5.9	-9.7
P_{15}	-3.9	-4.5	-4.6	-3.6	-2.8	-4.9
P_{17}	-1.8	-2.4	-2.2	-1.9	-1.3	-2.8
P_{19}	-0.7	-1.2	-0.9	-0.9	-0.7	-1.8
P_H	-238.7	-199.7	-199.0	-193.2	-183.50	-371.3
P_1+P_H	-6.9	98.3	139.5	176.8	227.5	37.2
$P_{average}$	43.0	86.0	128.9	171.6	214.2	43.9

The increased losses observed during period-1 ferroresonance in the laboratory distribution transformer are attributed to increased stray 60 Hz eddy-current losses in the tank and other core components and not to high frequency eddy-current losses in the iron-core. Frequency dependent eddy-current loss models have been proposed to increase the accuracy of modelling transients in the tens of kHz range [11]. Below 3 kHz, the conventional linear model is accurate to within 5% [11].

Shortly after the switch opens to insert the grading capacitance, an additional linear eddy-current loss resistor is switched on in parallel with the existing linear iron-core loss resistor. The resistance is inserted during the transition from nonferroresonance to ferroresonance.

Similar modifications were made to the iron-core loss model, in order to match the period-3 subharmonic case produced in the laboratory. In this case, the eddy-current losses were increased by a factor of three.

5.6 EXTENSION OF RESULTS TO STABILITY DOMAINS

Based on the experimental results of this chapter, it is prudent to re-evaluate the period-1 stability domain calculations. For example, Fig. 4.11 was calculated assuming a single 3.11 MΩ linear resistor represents the iron-core losses. During period-1 ferroresonance, stray eddy-current losses become significant. The stability domain boundaries are recalculated assuming a new iron-core loss resistor value of 0.622 MΩ (field measurements on the actual transformer are recommended to verify this assumption). The left-hand side stability boundary shifts significantly to the right as a result of the five-fold increase in iron-core losses.

Fig. 5.10 indicates new assessments of the level of risk of ferroresonance. The low risk area is bounded by two curves. The left-most curve assumes a base amount of iron-core losses while the other assumes a five-fold increase in iron-core losses. There is a finite probability of subharmonic states existing in this region; however, the average power loss of a subharmonic ferroresonance mode is generally less than the transformer's rated iron-core losses and therefore poses no concern to overheating. If the increase in iron-core losses is made artificially by loading resistors (see Section 4.5), the low risk region becomes a no risk region.

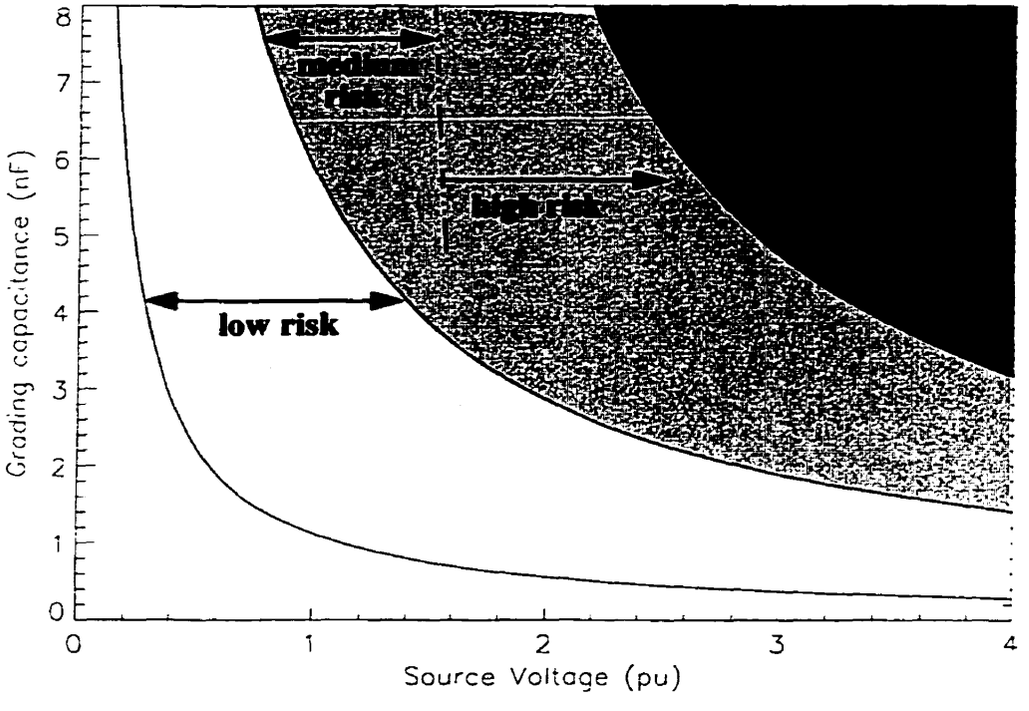

Fig. 5.10 Revised period-1 stability domain boundary locations after the inclusion of a five-fold increase in eddy-current losses.

5.7 SUMMARY

An experimental investigation of the iron-core loss behaviour in a distribution transformer has been completed. Comparisons are made between laboratory measurements and two digital models of the iron-core losses.

Either a pure eddy-current loss model or a mixed hysteresis/eddy-current loss model is able to adequately represent the iron-core losses up to rated voltage and rated frequency. Preference is given to the mixed form if the damping of subharmonics is to be modelled accurately.

During period-1 ferroresonance, the pure eddy-current loss model is able to match the steady-state shape of the voltage and current waveforms. In order to match fundamental frequency losses, the linear iron-core loss resistance must be decreased by a factor of five. Average power loss recordings do not give an accurate indication of the performance of iron-core loss models due to the high level of harmonic distortion. Harmonic power measurements are required to get a complete picture of the model's performance.

Control over the air-core reactance is essential to matching laboratory measurements. The hysteresis model available in EMTP does not allow adequate control over the shape of the magnetizing characteristic during extreme saturation.

Revised stability domain boundary calculations are made assuming high voltage transformers will also experience a five-fold increase in iron-core losses during period-1 ferroresonance.

Further work is recommended to investigate the iron-core losses during the transient phase of ferroresonance to determine whether a simple switched eddy-current loss resistor is sufficient or whether a nonlinear relation exists between flux linkage, frequency and the effective resistance of the eddy-current loss resistor. Different types and sizes of transformers should be studied as part of the investigation.

5.8 REFERENCES

[1] Westinghouse, *Electrical Transmission and Distribution Reference Book: 4th Edition*, Westinghouse Electric Corporation, pp. 126, September 1950.

[2] Kennedy, B.W., *Energy Efficient Transformers*, McGraw-Hill:New York, pp. 30-37, 1998.

[3] Swift, G.W.,"Power Transformer Core Behavior Under Transient Conditions", *IEEE Trans. on Power Apparatus and Systems*, Vol. PAS-90, No. 5, pp. 2206-2210, September/October 1971.

[4] Beckley, P.,"Modern Steels for Transformers and Machines", *Power Engineering Journal*, pp. 190-200, August 1999.

[5] Liorzou, F., Phelps, B., and Atherton, D.L.,"Macroscopic Models of Magnetization", *IEEE Transactions on Magnetics*, vol. 36, no. 2, pp. 418-428, March 2000.

[6] de León, F., and Semlyen, A.,"A Simple Representation of Dynamic Hysteresis Losses in Power Transformers", *IEEE Transactions on Power Delivery*, vol. 10 no. 1, pp. 315-312, January 1995.

[7] Koreman, C.G.A.,"Determination of the Magnetizing Characteristic of Three-Phase Transformers in Field Tests", *IEEE Trans. on Power Delivery*, vol. 4, no. 3, pp. 1779-1785, July 1989.

[8] Calabro, S., Coppadoro, F., and Crepaz, S.,"The Measurement of the Magnetization Characteristics of Large Power Transformers and Reactors Through DC Excitation", *IEEE Trans. on Power Delivery*, vol. 1, no. 4, pp. 224-234, October 1986.

[9] Magalhaes, M., *Measurement and Modelling of Distribution Transformer Losses During Sub-harmonic and Fundamental Frequency Modes of Ferroresonance*, B.Sc. Thesis, University of Manitoba, March 10, 2000.

[10] Morched, A.S., and Kundur, P.,"Identification and Modelling of Load Characteristics at High Frequencies", *IEEE Transactions on Power Systems*, Vol. 2, No. 1, pp. 153-160, February 1987.

[11] Tarasiewicz, E.J., Morched, A.S., Narang, A., and Dick, E.P.,"Frequency Dependent Eddy-Current Models for Nonlinear Iron Cores", *IEEE Trans. on Power App. and Systems*, Vol. 8, No. 2 pp.588-597, May 1993.

[12] Malewski, R., Train, D., and Kosztaluk, R., "Measurments of Iron Losses in Large Power Transformers", *CIGRE*, paper 12-01, 1988.

Chapter 6

Transformer-Terminated Double-Circuit Transmission Lines

6.1 INTRODUCTION

At system voltages at or above 66 kV, the most prevalent circuit configuration prone to ferroresonance occurs between circuit breaker grading capacitors and wound potential transformers. Another possible ferroresonant circuit occurs when a transformer is connected to a de-energized transmission line that is capacitively coupled with a parallel energized line. Manitoba Hydro's Ashern to Rosser transmission line (A3R) is a typical example and was investigated for the possibility of ferroresonance occurring in the transformers located in Silver station.

6.2 LITERATURE REVIEW

An extensive literature survey covering the last 90 years turned up over 100 papers discussing some aspect of ferroresonance. Of those papers, only 10 make reference to problems occurring in double-, or multiple-circuit lines having a transformer termination. These ten papers only report on four different occurrences of ferroresonance. Details of each configuration are discussed below.

Recently, Ontario Hydro reported on examples of ferroresonance occurring in their Dual Element Source Network (DESN) stations [A126], [A91]. On occurrence of a fault, the faulted circuit-transformer combination is disconnected. This system achieves high reliability by providing continuous voltage to the load during the disturbance. However, the close coupling of parallel circuits with similar or higher voltage increases the risk of ferroresonance in the disconnected transformer. An example is shown where 59 km of parallel 230 kV and 32 km of parallel 500 kV transmission were sufficient to cause ferroresonance in a 230-115 kV transformer [A91]. The problem was mitigated by installing a resistor (267 kW/phase) in the tertiary of the transformer.

Electricité de France (EDF) have reported on experiences with their 400 kV network

[A78], [A80]. Approximately 80% of the transmission lines in their 400 kV network are constructed with two circuits on a common support. It is quite common to tap one of these lines in order to supply power to local loads. Ferroresonance has been reported following uneven breaker pole operation (i.e. stuck breaker during single-pole switching operations). An example of a 113 km double-circuit 400 kV transmission line with a 150 MVA transformer tapped off one line is discussed in [A78], [A80]. The solution proposed in [A78] was to detect ferroresonance by using overvoltage and voltage distortion measuring devices and then to eliminate the situation by short-circuiting the secondary of the transformer to ground.

Some examples from Britain are given in [A55] and [A48]. These examples are slightly different because one of the double-circuit lines is not tapped. Instead, the lines are terminated by one or two step-down transformers. The normal practice is to drop the line-transformer combination because a disconnect switch rather than a circuit breaker is installed between the line and transformer. The simulation results for a 45 km, 400 kV double-circuit line terminating in a 1000 MVA transformer is described in [A55] while field observations of a 150 km, 400 kV double-circuit line terminating in a 500 MVA transformer are reported in [A48]. German and Davies [A48] observe that the length of the coupling tends to influence the type of oscillations observed. Very short lines (i.e. less than 20 km) do not experience ferroresonance. Period-1 ferroresonance is prevalent for medium length lines while subharmonic (period-3) oscillations dominate long lines (i.e. >150 km). Diseko *et al.* [A55] notices the zero sequence impedance of the transformer is a critical parameter in determining the probability of ferroresonance.

The first reported occurrence of ferroresonance in a transformer caused by capacitive coupling with a parallel energized line was at the Big Eddy Station of Bonneville Power Administration (BPA) in the U.S.[A35]. This incident was further analyzed by Wale [A38]. The circuit consisted of 31 km of parallel 525 kV circuits. One circuit was terminated by a 1000 MVA 525-241.5 kV autotransformer. Ferroresonance (period-1) lasted for 16-22 minutes in phase C but did not cause any damage to the transformer. Subsequent measurements showed the magnetizing current in phase C was 30% lower than phases A and B. Both period-1 and period-3 ferroresonance were observed in field tests. The problem was solved by closing the delta connected tertiary (i.e. the winding was originally open-delta). The coupled voltages were mainly composed of zero sequence components. The authors postulated that ferroresonance could be eliminated if the zero sequence impedance of the bank could be reduced. Field tests confirmed their hypothesis.

In summary, transformers can ferroresonate when connected to an open transmission line that is capacitively coupled to an energized line. The phenomenon has not been well studied. It is assumed at least 10 to 20 km of parallel high voltage transmission lines (i.e. 115 kV or greater) coupled with an unloaded transformer is necessary before ferroresonance can be initiated. The literature indicates ferroresonance will be excited only for a narrow band of initial conditions. Hence, the probability is low even if the configuration is of high risk.

In order to avoid any surprises at Manitoba Hydro, a search for candidate 230 kV configurations that might be susceptible to this form of ferroresonance was made. To date, Manitoba Hydro has three parallel circuit lines with lengths in excess of 10-20 km. The lines are A3R/A4D (200 km), G1A/G2A (234 km) and K21W/K22W (129 km). All three examples are single circuit lines constructed in the same right-of-way. The configuration chosen for further study was A3R/A4D since line A3R is the only one that is tapped.

6.3 SYSTEM DESCRIPTION

A single-line diagram representing the studied system is given in Fig. 6.1.

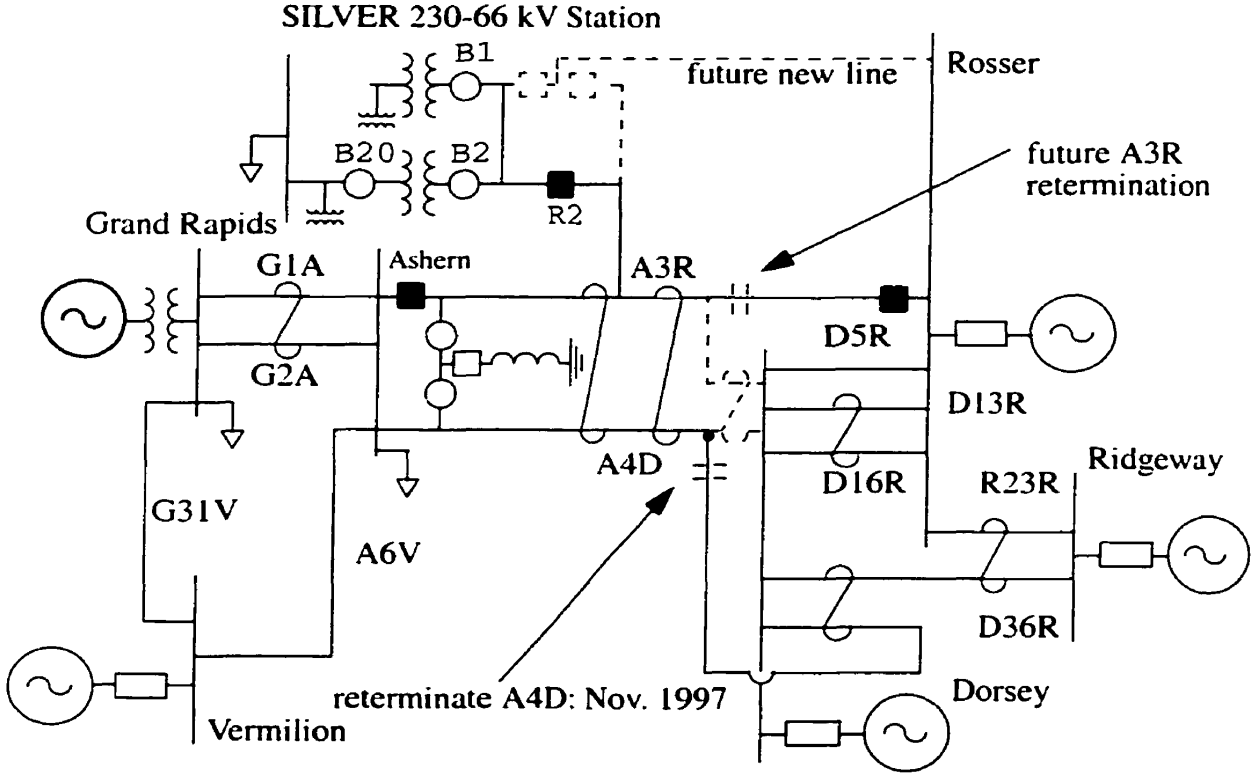

Fig. 6.1 Silver 230 kV EMTP model single-line diagram.

Based on the literature review, the Silver 230-66 kV transformer may be susceptible to ferroresonance if it is unloaded and remains connected to the de-energized line A3R. Manual clearing or energization procedures currently in place will not place the Silver transformers and line A3R in a configuration that is susceptible to ferroresonance.

In order for the Silver transformer to remain connected to the de-energized 230 kV line, two scenarios have been identified:

- automatic clearing of 230 kV line A3R, and
- automatic clearing of Silver Station.

Each scenario will be described in more detail.

6.3.1 Automatic Clearing of Faults on 230 kV line A3R

A fault on the 230 kV transmission line (A3R) will be detected by impedance relays and cleared by opening breakers at Rosser and Ashern. Breaker R2 at Silver is not equipped with line protection or communication and therefore will not open automatically.

The 66 kV breakers will open via an undervoltage relay after 200 milliseconds assuming the 66 kV is not networked (normal case). The purpose of sectionalizing the 66 kV bus automatically following undervoltages is to avoid the pickup of full station load current in addition to transformer inrush current following re-energization of line A3R.

Fig. 6.2 indicates the normal clearing sequence for line disturbances assuming the 230 kV circuit breakers have a 3 cycle clearing time and the 66 kV breakers have a 5 cycle clearing time.

Ferroresonance may develop if the transformer is unloaded. During a recent winter storm, crossarms were damaged on both 66 kV feeders leaving Silver resulting in a three hour outage. If the 230 kV line A3R had also tripped during the storm, the Silver transformers may have gone into ferroresonance and remained undetected.

There is some probability that the resulting ferroresonance condition will be removed automatically, either by an existing overvoltage or a neutral overcurrent relay.

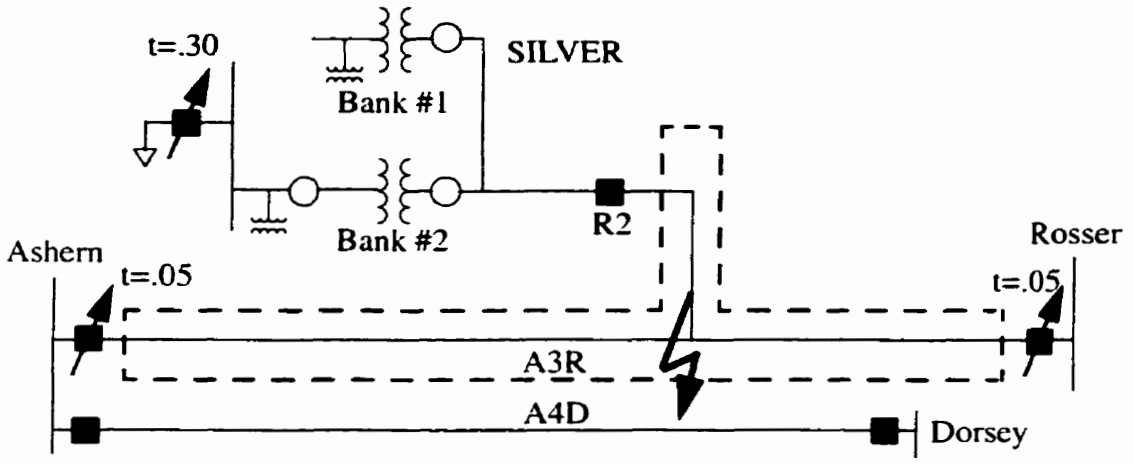

Fig. 6.2 Breaker timing for normal clearing of A3R.

An overvoltage relay on the 230 kV bus at Silver will trip breaker R2 if the voltage is greater than 112% for more than one second. The time delay is set high enough to avoid tripping due to temporary overvoltages caused by HVdc reductions. The purpose of the relay is to protect the bank in the event the 66 kV load is networked and A3R becomes isolated.

Breaker R2 will open by neutral overcurrent protection if a single line-to-ground fault on the 230 kV line A3R is not cleared. The neutral overcurrent relay is configured with a standard inverse characteristic curve and a 0.3 time multiplier setting. Equation 6-1[1] relates the neutral current to the relay operation time.

$$T = \frac{0.042}{\left(\frac{I_N}{97.5}\right)^{0.02} - 1} \tag{6-1}$$

For example, a neutral current of 2000 amperes results in a relay operation time of 0.67 seconds.

A ferroresonance condition resulting in voltages in excess of 112% or excessive neutral current will trip breaker R2, effectively eliminating any risks of damage.

---

1. The equation comes from the data sheets for a GEC MCGG overcurrent relay. The 97.5 A neutral current setting on the Ct primary is specific for the Silver transformer.

6.3.2 Automatic Clearing of Silver Station Faults

Internal fault detection for the transformers at the Silver station is provided by fast gas, pressure relief, temperature and differential relays. These relays trip and lockout breaker R2 and the 66 kV breakers. Normal clearing of Silver station disturbances will not result in a configuration that is prone to ferroresonance.

In the event one or more phases of R2 fail to open (e.g. loss of gas pressure), line A3R will trip as a backup (i.e. by zone 2 protection after a 250 msec. delay). Because the bank is unloaded before A3R trips, there is a risk of ferroresonance. The concern with this disturbance is that ferroresonance will not be removed by automatic protection. Existing overvoltage or neutral overcurrent relays may operate; however, the failed phases of breaker R2 cannot be opened.

Some possible alternatives that are available to remove this condition are:

- reclose circuit breaker at Rosser or Ashern,
- trip line A4D,
- install transformer loading resistors,
- permanently connect a line reactor to A3R,
- switch the existing line reactor onto A3R.

There is a risk that a reclose at Ashern or Rosser will not be successful if a permanent fault exists in the Silver station. Tripping line A4D is possible; however, this results in a double-circuit outage, which can have stability implications.

The use of switched [A91] or permanently connected [A127] loading resistors is sometimes the only feasible method that can be used to prevent ferroresonance. However, the method is costly and should be avoided if other techniques are available.

The existing line reactor cannot be connected permanently to A3R because it reduces operating flexibility. A new line reactor (e.g. 25 MVAr) could be connected to A3R, but this is costly. Temporarily switching the existing line reactor onto A3R to remove a ferroresonant condition is feasible if the reactor is available and inserted quickly.

Field tests and further analysis in later sections will address the concerns for ferroresonance posed by this circuit configuration.

6.4 FIELD TESTING

Tests were conducted on July 4, 1997, to assess the risk of ferroresonance occurring at Silver station. Preliminary EMTP studies showed a risk of ferroresonance if the line A3R trips and one or two unloaded transformers are connected at Silver. Controlled field tests were used to verify the accuracy of the EMTP model. Once the EMTP model is validated, simulations can be confidently carried out to design the appropriate mitigating procedures, if the risk of ferroresonance is verified. As well, the effectiveness of the Silver transformer's neutral current protection and overvoltage protection under distorted conditions had to be tested.

6.4.1 System Monitoring Setup

Recording instruments were installed in Ashern and Silver stations on July 4, 1997. The monitored potential and current transformers are indicated in Fig. 6.3.

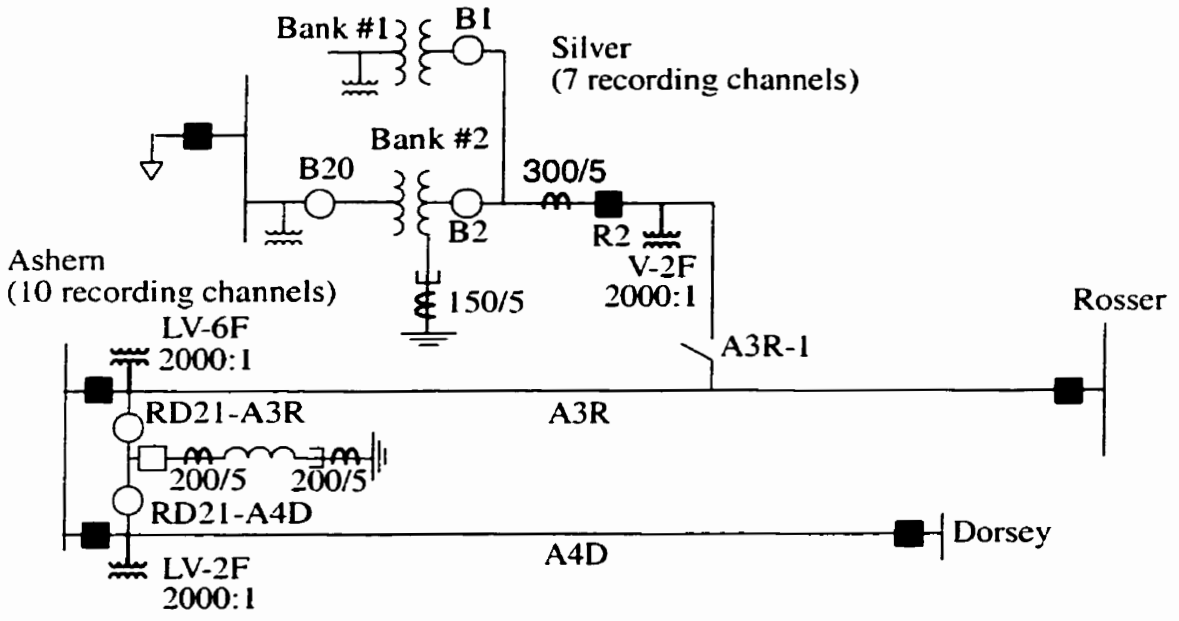

Fig. 6.3 Locations of monitored potential and current transformers used in Silver ferroresonance tests.

6.4.2 Summary of Field Tests

Several switching events were performed to determine if ferroresonance could be excited under controlled conditions. Tripping line A3R without the Ashern reactor connected could not be tested because the open-ended line voltage exceeds the steady-state rating of

line-end equipment.

The complete test procedure is given in Manitoba Hydro Operation Order No. 97-4834.

Prior to the tests, the following conditions were checked:

- ensure Ashern 230 kV ring is intact,
- ensure Rosser 230 kV ring is intact,
- ensure Ashern reactor connected to A3R (reactor disconnect RD21-A4D in open position),
- system o.k. for loss of reactor,
- all Silver 66 kV load transferred to alternative supply,
- Silver station service transferred to alternative supply.

Each test will briefly be described.

Test #1: 8:55 AM

Line A3R was tripped by first opening Ashern breakers R6 and R7 and then Rosser breakers R9 and R10 minutes later. This is the preferred manual de-energization procedure as the reactor at Ashern is used to hold the open-ended line voltage below 1.065 pu.

Prior to the line de-energization, motor operated disconnects B1 and B20 were opened (note: disconnects are rated for interrupting magnetizing current). Simulations have shown that there is a risk of ferroresonance occurring in the Silver transformers following the trip of line A3R. All 66 kV equipment (e.g. potential transformers) were removed in order to avoid any possible risks of damage.

The trapped charge on the line was dissipated through the Ashern reactor in three seconds. The frequency of the line discharge oscillations was 56 Hz. During the discharge, a 240 kV (1.27 pu) transient voltage appeared at the terminals of the Silver transformer without significantly saturating the core. No ferroresonance occurred.

Test #2: 9:40 AM

Test #1 was repeated with near simultaneous tripping of line A3R. It was assumed that

near simultaneous opening would be a more severe kick, which may excite ferroresonance. However, again no ferroresonance was observed. The discharge transients were similar to those in Test #1.

Field traces for Test #2 are shown in Fig. 6.4.

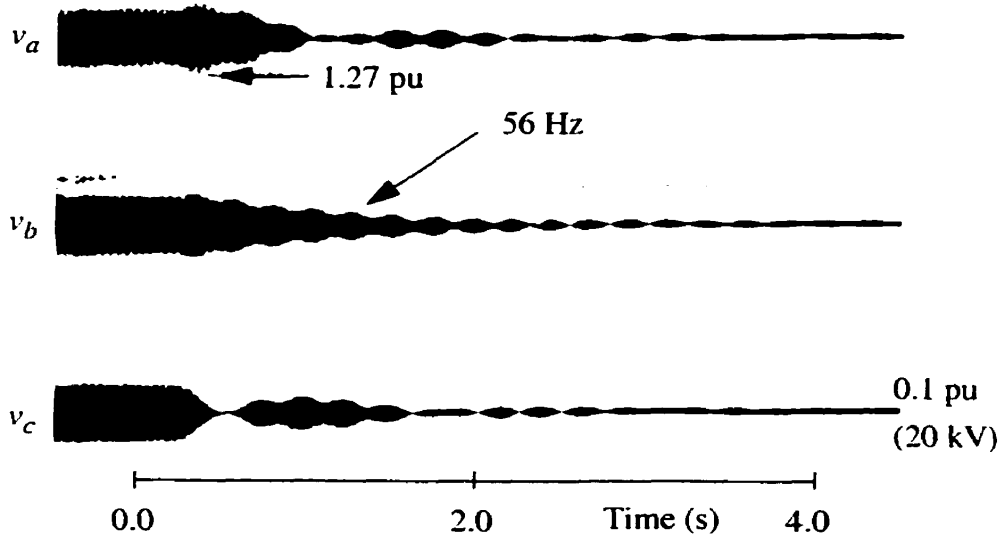

Fig. 6.4 Field Test #2: trip A3R with reactor and one transformer at Silver.

Test #3: 10:40 AM

With line A3R out-of-service, disconnect B1 was closed thus energizing Silver transformer bank #1.

Test #4: 10:45 AM

The Ashern reactor circuit switcher RD21 was opened. Simulations showed there was some probability of ferroresonance occurring. Low frequency discharge transients were observed but were highly damped and did not develop into sustained ferroresonance.

Test #5: 11:00 AM

The reactor was re-energized and Test #4 was repeated. Monitoring equipment was adjusted to better capture the discharge transients.

Fig. 6.5 represents the transients following de-energization of the Ashern reactor. Prior to the reactor circuit switcher opening, line A3R was open. The high coupled voltage (i.e. 20 kV) is due to parallel line resonance[2] [4], [5] between the reactor and line charging capacitance. After the reactor is removed, the coupled voltage reduces to 3.2 kV.

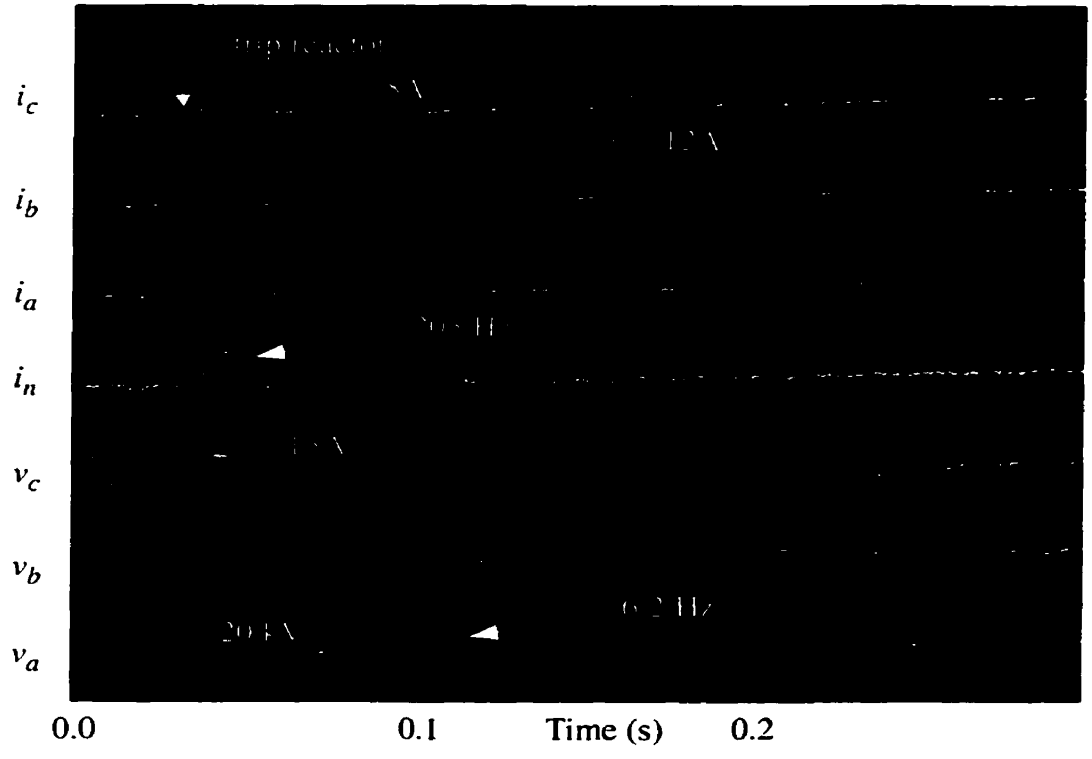

Fig. 6.5 Field test #5: reactor switching.

Test #6: 11:12 AM

With the reactor remaining de-energized, motor operated disconnect B2 was opened. This de-energized Silver bank #2.

Test #7: 11:15 AM

The final test was the trip of Silver Bank #1 via opening of 230 kV breaker R2.

After the completion of test #7 the system was returned to its original state.

---

2. For additional information on parallel line resonance refer to Section 6.10.

At no time during the tests did the Silver transformers go into ferroresonance. Sufficient information is contained in tests #2 and #5 for benchmarking the EMTP model.

The next sections will describe the various EMTP model components and refinements required to match field recordings.

6.5 EMTP MODEL DEVELOPMENT

An EMTP model of the Silver 230-66 kV station and the surrounding Manitoba Hydro 230 kV network was created. Details of the modelling techniques of various components follow.

6.5.1 Source Equivalents

Normally, ideal or constant voltage sources are used in creating the source equivalents in an EMTP model. However, in the case of ferroresonance, long duration simulations are often required (i.e. more than 5 seconds) in order to reach steady state. The inertial effects of generators can greatly influence transients in this case. Some simulations using the commercial stability program PSS/E (Power System Simulator for Engineering) were conducted to determine if a dynamic source model was required.

Fig. 6.6 shows the effect of tripping the Ashern to Rosser (A3R) transmission line following a four cycle 1-phase fault applied at Ashern. The key feature to note is the EMTP model using only Thévenin equivalents understates the increase in power flow on the Ashern to Dorsey (A4D) transmission line and the voltage drop at Ashern.

By replacing the equivalent at Grand Rapids with a representation of the generators, a closer comparison can be made between the PSS/E case and the EMTP case. It should be noted that the oscillations are not as damped in the EMTP dynamic case because the exciter and governor at Grand Rapids were not modelled. The increased complexity was not considered necessary for this study.

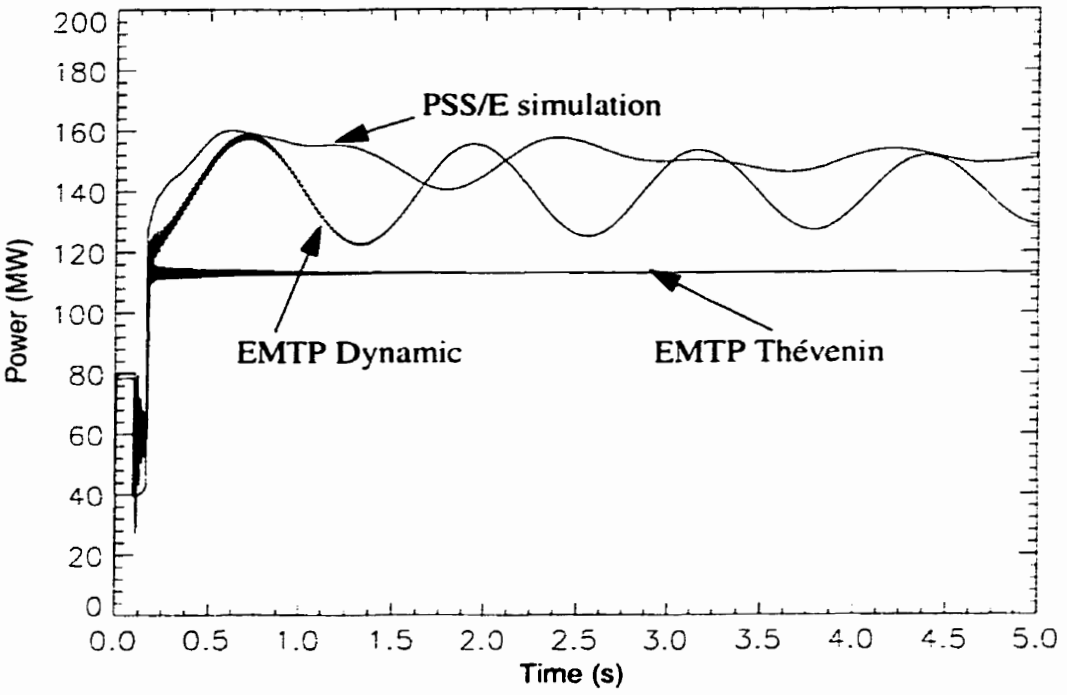

Fig. 6.6 EMTP and PSS/E case comparison of a 4 cycle 1-phase fault at Ashern followed by trip of transmission line A3R.

The worst case scenario for ferroresonance occurs when the transformer is lightly loaded or unloaded. Manitoba Hydro's daily summary load measurement database was consulted to determine what the typical minimum loading of the Silver transformer has been over the last two years and what the absolute minimum has been. The typical summer minimum is 9 MW and occurs in the months of June and July. The absolute minimum loading recorded was 4 MW and occurred July 27, 1995. A typical 1997 summer minimum load flow was setup and the load at Silver was adjusted accordingly.

6.5.2 Transmission Line Model

The transmission lines included in the model are indicated in Fig. 6.1. The critical lines to be modelled are A3R, A4D and the Silver tap. Frequency dependent line models are necessary if accurate transient recovery voltages are to be calculated or if a broad spectrum of transients are expected. Based on previous research, periodic signals based on 60 Hz or subharmonics of 60 Hz are expected, however, there is always the possibility of quasi-periodic or chaotic signals being excited. A frequency dependent line model was used as it is more accurate for signals that deviate widely from 60 Hz.

The transposition scheme must be explicitly modelled. Transpositions in each circuit have the effect of balancing the phase-to-neutral capacitance and phase inductance between each phase over the entire transposition cycle. By transposing phases in a double-circuit line at the same locations, the positive sequence coupling between circuits can be reduced. A pictorial representation of the A3R/A4D transposition scheme and conductor configuration is shown below in Fig. 6.7. The average separation between the two transmission lines A3R and A4D is 28.26 meters.

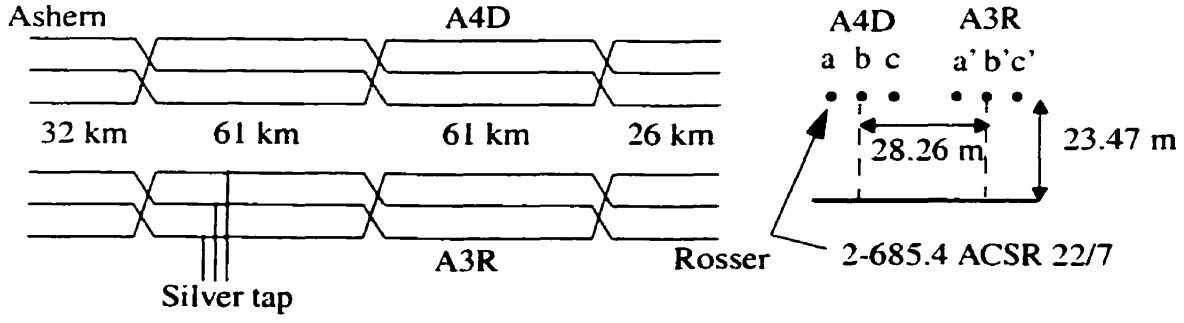

Fig. 6.7 A3R/A4D transposition locations and tower configuration.

The transmission line model affects coupled voltages and discharge transients. A comparison of steady-state coupled voltages on de-energized line A3R is made between field tests and the EMTP model and is summarized in Table 6.1.

Table 6.1 Coupled Voltage Comparisons

Case	Test #5 (kV peak)	EMTP Model (kV peak)
Reactor	18.7 ±1.5	29 ±2.0
No Reactor	3.2 ±0.4	2.8 ±0.4

The coupled voltages without the reactor connected to line A3R are very close. The EMTP model predicts higher voltages when the reactor is connected. The problem with duplicating the coupled voltages in this case is the reactor and line charging are near a 60 Hz resonance condition. A small change in line capacitance (e.g. 5%) can result in a 100% change in coupled voltage. Fig. 6.8 (repeat of Fig. 6.21) shows calculated induced voltages as a function of reactor MVAr. Given the reactor MVAr is comparable between the two models, the difference in coupled voltages indicates the EMTP line capacitance should be increased.

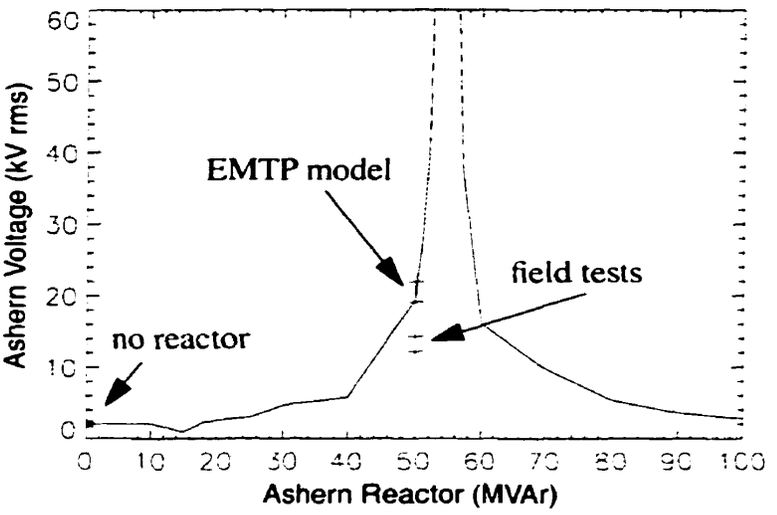

Fig. 6.8 Comparison between field tests and simulation of the induced voltage on A3R.

The line discharge oscillation frequency predicted from linear frequency scans using the parameters given in Fig. 6.7 is 58 Hz and the coupled voltage with the reactor connected is 30 kV. If the transmission line length is increased by 5%, the discharge frequency decreases and the coupled voltage decreases to match field measurements shown in Fig. 6.5.

Comparing the LC discharge frequency in Test #2 also indicates a slight modification in capacitance is needed. Field tests show a 56 Hz oscillation while EMTP simulations show 57.8 Hz. Given the rating of the reactor is 49.5 MVAr and the observed natural frequencies (f_n), the effective line charging capacitance can be calculated using (6-2). For the EMTP case, the line charging capacitance is calculated to be 53.3 MVAr. The calculated line charging capacitance for the field tests is 56.8 MVAr.

$$MVAr_{Cap} = MVAr_{ind} \cdot \left(\frac{\omega}{2\pi \cdot f_n}\right)^2 \tag{6-2}$$

The peripheral lines to the study area do not need frequency dependent modelling as they do not affect switching surges in the study area to a great extent. Therefore, all external lines were modelled as untransposed distributed parameter lines.

6.5.3 Ashern Reactor Model

The Ashern 50 MVAr reactor is constructed in a three-phase three-legged core configuration. The positive and zero sequence impedances given in the Manitoba Hydro data book are: X_1=100.71%, X_0=34.87%, and R_1=0.266% (all values on 230 kV, 50 MVA base). The X_0/X_1 ratio (0.35) is lower than typical values (0.5-0.7) [5]. The positive sequence quality factor (Q_1=379) is within typical ranges of 300 to 500. The zero sequence resistance was not given. Typically, Q_0 lies between 10 and 40 [5]. A value of 23 was chosen based on one author's 60 MVAr reactor [4]. The positive and zero sequence data was entered in a three phase coupled *RL* branch in EMTP. The zero sequence data is necessary to determine the effect of faults on coupled voltages.

Saturation data was not given in the Manitoba Hydro Reactor data book. The knee point of a reactor's saturation curve is normally at 150-160%. A linear model was chosen to be used as study voltages were not expected to exceed the reactor kneepoint.

Steady-state comparisons of reactor voltage and current in either test #2 or test #5 show the reactor impedance is roughly 1100 ohms which compares well with the digital model (1069 ohms - 49.5 MVAr).

6.5.4 Current Transformer

An ideal current transformer (Ct) model (or potential transformer model) is normally used or assumed in a system transient investigation. However, in order to explain the difference between field recordings and simulations in Test #5, a detailed Ct model is required.

A 150/5 Ct model was created[3] and inserted in series with the motor operating disconnect B2 shown in Fig. 6.3. Comparisons are made in Fig. 6.9 between the actual phase current and the secondary current in a Ct model. The subharmonic component saturates the Ct which in turn distorts the measured secondary current. The Ct secondary current looks very similar to field measurements. Modifying the flux-linkage/magnetizing-current characteristic of the Silver transformer will not produce similar transients. The Ct secondary output was scaled until the magnitude of the first few steady-state oscillations matched the magnitude of the primary phase current.

---

3. Detailed Ct parameters are listed in the EMTP data file included in Appendix B.3.

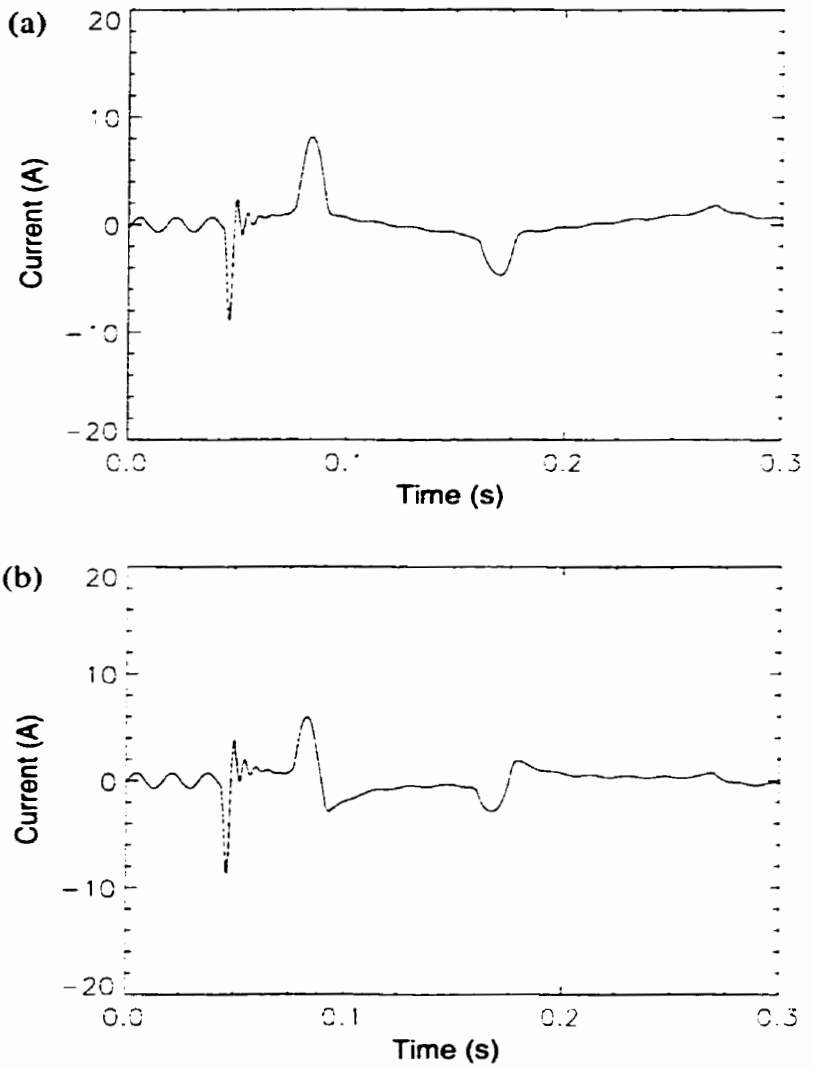

Fig. 6.9 Simulation results of Test #5 showing (a) primary phase current through two Silver transformers and (b) corresponding secondary current of a current transformer model.

6.5.5 Grading Capacitor

The normal simulation model of a circuit breaker with grading capacitance is a pure capacitor in parallel with an ideal switch. Energizing one of the Silver transformers using this default model resulted in numerical oscillations in the circuit breaker's current. The oscillations are a result of using trapezoidal integration [9]. A resistor in series with the grading capacitor of 50 ohms is sufficient to damp the high frequency oscillations by preventing excessive *dv/dt* across the capacitor. The value chosen is one order of magnitude lower than that given by Alvarado's formula 0.15x10μs/(2x1600 pF), which is consistent with Dummer's approach [9].

Resistors are sometimes added across a capacitor for damping low frequency transients. None were used in this EMTP model. The transients are sensitive to this resistor value. It is preferable and more realistic to modify the transformer model to achieve the required damping.

6.5.6 Future Network Plans

An alternative 230 kV transmission line is proposed to supply firm power to Silver from the existing Rosser Station. Manitoba Hydro planning studies indicate that an outage of the existing 230 kV transmission line (A3R) will require electrical load in the Interlake to be supplied through the existing 66 kV sub-transmission network. By 2004, the load cannot be fully supported by the 66 kV network, thus a second 230 kV transmission line is required to ensure a reliable supply. The addition of this new line will eliminate any risk of ferroresonance (due to 60 Hz capacitive coupling with an energized line) if it is in-service, therefore it was assumed out in this study.

The A4D line was reduced in length by 16 km in November, 1997. The retermination reduced the coupled voltages on A3R slightly. The onset of ferroresonance in the Silver transformers will not be impacted by the retermination. The coupled voltages on A4D with the reactor connected are reduced from roughly 40 kV to 12 kV due to the reduced positive sequence line charging capacitance. Field values may be slightly higher if the actual line capacitance is higher than the EMTP model (as was the case for A3R).

It is also proposed to terminate A3R at Dorsey in the future. It is estimated that this new termination will reduce the length of A3R by approximately 17 km. A reduction in length will lower the positive sequence line charging capacitance and result in higher coupled voltages (see Fig. 6.8). A reduction of 5-10 MVAr of line capacitance or 15 to 30 km of line length may result in excessive coupled voltages on de-energized line A3R and possible ferroresonance in the Silver transformers.

The retermination of line A3R is not recommended due to the possibility of damaging voltages and sustained ferroresonance in the Silver transformers and was not studied in this thesis.

This case is unique in that a strong 60 Hz resonant circuit is being influenced by a nonlinear device. Cases reported in the literature did not have transmission lines that were shunt compensated.

6.6 SILVER TRANSFORMER MODEL

The Silver transformer is a 230-66 kV grounded wye-delta three-phase transformer rated 50 MVA. Since 1995, a second 230-66 kV transformer has been in-service as a hot standby (i.e energized but not connected to the 66 kV load).

A 3-legged core configuration is used. Conversations with a transformer design engineer at Pauwel's indicate this design is the most economical and common for medium size power transformers (i.e. less than 200 MVA). When height becomes a problem, a low profile transformer would use a 5-legged core configuration.

It is well known that the asymmetry in the flux paths of a 3-legged core-type transformer results in unbalances in the phase and magnitude of the exciting currents [10]. A topological model is available in EMTP that enables modelling of the asymmetry by adding a fictitious winding as shown in Fig. 6.10. Because detailed information of the core topology was unknown, this type of model was not pursued. A preliminary look, using data from [11], showed that the asymmetry results in a double-pole low frequency positive sequence resonance.

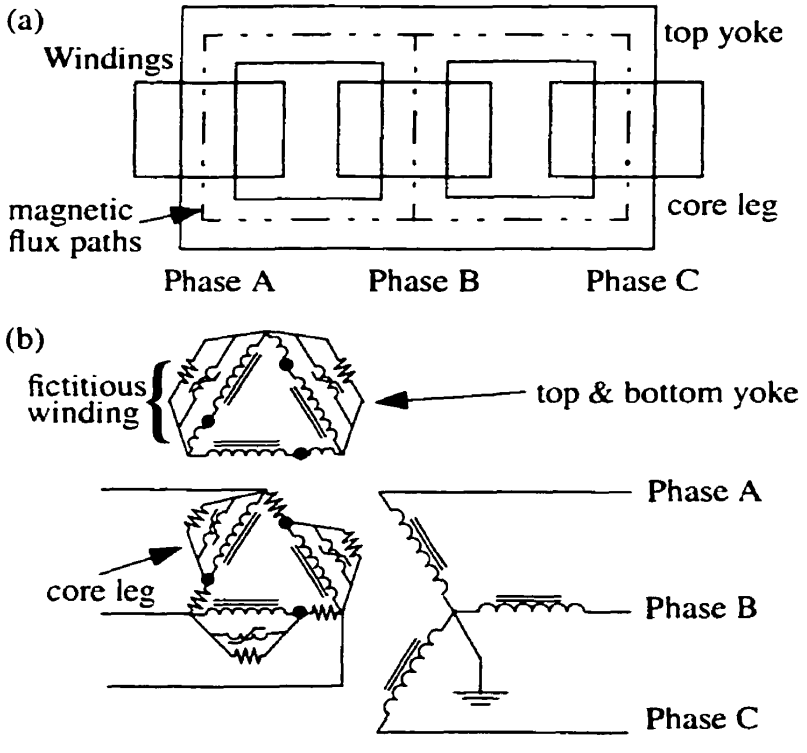

Fig. 6.10 Topological transformer model showing the (a) physical layout of the windings and (b) the electric circuit model.

A frequency dependent transformer model and frequency dependent eddy-current model [2], [3] are available in EMTP. The additional accuracy above 2-3 kHz is not required for ferroresonance studies.

Because of the direct magnetic coupling between phases, a three-phase transformer model must be used. Two models are currently available for use in EMTP: TRELEG and BCTRAN. Both models consist of coupled R-L branches that reproduce standard short circuit tests at 60 Hz. For frequencies up to 1 kHz both models behave similarly, however for zero sequence frequencies approaching dc the BCTRAN model correctly degenerates to a simple resistance (see Fig. 6.11b). The BCTRAN model was used in the study.

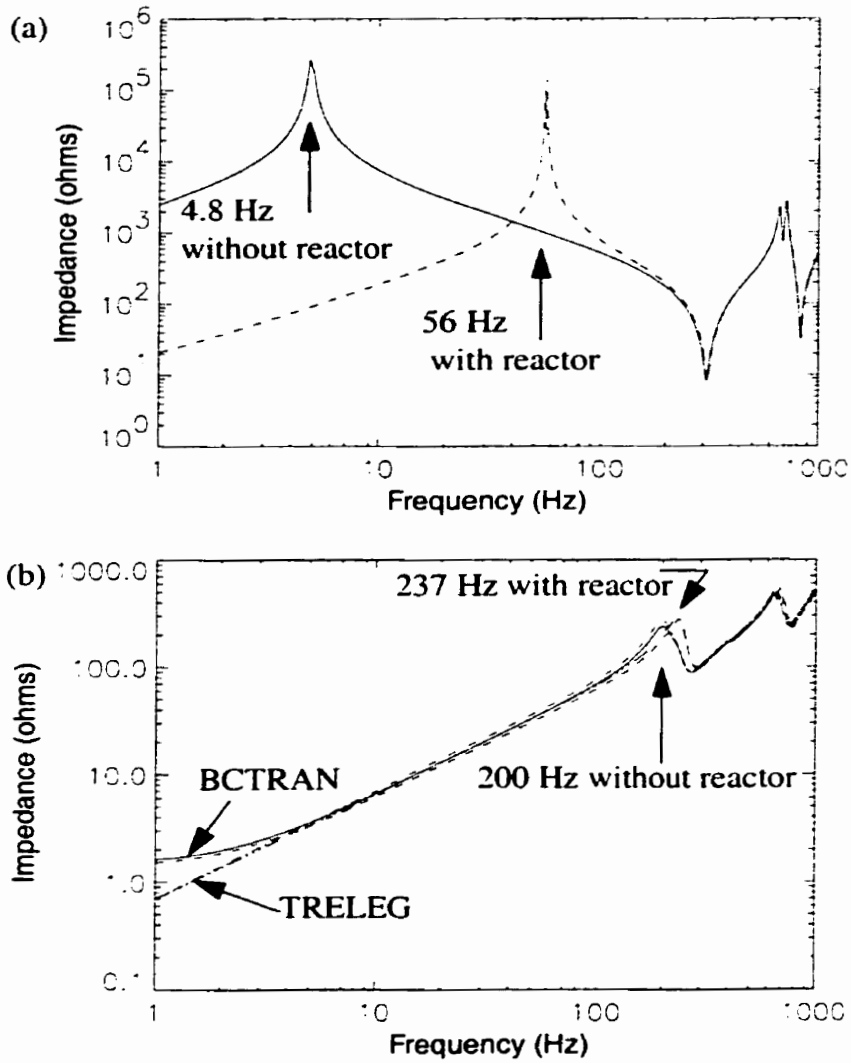

Fig. 6.11 Comparison of (a) positive sequence scan (BCTRAN model) and (b) zero sequence scan (BCTRAN and TRELEG models) looking into the system from the Silver 230 kV bus with A3R open at Ashern and Rosser and with two transformers connected.

6.6.1 Saturation and Iron-Core Loss Modelling

The location of the saturation curve is important. Of importance is the ability to match the transient flow of current in the neutral. With saturation modelled on the delta winding, all zero sequence current is trapped in that winding. With saturation modelled on the high-side wye winding, some third harmonic current will flow transiently through the neutral, for example. The best match to field measurements resulted when saturation was modelled on the low side as shown in Fig. 6.12.

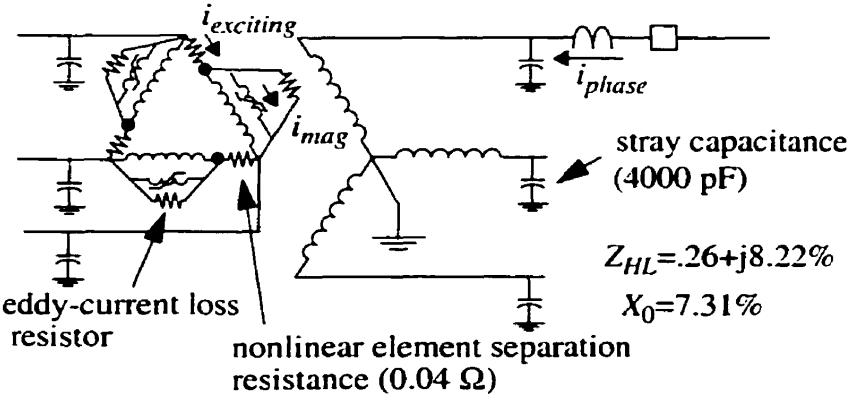

Fig. 6.12 Silver transformer equivalent circuit model.

Subharmonic damping in Test #5 can only be matched if hysteresis losses are modelled. A constant resistance is normally used to approximate the iron-core losses. This model is voltage dependent and not flux linkage dependent, which causes inadequate damping of low voltage subharmonics. The manufacturer has confirmed the core is constructed using grain-oriented steel with 4% silicon, therefore, the hysteresis losses are assumed to be 1/3 the eddy-current losses.

There are three models available in EMTP to represent saturation in an inductor. Each will be described briefly.

A. Type-98: Pseudo-Nonlinear Inductance

A normal piecewise-linear saturation curve was used in the initial modelling stages. Test data was given by the manufacturer for 90%, 100% and 110% open-circuit voltage. The air-core reactance was assumed to be twice the leakage reactance (Z_{HL}). Since the per unit flux contained by the iron-core under full saturation was unknown, a worst case was obtained by extrapolating the last measured point based on the assumed air-core reactance. A 10 μs time-step is used in all simulations.

The resulting 4-segment piecewise-linear curve did not match field tests. Fictitious oscillations resulted because of too low a knee-point and too abrupt a transition between curve segments. Examining only the current and spectrum of the current in Fig. 6.13 leads one to conclude that a period-1 ferroresonance state has been reached. However, the discontinuous nature of the flux-linkage/magnetizing-current trajectory and the frequency of oscillations in the phase current waveform likely mean a natural mode (i.e. 237 Hz zero seq. from Fig. 6.11) of the circuit has been excited.

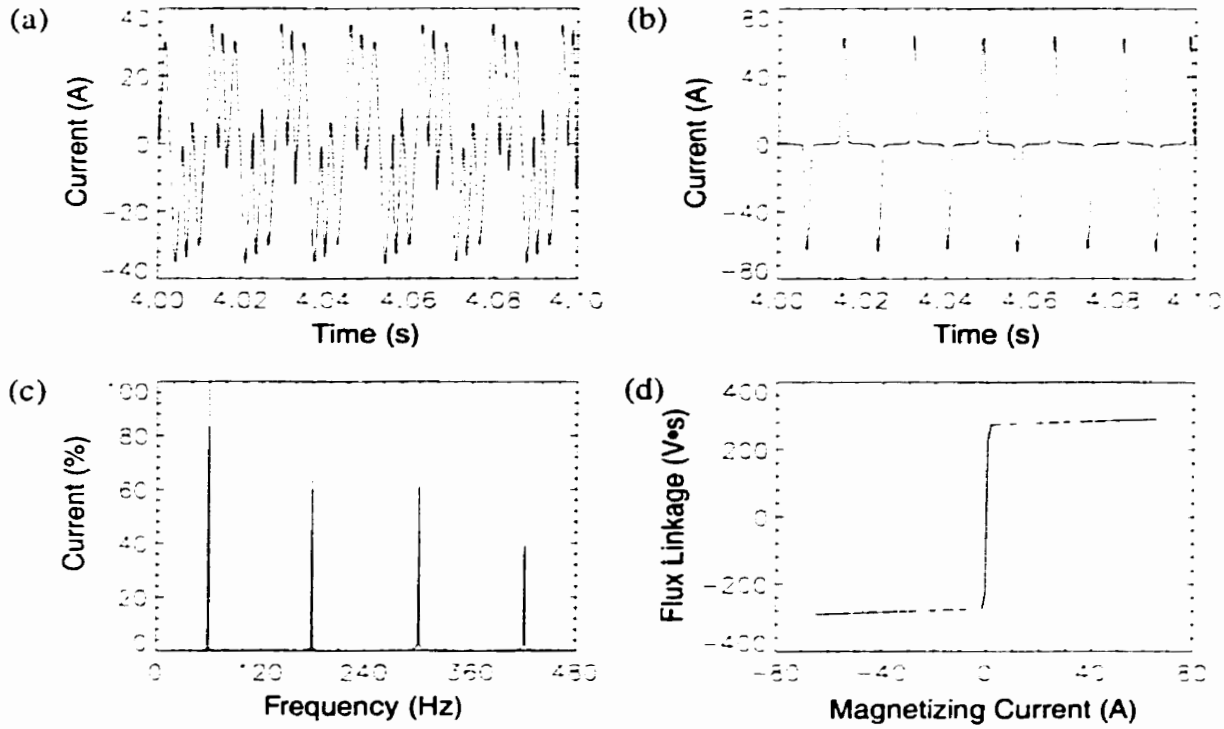

Fig. 6.13 Fictitious attractor's (a) primary phase A current, (b) magnetizing phase A current, (c) spectrum of primary current and (d) flux-linkage/magnetizing-current trajectory generated by tripping line A3R with the Ashern reactor connected.

An alternative model was developed using a two-term polynomial relation (6-3).

$$i_L(\lambda) = a_1 \cdot \lambda + a_n \cdot \lambda^n \tag{6-3}$$

An 11^{th} order polynomial (a_1=.0028, a_{11}=.0001) served as a starting point and was discretized into 28 segments. The flux-linkage coordinate points were scaled (i.e. 80%) until the first transient current peak in the reactor switching test matched field tests. A linear parallel resistor modelled the 50 kW iron-core losses. The modified model produces the transient flux-linkage/exciting-current loops shown in Fig. 6.14a.

B. Type-96: Pseudo-Nonlinear Inductance with Hysteresis

The Type-96 reactor model was setup to have roughly the same transient flux-linkage/ exciting-current loop shape as the Type-98 reactor shown in Fig. 6.14a. By using the default 22 segment hysteresis shape (Armco M4 grain-oriented silicon steel) and by modifying the slope through the linear region by adjusting the excitation current to 0.2% in the BCTRAN transformer model, this was achieved.

One input required in the hysteresis data setup routine is the coordinates where the saturation characteristic changes from being multi-valued to single-valued. The flux-linkage coordinate can be estimated from the Type-98 flux-current loop to be 290 volt-seconds. The current coordinate is adjusted until the total measured open-circuit losses is 50 kW. A linear eddy-current loss resistor is included representing 75% of the total iron-core losses.

C. Type-92: True-Nonlinear Inductance with Hysteresis

The new Type-92 nonlinear inductor with hysteresis model [3] is not a piecewise-linear model but rather a closed-form nonlinear function. This closed-form function takes the form of a two-term polynomial.

The closed-form functions are calculated using an auxiliary EMTP subroutine. A 10-segment single-valued saturation curve taken from the Type-98 reactor is input and the coercive current is adjusted until the total measured open-circuit losses is 50 kW. As with the Type-96 reactor, a linear eddy-current loss resistor representing 75% of the total iron-core losses is used.

The DCG/EPRI version of the EMTP, type-92 (or true nonlinear models) are solved using the compensation method [9]. Because of the way the compensation method is implemented in this version of the EMTP, delta-connected loops of Type-92 elements result in a singular matrix. One way of eliminating this problem is to separate the nonlinear elements by a small impedance. For this problem, a resistor was used as shown in Fig. 6.12. A value equivalent to 15% of the measured delta winding resistance eliminated the singularity, which allowed for rapid convergence. The additional resistance is insignificant compared with the iron-core loss resistance, for example, and did not affect the results.

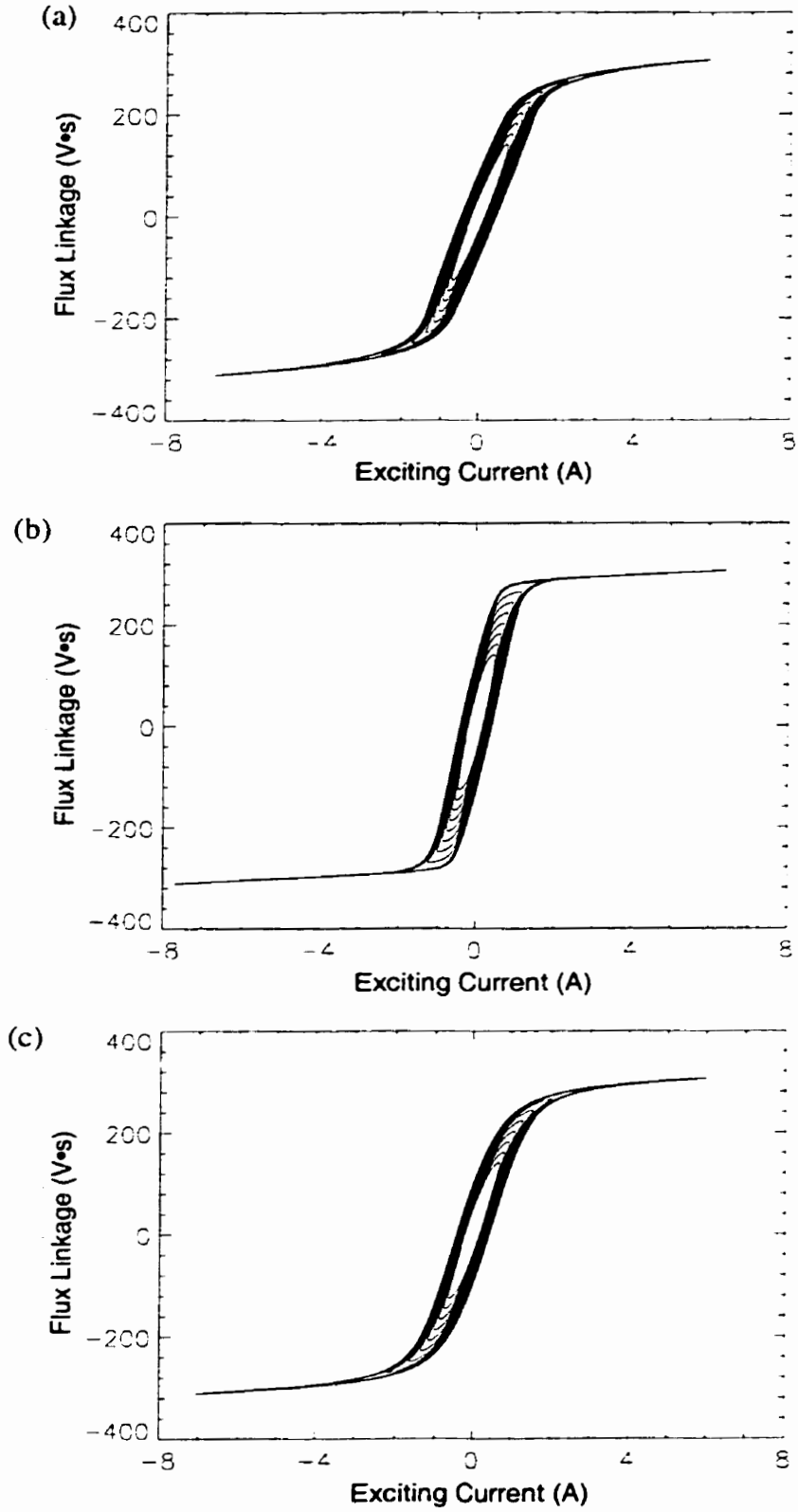

Fig. 6.14 Comparison of transient flux-linkage/exciting-current loops for (a) Type-98 reactor, (b) Type-96 reactor and (c) Type-92 reactor.

D. Comparison of the Models

As mentioned earlier in the Chapter, subharmonic damping is improved by including hysteresis losses. A comparison of the damping performance of the three models is shown in Fig. 6.15.

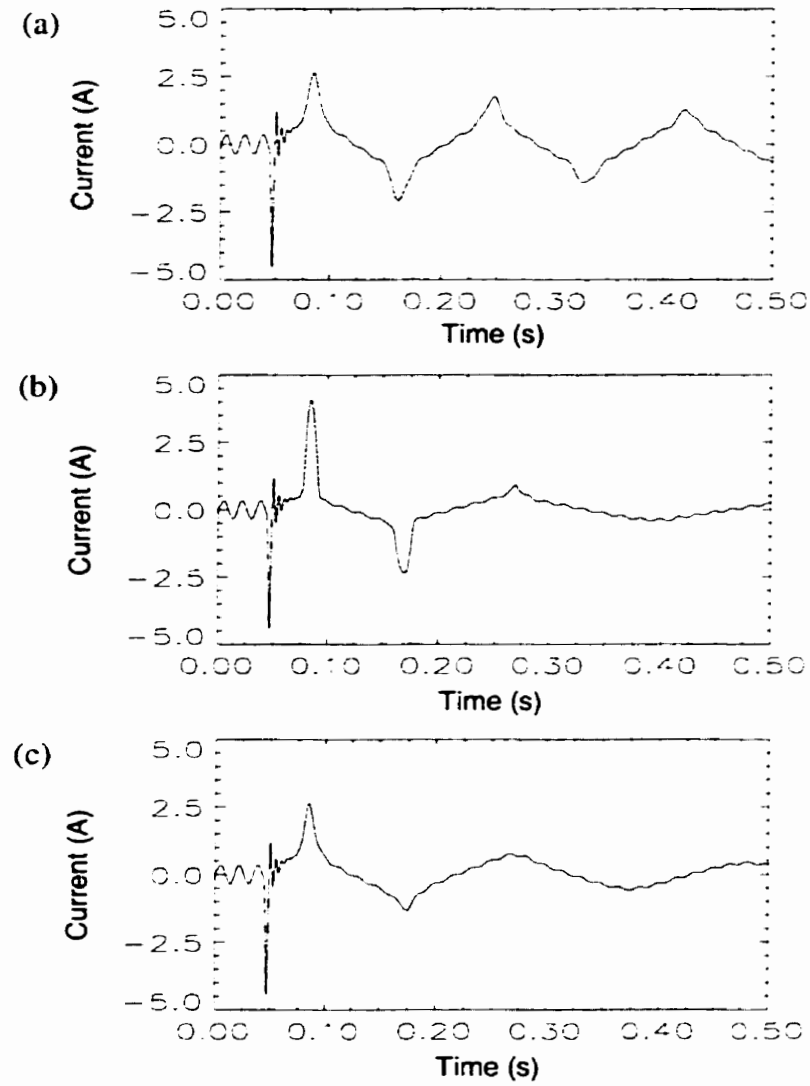

Fig. 6.15 Comparison of subharmonic damping in the Silver transformer's primary phase current between (a) Type-98 piecewise-linear reactor, (b) Type-96 pseudo-nonlinear reactor and (c) Type-92 true-nonlinear reactor.

Sustained numerical oscillations can be introduced following transitions between segments in piecewise-linear inductors. A small time step (10 μs), large number of segments and inclusion of a linear parallel eddy-current loss resistor effectively eliminated

any oscillations. The "Critical Damping Adjustment [9]" feature of EMTP was not enabled in these simulations.

In terms of cpu time, the Type-92 inductor requires approximately 25% more computation time than the Type-98 and Type-96 inductors.

The EMTP simulation[4] of the reactor switching test is shown in Fig. 6.16 and includes breaker R2 current (i.e. sum of two banks), neutral current and 230 kV bus voltages. The Type-96 reactor model matched the field measurements shown in Fig. 6.5 more closely than the other two models.

As previously mentioned in Section 6.5.4, a current transformer (Ct) model is required in the simulation in order to match the recorded current transients. The subharmonic current saturates the Ct which distorts the measured current. An ideal Ct model produces the transients shown in Fig. 6.15.

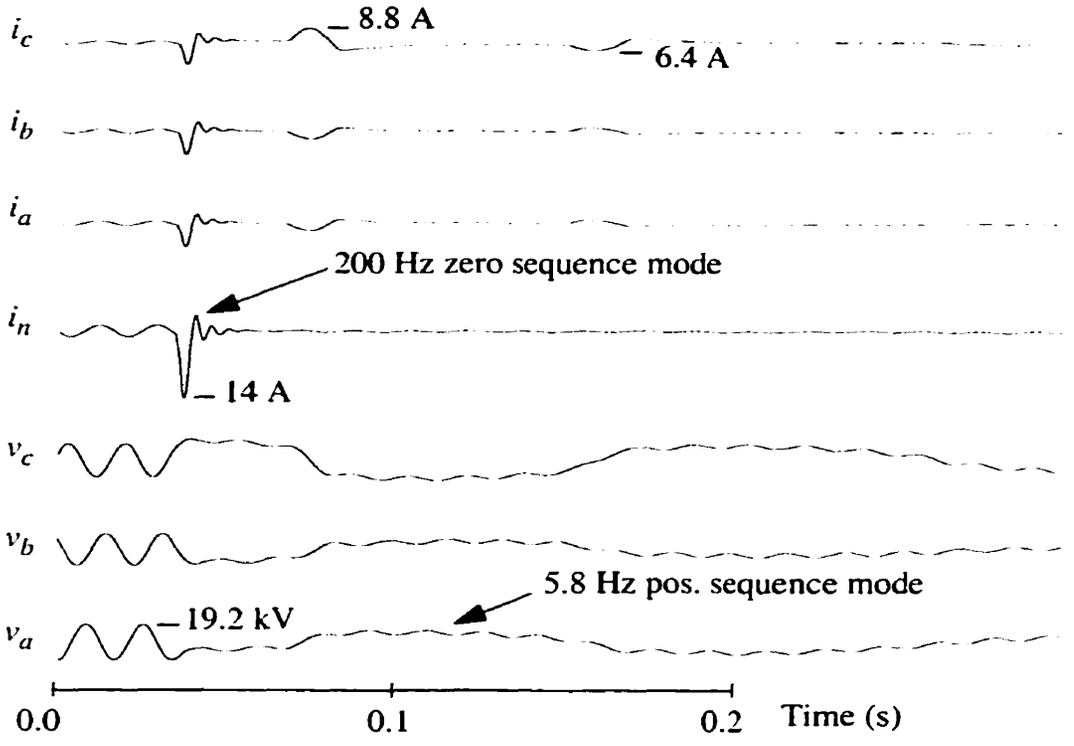

Fig. 6.16 EMTP simulation of the reactor switching test using the Type-96 pseudo-non-linear model.

4. A listing of the EMTP data file is included in Appendix B.3.

The large current pulse at 0.16 seconds indicated by field tests was not duplicated with the final EMTP model. A topological core model is required to match this transient.

6.7 EMTP FERRORESONANCE STUDY

Several cases that could not be field tested were investigated using the benchmarked EMTP model. In general, ferroresonance did not develop for any case which had the Ashern reactor connected or had loaded transformers. Ferroresonance did develop for the following cases:

- single-pole breaker failure at Rosser or Ashern,
- tripping A3R.

The parallel transmission line can be ignored in the case of single-pole failure at Rosser or Ashern as the energy required to sustain ferroresonance is derived from the remaining healthy phases on line A3R. This phenomenon has been extensively studied using laboratory models and field tests at distribution level voltages up to 35 kV originally by Hopkinson [A21] and later by Walling *et al.* [A106]. Analytical work has been done by Prusty [A63] using Rüdenberg's graphical approach and recently by Mozaffari *et al.* [A136] using nonlinear dynamics theory.

For distribution systems, single-pole failures are a real concern because there may be no backup protection. At transmission voltage levels, breaker failures are cleared within 250 milliseconds by backup breakers. The only concern is whether the transient recovery voltage (TRV) capability of the backup breaker is sufficient or whether ferroresonance will be sustained following breaker clearing. For this system, standard ANSI 230 kV TRV ratings were not exceeded and no ferroresonance modes were sustained.

Tripping A3R with no reactor and with no load at Silver also results in ferroresonance. The oscillations were predominantly subharmonic which supports the observations made by German and Davies [A48]. Long duration simulations (i.e. up to 10 seconds) are required to determine whether the ferroresonance oscillation mode is permanent.

Immediately following the trip of A3R, the transformer saturates and the first positive sequence resonance mode bends to the right.

The new "resonant" frequency that results following the trip of line A3R depends on a number of factors but typically shifts to between 25 and 30 Hz. During the subharmonic decay process, there is a chance that the oscillations will lock-in to a ferroresonant state. Two examples of ferroresonant states are shown in Fig. 6.17. For the majority of cases, the initial subharmonic oscillations decayed to a nonferroresonant state within 5-15 seconds.

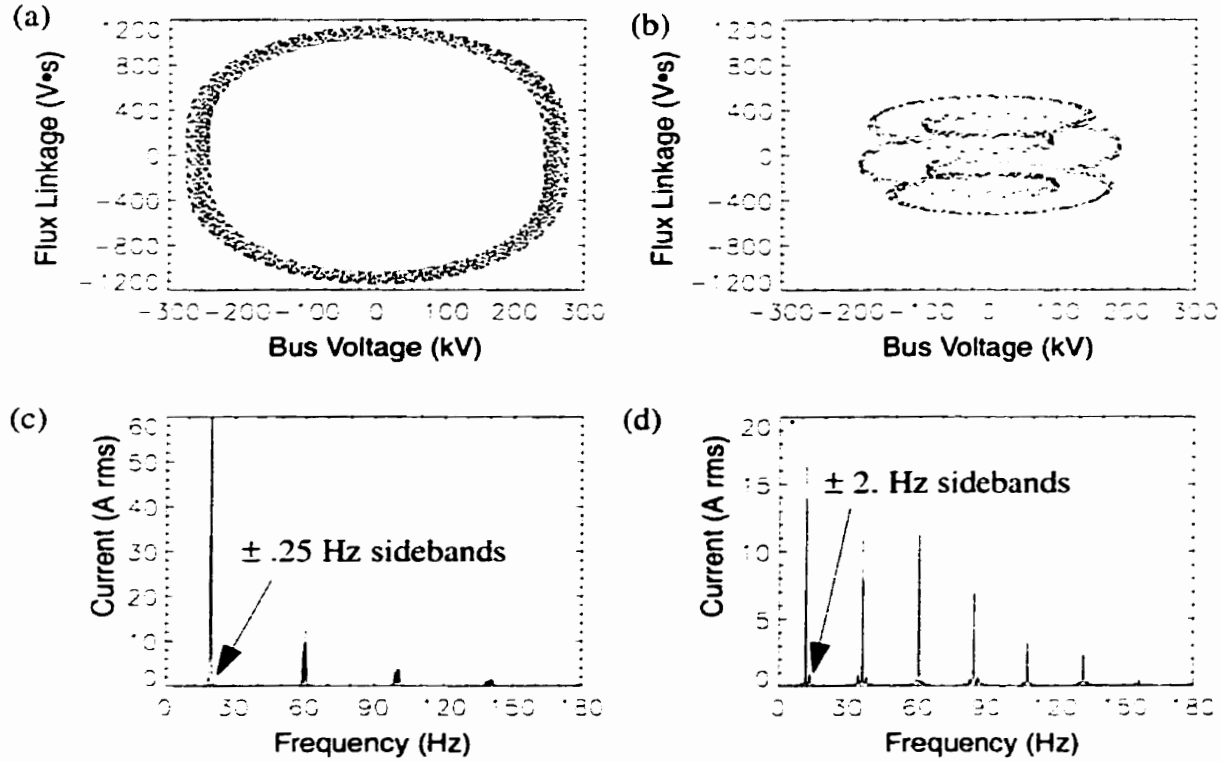

Fig. 6.17 Example of two typical subharmonic attractors, (a) state space trajectory of quasi-period-3 attractor which results after A3R trips using the Type-96 reactor model, (b) state space trajectory of quasi-period-5 attractor which results after A3R trips with single-pole breaker failure at Rosser using the Type-92 reactor model, (c) spectrum of secondary magnetizing current of QP-3 attractor, (d) spectrum of secondary magnetizing current of QP-5 attractor.

The oscillations observed in Fig. 6.17 are quasi-periodic because they are composed of two incommensurate frequencies. Instead of a Poincaré section showing three or five points indicating periodic behaviour, it would show three or five closed circles indicating toroidal motion around the main periodic attractor.

Two Poincaré sampled trajectories are shown in Fig. 6.18a and Fig. 6.18c. The new trajectories are showing some decay that is not evident in the original diagram.

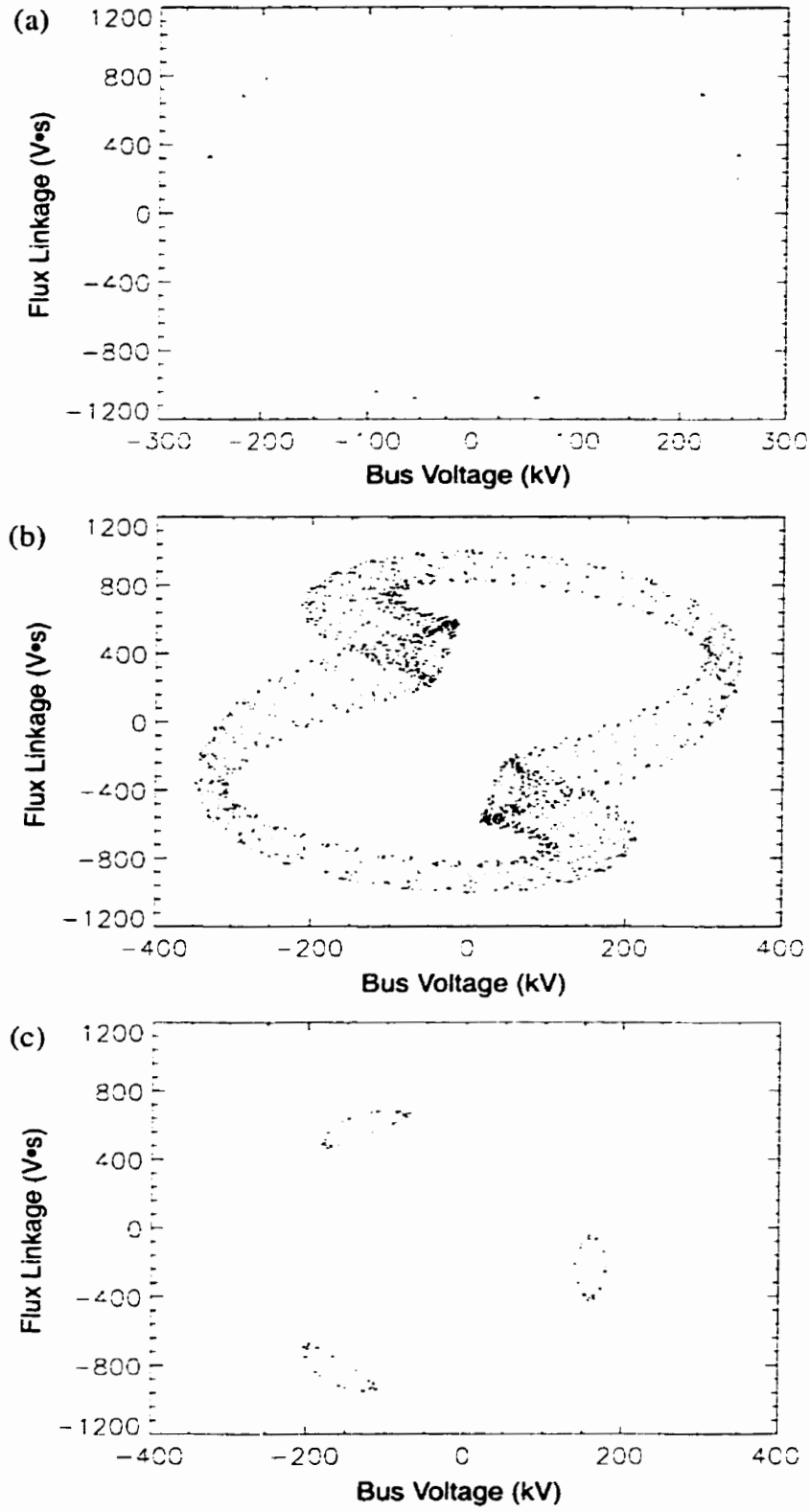

Fig. 6.18 Poincaré sampled state space trajectories showing (a) QP-3 attractor corresponding with Fig. 6.17a, (b) new QP-3 attractor, (c) Poincaré sampling applied to (b) .

A rough Poincaré sampler can be created in an EMTP simulation by adjusting the time step and print time. The original simulations used a time step of 10 microseconds and printed every 99^{th} point over a 10 second simulation. If the time step is adjusted to 10.01 microseconds and every 1665^{th} sample is saved, the output will be one sample point per 60 Hz period. The imperfect sampling causes a slight drift in the resulting Poincaré sampled curves (i.e. Fig. 6.18a and c).

It is interesting to note that the small change in time step (.01 microseconds) resulted in a completely different final attractor to that shown in Fig. 6.17b. The frequency spectrum has dominant components at 20 Hz, 60 Hz, 100 Hz and 140 Hz with 2 Hz sidebands around each.

If the final state is ferroresonant, damage due to excessive iron-core losses in the transformer will occur. An overvoltage relay is installed at Silver which will trip breaker R2 if the voltage is greater than 112% for more than one second. The relay will trip the transformer early in the subharmonic decay process preventing possible damage. If the Silver breaker fails, or the transient voltages do not trigger the overvoltage relay, the Ashern line reactor can be switched onto line A3R remotely by a system operator. Fig. 6.19 shows the smooth transition from ferroresonance to a normal line discharge transient (i.e. see Fig. 6.4).

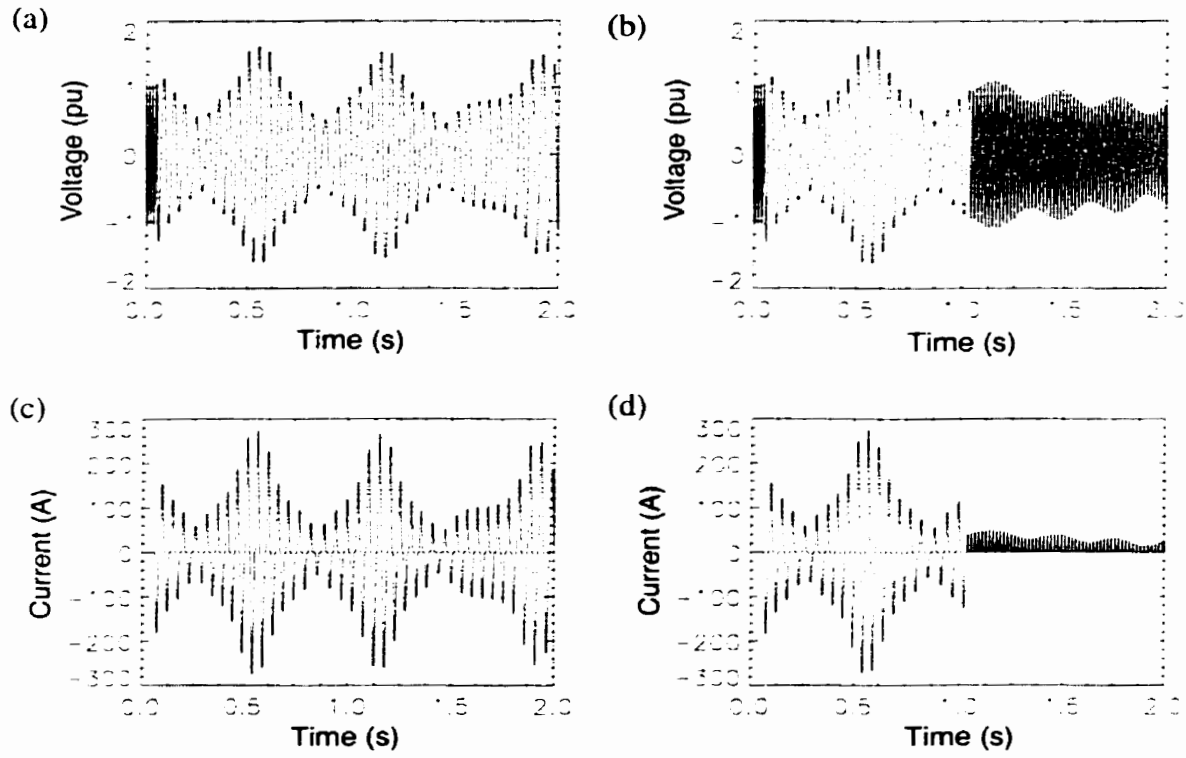

Fig. 6.19 Demonstration of effectiveness of reactor switching in eliminating ferroresonance, (a) Silver primary voltage with no reactor, (b) Silver primary voltage with reactor switched on after one second, (c) Silver secondary magnetization current with no reactor, (d) Silver secondary magnetization current with reactor switched on after one second.

6.8 SUMMARY

This chapter has focussed on double-circuit transmission lines and how ferroresonance can result in a de-energized transformer through capacitive coupling with a parallel energized transmission line. Through field tests, improvements have been made in modelling techniques. For example, in order to model the subharmonic damping behavior properly, the ratio of hysteresis losses to eddy-current losses can be adjusted. Alternatively, a flux-linkage dependent resistor model could be developed. Piecewise-linear representations of transformer magnetization curves can lead to numerical oscillations that may be interpreted as being chaotic or develop into a periodic state that is misinterpreted as being representative of the real system.

Field tests are required to verify transients resulting from de-energizing an unloaded transformer. An EMTP investigation has confirmed that the possibility of a permanent ferroresonant state exists and can be mitigated by reactor switching.

It is recommended to investigate simulation model simplification techniques such as, $\alpha\beta 0$ transformations or multi-port equivalencing of the external system. A simple network would permit analysis using analytical techniques or permit the setup of a laboratory model. A laboratory model would be very valuable to analyze the effects of different modes of ferroresonance on transformer losses/heating.

Further investigation into how modelling the detailed transformer topology may influence three-phase ferroresonance is recommended.

The possibility of non-linear frequency scans can be studied for the near 60 Hz positive sequence line reactor line charging capacitance resonance case. The effect of transformer saturation on the resonant frequency may be predicted.

6.9 REFERENCES

[1] Dommel, H.W., *Electromagnetic Transients Program Reference Manual: EMTP Theory Book*, Bonneville Power Administration: Portland, pp. 2.30-2.32, August 1986.

[2] Morched, A., Marti, L., and Ottevangers, J.,"A High Frequency Transformer Model for the EMTP", *IEEE Trans. on Power Delivery*, pp.1615-1626, July 1993.

[3] Tarasiewicz, E.J., Morched, A.S., Narang, A., and Dick, E.P.,"Frequency Dependent Eddy-Current Models for Nonlinear Iron Cores", *IEEE Trans. on Power App. and Systems*, Vol. 8, No. 2 pp.588-597, May 1993.

[4] Colapret, E.E., and Reid, W.E., "Effects of Faults and Shunt Reactor Parameters on Parallel Resonance", *IEEE Trans. on Power App. and Systems*, Vol. PAS-100, No. 2, pp. 572-584, February 1981.

[5] Reid, W.E., Gustin, R.F., and Zylstra, P.V.,"Guidelines for Determining Parallel Resonance on EHV Transmission Lines", *IEEE Trans. on Power App. & Systems*, Vol. 102, No. 9, pp. 3196-3204, September 1983.

[6] Fortescue, C.L.,"Method of Symmetrical Components Applied to the Solution of Polyphase Networks", *A.I.E.E. Trans.*, Vol. 37, Part II, pp. 1027-1140, 1918.

[7] Clarke, E., *Circuit Analysis of AC Power Systems, Volume I: Symmetrical and Related Components*, John Wiley & Sons: New York, pp. 308-362, 1943.

[8] Chua, L.O., Desoer, C.A., Kuh, E.S., *Linear and Nonlinear Circuits*, McGraw Hill: New York,1987.

[9] Dommel, H.W., *The EMTP Theory Book: Second edition*, Microtran: Vancouver, B.C., April 1996.

[10] Slemon, G.R.,"Equivalent Circuits for Transformers and Machines Including Nonlinear Effects", *Proceedings of the I.E.E.*, Vol. 100, Part IV, pp. 129-143, 1953.

[11] Dick, E.P., and Watson, W.,"Transformer Models for Transient Studies Based on Field Measurements", *IEEE Trans. on Power App. and Systems*, Vol. PAS-100, No. 1, pp. 409-419, January 1981.

6.10 APPENDIX: PARALLEL LINE RESONANCE

Parallel line resonance can result in overvoltages on a de-energized shunt reactor compensated circuit due to capacitive coupling with a parallel energized circuit [A80], [4], [5]. The possibility of resonance on line A3R/A4D is investigated.

The Ashern reactor was originally installed in the station for the purpose of controlling the voltage during normal daily and seasonal load variations. In June, 1990, the reactor was relocated to a selectable position between line A3R or A4D coincident with the addition of Silver station. The reactor is required to be connected to A3R when the Silver 66 kV system is networked. If line A3R were to trip while networked, there is a risk that a standard 230 kV breaker would restrike while attempting to interrupt line charging current. The reactor is required to hold the voltage below 1.2 pu allowing successful interruption for this contingency. As well, during a system restoration sequence, the reactor must be connected to A4D for voltage control.

With the change in reactor location, the possibility exists for high voltages due to parallel resonance following line de-energization. The probability depends on the reactor MVAr and transmission line parameters. However, even if the reactor voltages are below the reactor rating, reactor zero sequence currents may be a problem. Prolonged zero sequence currents can result in excessive reactor heating. Colapret and Ried [4] indicate the continuous zero sequence current rating is less than 10% of the positive sequence current rating in many reactor designs. Assuming the reactor has a 110% continuous overvoltage rating, the corresponding positive sequence phase current is 138 amperes. Therefore, the continuous zero sequence current shouldn't exceed 13.8 amperes. If it does the manufacturer should be contacted to confirm the actual rating.

Colapret and Ried [4] have determined formulae for hand calculating possible resonances. Assuming the resonances are a result of pure electrostatic coupling, the EMTP line constants program can be used to calculate the capacitance matrix of the equivalent phase conductors. A comparison of the line constants output with Colapret and Ried's naming convention for line A3R/A4D (i.e. geometry shown in Fig. 6.7) is given in Fig. 6.20.

(a)

	I: A4D			II: A3R		
I	C_{aa}	C_{ab}	C_{ac}	$C_{aa'}$	$C_{ab'}$	$C_{ac'}$
	C_{ba}	C_{bb}	C_{bc}	$C_{ba'}$	$C_{bb'}$	$C_{bc'}$
	C_{ca}	C_{cb}	C_{cc}	$C_{ca'}$	$C_{cb'}$	$C_{cc'}$
II	$C_{a'a}$	$C_{a'b}$	$C_{a'c}$	$C_{a'a'}$	$C_{a'b'}$	$C_{a'c'}$
	$C_{b'a}$	$C_{b'b}$	$C_{b'c}$	$C_{b'a'}$	$C_{b'b'}$	$C_{b'c'}$
	$C_{c'a}$	$C_{c'b}$	$C_{c'c}$	$C_{c'a'}$	$C_{c'b'}$	$C_{c'c'}$

(b)

10.15					
-1.88	10.53				
-.577	-1.83	10.31			
-.138	-.295	-.890	10.31		
-.065	-.114	-.295	-1.83	10.53	
-.046	-.065	-.138	-.577	-1.88	10.15

Fig. 6.20 Equivalent phase conductor capacitance matrix, (a) using Colapret and Ried's naming convention, (b) EMTP calculation of A3R/A4D example in nF/km.

For one reactor bank on the line with $X_0=kX_1$, the following two equations can be used to calculate the reactor inductance resulting in resonance on a transposed transmission line. Equation 6-4 refers to an unfaulted case while (6-5) refers to a single line-to-ground fault case.

$$L_1 = \frac{1}{\omega^2 \cdot (C_{a'a'} - C_{a'b'})} \tag{6-4}$$

$$L_2 = \frac{2+k}{3k \cdot \omega^2 \cdot (C_{a'a'} + C_{a'b'})} \tag{6-5}$$

As an example, assume the reactor is connected to de-energized line A4D. The length of A4D is 198 km and the X_0/X_1 ratio of the reactor is 0.35 (i.e. k). As a rough approximation, the transpositions have the effect of averaging the diagonal and mutual capacitances. Therefore, $C_{a'a'}$ is 2.045 μF and $C_{a'b'}$ is -0.283 μF. Inserting these values in the above equations results in 3.02 Ω (or 46.4 MVAr) for L_1 and 8.94 Ω (or 15.7 MVAr) for L_2. The hand calculations are very close to accurate steady-state EMTP calculations (see Fig. 6.22).

It is instructive to consider two popular transformations that can performed on a general set of three vectors. The symmetrical component system developed by Fortescue [6] and the alpha, beta, zero component system defined by Clarke [7]. These transforms were designed to aid the calculation of unsymmetrical three phase systems. Symmetrical components are used almost exclusively in the steady-state analysis of faulted power systems while Clarke's transform is popular for synchronous machine analysis. Because

the synchronous machine has two axes of rotor symmetry, the components best suited to its analysis are direct-axis, quadrature-axis and zero sequence.

The normalized Clarke's transformation (6-6) can be applied to the balanced partitioned matrix ($C_{II\text{-}II}$). in order to decouple the system into α, β, and zero components.

$$[Z_{0\alpha\beta}] = [T]^{-1} \cdot [Z_{abc}] \cdot [T] \tag{6-6}$$

Expanding the matrices and letting $C_g = C_{a\cdot a\cdot}$ and $C_m = -C_{a\cdot b\cdot}$ results in:

$$\begin{bmatrix} C_0 \\ C_\alpha \\ C_\beta \end{bmatrix} = \begin{bmatrix} C_g - 2C_m & 0 & 0 \\ 0 & C_g + C_m & 0 \\ 0 & 0 & C_g + C_m \end{bmatrix} = \frac{1}{\sqrt{3}} \begin{bmatrix} 1 & 1 & 1 \\ \sqrt{2} & \frac{-1}{\sqrt{2}} & \frac{-1}{\sqrt{2}} \\ 0 & \frac{\sqrt{3}}{\sqrt{2}} & \frac{\sqrt{3}}{\sqrt{2}} \end{bmatrix} \cdot \begin{bmatrix} C_g & -C_m & -C_m \\ -C_m & C_g & -C_m \\ -C_m & -C_m & C_g \end{bmatrix} \cdot \frac{1}{\sqrt{3}} \begin{bmatrix} 1 & \sqrt{2} & 0 \\ 1 & -\frac{1}{\sqrt{2}} & \frac{\sqrt{3}}{\sqrt{2}} \\ 1 & -\frac{1}{\sqrt{2}} & -\frac{\sqrt{3}}{\sqrt{2}} \end{bmatrix} \tag{6-7}$$

Similarly, the positive, negative and zero sequence components can be derived from (6-8).

$$[Z_{012}] = [A]^{-1} \cdot [Z_{abc}] \cdot [A] \tag{6-8}$$

The symmetrical component transformation matrix is complex with the operator a defined by the complex number $1 \angle 120^\circ$. Solving for the equivalent zero, positive and negative sequence components results in (6-9).

$$\begin{bmatrix} C_0 \\ C_1 \\ C_2 \end{bmatrix} = \begin{bmatrix} C_g - 2C_m & 0 & 0 \\ 0 & C_g + C_m & 0 \\ 0 & 0 & C_g + C_m \end{bmatrix} = \frac{1}{3} \begin{bmatrix} 1 & 1 & 1 \\ 1 & a & a^2 \\ 1 & a^2 & a \end{bmatrix} \cdot \begin{bmatrix} C_g & -C_m & -C_m \\ -C_m & C_g & -C_m \\ -C_m & -C_m & C_g \end{bmatrix} \cdot \begin{bmatrix} 1 & 1 & 1 \\ 1 & a^2 & a \\ 1 & a & a^2 \end{bmatrix} \tag{6-9}$$

The zero sequence impedance is the same in both cases and is true in general. The positive and negative sequence components are equal to the alpha and beta components in this case because we have a circuit with equal positive and negative sequence impedances and no mutual impedances between sequence networks. In general, the alpha and beta components are not equal to the sequence components. Notice that the capacitance ($C_{a\cdot a\cdot}$ - $C_{a\cdot b\cdot}$) in (6-4) is precisely the positive sequence capacitance.

The simplified averaging approach used by Colapret and Ried [4] can't be used for the

case of line A3R open because the 61 km tap to Silver station has a large influence on the line charging capacitance. Detailed calculations are necessary for an accurate prediction.

Steady-state coupled voltages are plotted in Fig. 6.21 and Fig. 6.22. The plots indicate the 50 MVAr reactor is quite close to a resonant point. It is predicted for an outage of A3R, the coupled voltage will be between 14.2 kV (no tap) and 21.5 kV (tap and 2 transformers). The resonance will shift depending on factors such as: the status of the Silver tap, the number of Silver transformers connected and the system frequency (60.0 Hz was assumed). Similarly, an outage of A4D plus reactor will result in coupled voltages of 28.8 kV. In both cases, neutral currents measured were much less than the assumed continuous rating (13.8 A). Table 6.2 summarizes some of the expected coupled voltages and reactor neutral currents for a 50 MVAr reactor.

Table 6.2 Coupled Voltage and Reactor Neutral Current

Configuration		Ashern Voltage (kV rms)	Neutral Current (A rms)
A3R	no tap	14.2	0.5
	Silver tap 0 transformers	19.3	0.6
	Silver tap 1 transformer	20.2	1.3
	Silver tap 2 transformers	21.5	1.4
A4D		28.8	0.9

The coupled voltages on A3R for the case of only the Silver tap connected (no transformers) have been observed at 23 kV. It should be noted that this parallel resonance occurs between the line reactor and the positive sequence line charging capacitance and is a 60 Hz steady-state phenomenon.

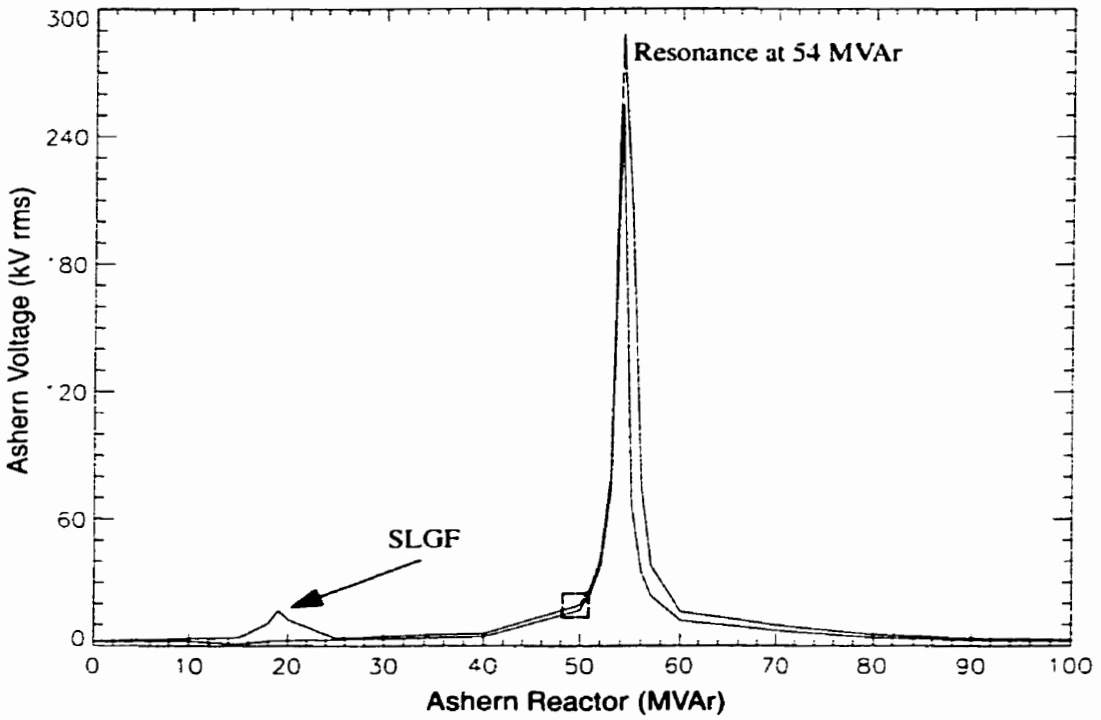

Fig. 6.21 Induced voltage on A3R with no transformers connected at Silver.

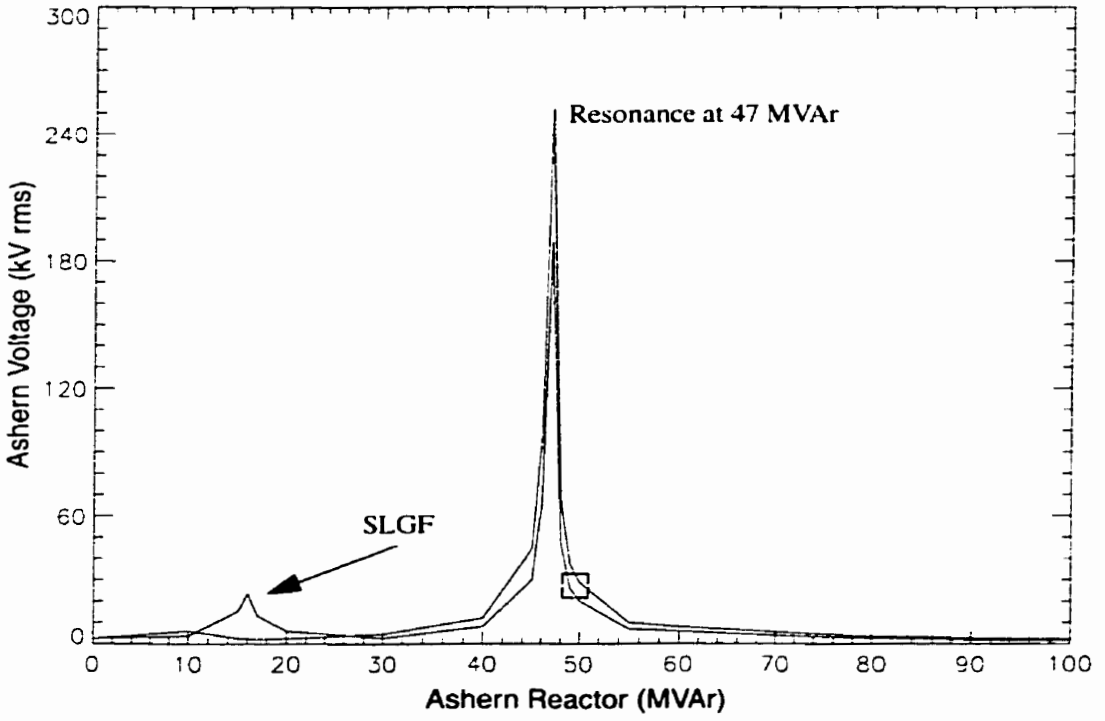

Fig. 6.22 Induced voltage on A4D.

Chapter 7

Conclusions

The main objectives of this thesis have been to improve upon the existing techniques of ferroresonance analysis and ferroresonance modelling. This chapter summarizes the main conclusions and contributions made in pursuit of the research objectives. Some suggestions for additional work are included at the end of the chapter.

7.1 FERRORESONANCE ANALYSIS

Utility engineers are used to thinking about protection margins in terms of insulation coordination or relay operation. For example, standard insulation coordination practice is to maintain a fifteen percent safety margin between switching surges and equipment withstand capabilities. Lightning arresters, installed near transformer banks, are sized based on this criteria. Out-of-step relays are designed to detect unstable power swings and trip critical lines in order to sectionalize the system and prevent widespread blackouts. The severity of a disturbance can be measured by how close the swing comes to violating protection margins.

A major contribution of this work is a new method of visualizing the margin between non-ferroresonant and ferroresonant states has been developed. A set of equations has been developed that can be used to create a two dimensional parameter plane map showing possible ferroresonance risks. Given an operating point on the two dimensional parameter plane, the margin to ferroresonance can clearly be seen. Utility engineers will benefit because they now have a tool that can be used to quickly screen their particular system for the potential risk of ferroresonance, thus preventing future disastrous equipment failures.

Quasi-static analytical approaches can be used to give a quick indication of the locations of zones of different ferroresonant states as a function of a set of parameters. However, such an approach does not give an accurate indication of safety margins if large signal perturbations are considered. A novel *kick*-initiated brute-force bifurcation diagram is developed and is found to be an ideal tool for displaying margins between ferroresonant and non-ferroresonant states on a parameter plane. The particular *kick* under study is the

opening of a circuit breaker, which de-energizes a transformer. In a high voltage power system (i.e. greater than 66 kV), the most prevalent ferroresonant circuit occurs between a de-energized transformer and the grading capacitance of an open circuit breaker.

One major disadvantage with the brute-force time-domain technique is computation time. As mentioned, direct calculation of the stability domain boundaries can be achieved quickly by using the Galerkin method of harmonic balance or by the method of averaging. In order to overcome the limitations inherent in a quasi-static approach, the method of averaging has been enhanced by considering the location of initial conditions on the basin of attraction. An improved prediction of the parameters necessary to cause a jump to fundamental frequency ferroresonance can now be achieved.

The Limacon of Pascal is found to be a good approximation to the geometric shape of the basin of attraction of the period-1 ferroresonant attractor and can be used to analytically calculate a better approximation of the stability domain boundary. The initial conditions at the time a transformer is de-energized can result in a jump to period-1 ferroresonance that is not predicted by quasi-static methods.

A general set of averaged equations is derived that permit the analysis of an n^{th} order polynomial approximation of the magnetization curve. Depending on the transformer, anything between a 9^{th} order and 19^{th} order polynomial may be necessary to adequately describe the shape of the curve. The location of the saddle points and slope of the stable manifold through the saddle points can be determined for a particular transformer under study. The critical parameters resulting in a crossing of the separatrix can then be found iteratively by solving the Limacon equations.

Rather than derive general equations for each possible subharmonic oscillation, the approach taken is to display the projection of the upper and lower period-1 turning points on a parameter plane. The enclosed region between the two curves contains all relevant subharmonic oscillations.

Based on laboratory experiments, the effective iron-core loss resistance of the transformer decreases by a factor of five during period-1 ferroresonance due to increased eddy-current losses in the tank and core components. An additional curve on the parameter plane reflecting the increased core losses is recommended to indicate a low risk of ferroresonance region.

7.2 MODELLING OF FERRORESONANCE

Several different ferroresonant circuits have been modelled and compared with field or laboratory measurements including: wound potential transformer/grading-capacitance, transformer-terminated double-circuit transmission line and a coupling capacitor voltage transformer. Field measurements are crucial in the development of an accurate model. Because of the high degree of nonlinearity in the magnetizing characteristic, general assumptions cannot be made about its low frequency behaviour, loss behaviour or shape in regions of high saturation.

Piecewise-linear representations of saturation curves may produce artificial ferroresonant states in commercial electromagnetic transient programs due to numerical problems with the solution technique. Rapid transitions from saturated to unsaturated states has been shown to excite fictitious zero sequence system resonances. The technique used in this thesis to overcome this problem is to first take the manufacturer's open-circuit voltage and current measurements and convert to a flux-linkage/magnetizing-current curve. A polynomial best-fit approximation to the measured data is then found and a piecewise-linear curve with a minimum of twenty segments created. The polynomial may require adjustment in order to match ferroresonance field tests, if available.

It should be noted that open-circuit measurements of the magnetizing characteristic performed on a tanked transformer are not accurate. The inherent stray capacitance-to-ground of the transformer is sufficient to distort the measurements leading to poor approximations to the true magnetizing characteristic.

Comparisons between two different iron-core loss models have been made. Either a pure eddy-current loss model or a mixed hysteresis/eddy-current loss model is able to adequately represent the iron-core losses up to rated voltage and rated frequency. Preference is given to the mixed form if the damping of subharmonics is to be modelled accurately.

Laboratory measurements indicate the effective resistance of the iron-core loss decreases during period-1 ferroresonance. It is postulated that increased stray eddy-current losses in the tank and other core components is occurring. Average power measurements do not provide adequate information to draw conclusions of iron-core loss model performance. The high level of voltage and current distortion requires harmonic power measurements to be taken. A very simple switched iron-core loss resistor is found able to model the losses during period-1 and period-3 ferroresonance modes in a laboratory transformer.

7.3 SUGGESTIONS FOR FURTHER STUDY

Even though the initial objectives of the research were met, several questions arise out of this research that could be explored by further research.

7.3.1 Iron-Core Loss Modelling

Further work is recommended into measuring the losses (i.e. effective iron-core loss resistance) during transient and steady-state ferroresonance. A nonlinear resistor could be developed that is a function of voltage, flux linkage, and frequency. Various transformer types and sizes should be investigated to determine the robustness of the new model.

7.3.2 Location of Ferroresonance Stability Domain Boundaries

The transformer/grading-capacitance circuit should be further investigated to determine the influence other disturbances, such as clearing of faults and filter switching, for example, have on the location of the period-1 stability domain boundary. Where are the initial conditions prior to crossing the separatrix? Which disturbance is the worst case?

Are there any benefits in using a higher order method, such as the Galerkin method of harmonic balance, for locating fixed points? How much accuracy is sacrificed by using the general form of the averaged equations?

7.3.3 Equivalent Network Determination and Simplification

Can a heuristic approach be used to simplify a complicated frequency dependent network to a minimum set of state variables? What circuit develops if a frequency dependent network equivalent is developed using a multi-port equivalencing technique? Is there any advantage to studying the states of the system in the DQ0 frame or $\alpha\beta 0$ frame versus a complete set of state variables?

Given a simple system with more than two state variables, can an analytical 2d bifurcation diagram be constructed?

7.3.4 Topological Modelling of Transformers

Are there any benefits to using topological modeling in a three-legged core configuration? What are the effects on iron-core losses if a topological model is used? Are there any modelling guidelines that can be stated regarding parameter selection?

7.3.5 Nonlinear Frequency Scans

Can the bending of the frequency scan in the subharmonic range be shown and/or predicted. Can Mork/Wrate's method (frequency modulated current injection) be used to any advantage in a general case or should a new technique like frequency modulated voltage sources be developed instead?

Appendix A

Ferroresonance Literature Review: 1907-1999

A.1 LITERATURE CLASSIFICATION

The vast majority of English language publications discussing some aspect of ferroresonance have been collected and were reviewed. Some French and German papers of historical interest or of archival value are also included. A short summary of each paper is included in Section A.2 .

The papers cover a wide variety of specific topics including field testing of transformers, simulation of the phenomena and theoretical calculations. In order to expedite the retrieval of appropriate papers, the literature has been classified. Table A.1 through Table A.5 summarizes each reviewed paper based on a few criteria.

Several analysis techniques have been used over the years to either explain the ferroresonance phenomenon or to try to predict system parameters which are necessary to cause a jump to a ferroresonant mode. The main techniques are: Rüdenberg's graphical approach, Swift's describing function method, Harmonic balance, and chaos/nonlinear dynamics. Other methods which don't fit one of these categories are labelled analytical.

The papers are also grouped by the particular circuit which was studied and the voltage class. Distribution voltages are defined by voltages less than 35 kV (dist <35kV) while transmission voltage levels (trm.>66kV) are defined by voltages greater than 66 kV. The two most prevalent circuits are wound potential transformers (PTs) and unbalanced operation of distribution transformers (open cond.). Three circuit configurations have been identified for the wound PT:

1. *grounded PTs in an ungrounded system,*
2. *PT/circuit breaker grading capacitance,*
3. *Unbalanced operation of grounded PT in a grounded system.*

Other circuits include: capacitor voltage transformers (CVTs), transformer-terminated/series-compensated lines (series cap), double-circuit transformer-terminated lines (dble. cct), or series compensated HVdc Converters (HVdc/cap.). One case identified generator overspeeding (ge) as being the cause of ferroresonance [A34]. In some applications, the influence of metal oxide varistors (MOVs) have been considered important. Ferroresonance usually occurs after a switching event such as energizing or de-energizing the circuit.

Rather than concentrating on a specific example, some authors chose to examine either a series or parallel RLC circuit. These papers are separated by selecting (series cap.) with no corresponding voltage level designation. Some theoretical calculations were performed on Duffing's equation because some ferroresonant circuits can be simplified into this form.

It is important to know whether the event described is resulting from an actual field observation or field test (fld. obs./tst), generated using laboratory equipment (lab. test) or simulated using mathematical techniques (simulation).

The simulation technique is further classified. Was a commercial simulation program such as EMTP (1) or EMTDC (3) used? If the circuit was simplified in order to be able to write the differential equations by hand, what integration technique was used to solve the nonlinear equations (i.e. Runge Kutta (2), Gear, Trapezoidal etc.)? The code (4) is present if either the author didn't specify the simulation technique or the technique/commercial program hasn't been used often. Some of the other techniques used include: Modified Euler [A60], Hamming[A65], MORGAT [A78] and AUTO [A96].

Early papers used a differential analyzer to calculate the transients. These papers are lumped together with the lab tests.

The transformer simulation models can be described by the following codes:

1. 1 phase

2. 3-1phase

3. Hysteresis modelled

4. 3 phase (5-legged core)

5. 3 phase (3-legged core)

The majority of simulations that have been conducted have used single-phase transformer models with a parallel linear resistor representing iron-core losses. If hysteresis was also modelled the tables include the number (3) beside the first entry.

Both piecewise-linear and polynomial representations of the saturation curve have been tested. The polynomial is the most popular because it allows several mathematical techniques to be used and doesn't suffer from numerical problems associated with switching between linear segments of the piecewise curve.

Table A.1 Literature Classification (papers 1-25)

category	Publication Reference																								
	1	2	3	4	5	6	7	8	9	10	11	12	13	14	15	16	17	18	19	20	21	22	23	24	25
graphical	X	X	X		X				X					X											
descr. fcn.																									
harm bal.													X						X			X			
chaos/nlin																									
analytical				X		X				X		X	X		X			X							
dist <35kV								X	X	X	X			X		X	X				X		X	X	X
trm.>66kV																				X					
PTs								1			1					1									
CCVTs																									
open cond									X	X				X							X			X	X
dble. cct.																									
series cap.	X	X	X	X	X	X	X						X		X		X	X							
HVdc/cap.																									
MOVs																									
fld obs./tst																	X								X
simulation																									
lab. test		X	X	X		X	X	X	X	X	X	X	X	X	X	X	X		X	X	X			X	X
Duffing's												X							X			X			
TF model	1	1	1	1	1	1	1		1			13	1	1	1		1	1	1			3			
paper date	07	20	21	38	38	39	41	41	50	50	51	56	57	58	59	59	59	60	64	64	65	66	66	67	68

Table A.2 Literature Classification (papers 26-50)

category	Publication Reference																							
	26	27	28	29	30	31	32	33	34	35	36	37	38	39	40	41	42	43	44	45	46	47	48	49	50
graphical						X													X						
descr. fcn.			X								X			X								X			
harm bal.								X								X					X				
chaos/nlin																									
analytical					X	X							X								X			X	
dist <35kV	X	X				X						X					X			X					
trm.>66kV			X				X		ge	X	X		X	X	X	X		X	X		X	X	X		X
PTs															12				12						2
CCVTs						X								X	X	X									
open cond.	X	X										X		X	X		X		X	X					
dble. cct.										X			X	X	X			X					X		
series cap.					X	X	X	X						X	X									X	
HVdc/cap.																									
MOVs																									
fld obs./tst		X								X			X										X		X
simulation															4			2					2	2	4
lab. test			X		X	X	X	X	X	X			X		X		X	X		X				X	X
Duffing's																									
TF model			1	53	13	1	2	13			1		1	1	23	1		13	1		1	1	2	13	13
paper date	68	68	69	69	70	70	71	71	72	72	72	73	73	74	74	75	75	76	76	76	76	77	78	78	78

Table A.3 Literature Classification (papers 51-75)

category	Publication Reference																								
	51	52	53	54	55	56	57	58	59	60	61	62	63	64	65	66	67	68	69	70	71	72	73	74	75
graphical													X					X			X				
descr. fcn.		X		X				X						X											
harm bal.	X					X																			X
chaos/nlin	X								X			X			X										
analytical							X		X															X	
dist <35kV			X					X				X		X				ge		X		X	X		
trm.>66kV		X		X	X	X	X		X	X			X			X			X		X			X	X
PTs						2				2		1				2			1		2			2	2
CCVTs									X																
open cond.			X				X						X							X		X	X		
dble. cct.					X																				
series cap.	X			X				X			X			X			X								
HVdc/cap.																									
MOVs																									
fld obs/tst						X				X						X		X	X			X		X	
simulation	2	4		4	2			4	4	4	1	4			24						1			4	2
lab. test	X							X			X	X		X			X		X			X			X
Duffing's															X										
TF model	1	13		5	4	1	1	1	1	1	13	23	1	1	1				2		1			1	1
paper date	78	78	79	79	80	81	82	82	82	82	83	83	85	85	85	86	86	87	88	88	89	89	89	89	89

Table A.4 Literature Classification (papers 76-100)

category	Publication Reference																								
	76	77	78	79	80	81	82	83	84	85	86	87	88	89	90	91	92	93	94	95	96	97	98	99	100
graphical						X	X					X													
descr. fcn.										X	X														
harm bal.				X								X			X										
chaos/nlin		X	X					X	X											X	X		X		
analytical																	X								
dist <35kV					X	X	X															X		X	X
trm.>66kV	X		X	X	X			X	X	X	X	X		X	X	X		X	X	X	X		X	X	
PTs				2	12					2					2			2							
CCVTs											X														
open cond.	X		X		X		X			X		X		X						X		X			X
dble. cct			X		X									X		X									
series cap.		X											X				X								
HVdc/cap.																									
MOVs	X					X																			X
fld obs/tst	X		X	X	X		X	X	X					X				X	X			X			X
simulation	1	2	4			2		12	24			2	4	1		1		1	2	2	24		12		1
lab. test		X	X	X						X	X		X											X	
Duffing's																							X		
TF model	1	1	2	1		1		1	1	1	1	1	13	5	1			1	1	1	1		1		4
paper date	90	90	90	90	90	91	91	91	91	91	91	91	91	91	91	91	92	92	93	93	93	93	93	93	94

Table A.5 Literature Classification (papers 101-125)

category	Publication Reference																								
	101	102	103	104	105	106	107	108	109	110	111	112	113	114	115	116	117	118	119	120	121	122	123	124	125
graphical																									
descr. fcn.																									
harm bal.															X		X								
chaos/nlin		X	X				X		X			X	X	X	X						X		X		X
analytical																X	X								
dist <35kV	X	X				X				X	X		X			X	X		X		X	X			
trm.>66kV				X	X		X	X	X					X	X			X		X			X	X	X
PTs				1				2									1			X	1		2	2	
CCVTs							X																		
open cond.	X			X		X			X										X						
dble. cct.																				X					
series cap.			X									X	X	X		X						X			X
HVdc/cap.																		X							
MOVs	X					X					X														
fld obs/tst	X	X			X	X											X			X					
simulation		1	4				2	1	24	4	4	2	4	2	2	4	2	3		1	2	4	2	4	3
lab. test			X	X												X					X			X	
Duffing's																									
TF model		4	13				1	1	1	53	53	1	1	1	1	1	2	5		23	2		1	13	1
paper date	94	94	94	94	95	95	95	95	95	95	95	95	95	95	95	95	95	95	95	95	95	96	96	96	96

Table A.6 Literature Classification (papers 126-150)

category	Publication Reference																								
	126	127	128	129	130	131	132	133	134	135	136	137	138	139	140	141	142	143	144	145	146	147	148	149	150
graphical	X																			X					
descr. fcn.																									
harm bal.																									
chaos/nlin	X	X	X	X		X			X	X	X	X	X			X	X			X	X	X	X	X	X
analytical																									
dist <35kV	X		X		X	X						X	X	X			X			X	X	X	X		
trm.>66kV	X	X		X			X	X			X			X	X		X	X		X				X	X
PTs	1	2				1	3			2				2		2	12		1	1	1		1		2
CCVTs								X										X							
open cond.	X						X				X			X	X		X			X				X	
dble. cct.	X													X						X				X	
series cap.			X		X				X			X	X	X											
HVdc/cap.																									
MOVs														X											
fld obs/tst	X	X					X	X		X				X				X		X		X		X	
simulation	1	12	4	4	4	2	1	1	2	2	24	4	4		1	2	1	2		1	2	1	2	1	2
lab. test					X	X		X	X					X							X		X		
Duffing's																									X
TF model	25	1	1	1	1	2	23		13	1	1	1	1	13	1	1	1	1		25	2	4	2	5	1
paper date	96	96	96	96	97	97	97	97	97	97	97	97	97	97	98	98	98	98	98	99	99	99	99	99	00

A.2 BIBLIOGRAPHY

[A1] Bethenod, J., "Sur le Transformateur à Résonance", *L'Éclairage Électrique*, Vol. 53, pp. 289-96, Nov. 30, 1907.

Bethenod discusses the possibility of multiple fundamental frequency operating points in a circuit where a saturable reactor is in series with a capacitor. A graphical approach is used to study the phenomenon. Ferroresonance is not used at this time to label the phenomenon. An interesting historical note: H. Poincaré was on the scientific board of this journal.

[A2] Boucherot, P.,"Éxistence de Deux Régimes en Ferrorésonance", *Rev. Gen. de L'Élec.*, pp. 827-828, Vol. 8, No. 24, December 11, 1920.

The author uses a graphical method to show the existence of two regions of ferroresonance: a high current and a low current mode. A physical explanation for this phenomenon was formulated in an earlier paper by Bethenod [A1]. The high current mode was discovered accidently and was mentioned in an earlier article (May 22, 1920, R.G.E).

[A3] Margand, F.,"Au Sujet de L'Éxistence de Deux Régimes en Ferro-résonance", *Rev. Gen. de L'Élec.*, Vol. 9, pp. 635-637, May 7, 1921.

Margand was intrigued by Boucherot's observation and further improves upon the graphical technique. He shows the effect of load resistance on the capacitor ellipse, for example, and explains why certain operating points are stable and others are not.

[A4] Travis, I., and Weygandt, C.N.,"Subharmonics in Circuits Containing Iron-Cored Reactors", *AIEE Trans.*, Vol. 57, pp. 423-431, August, 1938.

The authors analyze a series RLC circuit by applying a differential analyzer, a region-by-region (or piecewise-linear) method and a direct analytical solution by means of recursion formulae.

The following idealized assumptions are made:

1. winding resistances and distributed capacitances are equal to zero.

2. hysteresis effects may be neglected.

3. no eddy-current losses exist in the core.

The physical mechanism of subharmonic production is shown linked to the trapped charge on the series capacitors.

The recursion method suffers from the required idealization (i.e. neglect all resistance, piecewise-linear single-valued mag. characteristic) of the circuit in order to make the mathematics reasonable. The author claims the steady states can be calculated in terms of circuit parameters and the initial transient can be ignored.

[A5] Odessey, P.H., and Weber, E.,"Critical Conditions in Ferroresonance", *AIEE Trans.*, Vol. 57, pp. 444-452, August, 1938.

Classic paper on graphical approach with good references. The first case of describing the multitude of operating points was discussed by Bethenod in 1907. The method of graphical analysis was first introduced by Stark (1917) and refined by Rouelle (1934). Margand (1921) and Rüdenberg (1923).

The purpose of the paper is to explain the theory and how it could relate to relay and control problems.

Errors are present that are attributed to the presence of harmonics The errors influence the value of apparent resistance. Although, the errors don't seem to be any worse than some of the other approximate solutions.

[A6] Thomson, W.T.,"Similitude of Critical Conditions in Ferroresonance Circuits", *AIEE Trans.*, Vol. 58, pp. 127-130, March, 1939.

The author attempts to design a series RLC circuit for use in a resonant relay circuit. Critical conditions on the volt-amp curve are defined where $dE/di=0$.

This seems to be a pseudo-graphical approach. The in-phase and quadrature components of reactor voltage are also generalized based on detailed iron and core information.

[A7] McCrumm, J.D.,"An Experimental Investigation of Subharmonic Currents", *AIEE Trans.*, Vol. 60, pp. 533-540, 1941.

A very interesting and well written paper. The author uses metaphors such as lakes, islands and marshes to describe the phenomenon of subharmonic ferroresonance. The classic *jump* to period-1 ferroresonance avoids subharmonics if the applied voltage is slowly increased. The subharmonics are excited by *shocking* the system. Similar observations have been made in this study.

Contains a good bibliography review. The oldest paper is by Boucherot 1920.

The circuit analyzed is a series RLC. The circuit is *shocked* into subharmonic ferroresonance by closing a switch. Following the switch closing the inductor is momentarily short-circuited. The switching angle and the moment the short circuit is removed are important parameters. The initial conditions determined what mode of ferroresonance occurred. Period-3 was most common while periods-2, 6, and 9 were rare.

[A8] Shott, H.S., and Peterson, H.A.,"Criteria for Neutral Stability of Wye-Grounded-Primary Broken-Delta-Secondary Transformer Circuits", *Transactions on AIEE*, Vol. 60, pp. 997-1002, 1941.

The paper provides more details on the work published later in Peterson's book on power system transients [A11]. Ferroresonance in grounded-wye-broken-delta potential transformers connected in an ungrounded system is investigated. A transient network analyzer (i.e. miniature system setup) is used to investigate the circuit. Regions of stable 30 Hz quasi-periodic (QP-2), unbalanced fundamental (UF) and third harmonic (H-1/3) are presented. Installing line-line rated PTs in a line-ground configuration plus sufficient resistance (less than 45% of X_m) or reactance (less than 12% of X_m) across the break in the open-delta prevent ferroresonance from occurring. The ferroresonance mode was excited by shocking the system either by energization or by fault removal. Relatively long transients exist near the border line of two different stable oscillation regions.

[A9] Rüdenberg, R., *Transient Performance of Electric Power Systems*, New York: McGraw-Hill, pp. 642-656 and 689-695, 1950.

I incorrectly associated the graphical approach as being developed by Rüdenberg. Actually, Odessey [A5] refined an already existing method in an earlier paper. The approach is generally referred to as Rüdenberg's because the textbook is heavily referenced and can be considered as a classic.

The mechanism of subharmonic oscillations is qualitatively described in Chapter 50. He correctly identifies the fact that the subharmonics gradually disappear as losses are increased until only the period-3 is left. Eventually, this mode can also be made to disappear. The existence regions appear in narrow zones of capacitance and impressed voltage and appear in series and parallel connections of transformers and capacitors.

An example of single-pole operation of a 30 kV distribution transformer is discussed (pp. 652-656).

The differential analyzer is used to solve the differential equations of series and parallel RLC circuits. Various subharmonic modes were excited depending on the switching phase of the impressed voltage.

A comprehensive bibliography is contained in this book.

[A10] Clarke, E., *Circuit Analysis of A-C Power Systems: Volume II*, John Wiley & Sons: New York, pp. 174-209, 1950.

Clarke analyzes conditions necessary to create abnormal voltages on a system where one or two conductors are supplying power to an ungrounded transformer. Both calculations using sequence components and laboratory investigations are reported. The miniature system investigated banks of single-phase transformers and three-phase transformers of both the shell and core type.

Curves are developed comparing the open-circuit voltage vs. the ratio X_c/X_m. The symmetrical component calculations made by Clarke neglect transformer losses and do not take into account harmonics. Further, it is assumed the sustained voltages are nearly sinusoidal of fundamental frequency. The effective exciting reactance of the transformer is determined by the ratio of the rms voltage to the rms current. The calculations actually proved to follow lab measurements reasonably well.

[A11] Peterson, H.A.,*Transients in Power Systems*, John Wiley & Sons: New York, pp. 265-279, 1951.

Observations of grounded-wye PT with a broken delta or wye secondary in an ungrounded system are discussed. The author has seen quasi-periodic 1/2, period-3, fundamental and QP-2 oscillations following investigations on a miniature system.

Source of references from 1900-1950 are included.

[A12] Brenner, E.,"Subharmonic Response of the Ferroresonance Circuit with Coil Hysteresis", *AIEE Trans.*, Vol. 74, pp. 450-456, Sept., 1956.

The authors use a piecewise-linear analysis of a series RLC circuit. The source and coil characteristic are discretized permitting such an analysis. The circuit responded in a definite sequence as the amplitude of the supply voltage was decreased from a large value (fundamental, period-3, period-5, higher odd harmonics, even-order subharmonics in reverse order, unsymmetrical fundamental).

Minor loops were responsible for even order unsymmetrical subharmonic responses.

Trapped charge is considered as the basic explanation of subharmonics.

[A13] Plotkin, S.,"Discontinuous Transition Time Between Stable State in Ferroresonance Circuits", *AIEE Trans.*, Vol. 75, pp. 410-421, Sept., 1957.

A theoretical analysis of the transition time between nonferroresonant and ferroresonant states is presented. The bistable behavior of this circuit has been exploited in magnetic amplifiers, sensing devices, stabilizers and counting circuits. Transition speed is maximized while inductor losses ideally should be minimized. The differential equations are solved using the harmonic balance method and the Kryloff-Bogoliuboff method with similar solutions resulting.

Both series and parallel ferroresonant circuits are analyzed. The calculations are approximate and higher harmonic terms are neglected. The nonlinear characteristic is limited to a third order polynomial. Experimental results are also presented.

The hysteresis and eddy-current losses are very important in the determination of the transition time. For example, thicker laminations (note: eddy-current losses increase with the square of the lamination thickness) give faster transition speeds. I find this point hard to believe. If eddy-current losses are large enough the transition won't take place. The authors place an equivalent resistor in series with the coil and claim eddy-current losses are being modelled.

[A14] Kelly Jr., G.E.,"The Ferroresonance Circuit", *AIEE Trans.*, Vol. 77, pp. 843-848, Jan., 1959. (Discussion: pp. 1061)

Authors perform calculations and lab experiments on a 2 kVA 120-240 V transformer. Subharmonics are not initiated. A lot of qualitative discussion but no mathematics. The discusser recognizes his methods as the Odessey-Weber treatment (modified phasor analysis) and the Rouelle

method.

A three-phase distribution circuit with an open conductor is briefly analyzed. The circuit is simplified to a single-phase representation of the open phase.

[A15] Dennard, R.H.,"Behavior of the Ferroresonant Series Circuit Containing a Square-Loop Reactor", AIEE Trans., Vol. 77, pp. 903-911, Jan. 1959.

Dennard completed his dissertation on this subject in 1958 at the Carnegie Institute of Technology.

A series RLC circuit is analyzed under square wave and sinusoidal excitation. The square wave excitation can be analyzed analytically because transcendental equations do not arise. Some equations are derived defining the overshoot factor.

[A16] Karlicek, R.F., and Taylor Jr., E.R.,"Ferroresonance of Grounded Potential Transformers on Ungrounded Power Systems", *AIEE Trans.*, Vol. 77, pp. 607-618, Aug., 1959.

Interesting paper which discusses TNA and laboratory tests of grounded PTs in an ungrounded system. The PTs are used for ground fault detection on 480 V and 2400 V systems. The secondary is connected broken delta normally.

The authors refer to the phenomena as *ferroresonance* although *neutral inversion* and *neutral instability* have been used in the past.

Ferroresonance was initiated by energizing the PT or by momentary application of a single-phase grounding switch. Depending on the value of the line-to-ground capacitance, the ferroresonance that occurred following the transient, could occur more or less easily depending on the transient. For example, at high values of C, ferroresonance occurred more easily following SLGF removal. Whereas, at lower C, the switching transient more easily initiated ferroresonance.

The magnetizing reactance had no significant effect on the range of capacitance where ferroresonance occurred. The air-core reactance had a much more pronounced effect.

The authors come up with a simple relation for secondary resistance.

In the discussion, some experiences are related where in some situations, even a resistor of 100% thermal rating did not prevent ferroresonance. Other comments, such as the availability of air-core reactance data are made.

The authors curves are interesting. Only period-1, period-2 and period-4 oscillations were observed. Period-3 were rare and only occurred at low values of capacitance.

[A17] Kratz, E.F., Manning, L.W., and Maxwell, M.,"Ferroresonance in Series Capacitor-Distribution Transformer Applications", *AIEE Trans.*, Vol. 77, pp. 438-449, Aug., 1959.

Authors describe TNA (2.4 kV) and some full scale tests (7.6 kV) on energizing a series compensated distribution transformer. They seemed to concentrate on transient ferroresonance rather than period-1 or subharmonic ferroresonance. The effect of different parameters were studied. For example, as the source impedance was increased there was a gradual reduction in the severity of ferroresonance.

Several discussers question the validity of their conclusions because other parameters such as the magnetizing characteristic have an important effect on ferroresonance.

Various techniques of describing the zones of ferroresonance as a function of system parameters are presented.

[A18] Salihi, J.T.,"Theory of Ferroresonance", *AIEE Trans. (Communication & Electronics)*, Vol. 78, pp. 755-763, Jan., 1960.

Salihi completed his Ph.D. "Capacitive Loading on Nonlinear Magnetic Circuits" in 1958.

The author modifies the magnetizing characteristic to a square characteristic and the source to a square wave. By so doing, the analysis can be made simpler. A feedback diagram is derived.

The assumptions made make the analysis questionable at best. No mention is made of subharmonics.

[A19] Hayashi, C., *Nonlinear Oscillations in Physical Systems*, New York: McGraw Hill, 1964.

Classic book on the subject. Describes analytical and topological solutions of nonlinear differential equations. Duffing's equation is the closest to the series ferroresonant case.

Harmonic and subharmonic oscillations are discussed. The author performs experiments and calculates solutions analytically.

[A20] Aicher, L.C., and Thomas, C.H.,"Ferroresonance as a Transmission Problem", *American Power Conference*, pp. 854-860, 1964.

The authors analyze the effects of energizing a 500 kV autotransformer at the end of a transmission line. Depending on the values of: source reactance, transmission line length, MVA rating of transformer, knee point of transformer, ratio of transformer unsaturated reactance to saturated reactance, ferroresonant overvoltages could result. Some of the overvoltages may be harmonic overvoltages due to tuning of the network to the fifth or seventh harmonic.

[A21] Hopkinson, R.,"Ferroresonance During Single-Phase Switching of 3-Phase Distribution Transformer Banks", *IEEE Trans. on Power App. & Systems*, Vol. 84, No. 10, pp. 1258-1265, April 1965.

Curves are defined in this paper that are still used by distribution engineers. He defines the X_c/X_m ratio (phase-to-ground capacitance to transformer magnetizing reactance) and says a ratio greater than 40 is required to prevent excessive overvoltages.

Representative capacitance data are given for pole-type distribution transformers.

[A22] Hayashi, C.,"The Influence of Hysteresis on Nonlinear Resonance", *Journal of the Franklin Institute*, vol. 281, no. 5, pp. 379-386, May 1966.

Hayashi presents a very interesting paper where he extends his previous work [A19] to include the effects of hysteresis on the period-1 attractor. Assuming the magnetic flux varies sinusoidally, the following equation is chosen to represent a magnetization curve with hysteresis. The third term is an ellipse and is associated with hysteresis.

$$i = c_1\lambda + c_3\lambda^3 + \frac{1}{\nu}\frac{a}{1+br^2}\frac{d\lambda}{d\tau} \qquad \text{(A-1)}$$

The parameters, c_1, c_3, a, and b are chosen to represent the magnetization curve under study.

The method of harmonic balance and slowing varying averages are used to determine the steady-state solutions and stability of solutions. It is shown that the resonance curve can have an isolated portion depending on the value of parameters chosen.

Hysteresis losses are compared with ohmic losses. It is observed that when the amplitude of the forcing function is small, the influence of hysteresis on the resonance is large.

[A23] Turley, S.,"Ferroresonance Oversimplified", *Transmission & Distribution*, pp.36-40, Oct. 1966.

Discusses ferroresonance qualitatively and describes some circuits where ferroresonance might or might not occur. Some mitigation measures are discussed. The author has some lack of understanding of the types of overvoltages that can occur. He feels more work is required that will define the causes and effects of ferroresonance.

[A24] Hopkinson, R.,"Ferroresonant Overvoltage Control Based on TNA Tests on Three-Phase Delta-Wye Transformer Banks", *IEEE Trans. on Power App. & Systems*, Vol. 86, No. 10, pp. 289-293,

Oct. 1967.

Identical study to the one presented in [A25] except delta-wye transformers are studied instead of wye-delta.

The authors mention that they calculate the expected overvoltages analytically by drastically simplifying the nonlinear differential equations such that steady-state methods can be used. No details are given except a reference to Clarke's circuit analysis book [A10].

[A25] Hopkinson, R.,"Ferroresonant Overvoltage Control Based on TNA Tests on Three-Phase Wye-Delta Transformer Banks", *IEEE Trans. on Power App. & Systems*, Vol. 87, No. 2, pp. 352-361, Feb. 1968.

TNA tests on wye-delta transformer banks are performed during single-phase switching. Results show the effect of transformer size and lateral cable length.

Neutral resistors and secondary loads are attractive mitigation measures.

In the discussion section of this paper, the authors of [A27] ask why there is a discrepancy between their full scale tests and the authors TNA tests. The author counters by saying the TNA tests were substantiated by two independent full scale tests with similar results. He says something is apparently wrong with the discusser's tests! Who is correct?

[A26] Hopkinson, R.,"Ferroresonant Overvoltages Due to Open Conductors", *Distribution*, Fourth Quarter, 1967.

This article summarizes some of the results presented in [A25],[A24],[A21].

[A27] Young, F., Schmid, R., Fergestad, P.,"A Laboratory Investigation of Ferroresonance in Cable-Connected Transformers", *IEEE Trans. on Power App. & Systems*, Vol. 87, No. 5, pp. 1240-1249, May 1968.

Full scale laboratory investigations, consisting of energizing and de-energizing a three-phase 13 kV distribution transformer via a single-phase cutout, are presented. Based on these experiments, it is concluded that a simple relation doesn't exist between the normal exciting current, and cable length required for ferroresonance. For example, Hopkinson's work [A25][A21] showed ferroresonance occurred at 4 ft. of cable for a 13.2 kV, 150 kVA delta-grounded wye transformer. System tests performed by the authors showed ferroresonance occurred at 100 feet. I would say the TNA model losses are not accurate and provide too pessimistic a result.

One interesting fact the authors found was there is a higher probability of obtaining overvoltages during de-energizing than energizing sequences.

There is a linear relationship between the percent of secondary load and the increase in cable length before ferroresonance is experienced. 1-4% resistive loads were tested. Cable lengths increased from 1000 to 4000 ft. using the aforementioned loads. The winding connections had some influence on the effectiveness of the resistive load.

[A28] Swift, G.,"An Analytical Approach to Ferroresonance", *IEEE Trans. on Power App. & Systems*, Vol. 88, No. 1, pp. 42-46, Jan. 1969.

Classic paper on analyzing ferroresonance using incremental describing functions (i.d.f.) or also known as the dual-input describing function (d.i.d.f).

The parallel ferroresonance case is examined (i.e. a line or cable charging capacitance in parallel with a transformer's magnetizing branch). Only the spontaneous jump to ferroresonance is considered. Switching surge initiated or subharmonic ferroresonance are not considered. Further analytical work in this direction would be useful. A 5th order polynomial representation of the magnetization curve is analyzed.

Analog computer simulations were made for verifying the analytical work.

[A29] Wright, I.A., and Morsztyn, K.,"An Improved Method of Simulating the Transient Performance of Power System Transformers", Int. J. Elect. Eng. Educ., Vol. 6, No. 4, pp.499-516, 1969.

This paper describes a TNA transformer used at the University of Monash. An interesting feature of the transformer is the nonlinear inductor simulator.

[A30] Santesmases, J.G., Ayala, J., Cachero, A.H., "Analytical Approximation of Dynamic Hysteresis Loop and its Application to a Series Ferroresonant Circuit", *Proc. of IEE*, Vol. 117, No. 1, pp. 234-240, Jan., 1970.

The authors derive a simple analytical expression for modelling the hysteresis loop dynamics. The end result is similar to the one used by Pierrat and Tran-Quoc [A110].

The paper contains a lot of mathematics. The nonlinear equation is solved by the asymptotic method of Bogoliubov and Mitropolsky. A first order approximation is given. In other words, a solution with a single frequency is found.

An equation is derived which defines where ferroresonant jumps can occur.

[A31] Wright, I.A. and Morsztyn, K.,"Subharmonic Oscillations in Power Systems: Theory and Practice", *IEEE Winter Power Meeting*, Paper 70 TP 107-PWR, T-PAS-90, No. 3, pp. 1805-1815, Dec., 1970.

The author describes subharmonic ferroresonance using a single-phase circuit approach.

Swift submits several very pointed remarks concerning this paper. The elimination of the linear portion of the mag. curve can be justified at one frequency perhaps but not several. The exclusion of hysteresis effects, eddy-current losses etc. are not justified as subharmonic stability critically depends on these factors.

I don't totally understand the authors method. It appears to based on a modified graphical technique. He claims the results are verifiable with TNA and real tests on a 5 kVA power transformer.

[A32] Wright, I.A.,"Three-Phase Subharmonic Oscillations in Symmetrical Power Systems", *IEEE Summer Power Meeting*, Paper 70 TP 625-PWR, T-PAS-90, No. 3, pp. 1295-1304, May, 1971.

The author describes the results of a TNA investigation performed at Monash University. The base frequency of the TNA was 500 Hz. A symmetrical three-phase series RLC ferroresonant circuit was analyzed. The different modes and transitions between modes are discussed. The magnetizing curve is represented by a 7th order truncated polynomial. This paper is an extension of his original work [A31],[A29].

One aspect of his Ph.D. work is brought out in the discussion where he says polynomial vs. piecewise-linear mag. curves were compared. He favors polynomial representations.

[A33] Baycura, O.M., and Donovan, J.C.,"An Unsymmetrical Mode of Ferroresonance", *IEEE Trans. on Magnetics*, Vol. MAG-7, pp. 890-895, Dec., 1971.

The author performs experiments on a series ferroresonant circuit using a source frequency of 21 kHz and 3 kHz. An unsymmetrical mode of ferroresonance is found exhibiting a minor loop. The phenomenon is explained qualitatively and quantitatively, I believe using the harmonic balance method. The authors propose using this circuit as a logic or memory element.

[A34] Clerici, A., and Didriksen, C.H.,"Dynamic Overvoltages and Ferroresonance Found in Switching Surge Studies For IRAN 400 kV System", *IEEE Winter Power Meeting*, Paper 71 TP 142-PWR, T-PAS-91, No. 1, pp. 195-203, Jan./Feb., 1972.

Ferroresonance is reported for a 400 kV system in Iran. Large nonlinear overvoltages occur when using one isolated generator to energize a 160 mile line or following load rejection. Frequencies in excess of 50 Hz are experienced following load rejection due to generator overspeed. TNA studies

were used to define ferroresonant regions. Curves are presented as a function of system parameters. For a fixed frequency and parameter set, the voltage behind subtransient reactance was slowly raised until ferroresonance occurred. This kick may not be the most realistic for the circuit under study.

Operating restrictions will prevent ferroresonance problems.

[A35] Dolan, E., Gillies, D., and Kimbark, E.,"Ferroresonance in a Transformer Switched with an EHV Line", *IEEE Summer Power Meeting*, Paper 71 TP 533-PWR, T-PAS-91, No. 3 pp. 1273-1280, May/June, 1972.

The authors describe ferroresonance that occurred in a 1000 MVA 525/241.5 kV wye connected bank of autotransformers. 30.5 km of disconnected line was capacitively coupled to an energized 525 kV line (neither line is transposed). Ferroresonance lasted for 16-22 minutes and no damage occurred although gas relays did alarm after 9 minutes. The increased gassing/heating were caused by localized stray flux linkages, especially in the tank lid.

The authors solved their problem by closing the delta connected tertiary through a resistance. Other methods include: reducing the coupled voltage by transposing the lines, decreasing the trapped charge by using opening resistors, decrease the zero sequence inductance, increase the losses of the circuit while it is in ferroresonance, disconnect the transformer from the line manually or automatically.

Comments are made that adequate information is required during normal and abnormal conditions of the line and transformer parameters, in order to adequately predict ferroresonance.

The paper stimulated significant discussion. Some comments included more information is needed on transformer operation above the knee of the saturation curve.

Mr. Alan Forrest (Teshmont) was involved with testing and inspecting of the autotransformers at English Electric.

The transmission line trapped charge was shown to be very important in the development of ferroresonance. The capacitive coupling only helped to sustain the resonance.

[A36] Ashok Kumar, B.S., Tripathy, A.K., Parthasarathy, K., Kothari, G.C., "Approach to the problem of Ferro-Resonance in E.H.V. Systems", *Proc. of IEE*, Vol. 119, No. 6, pp. 672-676, June, 1972.

Authors first paper using the incremental describing function or Swift method. They point out an error made in the analysis performed by Swift.

The authors examined 3^{rd}, 5^{th}, and 7^{th} order nonlinearities. One conclusion made is the higher the order of the nonlinearity, the more susceptible the transformer is to ferroresonance.

One drawback of this method is closed form solutions for the jump-to points can't be obtained for nonlinearities higher than five due to the difficulty in isolating complex roots. A closed form analytical solution for a third order polynomial is obtained.

[A37] Lister, E.C.,"Ferroresonance on Rural Distribution Systems", IEEE Trans. on Industry Applications, Vol. IA-9, No. 1,pp. 105-111, Jan./Feb., 1973.

A good summary of the situations (unbalanced) where ferroresonance occurs on distribution systems and the possible preventive measures is provided.

Summary of available corrective measures:

1. Circuit design

    a) limit cable length

    b) use three-phase switching device

c) provide secondary dummy load

2. Operating procedures

a) Use special switching sequence

b) Temporarily ground the neutral of wye-delta transformers

3. Three-phase transformer connections

a) Use grounded wye-grounded wye banks

b) use grounded open wye-open delta banks

c) solidly ground wye-delta banks (if there are many close together)

d) use resistance grounded wye-delta banks

No mention is made of problems with 4 and 5-legged transformers.

[A38] Wale, G.,"Ferroresonance in a Disconnected EHV Power System", *GEC Journal of Science & Technology*, Vol. 40, No. 2, pp. 79-86, 1973.

The author analyzes the problem reported in [A35] in more detail. The problem of ferroresonance resulting from capacitive coupling from an energized line (double-circuit tapped line).

The comment is made that the core loss is made up of the hysteresis component (dependent on peak flux density) and the eddy-current component (dependent on rms value of line voltage). Additional losses in structural metalwork are present under overfluxing conditions (measurements are required). Copper loss and corona losses are negligible.

Laboratory experiments on a toroidal core (440 V system voltage) were made in order to reproduce the phenomenon. The model had a much higher Q than the real system which didn't allow the generation of low order subharmonics.

A strong influence of phase angle between the two systems was observed.

The actual i-flux curve was obtained using the method of current reversals. Note, for safety reasons the current must be reversed slowly. As well, the winding losses are significant and must be eliminated in the integration circuit.

The solution to the nonlinear equation was found using a graphical method and numerical integration.

[A39] Kothari, G.C., Ashok Kumar, B.S., Parthasarathy, K., Khincha, H.P.,"Analysis of Ferro-Oscillations in Power Systems", *Proc. of IEE*, Vol. 121, No. 7, pp. 616-622, July, 1974.

The authors use the dual input describing function (d.i.d.f.) method for determining regions of ferroresonant oscillations. They try to signify the role of physical parameters by graphically illustrating Nyquist plots as parameters such as capacitance are varied. This paper extends their original work [A36].

One limitation is the assumption that the subharmonic oscillations have predominantly two frequency components (ω and 3ω).

The magnetizing curve is represented as a power series of the form:

$$I_L = a_1\lambda + a_3\lambda^3 + a_5\lambda^5 \qquad \text{(A-2)}$$

Two circuits were analyzed (A,B) while others were commented on:

A. Capacitor Voltage Transformer

They show that subharmonics will occur, however, the jump to period-1 ferroresonance is not

possible.

B. Series Compensated Transmission Lines

Ferroresonance is possible between the series capacitors and receiving end transformers upon line energization. Energization through pre-insertion resistors or bypassing the series capacitors will avoid the resonance.

C. Distribution Systems

During unbalanced operation, the transformer nonlinear magnetizing impedance is in series with the inherent shunt capacitance of the system.

D. Capacitive Coupling on Double-Circuit Lines

On untransposed lines, no effective capacitance appears between the phase sources and the transformer windings unless there is a fault.

[A40] Germay, N., Mastero, S., and Vroman, J.,"Review of Ferroresonance Phenomena in High Voltage Power System and Presentation of a Voltage Transformer Model for Predetermining Them",*1974 CIGRE*, paper no. 33-18, 1974.

The authors review ferroresonance in a high voltage power system and propose a transformer model for the accurate calculation or prediction of this nonlinear phenomenon.

Typical ferroresonant circuits:

1. 1 phase ferroresonance on a transformer connected to a de-energized high voltage line running in parallel with another energized line.

2. 1 phase ferroresonance between PTs and the capacitance of a supply transformer

3. 1 phase ferroresonance between a PT and the capacitance of an open high voltage circuit breaker.

4. 3 phase ferroresonance of PT connected to a system with an insulated neutral and very low zero sequence capacitance.

5. ferroresonance with an unloaded transformer supplied accidently on one or two phases.

6. 1 phase ferroresonance which can occur in a CCVT. No influence on high voltage system

7. Long series compensated lines exhibit ferroresonance effects.

The hysteresis model is based on Preisach's theory on magnetism as modified by Wilde and Girke. They comment that better physical knowledge during heavy saturation of the magnetic material would enable the model to be improved as regards to the extension of the static loops beyond the loop adopted as the limit cycle and also in the choice of series impedances. They don't specify which numerical technique was used.

The authors laboratory measurements and computer simulations appear quite good.

[A41] Germond, A.,"Computation of Ferroresonant Overvoltages in Actual Power Systems by Galerkin's Method", *IEEE PICA 1975 Conf.*, New Orleans, pp. 127-135, June, 1975.

Classic paper that describes Galerkin's method for ferroresonance evaluation. Germond completed his thesis in 1975 at the École Polytechnique Fédérale de Lausanne entitled, "Conditions de ferroré-sonance dans des systemes triphasés".

Steps of the Algorithm:

1. build the differential equations - a single valued polynomial relation between flux and current was used and linear series and parallel resistances representing losses. Ideally, a model such as the one developed by Germay [A40] should be used. Due to the difficulty in obtaining the necessary

data, and the fact that the simple model gives reasonable results, even in the subharmonic regime, the detailed model was not used.

2. Initiate Newton-Raphson method - for solving a system of nonlinear algebraic equations.

3. Evaluate fourier coefficients - of the currents for the appropriate magnetic flux.

4. Calculate the residuals - the residuals are obtained by replacing the unknown fourier coefficients by their approximation and by their evaluation.

5. Evaluate the Jacobian - If the residuals calculated above are larger than prescribed tolerances, evaluate the non-zero elements of the Jacobian matrix (the partial derivatives of the residuals over the unknown amplitudes).

6. Solve the linear system - solve for the correction of the unknown amplitudes and return to step 3

Drawbacks:

1. If a given type of solution is not possible, Newton's process will not converge. New initial conditions have to be found.

2. The solution found is derived for a truncated Fourier series. It remains to be shown that this solution is close to the actual periodic solution of the system.

3. The solutions given by Galerkin's method can be stable or unstable. The differential system is tested for small variations in the solution variables. If the absolute value of the eigenvalues are less than 1, the solution is stable.

Two cases were examined:

A: Capacitively Coupled Voltage Transformer: What domains of the applied voltage will ferroresonance develop? Subharmonic and period-1 ferroresonance were found. Tests show ferroresonance was obtained after opening a short circuit at the secondary of the intermediate transformer.

B: Transformer - cable de-energization: not well explained

It is not clear what speed advantage is gained by this method. As well, the accuracy and effect of different kicks on exciting different ferroresonant modes was not discussed.

[A42] Smith, D., Swanson, S., and Borst, J.,"Overvoltages with Remotely-Switched Cable-Fed Grounded Wye-Wye Transformers", *IEEE Trans. on Power App. & Systems*, Vol. 94, No. 5, pp. 1843-1853, Sept./Oct. 1975.

Full scale laboratory investigations of 4 and 5-legged grounded wye-wye distribution transformers (12.5-25 kV) are presented. Overvoltages (up to 2.1 pu on five legged core and 2.35 pu on four legged) can occur when energizing one of these transformers through single conductor shielded cable (single-pole switches). The allowable cable length is considerably longer than that permitted on ungrounded transformers. Overloading after energization can be avoided by ensuring 10% resistive loading, using three-pole ganged switching or non-coupled core transformers. Lab tests were conducted due to the difficulty in accurately modelling the iron core inductances.

The ferroresonance modes are categorized according to types:

A: symmetrical, 60 Hz periodic

B: asymmetric, 60 Hz base frequency.

C: non-cyclic response sometimes proceeding another type [i.e. transient chaos]

D: 20 Hz subharmonic

E: 30 Hz subharmonic

F: 180 Hz component with 60 Hz modulation

Each type are plotted on a peak voltage vs. cable capacitance diagram. The peak voltage is necessary for determining transformer stresses. The effect of different kicks are shown. The presentation of results and categorization is not as clear as the ones I have used. I don't differentiate between asymmetric and symmetric attractors only the periodicity of each. Transient chaos is identified.

[A43] Teape, J.W., Slater, R.D., Simpson, R.R.S., and Wood, W.S.,"Hysteresis Effects in Transformers, Including Ferroresonance", Proc. of IEE, Vol. 123, No. 2, pp. 153-158, Feb. 1976. "Discussion of:", Proc. of IEE, Vol. 123, No. 11, pp. 1234-1238, Nov. 1976.

The paper describes experimental and computer simulations (4th order Runge Kutta) of inrush and ferroresonance phenomena. The ferroresonant circuit represents the disconnection of an unloaded transformer that is being supplied from one-circuit of a double-circuit line. A 1 kVA lab transformer was used in the simulation. The details of the transformer model is described in another paper.

This paper generated a very lively discussion from the likes of Mastero/Germay[A40] to Wale [A38], Janssens[A117] and others. It seems the fundamental problem appears to be in the transformer modelling. Janssens, for example, says in order to model the secondary cycles of hysteresis with enough accuracy the Preisach type of modelling should be used rather than the Duhem type. It is admitted that losses play an important role in the initiation process. Hysteresis and eddy-current losses can't be adequately modelled in an analytical or phase plane technique. Eddy-current losses were ignored.

Wale described some results from his study of coupling from an energized line. The most significant factor in determining ferroresonance was the phase angle between the line and spur voltages, which modelled the effect of different transposition arrangements.

[A44] Lapierre, J.,"Ferroresonance Made Easy", *CEA Spring Meeting*, March, 1976.

Author uses Rüdenberg's approach to graphically illustrate when ferroresonance could occur. Typical situations are briefly described.

[A45] Hopkinson, R.,"TNA is used to Study Ferroresonance", *Electrical World*, T&D, pp. 74-75, June 1976.

This article summarizes the results of TNA studies made on 15-35 kV distribution transformers. The new tests show agreement with earlier work, in that if the X_c/X_m ratio is greater than 40 ferroresonant overvoltages will not exceed 1.25 pu. The results are valid for remote energizing of one or two conductors. Ferroresonance does not develop on 3 single-phase units or three-phase three-legged core units. Wye-wye connected five-legged cores have the possibility of ferroresonance but were not tested.

[A46] Maklad, M.S., and Zaky, A.A.,"Multimodal Operation of a Ferroresonant Circuit with Quintic Nonlinearity", IEEE Trans. on Magnetics, Vol. 12, No. 4, pp. 380-384, July, 1976.

The authors analyze Swift's circuit using West's method of frequency-damping boundaries. Upper and lower boundaries of the jump region are calculated. The describing function method gives only a certain value for the applied voltage which will produce a jump if this value is exceeded. The authors claim this value lies between the limits determined by the frequency-damping boundary method. However, no experimental evidence supports this claim.

The method appears to be a form of harmonic balance. A crude solution is assumed. The steady-state flux is sinusoidal and higher harmonic terms are neglected.

[A47] Prusty, S., and Sanyal, S.K.,"Some New Solutions to Ferroresonance Problem in Power System", Proc. of IEE, Vol. 124, No. 12, pp. 1207-1211, Dec. 1977.

The authors improve upon previous work using describing function methods. The magnetization characteristic is represented by a 5th order nonlinearity and a closed form analytical solution obtained (an improvement over previous 3rd order nonlinearities [A36]). With higher order nonlinearities, it is normally difficult to isolate the complex roots and graphical techniques must be relied upon. A new jump severity index is proposed for evaluating overvoltages/undervoltages experienced in transformer windings.

Previously, graphical techniques were used to determine the onset of a jump. An equation of the envelope has been developed that enables more accurate determination of the threshold frequency.

Swift's circuit is analyzed.

[A48] German, D.M., and Davies, A.E.,"Ferroresonance on EHV Transmission Systems", 1978 IEEE PES Winter Meeting, Paper No. A78 116-6, Feb., 1978.

Considers the case when ferroresonance occurs following the isolation of a transmission line terminated in a transformer electrically coupled to a second energized line.

Field tests performed on a double-circuit 400 kV line, 150 km long and terminated in a 500 MVA transformer are shown. A period-3 ferroresonant wave was excited depending on the point-on-wave of switching and circuit breaker opening sequence. Computer simulations of a double-circuit 275 kV, 25 km long line terminated in 3 single-phase transformers is also shown.

Concerns with a sustained ferroresonance include: severe overfluxing and overheating due to eddy-currents induced in leakage paths, large magnetizing inrush currents following transformer energization, possible arrester operation following energization.

Runge-Kutta integration is used to solve the state equations. The flux-i equation used was:

$$\lambda = a_1 i + a_2 \tanh a_3 i \qquad \text{(A-3)}$$

The authors note the constant loss resistance is too low to represent losses following switching. A higher value based on field tests resulting in too long a transient period under non-ferroresonant conditions. Further study is required.

The type of transformer, three single-phase, 3 or 5 limb three-phase affected the resulting mode of ferroresonance. It appears the authors performed simulations for the three single-phase case.

The model showed short lines oscillating at the supply frequency or a subharmonic while long lines oscillate mainly as a period-3 ferroresonance.

[A49] Feldman, J.M., and Cappabianca, A.L.,"On the Accuracy and Utility of Piecewise-Linear Models of Ferroresonance", *IEEE Trans. on Power App. and Systems*, Vol. 97, No. 2, pp. 469-477, March/April 1978.

Very wordy description of the turn-on/turn-off process of ferroresonance. The authors perform some lab experiments and computer simulations of a series ferroresonant circuit. A 220/110/110 V transformer is tested. I don't like the fact that the isolation transformer is the same as the transformer under test and an induction regulator is used in parallel. The authors use a piecewise-linear hysteresis model. Equations are developed for predicting the turn-on/turn-off voltages vs. capacitance.

Good agreement was reached between lab and computer results only after very detailed measurements were made. The voltage and current waveforms were captured using an A/D and analyzed on the computer.

[A50] Germay, N., Mastero, S., and Vroman, J.,"Single-Phase Ferroresonance on a 150/$\sqrt{3}$ kV Voltage Transformer: Comparison of Measured and Computed Results", *Proc. of IEE*, Vol. 125, No. 6, pp. 533-535, June 1978.

This paper is a brief extension to the work presented in [A40]. Single-phase ferroresonance in a 150 kV PT is reproduced (both period-1 and period-3). An improvement to the hysteresis model was made. Stray capacitance data is not given. A grading capacitance of 200 and 400 pF were used. If the circuit breaker was opened near a peak, it was observed that period-1 oscillations were more probable than a voltage zero.

[A51] Janssens, N.,"Calcul des zones d'existence des régimes ferrorésonants pour un circuit monophasé", *Proc. of the 1978 IEEE Canadian Communications & Power System Conference*, Cat N° 78CH1373-0 REG7, pp. 328-331, October 1978.

Janssens has written several other papers including: [A62], [A75], [A79], [A117], [A121], [A131] and [A148].

A single-phase RLC circuit is modelled and the Galerkin method of harmonic balance used to find the steady state modes of ferroresonance.

He calculates the characteristic exponents in order to derive stability zones of the period-3 subharmonic and fundamental modes of ferroresonance. Experimental verification is made using a 140 Volt transformer arrangement.

The paper contains an interesting discussion on loss modelling. Janssens modifies the conductance depending on the frequency of oscillation.

[A52] Hirst, D.E., and Baràkat, E.E.,"Improved Analysis of Jump Resonance in Single-Phase Circuits", *Proc. of IEE*, Vol. 125, No. 12, pp. 1380-1382, Dec. 1978.

The authors first propose a combined Swift/time-domain simulation method. Close agreement is found between their analysis, lab experiments and Swift's results on a single-phase circuit.

[A53] "Dual Prescription for Ferroresonance", *Electrical World*, T&D, May, 1979.

This article briefly describes some of the conditions which lead to ferroresonance. Triplex transformers are recommended in situations where ferroresonance arises in three-phase common-core transformers due to mutual coupling. Some of Hopkinson's work is rehashed.

[A54] Baràkat, E.E., and Hirst, D.E.,"Susceptibility of 3-Phase Power Systems to Ferro-Nonlinear Oscillations", *Proc. of IEE*, Vol. 126, No. 12, pp. 1295-1300, Dec. 1979.

Authors use describing function (Swift's) approach. They modify it to include some time-domain simulation in order that three-phase systems can be analyzed. The new hybrid approach is described. A continuation of the results presented in [A52]. The set of nonlinear equations are solved using a Newton-Raphson iterative method.

The authors analyze a three-phase series compensated transformer feeder. A scaled down representation of a three-phase three-limb 750 MVA transformer is tested in their laboratory. Computer simulations use a transformer model developed by Nakra and Barton.

The authors comment that jump resonance and subharmonic oscillations are distinct phenomena. Subharmonics are a form of forced oscillation, requiring a switching condition to excite them.

The differences between experimental and computed results are not as accurate as desired and may be improved by a more detailed core characteristic. More work is needed to establish how well this method deals with wider ranges of circuit and transformer configurations.

Simulations still remain the best means of studying the switching transients needed to initiate ferroresonance.

[A55] Diseko, N.L., and Bickford, J.P.,"A Method of Simulating Linear and Nonlinear Resonant Phenomena Associated with Transformer Feeders", IEE Proceedings, Vol. 127, Pt. C, No. 3, pp. 169-178, May 1980.

The purpose of this paper is to present a new method for simulating transient phenomena (i.e. a

combination of travelling wave transmission line calculations and direct solution of transformer equations in state space).

Of interest are the simulation results of a double-circuit 45 km long 400 kV transmission line. The 1000 MVA grd.-wye/grd.-wye/earthed-delta tertiary winding transformer experienced ferroresonance if a three-limb representation was used. A five-limb representation has a relatively high zero-sequence impedance and consequently the energy induced from the energized line is not sufficient to sustain the oscillations.

[A56] Aggarwal, R.P., Saxena, N.S., Sharma, B.S., Kumar, B., and Krishan, S.,"Failure of Electromagnetic Voltage Transformer Due to Sustained Over-Voltage of Switching: An In-depth Field Investigation and Analytical Study", *IEEE Trans. on Power App. and Systems*, Vol. 100, No. 11, pp. 4448-4455, Nov. 1981.

A wound PT was damaged following a 220 kV busbar de-energization in India. Very similar recordings were obtained for their PTs as we measured at Dorsey.

The principle of harmonic balance is used to analyze this problem. Only fundamental and third harmonics are considered. It is not clear what the authors do with the results. I guess they see if a period-1 ferroresonant solution is possible given a set of circuit parameters. The tabular form of presentation is difficult if not useless to decipher.

Field tests of the v-i characteristic show significant distortion due to stray capacitance. They use a three segment piece-wise linear approximation.

The field data used is as follows:

C_g=1300 pF, C_b=2000-3200 pF, L_1=13x10^5H, L_{air}=700-1000 H

The parallel losses were ignored. The 220 kV bus is 108 m long and the capacitance of the PT is taken as 600-800 pF. I think the air core reactance chosen may be high.

The failure mode was due to excessive current causing heat losses and insulation stress, which was similar to the Dorsey event described in this thesis. The authors recommend using a CVT as failures are not expected.

I would expect, based on my study results, failure to occur at 1300 pF following circuit breaker clearing.

[A57] Staats, G.W., and Ebert, J.A.,"Overvoltages in Medium Power Transformers", *IEEE Trans. on Power App. & Systems*, Vol. 101, No.4, pp. 877-885, April, 1982.

The authors calculate the probability of ferroresonance using a method based on symmetrical components. The saturated air-core reactance of the transformer is used in the equations. Equations for the case of one and two lines being open are analyzed. Prusty has some objections to this analysis method [A63]. A discusser also has some problems with the method (i.e. accuracy and practicality).

[A58] Masson, L.,"Control of Ferroresonance in Transformers", CEA Research Project 087 D 166, June 1982.

The author uses Swift's describing function method to design an anti-ferroresonance device. The device is essentially an additional reactor in series with the transformer.

Through lab tests (120 V), digital simulation (CSMP) and cost calculations of a series compensated 25 kV ferroresonant circuit, it is determined that the proposed circuit works but is not practical due to its cost. The controlled insertion of a series or parallel resistor is preferred.

[A59] Chua, L., Hasler, M., Neirynck, J., Verburgh, P.,"Dynamics of a Piecewise-Linear Resonant Circuit", *IEEE Trans. on Circuits and Systems*, Vol. CAS-29, No. 8, pp. 535-547, Aug. 1982.

The authors analyze a series RLC circuit from a circuit theoretic point-of-view. The nonlinearity is represented by a (crude) three-segment piecewise-linear curve. The parameters are obtained from [A41]. In each linear region, exact analytic formulae are produced. An iterative back-and-forth process is used at the boundaries of the linear regions until a prescribed precision is reached. Why wasn't interpolation used?. Errors do accumulate over time using this method.

The phenomenon of multiple periodic solutions is generally referred to as *ferroresonance* because the nonlinearity of the inductor is caused by the iron core.

Long time computer simulations have been criticized as having questionable validity. They show that solutions obtained by numerical integration will diverge rapidly from the actual waveform (obtained by using exact analytical formulae). As well, they attempt to prove the drifting apart of neighbouring solutions is a real phenomenon of chaotic systems not caused by numerical instability or imprecision. This is the first time *chaos* is mentioned in a power system circuit.

The attractors are mapped for voltages between 0 and 4500 V (180 V base?).

[A60] Aggarwal, R.P., Saxena, N.S., Gupta, J.C., and Sharma, B.S.,"Failure of Electromagnetic Voltage Transformer due to Sustained Over-Voltage on Switch Off-Preventive Measures", IEEE Trans. on Power Apparatus and Systems", Vol. 101, No. 12, pp. 4536-4541, Dec. 1982.

The authors continue their previous work [A56]. The modified Euler method is used for solving nonlinear d.e.

They analyzed the sensitivity of the simulations to variations in grading capacitance, bus capacitance, current chopping angle, and saturation characteristic. Practical ranges of grading capacitance (250-1300 pF) and bus capacitance (600 and 4000 pF) were determined for 220 kV busbars.

Some preventive measures were evaluated such as: switching sequence, resistance/saturable reactor in PT secondary, series or parallel resistance in primary, control of switching angle, control of saturation characteristic. The control of the saturation characteristic is found superior, although I have my doubts.

[A61] Mork, B.A., Stuehm, D.L., and Rao, K.S.,"Modelling Ferroresonance with EMTP", *EMTP Newsletter*, Vol. 3, No. 4, pp. 2-7, May, 1983.

This is the authors first paper, see also [A72], [A102], [A126].

Comparisons are made between various EMTP transformer models and a laboratory 120/240 1.5 kVA transformer/series capacitor arrangement.

Good results were achieved using a single valued sat. curve derived from measurements up to 1.5 puV. The type-96 hysteresis model was found not useful.

[A62] Guuinic, Ph., and Janssens, N.,"Full Scale Laboratory Investigations of the Three Single Phase Ferroresonance Phenomenon", IEEE Trans. on Magnetics, Vol. MAG-19, No. 5, pp. 2106-2108, Sept. 1983.

The results of energizing a bank of three 10 kV, 50 VA single-phase PTs 100 times is presented. The source voltage can be varied 10 kV ±25%. Variable grounded-wye capacitors between 5.4 nF and 24.5 nF were studied. It seems the PTs are energized on a three-phase basis and the resonance involved is a parallel LC [not a series LC as for Dorsey]. The authors attempt to Poincaré sample the initial transients with unusual results.

The domains of attraction method has several drawbacks in their opinion. In particular cases, the definition of the domains of attraction becomes impossible.

The authors also perform computer modelling using a piecewise-linear-inductor/linear-resistor and a Preisach-Biorci-Pescetti hysteresis model/linear resistor. They note the parallel resistor depends

on the amplitude of the flux for the hysteresis and eddy-current losses. As well, they see the need for better theoretical modelling of hysteresis/eddy-current losses during the transient periods which contain subharmonics and harmonics.

[A63] Prusty, S., and Panda, M.,"Predetermination of Lateral Length to Prevent Overvoltage Problems due to Open Conductors in Three-Phase Systems", *IEE Proceedings*, Vol. 132, Pt. C, No. 1, pp. 49-55, Jan. 1985.

The authors use a graphical approach (Rüdenberg's) to calculate general equations for ungrounded-wye and delta connected primary transformers connected to shielded cables or overhead lines. The equations represent the allowable length to prevent ferroresonant overvoltages.

Only period-1 ferroresonance is considered. Subharmonics are ignored. The author doesn't reference his earlier work using describing functions [A47] for some reason.

Good agreement was reached with Hopkinson's earlier work. The authors had some conflict with the work of Staats *et al.* [A57].

[A64] Bhadra, S.N.,"A Note on Some Computational Aspects of the Jump-Resonance Problem in 3-Phase Systems", *Proceedings of the IEE*, Part C, Vol. 132, no. 5, pp. 248-250, Sept. 1985.

The author is studying a series compensated feeder terminated in an unloaded transformer. A fifth order polynomial is used to represent the saturation characteristic of the center and outer limbs of a three-phase core-form transformer.

A set of 6 nonlinear equations are reduced to 2 nonlinear equations by only retaining the real and imaginary components of zero sequence flux. The initial set of equations are derived using describing function analysis. Guass-Seidel and Newton-Raphson methods used to calculate the steady state of a three-phase ferroresonant circuit.

Lab experiments on a 5 kV transformer seem to verify the computations. Although only the magnitude of flux and supply voltage are compared.

[A65] Ueda, Y.,"Random Phenomena Resulting from Nonlinearity in the System Described by Duffing's Equation", *Int. J. Non-Linear Mechanics*, Vol. 20, No. 5/6, pp. 481-491, 1985.

The author analyzes a series-resonant circuit and tunes the nonlinearity so that it corresponds with the well-known Duffing's equation. Comparisons of Runge-Kutta-Gill and Hamming's methods with various step sizes using both single and double precision compare well. Depending on the method and step size, different random oscillations are produced. However, this is to be expected in a chaotic system. Some heavy concepts such as diffeomorphism, stable manifolds, domains of attraction, random transitional oscillation and structural stability are mentioned and discussed.

[A66] Mareachen, R., Christesen, A., and Poletto, G., "Ferroresonance on 345 kV Bus Kills PT", *Electrical World*, T&D, pp. 69-70, April 1986.

Paper describes the failure of a 345 kV wound PT in Northern Indiana. The wound PTs were used because of their higher accuracy and stable lifetime voltage transformer characteristics. The configuration is similar to Dorsey.

The authors recommend several remedial measures:

- reconfiguring the bus so a large capacitance/reactance is connected in parallel with the PT.

- connect a resistor in the corner of an open-delta secondary winding. This is the preferred method as current will flow only when there is a voltage unbalance. This method will affect the performance of relays monitoring the unbalanced zero sequence voltage and will not always work if 2 or more breakers open.

- switch a wye connected loading resistor onto the secondary during ferroresonance. The resistors are switched out after a time delay. If ferroresonance reoccurs the resistors are reinserted. Failure to

switch out the resistors could thermally overload the PT. Final resistor sizes were selected in the field. They installed a switched 1 ohm resistor.

[A67] Blanc-Russac, J., and Picard, E.,"Study of a Particular Type of Ferroresonance-The Cyclic Resonance", *IEEE Trans. on Magnetics*, Vol. 22, No. 3, pp. 192-195, May 1986.

An experimental investigation of period-1 ferroresonance is made. The hysteretic mode transition (or jump resonance) is demonstrated as the source voltage is varied. The purpose is for the analysis of a constant voltage transformer or ferroresonant transformer. [Nothing useful here.]

[A68] Gish, W., Ferro, W., and Greuel, S.,"Ferroresonance and Loading Relationships for DSG Installations", *IEEE Trans. on Power Delivery*, Vol. 2, No. 3, pp.953-959, July 1987.

The paper describes possible ferroresonance that can result from isolating a distribution system generator (DSG) on a feeder which contains power factor correction capacitors or long underground cables. The condition is sustained because the generator protection doesn't recognize the abnormal condition and the energy is available from the prime mover inertia.

Field tests have verified the existence of ferroresonance using diesel driven three-phase induction generators, three-phase synchronous generators and single-phase induction generators.

[A69] Crane, D.R., and Walsh, G.W.,"Large Mill Power Outages Caused by Potential Transformer Ferroresonance", IEEE Trans. on Industrial Applications, Vol. 24, No. 4, pp. 635-640, July/Aug. 1988.

Describes the power outage caused by PT misoperation during ferroresonance. A 60 ohm resistor was placed in the broken-delta path of the PT secondary but was not sufficient in preventing ferroresonance. TNA studies showed a value of 3 ohms was necessary to damp out oscillations in one second. Overvoltage relays are connected across the open-delta to detect ground faults. Ferroresonant oscillations caused the false tripping of the mill bus. An alternative solution recommended called for the replacement of PTs with CCVTs.

Data is given for a 161 kV PT and associated buswork. The range of bus capacitance studied was 4000 to 30000 pF.

Oscillographs showing a 30 Hz mode are provided.

[A70] CEA Report prepared by Ontario Hydro Research Division, "Application Guide for Surge Arresters on Distribution Systems", *Canadian Electrical Association*, Report No. CEA 077 D184A, pp. 124-126, Sept. 1988.

This report is referenced by Mr. Brewer in his discussion of [A100]. The guide gives rules of thumb for ferroresonance based on TNA work performed by Hopkinson.

Properties:

- high overvoltages (>4.5 pu)

- resonance can occur over range ($0.1 < X_c/X_m < 40.$) for one or two energized phases.

For Manitoba Hydro's Dorsey station: $10000 < C_{eq} < 30000$ pF or $88K<X_c<265K$

and $6\ M\Omega < X_m$ (magnetizing reactance at rated voltage)$< 48M\Omega$

Therefore $0.002 < X_c/X_m < 0.044$ for three phases energized.

- resonance possible if load is less than 10% rated.

Minimum capacitance limits for ferroresonance are given for 8 kV to 25 kV typical transformers. General tables can't be given for 4/5 legged transformers because no typical X_m is available. X_m is dependent on construction details.

[A71] Shein, D., Zissu, S., Schapira, W.,"Voltage Transformer Ferroresonance in one 400 kV GIS Substation", *IEEE Conf. on Electrical and Electronics Engineering in Israel*, pp. 4.3.2.1-4.3.2.5, 1989.

The results of a utility study of PT ferroresonance in a 400 kV station are presented. Rüdenberg's graphical approach is used to qualitatively explain the phenomenon. The grading capacitors were 930 pF each (2 parallel breakers). Stray capacitances of 660 pF ±200 pF were measured.

EMTP studies were made in order to size loading resistors. Sensitivities to the current chopping angle, secondary loading, and capacitance to ground were calculated.

[A72] Mairs, D., Stuehm, D.L., and Mork, B.A.,"Overvoltages on Five-Legged Core Transformers on Rural Electric Systems", *IEEE Trans. on Ind. Appl.*, Vol. 25, No. 2, pp. 366-370, March/April 1989.

Other papers by Mork: [A61], [A102] and [A126].

This paper describes field and laboratory experiments on five-legged 75 kVA, 12.47 kV grd. wye/ 208 V grd. wye units. Of interest, are the plots of component values vs. excitation voltage.

Recommendations were made to:

- minimize the cable length

- ensure a minimum of 15% load will always be connected

- Open all three phases of a transformer not supplying load.

- Move triplex core units to lightly loaded areas and 5-legged units to heavy load areas

[A73] Hoerauf, R., and Nichols, N.,"Avoiding Potential Transformer Ferroresonant Problems in Industrial Power Systems", *Industrial and Commercial Power Systems Technical Conference*, pp. 61-68, May, 1989.

This paper describes incidents of ferroresonance occurring in industrial power systems. The occurrence of ferroresonance in industrial systems is generally lower because the voltages tend to be less, the capacitances lower and the transformers larger than those in utility distribution circuits. The absence of single-phase switching also helps, however, any single-phase switching performed by the utility may cause industrial problems. Resistive loading is recommended.

[A74] Andrei, R., and Halley, B.,"Voltage Transformer Ferroresonance from an Energy Transfer Standpoint", *IEEE Trans. on Power Delivery*, Vol. 4, No. 3, pp. 1773-1778, July 1989.

The authors discuss ferroresonance in their 138 kV and 345 kV wound potential transformers. The physical parameters used by the authors were:

C_g=1200 pF, C_b=2800 pF, L_{air}=400 H

C_g=2400 pF, C_b=1600 pF, L_{air}=500 H

C_g=600 pF, C_b=2400 pF, L_{air}=1200 H

NOTE: 62 H for a 230 kV PT in this thesis

The authors conclude that the critical factor for initiating ferroresonance is the energy transferred from the system to the PT during the switching transient following de-energization. The energy is dependent on the current chopping angle. I assumed there is no current chopping taking place in this thesis.

W_{1max} is an estimate of the maximum energy which the PT can receive in one cycle from the system:

$$W_{1max}=\left(1+\frac{K_C}{1-f_{01}^2}\right)^2+\frac{1}{2}\cdot\left(\frac{K_C}{1-f_{01}^2}\right)^2 \qquad \text{(A-4)}$$

where $K_c=C_g/(C_g+C_b)$ and

$$f_{01} = \frac{1}{\omega_0 \sqrt{L_1 (C_g + C_b)}} \tag{A-5}$$

W_2 is the energy received by the transformer during one cycle:

$$W_2 = \frac{1}{2} \cdot \left[\left(\frac{K_C}{1 - f_{02}^2} \right) + \frac{4 K_S f_{02}^2}{\pi (1 - f_{02}^2)} \right] \tag{A-6}$$

where:

$$f_{02} = \frac{1}{\omega_0 \sqrt{L_2 (C_g + C_b)}} \tag{A-7}$$

and:

$$K_S = \frac{\omega_0 \phi_S}{\sqrt{2} V_{sy}} \tag{A-8}$$

The assumptions made include:

- transient damping is neglected

- current interruption occurs at a current zero

- the energy the transformer receives from the system via the harmonic components is less than 10% of the 60 Hz energy.

One of the 138 kV PTs was found susceptible to ferroresonance and was replaced with a CCVT.

Disadvantages:

- equations are specific for circuit breaker opening. Other kicks would require different equations. Three phase cases with faults may be too detailed to analyze this way.

- the equations didn't seem to work for Dorsey (see table)

- difficult to make comments about margins because of the assumptions.

Table A.7 Analysis of Energy Transfer Method

Example	**AEP**	**Dorsey**
Bus L-L (kV)	138 kV	230 kV
Breakers		
Number	4	11
Interrupters/pole	2	2-4
Capacitance/gap	1200	1250-1500
Voltage Transformer		
Primary voltage (V_s)	80500 (1.01 pu?)	138800 (1.045 pu)
Secondary voltage	115/67	115/69

Example	**AEP**	**Dorsey**
Saturation Factor (K_S)	1.1	1.34
Nonsat ind. L_1 (H)	45000	127314
Sat. ind. L_2 (H)	500	62.4
Measured Quantities		
Voltage Divider (K_C)	0.6	0.33
Calculated Parameters		
Equiv. Grading (pF)	2400	5080
Equiv. Bus (pF)	1600	10400
Solution Parameters		
ω_{01} (rad/sec)	74	22.52
f_{01}	0.196	0.0597
ω_{02}	707	1017.5
f_{02}	1.88	2.699
W_{1max}	2.83	1.827
W_2	2.41	2.061

[A75] Janssens, N., Even, A., Denoel, H., Monfils, P.A.,"Determination of the Risk of Ferroresonance in High Voltage Networks. Experimental Verification on a 245 kV Voltage Transformer", Sixth International Symposium on High Voltage Engineering, New Orleans, paper No. 11.03, pp. 1-4, Sept. 1989.

This paper contains a brief account of [A79].

The harmonic balance method is used to define the existence regions of ferroresonance in a single-phase PT circuit. The RK4 algorithm was used for validation.

The method shows that particular modes of ferroresonance can exist but does not tell you if they will be excited by a particular transient.

[A76] Durbak, D., Lambert, S., and Ringlee, R.,"Ferroresonance-Induced Failures in High Voltage Transformers by Air Break Switch Operations", *Doble 90*, Section 6-3.1, 1990.

The failure of an air break switch to open or close on 1 or 2 phases caused high voltages to appear on the winding of 115 kV (delta-wye) transformers.

The authors performed low voltage, high frequency scans on an untanked transformer. The authors perform EMTP simulations but their plots don't look ferroresonant. I wonder if they included saturation in the model? Basically, this paper is weak.

MOVs had little effect.

[A77] Paap, G.C., Vos, E.J.A.,"On the Steady-State Determination of Networks Containing Magnetic Nonlinearities", *Archiv für Elektrotechnik*, Vol. 73, No. 2, pp. 109-114, 1990.

Paap was involved in another study which is reported in [A105].

The paper discusses the implementation of the Newton algorithm for finding the steady-state solution of a ferroresonant circuit. The problem is the initial conditions are difficult to find.

The energization of a simple RLC circuit is analyzed with the initial capacitor voltage and inductor current equal to zero. A second order set of nonautonomous equations are solved using a 4th order Runge Kutta method. Convergence within 5 periods results with the Newton method compared with tens to hundreds of periods (i.e. depending on circuit damping) for the brute-force integration method. All results compare favorably with lab measurements.

The magnetization curve cannot be represented by exponential functions because continuous second order derivatives are required by the author's method. Instead, hyperbolic tangent functions are used.

The authors comment that the solution the Newton method converges to may be different from the solution brute-force integration produces.

[A78] Bornard, P., Collet Billon, V., and Kieny, C.,"Protection of EHV Power Systems Against Ferroresonance", *1990 CIGRE*, paper 34-103, pp. 1-8, Sept. 1990.

This is Kieny's first paper. See also [A83], [A84], [A90], and [A96].

He describes the problem of tapping a double-circuit line. If the step down transformer is directly fed by one or two phases, an overvoltage can appear on the free phases because of a resonance between the line conductor capacitance and the transformer reactance. Duration is short in this case. However, long duration overvoltages may appear due to capacitive coupling with the energized line (i.e. assume the tap is on the de-energized line).

The circuit breaker pole opening sequence affected the results (i.e. initial conditions changed).

Bifurcation theory is proposed to provide an overall vision of the system's behavior and to define a security margin with respect to the existence limits of various states. The theory is presented in an appendix but is not expanded until later papers.

The study showed the minimum induced voltage necessary for the fundamental and 3rd subharmonic states to be maintained was only a few kV for typical line lengths of 100 km.

The proposed protection system consisted of overvoltage relays, a ferroresonance relay that detects secondary voltage distortion and a short circuit switch, which seems a little drastic.

[A79] Janssens, N., Vandestockt, V., Denoel, H., and Monfils, P.A.,"Elimination of Temporary Overvoltages Due to Ferroresonance of Voltage Transformers: Design and Testing of a Damping System", *1990 CIGRE*, paper 33-204, pp. 1-8, Sept. 1990.

This is the authors third paper, see also [A62], [A75], [A117], and [A121].

Single-phase ferroresonance is analyzed in great detail. The existence zones of this phenomenon are calculated using the Galerkin method of harmonic balance.

This paper contributes a detailed voltage transformer model. A parabolic spline (a succession of parabola arcs with a continuity of derivatives) is used to model the saturation curve. Eddy-current and hysteresis losses are separately represented. Their voltage-current relation is linear but their value is adapted at each iteration to reproduce the losses as a function of amplitude and shape of the computed oscillation. Eddy-current losses: depends on the rms voltage across magnetizing branch. Hysteresis losses: depends on the fundamental oscillation frequency and the extreme flux value (takes into account secondary flux cycles). Assumes 50:50 split between hysteresis and eddy-current. Supplementary losses in extreme saturated states: eddy-currents in deflector screens and tank, corona losses. Comments are made on the measurement of PT parameters.

On the boundary of the zone of existence, the Jacobian determinant of a set of equations is zero. The harmonic balance method was used in order to reduce the excessive computation times

involved from numerical time-domain simulation. The minimum voltages for fundamental, 1/2, 1/3, 1/5, 1/7 subharmonic states were calculated

Full scale 245 kV (1 phase) lab tests were performed on a 245 kV gas insulated PT. Depending on the length of busbar the following capacitances were possible:

C_g=1800 pF, C_b=7200 pF

C_g=1200 pF, C_b=3600 pF

C_g=600 pF, C_b=1200 pF

The damping system tested was a saturating inductor/resistor combination.

[A80] IEEE Task Force on TOV, "Temporary Overvoltages: Causes, Effects and Evaluation", *1990 CIGRE*, paper 33-210, pp. 1-15, Sept. 1990.

This paper defines TOV, describes their characteristics and effects on insulation requirements. Very general, however it serves as a good overview. Some waveforms are provided of the French ferroresonance problem of coupling from parallel energized lines.

[A81] Greenwood, A., *Electrical Transients in Power Systems: Second Edition*, New York: John Wiley & Sons, pp. 116-122, 397-398, 1991.

Greenwood explains the phenomenon using Rüdenberg's graphical approach. A very brief description of a computer simulation of the energization of a 13.8 kV transformer through an underground cable is presented. The interesting feature is the author's choice of an analytical expression for inductance (rather than current):

$$L = \frac{d\lambda}{di} = Ae^{-\frac{i}{B}} \tag{A-9}$$

[A82] Bohmann, L., McDaniel, J., and Stanek, E.,"Lightning Arrester Failures and Ferroresonance on a Distribution System", *1991 Rural Electric Conference*, pp. B4_1-B4_6, 1991.

The authors discuss the failures of lightning arresters in their distribution system that are close to an ELF (Extremely Low Frequency) antenna. Rüdenberg's approach is used to describe the phenomenon but the authors realize the limitations of the method. Single-phase switching was recommended not to be used. UPPCO is in the process of implementing a three-phase procedure. The paper does not show a lot of analysis. I requested McDaniel's M.S. paper for interest. It did not contain anything new. This paper was also printed in IEEE IA-29, No. 6, pp. 1189-95, Nov.-Dec. 1993.

[A83] Quivy, L., and Kieny, C.,"Pseudo-Periodic Ferroresonant Solutions Stability in Power Networks: Application of Bifurcation Theory and Lyapunov Exponents", Modelling and Control of Electrical Machines: New Trends, IMACS '91: Elsevier Science Publishers, pp. 297-304, 1991.

This is Kieny's second paper. See also [A78], [A84], [A90], and [A96].

Bifurcation theory is used to explain the existence of a pseudo- or quasi-periodic state. The paper goes into more details concerning the theory. Whereas, a companion paper [A84] discussed the event which generated the quasi-periodic mode in more detail.

EMTP simulations and RK4 simulations are made. The program AUTO is used to analyze the bifurcation problem. The program uses the continuation method to follow solutions as a bifurcation parameter is varied. The stability of solutions is determined using Floquet exponents. Poincaré sections of a RK4 time-domain solution show the tendency towards creating a closed curve (i.e. cut through an invariant torus). Lyapunov exponents calculated as the supply voltage is varied showed what voltage is required to bifurcate to an invariant torus (i.e. one exponent equals zero).

[A84] Kieny, C.,"Application of the Bifurcation Theory in Studying and Understanding the Global Behavior of a Ferroresonant Electric Power Circuit", *IEEE Trans. on Power Delivery*, Vol. 6, No. 2, pp. 866-872, April 1991.

This is Kieny's third paper. See also [A78], [A83], [A90], and [A96].

Bifurcation theory is the correct mathematical framework for describing the general behavior of a ferroresonant circuit. A 400 kV transformers fed from a 225 kV, 90 MW source over a long transmission line is analyzed. The authors' bifurcation diagram shows the existence of stable pseudo-periodic states in the typical source voltage operating region. Saddle-node bifurcations and Hopf bifurcations are discussed. He uses the RK4 algorithm plus a search for new solutions as a parameter is slowly varied.

The first example of a quasi-periodic state occurring in a high voltage power system is presented. Previously, quasi-periodic (QP-1/2 and QP-2) oscillations were known to exist in ungrounded distribution networks [A11].

[A85] Daay, B.P., "Ferroresonance Destroys Transformers", IEEE Proceedings of SOUTHEASTCON'91, Vol. 1, pp. 568-578, April, 1991.

Mr. Daay completed a dissertation (M.Sc.) at Iowa State University in 1985 on methods for studying ferroresonance.

He uses the incremental describing function method to analyze the problem. His research was sparked by the 1986 electrical world article [A66]. The theoretical analysis is weak, however.

Various ferroresonant connections and mitigation measures are mentioned. Some experience at Omaha Public Power with 345 kV PTs is presented.

[A86] Ashok Kumar, B.S., and Ertem, S.,"Capacitor Voltage Transformer Induced Ferroresonance-Causes, Effects and Design Considerations", *Electric Power Systems Research*, Vol. 21, No. 1, pp. 23-31, April, 1991.

Ashok Kumar continues his previous work [A39] and [A36]. He presently is an assistant prof. at the University of Southwestern Louisiana (email: bsa7332@usl.edu).

This paper is an interesting study of ferroresonance in capacitor voltage transformers. The author uses describing functions and laboratory simulation on an analog computer as study tools.

The circuit is free from jump resonances due to the tuned LC circuit; however, it is possible to excite subharmonic states. An inadequate ferroresonance suppression circuit (FSC) can eliminate these subharmonics but leave a long transient subharmonic period, which can affect the operation of relays. The use of switched suppression circuits and saturable reactors is questionable because subharmonics can appear in the first cycle.

[A87] Marti, J., and Soudack, A.C.,"Ferroresonance in Power Systems: Fundamental Solutions", *IEE Proc.-C*, Vol. 138, No. 4, pp. 321-329, July 1991.

This is the authors first paper on the subject. Others by Soudack include: [A95], [A98], [A109], and [A136].

The unbalanced operation of a 25 MVA, 110 kV transformer is considered. Thévenin's theorem is used to reduce the single-phase open case to an equivalent single-phase circuit.

They study the problem from a steady-state point of view. Rüdenberg's graphical approach and Ritz's method of harmonic balance are used. As well, a Runge Kutta solution of one operating point is compared with Ritz's solution.

[A88] Ray, S.,"Analysis of Transient Behaviour of Power System Circuits Containing Iron Cored Coils", *Proceedings of the IEE*, Part C, Vol. 138, no. 4, pp. 275-282, July 1991.

The author proposes a piecewise-linear hysteresis model. Swift's approach for representing iron-

core losses is used (i.e. eddy-current losses are three times hysteresis and represented by linear resistor).

Reasonable comparisons are made with a 40 V experimental lab setup.

[A89] Morched, A.S., Brierley, R.H., and Grainger, T.E.,"How to Operate Lines on Multi-Voltage Towers", Electrical World, pp. 33-36, Aug. 1991.

Other work by Morched includes: [A91], [A126] and [A132].

Practical problems associated with operating multi-voltage towers (i.e. 115 kV + 500 kV) are described. Ferroresonance problems associated with de-energizing the line/transformer with and without a stuck breaker are mentioned. The solution adopted is the use of switched damping resistors. Cross-tripping parallel energized circuits also can be used occasionally. Transient oscillations may stress transformer insulation or cause circuit breaker restrike.

[A90] Kieny, C., Le Roy, G., and Sbai, A.,"Ferroresonance Study Using Galerkin Method with Pseudo-Arclength Continuation Method", *IEEE Trans. on Power Delivery*, Vol. 6, No. 4, pp. 1841-1847, Oct. 1991.

This is Kieny's fourth paper. See also [A78], [A83], [A84], and [A96].

The Galerkin method (special case of harmonic balance method) is an analytical method used in finding an approximate solution to a nonlinear differential equation. An iterative (Newton-Raphson) method is used to calculate when the determinant of a Jacobian is equal to zero, which creates initialization problems. The author proposes using a pseudo-arclength continuation method that avoids the non-invertibility of the Jacobian at the limit points. One equation is added to the system so that the new system is invertible.

A 400 kV wound PT is studied. The system parameters used are: C_g=200 pF, C_b=200 pF, R_s=32 kΩ, R_m=714 MΩ, and a 9th order polynomial saturation curve. They discovered fundamental frequency ferroresonance and installed another transformer with more losses for mitigation.

A second case examined a longer busbar (C_b=1000 pF). Third subharmonic states were discovered.

[A91] Brierley, R.H., Morched, A.S., and Grainger, T.E.,"Compact Right-of-Ways with Multi-Voltage Towers", *IEEE Trans. on Power Delivery*, Vol. 6, No. 4, pp. 1682-1689, Oct. 1991.

Other work by Morched includes: [A89], [A126] and [A132].

The authors mention several problems that can occur with multi-voltage towers (i.e. ferroresonance due to coupling with energized lines). Nothing new is presented; only a qualitative description.

They mention EMTP studies are limited due to the accuracy of transformer models and information on saturation characteristics.

[A92] Mitrea, S., and Adascalitei, A.,"On the Prediction of Ferroresonance in Distribution Networks", *Electric Power Systems Research*, Vol. 23, No. 2, pp. 155-160, March 1992 [ISSN: 0378-7796].

The authors investigate the effects of single-phase switching on a transformer-terminated cable circuit. Piecewise-linear modelling is used to produce exact equations within each linear region. Similar analysis was performed by Chua [A59]. The minimum voltage required to sustain ferroresonance is determined analytically. Not enough work is presented to make me comfortable with this method.

[A93] Vilcheck, W.S., and Haddad, M.V.,"Voltage Transformer Ferroresonance in Cogeneration Substation", *1992 Annual Pulp and Paper Industry Technical Conference*, pp. 148-158, June 1992.

This paper describes an example of ferroresonance occurring between the grading capacitance of a 230 kV breaker and a wound PT. The mitigation solution chosen was to install a permanent resistor in the broken delta winding and switched wye-connected resistors. The power rating of the resistors was 1/2 the thermal rating of the PT. The ATP version of EMTP was used to test several methods of

suppression, although no results are reported. Field tests verified operation of the resistor.

The authors investigate in detail the source of stray capacitance. Some work is required to relate the cogen SLD, the individual measurements and the steady-state coupled voltage. It appears the total grading capacitance is 2100 pF and the stray capacitance is 8000 pF.

[A94] van Riet, M.J.M., and Buesink, D.J.W.,"The advantage of Implementing Corrective Capacitors Mounted Directly on the Low Voltage Side of a High Voltage Power Transformer", *12th International Conf. on Electricity Distribution*, pp.2.11.1-2.11.5, May 1993.

The authors use capacitors on the low side of a 150-11 kV transformer for demagnetizing. The purpose is to minimize the remnant flux and therefore reduce the inrush current.

The only mention of ferroresonance is that they installed 2 μF capacitors on the low side to avoid ferroresonance in normal operation.

Their transformer model is single-phase and uses a 13^{th} order polynomial. Eddy-current and hysteresis losses were measured by the manufacturer as a function of voltage. The fourth order Runge-Kutta method was used in simulations.

[A95] Araujo, A., Soudack, A., and Marti, J.,"Ferroresonance in Power Systems: Chaotic Behavior", *IEE Proc.-C*, Vol. 140, No. 3, pp. 237-240, May 1993.

One of the authors many papers in this area. Others include: [A87], [A98], [A109], and [A136]. The importance of including transformer losses is shown.

A RK4 solution technique is used. Some nonlinear dynamics visualization techniques are shown: power spectral density, Poincaré maps. Chaos occurs in their system at 25.26 pu voltage!

[A96] Ben Driss, K., Kieny, C., and Lorcet, B.,"Perturbation Method for the Continuation of Sub-Harmonic and Harmonic States of Parallel Ferroresonant Circuits", IMACS-TC1 '93, pp. 549-554, July 1993.

This is Kieny's fifth paper. See also [A78], [A83], [A84], and [A90].

A single-phase parallel RLC circuit is analyzed. The model corresponds to an unloaded transformer connected to a long 225 kV transmission line.

The AUTO software is used to calculate the steady state of the system using the pseudo-arc-length continuation method. Previously, it was not possible to study states rich in harmonics using this method due to the difficulty in determining an initial solution. The perturbation method described by the authors to solve this problem seems complicated. First, a solution of the lossless system is found. Second, the system is perturbed by a periodic forcing term. Finally, the losses are slowly reintroduced. I don't see the advantages of this method.

[A97] Walling, R., Barker, K., Compton, T., and Zimmerman, L.,"Ferroresonant Overvoltages in Grounded Wye-Wye Padmount Transformers with Low-Loss Silicon Steel Cores", *IEEE Trans. on Power Delivery*, Vol. 8, No. 3, pp. 1647-1660, July 1993.

This is Walling's first paper. For others see: [A101], [A106], and [A126].

Field evaluations of low loss grounded wye-wye three-phase padmount distribution transformers using five-legged silicon-steel wound cores are made. A number of 15, 25 and 35 kV class transformers were tested to evaluate the relationship between cable capacitance and ferroresonant overvoltages.

Overvoltages can reach 2.5 pu. Most severe cases result after the first phase opens or the next-to-last is closed. Exciting currents measured were small with respect to the transformer rating and no thermal overload is expected. Ferroresonance susceptibility is directly related to core loss.

[A98] Araujo, A., Mozaffari, S., Soudack, A., Marti, J.,"Chaos in Power Systems: EMTP Simulations",

11th Power System Computations Conference, pp. 671-677, Aug. 1993.

Comparisons are made between the MicroTran version of EMTP (trapezoidal) and the 4th order Runge Kutta (stepsize control considered not necessary) numerical integration methods. Duffing's equation and a more practical system [A109] were studied. The solutions to Duffing's equation compared favorably using either integration method.

The transformer nonlinear characteristic was discretized in the EMTP ferroresonant circuit using both 49 points and 9 points. An 11th order polynomial was used in the RK4 version. An example is shown where the RK4, 49 point EMTP show similar chaotic attractors but the 9 point EMTP representation shows no ferroresonance. They conclude that the high order nonlinearity requires accurate discretization of the nonlinear characteristic.

[A99] Vukelja, P.T., Naumov, R.M., Vucinic, M.M., Budisin, P.B.,"Experimental Investigations of Overvoltages in Neutral Isolated Networks", *IEE Proc. C: Gen. Trans. & Distr.*, Vol. 140, No. 5, pp. 343-350, Sept. 1993.

As the title states, this is an experimental investigation. Ferroresonance occurred following switching operations (i.e. switching in an unloaded 110 kV transformer) or fault interruption. Several examples of ferroresonance occurring in Yugoslavia are given.

A resistor installed between the ends of the broken delta secondary winding prevented ferroresonance.

[A100] Short, T., Burke, J., Mancao, R.,"Application of MOVs in the Distribution Environment", *IEEE Trans. on Power Delivery*, Vol. 9 No. 1, pp. 293-305, Jan. 1994.

T. Short is an analytical engineer with PTI. email: ta.short@pti-us.com

This interesting paper generated a lot of discussion. The paper investigates areas which could lead to distribution MOV failures. The topics included: voltage regulation, overvoltages (due to SLGF), ferroresonance, cogeneration, and switching surges. A utility survey indicates they are having reliability problems with MOVs. If a 9 kV arrester is used at 12.47 kV instead of a 10 kV arrester, reduced reliability can be expected because there is less margin for error than with previous gapped silicon carbide arresters.

On distribution systems, the most common case where ferroresonance occurs is during single-pole switching of a three-phase transformer fed by an underground cable. If the primary is ungrounded or grounded-wye with five-legged core then resonance can occur. Preliminary tests on five-legged, low-loss transformers indicate the impact of ferroresonant overvoltages on MOVs is small because the ferroresonant source is weak.

Some EMTP simulations are presented (Mork's 3 phase 5-legged core model is used). R. Walling makes the comment that field tests are less severe than that predicted by digital simulation. The nonlinear behavior of core losses is extremely difficult to model (i.e. losses increase rapidly as core saturates) and is critical to ferroresonance prediction. The authors feel the nonlinear magnetization curve dominates and the core loss simplification (linear R_m) does not affect the conclusions.

Another case where overvoltages occur is when a Distribution System Generator (DSG) is separated from the utility (islanding). The overvoltages can be caused by ungrounded transformer connections, self excitation and ferroresonance. The authors don't consider MOVs to be at peril if the DSG is tripped after a few seconds. If large cogens are used, higher rated MOVs may be required.

New gapped MOVs absorb more energy than standard MOVs during ferro. and should be tested.

[A101] Walling, R., Hartana, R., Reckard, R., Sampat, M., and Balgie, T.,"Performance of Metal-Oxide Arresters Exposed to Ferroresonance in Padmount Transformers", *IEEE Trans. on Power Delivery*, Vol. 9, No. 2, pp. 788-795, April 1994.

Walling continues his work. For other papers see: [A97], [A106], and [A126].

An extensive series of tests were performed to determine the electrical and thermal performance of MOV arresters subjected to long duration ferroresonant overvoltages. Only five-legged grounded-wye (13.8-34.5 kV) padmount transformers were studied as they are the most common three-phase underground transformer in use in the U.S.

Complex long-term interactions between the MOV and the ferroresonant circuit were discovered. A direct current flow through the primary winding causes a minute dc voltage. The integration of this voltage causes the flux-linkage to drift. When the flux offset reaches a critical point, the voltage wave asymmetry abruptly reverses and the arrester discharge currents are of opposite polarity. The period is roughly 10-340 seconds. The cyclic conduction was limited to silicon-steel cores and was not observed in amorphous-metal transformers.

Erratic (or transitional) ferroresonance was observed as the cable capacitance increased. Ferroresonance occasionally dropped out in some silicon-steel cores.

Liquid-immersed (internal, under-oil) arresters are more capable of withstanding ferroresonance than porcelain riser pole arresters. Both are not comparable on an application basis, however, as they serve different lightning protection needs. With the application of under-oil arresters at the transformer, switching options can be broadened from three-phase switches to single-phase cutouts.

[A102] Mork, B.A., and Stuehm, D.L.,"Application of Nonlinear Dynamics and Chaos to Ferroresonance in Distribution Systems", *IEEE Trans. on Power Delivery*, Vol. 9, No. 2, pp. 1009-1017, April 1994.

Mork completed his Ph.D. in this subject in 1992. Other papers in this area include: [A72], [A61] and [A126]. He is a professor at Michigan Technical University: **//www.ee.mtu.edu**.

Full scale ferroresonance tests were performed on a 75 kVA five-legged 12.5 kV/480 V grd.-wye/grd.-wye distribution transformer. A variable 0-150 μF shunt capacitor was used to simulate cable capacitance. Period 1,2, 3 and 5 periodic ferroresonance and some chaotic modes were observed. Laboratory tests should not use step-up transformers if possible. The impedance of the source should not be of the same order as the leakage impedance of the transformer or ferroresonance performance will be affected.

EMTP modelling was used to create bifurcation diagrams where the bifurcation parameter used was the cable capacitance. A slow parameter varying approach was used which exhibited hysteretic mode transitions. Some transient mode transitions were recorded.

The author did not measure core losses for the various modes (subharmonic/chaotic).

Integration time steps of 2 μs may be necessary if resonances in the 3-4 kHz range are experienced.

[A103] Deane, J.,"Modelling the Dynamics of Nonlinear Inductor Circuits", *IEEE Trans. on Magnetics*, Vol. 30, No. 5, pp. 2795-2801, Sept. 1994.

Deane completed his Ph.D. on this topic in 1990. For more information, see // **www.ee.surrey.ac.uk/Personal/J.Deane**.

This paper compares experimental vs. simulations of a series RLC circuit excited by a square wave voltage source.

The Jiles-Atherton (J-A) model of ferromagnetic hysteresis was used to verify experimental bifurcation/phase-plane plots.

His experimental setup did not exhibit chaos when driven by a sine wave.

[A104] Damstra, G. C.,"Ferroresonance in Gas-Insulated Substation Voltage Transformers", *Power Technology International*, pp. 87-91, 1994.

An experimental approach is used to investigate the boundaries and verify the remedies against

ferroresonance in gas-insulated voltage transformers in ungrounded networks. Several examples are given of tests performed at KEMA (Netherlands). Very good waveforms are presented comparing the unbalanced fundamental (UF) mode with the quasi-periodic-1/2 mode (QP-1/2).

A reactor/resistor scheme in parallel with an open delta winding is proposed for voltage transformers in ungrounded networks.

Damstra is affiliated with the Eindhovan University of Technology (Netherlands) at // **www.eeb.ele.tue.nl/~evt/eeg.**

[A105] Paap, G.C., Alkema, A.A., and van der Sluis, L.,"Overvoltages in Power Transformers Caused by No-load Switching", *IEEE Trans. on Power Delivery*, Vol. 10, No. 1, pp. 301-307, Jan. 1995.

The authors describe the energization of a 150 kV/50 kV wye/grd.-wye 120 MVA Dutch transformer. The transformer was energized via a short 12.5 m cable. High voltages appeared at the secondary of the power transformer which eventually led to a flashover from winding to core. Ferroresonance was disqualified in this case. Their studies showed a high frequency resonance (12-25 kHz) exists. Saturation plays a negligible role in this case. A simple solution was to change the length of the cable to 50m. Secondary capacitors or surge arresters could also help.

[A106] Walling, R., Hartana, R., and Ros, W.,"Self-generated Overvoltages due to Open-Phasing of Ungrounded-Wye Delta Transformer Banks", *IEEE Trans. on Power Delivery*, Vol. 10, No. 1, pp. 526-533, Jan. 1995.

Walling has extensive experience with field testing of transformers [A97], [A101], [A126].

The authors perform field tests and analyze the overvoltages resulting from the open-phasing of 12.5 kV and 25 kV transformer banks. Previous studies have shown the voltages could only be sustained at the 25 and 35 kV class.

The overvoltages are due to a shift in the neutral voltage and ferroresonance caused by the interaction of the nonlinear core with the transformer winding inherent capacitance.

The authors recommend temporarily grounding the bank during switching operations. Gapless arresters should be installed to protect the transformer in the event a fuse cuts out. The arrester may fail if prolonged unbalanced operation is experienced.

[A107] Chakravarthy, S.K., and Nayar, C.V.,"Ferroresonant Oscillations in Capacitor Voltage Transformers", *IEE Proc. - Circuits Devices Syst.*, Vol. 142, No. 1, pp. 30-36, Feb., 1995

This is the authors' first published work. Additional papers include: [A112], [A115] and [A129].

A CVT (represented by a series ferroresonant circuit) is analyzed.

The Runge Kutta-Merson routine is used to perform numerical simulations. The voltage applied to the CVT is increased to 6 pu in order to stimulate some different ferroresonant waveforms.

His objective was to establish a method for identifying all possible initial conditions and consequently the different types of ferroresonant oscillations. The system is linearized about a fixed point and eigenvalues calculated. He notes that the linearized form can't reveal all possible oscillations but provides some insight. The SVA method is applied to the polar form of the flux solution.

[A108] Shein, D., and Zissu, S.,"Domains of Ferroresonance Occurrence in Voltage Transformers with or without Damping Reactors", *Eighteenth Convention of Electrical and Electronic Engineers in Israel*, pp. 1.5.2/1-5, March 1995 [ISBN: 0 7803 2498 6].

This paper provides background information for a follow-up study reported in [A123].

The authors use EMTP to simulate ferroresonance in a 400 kV wound PT-grading capacitor circuit. It is claimed chaotic ferroresonance results when no damping reactor is connected. Current in the

order of 1000 times normal results. The current is a function of the shape of the saturation curve simulated. I would say they have too low a knee, too low an air core reactance and not enough core losses modelled. The correct term for the observations seen is chaotic transients.

Also, the stray capacitance modelled appears too low. Values between 600 and 2300 pF were investigated. Open air stations typically have stray capacitance of the order of 5000 pF. The stray capacitance is lower in a GIS station.

[A109] Mozaffari, S., Henschell, S., and Soudack, A.C.,"Chaotic Ferroresonance in Power Transformers", *IEE Proc. Gener. Transm. Distrib.*, Vol. 142, No. 3, pp. 247-250, May 1995.

The authors continue their previous work [A136], [A109], [A98], [A95], [A87].

A 25 MVA 110/44/4 kV (Y/Y/delta) autotransformer fed by a 100 km transmission line is studied under a single-pole open condition. The source voltage is the bifurcation parameter. Chaos is observed at 1.9 pu. No subharmonics are observed, other than period doubling type. Note: an equivalent series capacitor is calculated: $C_e=C_g+2C_m$ or 541 nF+2(118 nF)=777 nF.

The authors advocate using an 11th order polynomial for modern high-capacity transformers.

$$i = 0.0028 \cdot \phi + 0.0072 \cdot \phi^{11} \tag{A-10}$$

The following differential equation is solved:

$$\frac{d^2\phi}{dt^2} + \frac{1}{RC}\frac{d\phi}{dt} + \frac{1}{C}(a \cdot \phi + b \cdot \phi^{11}) = \omega_s E \cos(\omega_s t) \tag{A-11}$$

The fourth order Runge-Kutta method is compared with a variable-order multi-step Gear method and a trapezoidal method of numerical integration. No significant differences were found. The precision of the variable did have some impact.

Lyapunov exponents and the Lyapunov dimension are calculated for the Poincaré sampled system. The Lyapunov dimension was not calculated correctly. The definition of Lyapunov dimension given two Lyapunov exponents $\{\lambda_1=.09, \lambda_2=-.16\}$ is:

$$D_{Ly} = 1 + \frac{\lambda_1}{\lambda_2} \tag{A-12}$$

Therefore, the quoted dimensions should be 1.56 and 1.99 not 2.56 and 2.99.

Long lasting chaotic transients are observed

[A110] Tran-Quoc, T. and Pierrat, L.,"An Efficient Nonlinear Transformer Model and its Application to Ferroresonance Study", *IEEE Trans. on Magnetics*, Vol. 31, No. 3, May, 1995.

The authors talk more about their magnetization curve (A-15). The main saturation flux-current curve is represented by a p^{th} order polynomial (they chose p=11):

$$i_s = C_1 \cdot \lambda + C_2 \cdot \lambda^p \tag{A-13}$$

while the hysteresis current is determined by a q^{th} order even polynomial (they chose q=4):

$$i = \left[C_3 + C_4\left(\frac{d\lambda}{dt}\right)^q\right] \cdot \frac{d\lambda}{dt} \tag{A-14}$$

A three-phase 62.5/20 kV, 36 MVA wye-wye ungrounded transformer is energized/de-energized over a 2.2 km underground cable. The simulations are conducted on EDF's MORGAT program (i.e.

best guess as the author's don't specify). A three-phase three-legged core model is used.

[A111] Pierrat, L., and Tran-Quoc, T.,"Influences of MOV Arrester During Ferroresonance in Underground Distribution System", *IEEE/KTH Stockholm Power Tech Conference*, Paper SPT HV 11-02-0197, June, 1995.

Paper attempts to answer the questions: Will an MOV mitigate ferroresonance or will the MOV fail during ferroresonance?

Digital simulation (EMTP?) of the energization and de-energization of a 20 kV delta-wye (three-legged core) transformer is presented. An unusual magnetization curve is used:

$$i = C_1 \cdot \lambda + C_2 \cdot \lambda^p + \left[C_3 + C_4\left(\frac{d\lambda}{dt}\right)^q\right] \cdot \frac{d\lambda}{dt} \qquad \text{(A-15)}$$

The constants are determined by least squares fitting. A nonlinear R_m is also proposed but not described.

Authors show MOVs reduce the overvoltages in both the energizing and de-energizing cases. Ferroresonance is not eliminated however. There seems to be some nasty oscillations following individual phase energization, which don't look realistic.

No comments are made on the possibility of MOV failure.

[A112] Chakravarthy, S.K., and Nayar, C.V.,"Series Ferroresonance in Power Systems", *International Journal of Electric Power & Energy Systems*, Vol. 17, No. 4, pp. 267-274, Aug., 1995.

This is the authors' second published work. Additional papers include: [A107], [A115] and [A129].

A similar analysis approach, as presented in [A115], is used to analyze a series ferroresonant circuit.

Again the autonomous and nonautonomous systems are analyzed. The method of slowly varying amplitude (SVA) is presented. This method was devised by Van der Pol. It is an approximate method that can be applied to a limited class of nonlinear oscillating systems to obtain the amplitude and frequency at any instant in time for arbitrary initial conditions. He derives an equation that is a measure of the detuning of the system from fundamental frequency resonance.

The use of SVA analysis has two drawbacks: If the initial conditions are far removed from the steady state, the SVA will be inaccurate. As well, when different types of responses coexist, the SVA does not provide accurate results.

His analysis gets into bifurcation theory and eigenvalue analysis. For example, the possibility of cyclic fold bifurcations (coexistence of two saddle-node bifurcations) existing causes ferroresonant oscillations with two stable states to coexist. Each state can be either harmonic, periodic, subharmonic or aperiodic.

[A113] Naidu, S.R., and Souza, B.A.,"A Newton-Raphson Scheme for the Analysis of Ferroresonant Circuits", *38th Midwest Conference on Circuits and Systems*, Rio de Janeiro, Brazil, pp. 1293-1296, August, 1995.

Authors first paper on the subject. For others see: [A128], [A137], and [A138]. The formulation of the Jacobian used in the Newton Raphson iteration scheme is described in more detail than their other papers. Essentially the technique begins with a set of initial conditions and calculates the next state using a continuation method for small changes in a bifurcation parameter.

[A114] Gagnon, R., Viarouge, P., Sybille, G., and Gagnon, F.,"Study of Ferroresonance in a Series Compensated Network", *Canadian Conference on Electrical and Computer Engineering*, Vol. 1, pp. 447-452, September, 1995

The authors present a well written French article concerning ferroresonance in a 735 kV series

compensated, transformer-terminated transmission line. The 4th order Runge Kutta method was used to simulate the differential equations. Hysteresis was neglected and an 11th order polynomial was used to represent the saturation curve. The system was simplified to a single-phase equivalent.

Period-3 ferroresonance was discovered following fault removal. Poincaré methods (i.e. determine the fixed point by linearization) have shown at most two solutions are possible (fundamental and period-3). Basins of attraction can't be found because ferroresonance can be initiated from a perturbation which requires numerical techniques to determine.

They mention it is critically important to model the saturation curve correctly in order to simulate physically realizable modes of ferroresonance.

[A115] Chakravarthy, S.K., and Nayar, C.V.,"Parallel (Quasi-Periodic) Ferroresonant Oscillations in Electric Power Systems", *IEEE Trans. on Circuits and Systems I: Fundamental Theory and Applications*, Vol. 42, No. 9, pp. 530-534, Sept., 1995.

Chakravarthy completed his Ph.D. in 1995 at the Curtin University of Technology in Perth, Australia. So far, four papers have been written by him. See also: [A107], [A112] and [A129]. For more info see **//www.ece.curtin.edu.au/ECE/report93/electronics.htm**

This is a brief theoretical paper describing *quasi-periodic* oscillations. An irrational relation between the driving frequency and the natural oscillation frequency of the circuit results in quasi-periodic oscillations. Core losses influenced the emergence of frequency locked or quasi-periodic oscillations.

A simplified approach and numerical solutions are presented. A parallel ferroresonant circuit representing an unloaded transformer at the end of a long line is investigated (French grid: 275 kV, 400 km transformer terminated line).

A simplified autonomous (i.e. no driving force) and non-autonomous system are analyzed. Eigenvalue analysis revealed some properties of the linearized system. The harmonic balance method is used on the conservative system while the Melnikov method is applied for the lossy system.

[A116] Barr, R.A., and Platt, D.,"Modelling and Mapping Ferroresonant States in Series Compensated Distribution and Subtransmission Lines",*1995 IEEE/PES Summer Meeting*, paper 95 SM 372-3 PWRD.

Barr is completing his Ph.D. in this area at the university of Wollongong (// **www.elec.uofw.edu.au**). More information can be found at his personal website: // **www.shoal.net.au/~epc/**

A single-phase 33 kV series compensated distribution line is investigated for the possibility of ferroresonance with an unloaded transformer. A small scale laboratory model (200 V) is compared with a crude simulation model. The transformer was modelled with a 5th order polynomial.

The stability of the solution was tested in the frequency domain. A DC component in the transformer flux in the even subharmonic case was predicted.

Janssens disagrees with the author's statement that the stability of the oscillations is related to crossing of trajectories in state space.

[A117] Janssens, N., Van Craenenbroeck, T., Van Dommelen, D., Van de Meulebroeke, F.,"Direct Calculation of the Stability Domains of Three-Phase Ferroresonance in Isolated Neutral Networks with Grounded-Neutral Voltage Transformers", *1995 IEEE/PES Summer Meeting*, paper 95 SM 420-0 PWRD.

Janssens continues his previous work [A62], [A75], [A79]. Janssens is an adjunct professor and he maintains the following web site **//www.lei.ucl.ac.be./9_lei_main.html**. Both Janssens and Van Craenenbroeck have a second paper [A121].

Stability domains of ferroresonant oscillations are computed using the harmonic balance method.

A fifth-order polynomial is used for the $i(\lambda)$ curve of a 6.6 kV PT. The three-phase state equations are transformed to $(0,\alpha,\beta)$ equations using Clark's transformation. He admits a crude transformer model was used. A more detailed model will be considered later. His display of stability domains is interesting (i.e. source voltage vs. zero sequence capacitance).

The authors are able to apply the harmonic balance method to a quasi-periodic case by assuming an approximate periodic solution.

The authors don't specify the technique used for time simulations. Based on Janssens previous work[A79], I would guess RK4.

Van Craenenbroeck is researching ferroresonance with the Research Group Electrical Energy and expects to finish in 1998. See the following web site for more information: **//www.esat/kuleuven.ac.be/elen.html/**

[A118] Woodford, D.A.,"Solving the Ferroresonance Problem when Compensating a DC Converter Station with a Series Capacitor",*1995 IEEE/PES Summer Meeting*, paper 95 SM 528-0 PWRS.

For the case of series compensation on the system side of a converter transformer, ferroresonance has been shown to exist. An air-cored reactor in parallel with the series capacitor has been shown to prevent ferroresonance. An alternative method is to monitor the voltage across the capacitor (or current through the capacitor) and switch to current control at the inverter. The DC link acts as negative damping following a single-line to ground fault. The control switchover increases the damping. Supplementary damping can be provided by an extra function added to the current controller.

The ferroresonant state has positive, negative and zero sequence components. It is predominantly 19 Hz positive sequence. I would agree with Janssens that the mode is a type of quasi-periodic oscillation.

[A119] Bishop, M.,"Ferroresonance: Part 1-6", Cooper Systems Engineering Technical UPdate, 1995-1996.

Describes conditions necessary for ferroresonance to occur on energization of a three-phase delta-wye distribution transformer. The transformer is energized by closing distribution fuse cutouts one at a time. They use $(X_c/X_m) > 40$ as a criteria (see also [A70]). It is less likely for large transformers to be susceptible to ferroresonance. Higher system voltages (25-35 kV) increase the probability.

Ferroresonance is possible with delta, ungrounded-wye, and ungrounded-TEE connections. Grounded-wye connections are not normally a problem unless the transformer is a three-phase unit constructed with a four or five-legged core or there is a floating-wye or delta connected capacitor bank connected between the open point and the capacitor bank. Overvoltages with four and five-legged cores are approximately 2.0 pu, whereas 5.0 pu can be reached with delta or ungrounded-wye banks.

Three-phase switching or switching directly at the transformer terminals reduces the probability of ferroresonance. Some small transformers connected at high voltages have sufficient internal capacitances to also be at risk. A secondary load of 5-10 percent of the transformer rating is generally sufficient to eliminate the risk.

[A120] Köppl, G., Läderach, S., Lüke, E., and Kunde, K.,"Ferroresonanz auf einer abgeshalteten 220 kV Leitung durch eine parallelgeführte 380 kV Leitung", *Elektrizitätswirtschaft*, Vol. 94, No. 21, pp.1352-1358, Oct. 2, 1995.

Kunde discusses some of the results of this paper without referencing it in [A124].

Ferroresonance has occurred in a 220 kV PT connected to 9.6 km of 220 kV transmission line that is capacitively coupled with a 380 kV parallel transmission line. The tower consists of 4 circuits: 2-

280 kV and 2-220 kV. One phase of the 220 kV line is closely coupled to one of the 380 kV circuits. Period-3 oscillations were experienced and led to the explosive failure of one of the PTs.

EMTP simulations are used to study the problem and design a resistive damping device. A three-phase model including hysteresis was used.

New SF6 gas insulated PTs with gapped cores are being developed by Haefely-Trench as a possible solution to the ferroresonance problem.

[A121] Van Craenenbroeck, T., Van Dommelen, D., Janssens, N., and Van de Meulebroeke, F.,"Stability Analysis of Ferroresonant Oscillations in Networks with Isolated Neutral", *Proceedings of the 1995 First IEEE International Caracas Conference on Devices, Circuits and Systems* (Cat. No. 95TH8074), pp. 41-45, Dec. 12, 1995. (ISBN: 0 7803 2672 5)

This is Van Craenenbroeck's second paper, see also [A117], [A146], [A148]; or Janssens' fifth, see also [A62], [A75], [A79], and [A117].

A grounded 6.6 kV PT in an ungrounded system is analyzed. The oscillation modes discovered experimentally by Peterson [A11] are calculated. Two techniques are used to find the stability domain of each oscillation mode. The first method calculates the Floquet-multipliers while the second method calculates the eigenvalues of the Jacobian. The second method is more promising because no transients are present in the solution. The method is similar to the one described by Quivy[A83].

Very good correlation was actually found between the calculations and experimental work. Further work will look at more accurate transformer models.

[A122] Anderson, P.M., and Farmer, R.G.,*Series Compensation of Power Systems*, PBLSH!, pp. 325-328, 1996.

The case of energizing an unloaded transformer through a series compensated line is described. Development of ferroresonance depends on: point-on-wave of the energization, source voltage magnitude, residual magnetism in transformer and relative sizes of circuit components. Period-1 or subharmonic ferroresonance can be expected.

An easy solution to the problem is to bypass the capacitor with a circuit breaker or damping resistor prior to energization. Some simulation results on a 20 kV system are presented showing period-2 ferroresonance.

[A123] Ben-Tal, A., and Shein, D.,"Domains of Ferroresonance Occurrence by Bifurcation Diagrams", *Nineteenth Convention of Electrical and Electronic Engineers in Israel*, pp. 87-90, 1996.

The authors study ferroresonance in a potential transformer-grading capacitor circuit connected in a 400 kV gas-insulated station. The steady-state is solved for by using the harmonic balance (i.e. Galerkin) method. A set of non-linear algebraic equations result and is solved using a Newton-Raphson routine taken from an IMSL math library. A seventh order nonautonomous system of equations is discussed but not presented. Shein also discussed this project in [A108].

Difficulty was noted in providing the initial conditions for the first solution. Once the initial state was found, the continuation method was used to find the remaining solutions as a parameter was varied. Floquet multipliers determined the stability of the solution. Gear's method was used to develop time simulations for verifying the Galerkin method results.

The authors propose using a series resistor-damping reactor combination to eliminate ferroresonance. Their results show this method to be feasible for only a narrow band of resistor values. I wouldn't recommend such a circuit for general use. Only period-3 and period-5 subharmonic solutions were discovered.

Further work on quasi-periodic oscillations is proposed.

[A124] Kunde, K., Niedung, L., and Umlauf, A.,"Damping Ferroresonance in Transmission Networks", *Power Technology International*, pp. 100-103, Spring 1996.

An earlier work by Kunde can be found in [A120].

Gapped core PT proposed to eliminate ferroresonance in gas-insulated voltage transformers.

I asked the manufacturer, Haefly Trench, why this PT is not recommended for 230 kV applications. They had proposed using a CVT at Dorsey. They replied by saying cost was the biggest factor. CVTs are much cheaper than gapped core PTs.

They performed field tests only up to 1200 pF stray and grading capacitance. Their plot of stable ferroresonance was not clear.

Depending on the type of transformer model chosen, the ability to damp ferroresonance was changed. The real observed loss efficiency was always greater than what the model predicted. Additional non-measurable losses are occurring in the PT. The authors don't specify the method of simulation used.

[A125] Bodger, P.S., Irwin, G.D., Woodford, D.A., Gole, A.M.,"Bifurcation Route to Chaos for a Ferroresonant Circuit Using an Electromagnetic Transients Program", *IEE Proc. Gener. Transm Distrib.*,Vol 143, No. 3, pp. 238-242, May 1996.

The authors investigate a series capacitor unloaded transformer configuration using EMTDC. Bifurcation diagrams, Poincaré mapping etc. are discussed.

The simulation required a 2 usec. time step to get a reasonable bifurcation diagram. A 50 Hz system was studied to eliminate inaccuracies associated with 60 Hz (i.e. T=16.6666... msec.). Hyperbolic bifurcation points were observed. No subharmonics were excited in the low voltage region.

They talk about phantom bifurcation points. What looks like period doubling is not according to their simulations.

[A126] Mork, B.A., Morched, A.S., and Walling, R.,"Modelling and Analysis Guidelines for the Investigation of Slow Transients in Power Systems: Part III-Study of the Phenomenon of Ferroresonance", *Slow Transients Task Force of IEEE Working Group on Modelling and Analysis of System Transients Using Digital Programs*, July 27, 1996.

This guide is composed mainly of sections taken from Mork's Ph.D. thesis and ([A61], [A72], [A102]) Also included are field cases from work done by Morched ([A89], [A91], [A132]) and Walling ([A97], [A101], [A106]).

The main conclusion was a proper transformer model must be used or developed in order to correctly simulate the phenomenon. Bifurcation analysis is mentioned as a useful visualization technique. Rüdenberg's graphical approach is used to explain the multi-operating point characteristic.

Case studies presented in this report include: 50 kV PT in an ungrounded system, unbalanced operation of a 5-legged distribution transformer and ferroresonance in a 230 kV autotransformer due to capacitive coupling with an energized line.

[A127] Jacobson, D.A.N., Swatek, D., and Mazur, R.,"Mitigating Potential Transformer Ferroresonance in a 230 kV Converter Station", *IEEE T&D Conference*, Los Angeles, Sept. 15, 1996.

This paper was selected for publication in: Martinez, J.A. (Editor), *Computer Analysis of Electric Power Systems Transients: Selected Readings*, IEEE Press: Piscataway, New Jersey, 1997.

The authors describe the investigation of an actual ferroresonant event that occurred between a 230 kV PT and the grading capacitance of nearby open circuit breakers. Mitigation measures are described. A novel 2D bifurcation diagram is proposed for visualizing the dynamics.

Both EMTP and RK4 simulations are performed.

[A128] Naidu, S.R., and Souza, B.A.,"Analysis of Ferroresonant Circuits Using a Newton-Raphson Scheme", *IEEE Paper No. PE-431-PWRD-0-12-1996*, December 1996.

Authors first paper. A follow-up paper can be found in [A137]

A series RLC circuit is analyzed.

The pseudo-arc-length continuation method is used to trace out a solution branch given a known solution condition. The authors admit that there is no guarantee that the technique can locate every possible steady-state solution.

A hybrid frequency-domain time-domain technique is used to validate the steady-state responses. The authors find the hybrid technique slower than a time-domain solution.

Parameters used in a previous analysis by Kieny [A90] are used here. The authors duplicate Kieny's results and also validate the final states using a time-domain method.

Refinements are being studied to be able to handle larger networks.

[A129] Chakravarthy, S.K., and Nayar, C.V.,"Frequency-Locked and Quasiperiodic (QP) Oscillations in Power Systems", *IEEE Paper No. PE-096-PWRD-0-12-1997*, Dec. 1996.

This is the authors' fourth published work. Additional papers include: [A107], [A115] and [A112].

I submitted a discussion paper requested more information on their analytical techniques and to provide some simulation results to verify whether the quasi-periodic state is stable or not.

The authors analyze quasi-periodic oscillations that can result following energization of an unloaded transformer through a long transmission line. Some methods identified for calculating possible bifurcations include: harmonic balance, trial-and-error, slowly-varying-amplitudes, integral curves and Melnikov's method. The author's propose transforming the nonlinear o.d.e. into a simpler form which is valid in the neighbourhood of an equilibrium point. Applying Euler's algorithm to a manipulated equation results in the sine circle map form of the system.

$$\theta_{n+1} = \theta_n + \Omega - \frac{K}{2\pi}\sin(2\pi\theta_n) \qquad \text{(A-16)}$$

The sine circle map is a recursive relation that differentiates between frequency locked and quasi-periodic behavior. The relation has been verified against numerical simulation of the complete nonlinear o.d.e [one limitation is the devil's staircase plots don't give any information regarding the behavior of the frequency-locked signal. The plots show winding number vs. frequency ratio. The actual system quantities are buried within these parameters.]

[A130] Barr, R.A., and Platt, D.,"Use of a Saturating Choke in the Series Capacitor Compensation of Distribution Lines", *IEE Proc.-Gener. Transm. Distrib.*, Vol. 144, No. 1, January 1997.

Authors most recent paper. Additional work: [A116].

Single-phase lines in Australia are constructed up to 33 kV. These lines could see improved voltage regulation if they were series compensated. However, if they are radial fed there is some probability of ferroresonance occurring following energization of the line and transformer. The authors propose a saturable reactor/damping resistor would eliminate any subharmonic ferroresonant states. Calculations and lab tests prove their theory. They are looking for an 11 kV network for implementation.

I wonder how well this scheme would work if period-1 or quasi-periodic oscillations develop?

[A131] Stuckens, C., Monfils, P.A., Janssens, N., Van Craenenbroeck, T., Van Dommelen, D.,"Risk of Fer-

roresonance in Isolated Neutral Networks and Remedies", *IEE Conference Publication No. 438, CIRED*, pp. 1.18.1-1.18.6, June 1997.

One of the authors' many papers discussing ferroresonance in a low voltage network with isolated neutral, see also [A148] for example. At 15 kV, risk of "three single-phase" ferroresonance occurs when you have between 0 and 500 meters of underground cable.

Discusses some aspects of the experimental setup. Errors between 10-20% are found between model and experiment. The errors are attributed to losses in the measuring devices and the inadequate representation of the source.

[A132] Sagardía, S.R., and Morched, A.S.,"Potential Transformer Failure due to Ferroresonance", *IPST'97*, pp. 191-196, June 1997.

Other work by Morched includes: [A89], [A91] and [A126].

The authors describe the failure mechanism in a 115 kV PT. The individual phase midspan openers located several kilometres away from the PTs were sequentially opened. It is believed that damage occurred to the PT during this time and upon later re-energization, the PT exploded.

EMTP simulations show period-3 ferroresonance is prevalent for 1-4 km of line length. The PT is modelled by three single-phase transformers and the EMTP pseudo-nonlinear reactor was used. Waveforms are very similar to some of my cases.

[A133] Bolduc, L., Bouchard, B., and Beaulieu, G.,"Capacitor Divider Substation", IEEE Trans. Power Delivery, Vol. 12, No. 3, pp. 1202-1209, July 1997.

Interesting discussion of a substation designed using a capacitor divider. The scheme is cost effective (i.e. 1/4 the cost of a normal station) for tapping HV lines (115-230 kV) for feeding small loads (<2MW). For higher loads, the VAr injection may be too high or there may be equipment size limitations (inductors and arresters) or cost limitations.

The configuration is identical to a CCVT. The authors recognize that ferroresonance will be a concern. The distribution transformer is chosen to avoid period-1 ferroresonance. Subharmonic ferroresonance is prevented by installing a damper-filter. The notch filter blocks 60 Hz but passes lower and higher frequencies.

EMTP simulations verified the theory. A full scale prototype was built and successfully tested. Energizing and short circuit tests show the design is immune to ferroresonance. Finally a 1.5 MW substation was built for S2 M and has been operating since Aug. 1994.

[A134] Lamba, H., McKee, S., and Simpson, R.R.S.,"Subharmonic Ferroresonance in an LCR Circuit with Hysteresis", IEEE Trans. on Magnetics, Vol. 33, No. 4, pp. 2493-2500, July 1997.

Simpson was interested in ferroresonance several years ago [A43].

A single-phase series RLC circuit is investigated. The authors use the Preisach model of hysteresis and show that period-3 ferroresonance is heavily influenced by the width of the hysteresis loop (i.e. hysteresis losses). If the hysteresis function is removed and a linear parallel resistor is placed in the circuit to model the losses, period-3 ferroresonance could not be excited in their circuit. [I came to a similar conclusion for the Silver transformer model. For the PT case, I was able to simulate several subharmonic modes with a single-valued saturation curve. I would guess the slow voltage variation that the authors used was not a severe enough perturbation.]

The bifurcations in the hysteresis model could only be guessed at. Existing software, such as AUTO, can only identify bifurcations if a single-valued saturation curve is used.

[A135] Emin, Z., Al Zahawi, B.A.T., and Tong, Y.K.,"Ferroresonance in Electromagnetic Voltage Transformers: A Study Based on Nonlinear Dynamics", IEE Proc.-Gener. Transm. Distrib., vol. 144, no. 4, pp. 383-387, July 1997.

The authors analyze a ferroresonant incident that occurred in a wound potential transformer at a 275 kV London substation. Additional work is published in [A141]. Simulations show period-1 and period-2 ferroresonance are possible. The typical grading capacitance in the substation was 500 pF and the stray capacitance was 1250 pF. At 3000 pF of stray capacitance, no ferroresonance was observed. The numbers are consistent with my analysis of 230 kV power systems.

Runge-Kutta-Fehlberg simulations were performed using initial conditions of peak voltage and zero flux. A seventh order polynomial represented the PT.

Unrealistic values of C_g, C_b and losses resulted in chaotic ferroresonance. The results look more quasi-periodic to me.

The authors make the comment that an operator on site wants to know that he has an adequate safety margin before he takes action. However, in general a very large number of simulations are required before a reasonable assessment of the level of risk of ferroresonance can be made.

[A136] Mozaffari, S., Sameti, M., and Soudack, A.C.,"Effect of Initial Conditions on Chaotic Ferroresonance in Power Transformers", *IEE Proc.-Gener. Transm. Distrib.*, Vol. 144, No. 5,pp. 456-460. Sept. 1997.

Mozaffari/Soudack continue their previous work: [A87], [A95], [A98], and [A109]. Mozaffari received his Ph.D. in August 1996 from UBC. The thesis was entitled, "Chaotic Ferroresonance in Power Transformers".

The same circuit is analyzed as in previous papers. Basically the same plots are also included. However, the author goes a little further by plotting the basin of attraction for some chaotic attractors that occur at 25 pu voltage! The program INSITE is used in making their investigation.

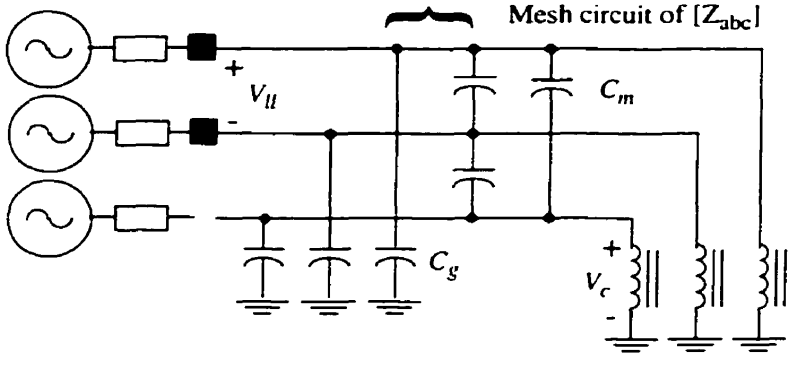

Figure A.1 Equivalent circuit showing line capacitance and transformer primary winding.

Mozaffari *et al.*[A136] applied Thévenin's theorem to the circuit given in Fig. A.1 for the case where one phase is open in order to derive the equivalent circuit shown in Fig. A.2. There are several assumptions which must be made when applying Thévenin's theorem to this circuit. The theorem only applies to well-defined linear time-invariant networks. A network is said to be ***well-defined*** if and only if it does not contain any element which is coupled to some variable outside of the network (i.e. transformer winding). Mozzafari *et al.* argue that by limiting the case to unloaded wye-wye transformers Thévenin's theorem may be applied.

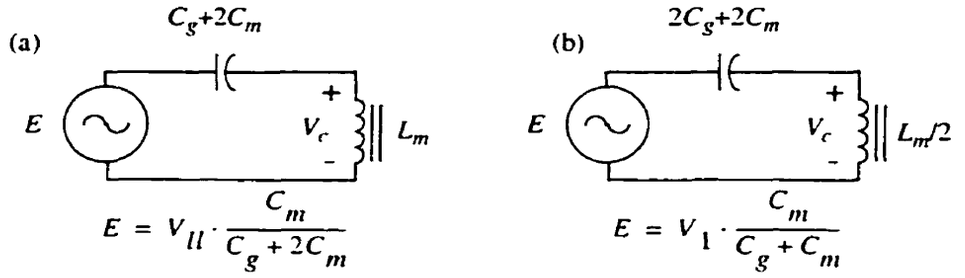

Figure A.2 Thévenin equivalent circuits of (a) single-phase open. (b) two-phase open conditions.

Using the data given in Section 6.10. a rough estimate for C_g is 10.33 nF/km and C_m is 1.43 nF/km. The parallel transmission line can be ignored in the case of a single or double-pole breaker failure at Rosser because the energy required to sustain ferroresonance is derived from the remaining healthy phases on line A3R.

Since we know the effective line charging of the line and tap is 54 MVAr. the effective length of the line can be calculated to be 230.2 km using (A-17). Therefore. the value of C_g and C_m to use in the Thévenin relation is 2.38 μF and 0.329 μF respectively.

$$l = \frac{MVAr}{V^2\omega(C_g + C_m)} \qquad \text{(A-17)}$$

The performance of the Thévenin equivalent is compared against an EMTP steady-state solution for one Silver transformer. The results are summarized in Table A.8. The transformer greatly influences the voltage across the open-circuited winding. Mozaffari's method cannot be applied to wye-delta transformers. which are the most common in practice.

Table A.8 Steady-state comparison with Thévenin Equivalent

Solution	Phase Voltage (V_c)	
	Phase C open	Phase B and C open
Thévenin equivalent formula	26.2 kV	16.9 kV
EMTP: transformer (wye-wye)	21.6 kV	24.0 kV
EMTP: transformer (wye-delta)	512 kV	96.5 kV

[A137] Naidu. S.R., and Souza. B.A.,"Newton-Raphson Approach for the Analysis of Ferroresonant Circuits", *IEE Proc.-Gener. Transm. Distrib.*, Vol. 144. No. 5. pp. 489-494. Sept. 1997.

Additional work: [A128]. [A138].

This paper is nearly identical to their original work. The only addition is Barr and Platt's circuit [A116] is analyzed using their technique. Asymmetrical period-2 and symmetric period-3 solutions are found. Asymmetrical responses result whenever the solution admits a direct component in the flux-linkage. Such waveforms occur in pairs when the magnetization characteristic has odd symmetry.

[A138] Naidu, S.R., and Souza, B.A.,"Analysis of Ferroresonant Circuits in the Time and Frequency Domains", *IEEE Trans. on Magnetics*, Vol. 33, No. 5, pp. 3340-3342, September 1997.

Repeat of authors' other work [A128], [A137]. Bifurcation diagrams of Kieny's circuit [A90] and Barr and Platt's circuit [A116] are calculated. Their hybrid time-domain Newton-Raphson method looks promising but not enough details are given as to how it should be implemented. The method is based on slow parameter variations (i.e. continuation method is used).

Naidu's email: **naidu@dee.ufpb.br.**

[A139] Rye, J.E., McKee, S., Simpson, R.R.S., Tong, Y.K., Wareing, J.B., Perrot, F., *IEE Colloquium on Warning! Ferroresonance Can Damage Your Plant* (Digest Number 1997/349), Publ: IEE, London, U.K., 48 pages, November 12, 1997.

Four papers are contained in this IEE publication.

The first paper, "Tales of the Unexpected", by Rye contains a basic discussion of ferroresonance. Resonance and ferroresonance are compared. A SPICE model of an 11 kV single-phase transformer with series capacitor is created and an odd looking subharmonic mode is simulated. Unbalanced operation of 33 kV circuit are shown to be susceptible to ferroresonance.

The second paper, "Ferroresonance and Preisach Theory", by McKee and Simpson, is an academic paper that discusses how hysteresis can be modelled using Preisach theory. Laboratory results from a single-phase 25 kV/275 V, 15 MVA transformer are compared with computer simulations. Field tests from a distribution substation are also presented. Computations show a period-3 subharmonic should exist; however, field tests did not excite any subharmonic modes.

The third paper, "NGC Experience on Ferroresonance in Power Transformers and Voltage Transformers on HV Transmission Systems", by Tong (National Grid Company), gives a Utility engineer's perspective on the problem. Two HV examples are described: transformer terminated double-circuit line, and a wound PT with circuit breaker grading capacitance. Transformers terminated on double-circuit lines are fitted with ferroresonance detection circuits, which automatically isolates the transformer at the onset of ferroresonance detection. Field measurements of the wound PT indicate period-3 subharmonic oscillations. He mentions fully reliable analytical tools that can predict the onset of ferroresonance are not available due to the difficulty in obtaining accurate system data.

The final paper, "Ferroresonance Overvoltages in Distribution Networks", by Wareing and Perrot, discuss examples of 11 kV distribution transformer ferroresonance. Over 4 pu overvoltages are possible under open-phase conditions, which impact nearby metal-oxide varistors. They recommend using higher rated MOVs on 11 kV circuits, although the high voltages will impact other components. Three-phase switching or adding resistive loading to the transformer secondary can reduce the probability of ferroresonance.

[A140] Sowa, P., Walczak, J., and Pasko, M.,"Evaluation of the Influence of the Chaotic ferroresonance in Transformer on the Power System Work Conditions", 9th Mediterranean Electrotechnical Conference, *MELECON 98*, Vol. 2, pp. 1126-1130, 1998.

Authors use Microtran version of EMTP to study a 115 kV transformer terminated circuit. Although not clear, they appear to be investigating single-pole autoreclosing (i.e. transformer is energized via two phases). The simulation results are highly suspect. A modified least squared approach is used to reduce the model of the system. The paper is poorly written and has little value.

[A141] Al Zahawi, B.A.T., Emin, Z., and Tong, Y.K.,"Chaos in Ferroresonant Wound Voltage Transformers: Effect of Core Losses and Universal Circuit Behaviour", IEE Proc.-Sci. Meas. Technol., vol. 145, No. 1, pp. 39-43, January 1998.

The authors continue their previous work [A135]. They waste their time investigating chaotic operation of the ferroresonant circuit using unrealistic parameter values. Fiegenbaum's number is

calculated.

[A142] Ferracci, P.,"Ferroresonance", *Groupe Schneider: Cahier technique n° 190*, pp. 1-28, March 1998.

This document can be downloaded from the following web site: **//www.schneiderelectric.com/en/pdf//ect190.pdf**

The document provides:

- a basic understanding of ferroresonance,

- overviews of scenarios where ferroresonance may exist,

- methods of preventing ferroresonance, and

- methods for predicting ferroresonance.

He proposed the following study plan:

(a) identify configuration at risk,

(b) simplify the circuit,

(c) determine power system parameters,

(d) determine areas of risk by steady-state computation methods (i.e. bifurcation analysis),

(e) if risk is apparent, then perform time-domain simulations,

(f) determine thermal/mechanical/dielectric withstand,

(g) propose solutions.

In general, I concur with his approach. Through steady-state analysis he shows a broad region where fundamental ferroresonance can exist. In this thesis, I am expanding this region to show where pockets of subharmonics can exist. As well, areas that are at high risk of experiencing fundamental ferroresonance based on the initial conditions are identified.

The follow-up time-domain analysis (i.e. step (e)) is meant to determine whether the initial conditions are feasible and determine expected transient and sustained overvoltage and overcurrent levels. He mentions it is not feasible to use time-domain analysis to study all possible combinations of parameters and initial conditions.

[A143] Iravani, M.R., Wang, X., Polishchuk, I., Ribeiro, J., Sarshar, A.,"Digital Time-Domain Investigation of Transient Behavior of Coupling Capacitor Voltage Transformer", *IEEE Trans. Power Delivery*, Vol. 13, No. 2, pp. 622-629, April 1998.

I sent a detailed discussion of this paper to the authors and the results are published along with the paper. The response to my query provided some additional modelling details that weren't covered in the paper.

The model proposed by the authors is similar to other published CCVT models except more details are provided on the ferroresonance suppression circuit (FSC). Sustained modes of ferroresonance do not result when a FSC is connected.

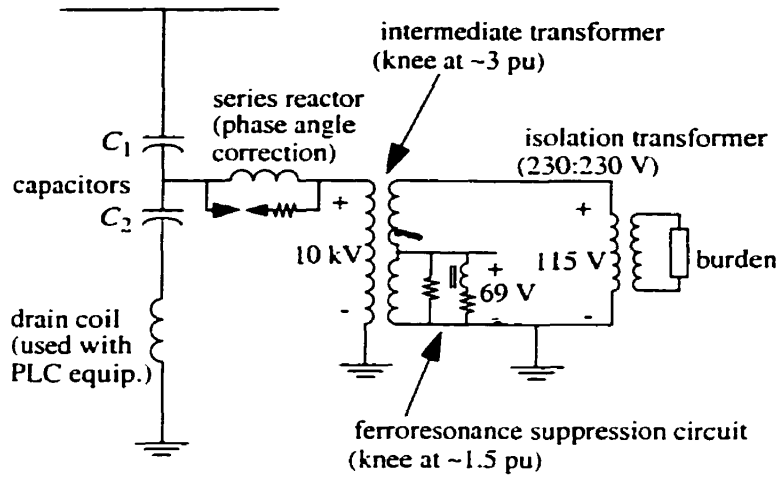

Figure A.3 Coupling capacitor voltage transformer equivalent circuit.

The EMTP program is used to simulate transients in the paper. Using the new information provided by the authors in the reply to my discussion, I was able to generate the following waveforms. Transients damp within 10 cycles as required by the CSA ferroresonance test if the FSC is enabled. Without the FSC, transients take over 60 cycles to damp out. The transients match the results of figures 10, 11 and 13b of the paper reasonably well. This circuit will not be investigated in this thesis because the high damping results in sustained ferroresonance being very unlikely. An unfortunate incident happened during commissioning of CCVTs at Manitoba Hydro. The isolation transformer shown in Fig. A.3 was not 230:230 but 115:115 initially. Switching events resulted in this transformer developing ferroresonance. However, all such isolation transformers have since been replaced.

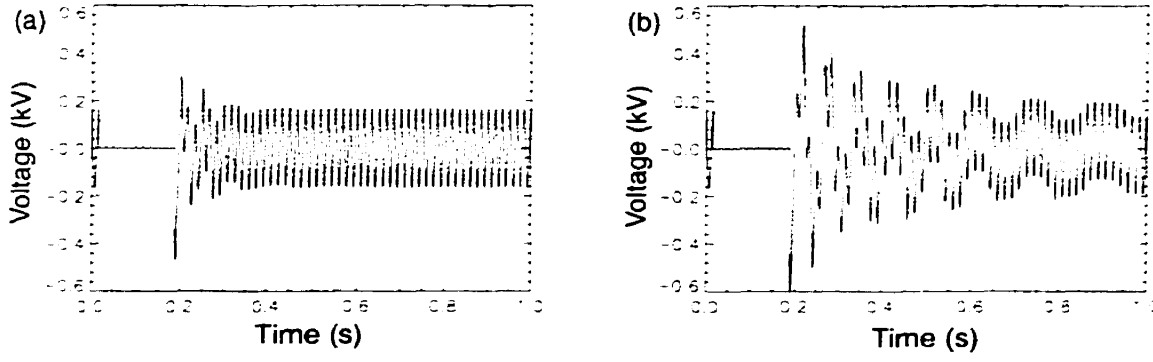

Figure A.4 CSA ferroresonance test comparison with, (a) ferroresonance suppression circuit (FSC) enabled and with, (b) FSC disabled.

Future work by the authors will show a comparison between field tests and EMTP simulations.

[A144] Bowden, J.,"How to Stop Ferroresonance", *Electrical World*, pp.90, June 1998.

The magazine article implies ferroresonance is similar to an LC resonance condition. I don't agree; the phenomenon is much more complex.

Generic guidelines for eliminating ferroresonance in a PT connected in an ungrounded network are given; simply install a resistor with a power dissipation of 50% of the PTs thermal rating across the break of the broken-delta winding.

[A145] IEEE Working Group 15.08.09, *IEEE PES Special Publication: Modelling and Analysis of System Transients Using Digital Programs*, IEEE Catalog No. 99TP-133-0, Chapter 3: Slow Transients, Feb. 1999.

The IEEE task force's report [A126] on slow transients (0.01-1000 Hz) is contained in this document. Nothing new was added other than a more up-to-date bibliography.

[A146] Van Craenenbroeck, T., Michiels, W., Van Dommelen, D., Lust, K.,"Bifurcation Analysis of Three-Phase Ferroresonant Oscillations in Ungrounded Power Systems", *IEEE Trans. Power Delivery*, Vol. 14, No. 2, pp. 531-536, April 1999.

The authors continue evaluating a PT connected in an ungrounded network. Previous studies were published in [A117] and [A121]. Also see [A148].

The bifurcation software AUTO is used to analyze the system. The original 4th order nonautonomous set of equations is transformed into a 6th order autonomous set of equations by representing the forcing function as a stable nonlinear oscillator. The normalized Clark transform derived the original set of equations. A 5th order polynomial represented the transformer saturation curve.

The unbalanced fundamental (UF) mode can only be excited by a transient. The bifurcation diagram has the shape of a closed loop and is called an *isola*. I've seen similar results on a 66 kV system where medium values of stray capacitance result in the UF mode and high values result in the QP-1/2 mode. The authors also discover a bifurcation to a QP-2 mode at low values of capacitance. I've only seen the H3 oscillations.

Future work will look at nonlinear protective devices which can be important in situations where the thermal dissipation of damping resistances become excessive. Also, future studies will investigate more accurate transformer models.

[A147] Mork, B.A.,"Five Legged Wound-Core Transformer Model: Derivation, Parameters, Implementation, and Evaluation", IEEE Trans. Power Delivery, Vol. 14, No. 4, pp. 1519-1526, October 1999.

Mork combines previous published work from [A102] and [A72] into a single paper.

He mentions that existing linear core loss models are not adequate and future work should address such inadequacies. Also, fractal dimension measures were found not to be very useful.

A combination of time-step (50.05005 μs) and print-step (333) were calculated that is very close to perfect Poincaré sampling.

An interesting observation was made in terms of state variables. A classical state diagram would show voltage and dv/dt. The current through the capacitor is Cdv/dt. Therefore, the only needed outputs from the EMTP model is capacitor voltage and capacitor current.

[A148] Van Craenenbroeck, T., Van Dommelen, D., Stuckens, C., Janssens, N., and Monfils, P.A.,"Harmonic Balance Based Bifurcation Analysis of Three-Phase Ferroresonance with Full Scale Experimental Validation", Paper 99 TD034, *Proc. of the 1999 IEEE T&D Conference*, vol. 2, pp. 772-777, April 1999.

Van Craenenbroeck continues his work [A117], [A121], [A146] on the study of ferroresonance in voltage transformers connected to cables in an ungrounded network. He completed his Ph.D. in May 1998.

The main contribution is a comparison is made between two approximation methods for studying the quasi-periodic 1/2 oscillation mode. The Galerkin method of harmonic balance is used to calculate the theoretical stability domains. Multiple nonlinearities in an ungrounded system are handled by applying Clark's transformation to decouple the nonlinear network. Comparisons are made between experiments on a 15 kV laboratory model and theoretical calculations. A slowly varying source voltage is used to discover the stability limits of the UF and QP-1/2 modes.

[A149] Jacobson, D.A.N., Martí, L., and Menzies, R.W.,"Modelling Ferroresonance in a 230 kV Transformer-Terminated Double-Circuit Transmission Line", *Proc. of the 1999 Intl. Conf. on Power System Transients*, pp. 451-456, June 1999.

Field measurements of a 230 kV double-circuit line are made and an EMTP model is developed. Effects of different transformer representations are studied with the result that field measurements could be duplicated with a digital model. Low voltage subharmonics require hysteresis modelling to match the damping of transients. A switched reactor is proposed for eliminating ferroresonance.

[A150] Jacobson, D.A.N., Lehn, P.W., and Menzies, R.W.,"Stability Domain Calculations of Period-1 Ferroresonance in a Nonlinear Resonant Circuit", under review by the PES society as of Dec. 1999.

Other papers by the same author include [A149] and [A127].

Jacobson describes how prediction of the stability domain boundary of period-1 ferroresonance can be improved upon by considering the shape of the basin of attraction. The quasi-static stability domain boundary is calculated using the SVA method. It is shown that network switching results in premature transitions to period-1 ferroresonance that are not predicted by the quasi-static method. Improvements in calculation are made by noting that the period-1 basin of attraction resembles the Limacon of Pascal.

A simple third order polynomial representation of the saturation curve is used to illustrate the method. Reasonable comparisons are made between brute-force calculations and the analytical calculations.

A.3 AUTHOR INDEX

Appendix B

EMTP Data Files

Three EMTP data file cases are included in this appendix.

The first case is listed in B.1 and corresponds to the May 25. 1995 ferroresonant event. The case will produce the output shown in Fig. 4.4b.

The second case is listed in B.2 and corresponds to the single-phase laboratory model. The case will produce the output given in Fig. 5.8.

The third case is listed in B.3 and corresponds to the transformer-terminated double-circuit line example. The case will produce the output shown in Fig. 6.16. Frequency dependent line data has been omitted to reduce the file size

B.1 TRANSFORMER/GRADING-CAPACITOR

```
BEGIN NEW DATA CASE
C
C
C              ************************************************
C              ***                                          ***
C              ***  EMTP FERRORESONANCE MODEL               ***
C              ***                                          ***
C              ***  VERSION 1.0                             ***
C              ***                                          ***
C              ************************************************
C
C   CASE NAME: FERRO_bm.DAT --- STRONG Dorsey --- Benchmark case
C   DATE: November 22, 1995
C
C   DESCRIPTION: POTENTIAL TRANSFORMER CONNECTION TO A 230 KV BUS THROUGH
C                THE GRADING CAPACITANCE OF x BREAKERS IN PARALLEL (5080 pF).
C                NO FAULT.
C
C   MITIGATION: (NONE)
C               1. USING SST2 (INCLUDE NEUTRAL R)
C               2. SECONDARY PT LOADING
C               3. EXTRA SHUNT CAPACITANCE
C               4. MOD DISCONNECTS
C               5. FILTER SWITCHING
C
C FIRST CARD
C                    ohms      uF
C DELTAT<---TMAX<---XOPT<---COPT<-EPSILN<----TOL
  25.E-6     1.0      60.       0.   1.E-10  1.E-10
C SECOND CARD
C
C   IOUT   IPLOT  IDOUBL  KSSOUT  MAXOUT    IPUN  MEMSAV    ICAT  NENERG IPRS
```

```
    9999      11       0       3       1       0       0       1       0
C
TACS HYBRID
C
C
BLANK ENDS TACS
C
C ------------------------------------------------------------------------------
C EQUIVALENT SOURCE MODEL
C
C POS. SEQ. DATA; calculated from PSSE SC Model
C i.   strong system Z: .2116+j4.3801   MVA:13133
C
C ZERO SEQUENCE DATA: FROM PSSE SC MODEL
C i.   strong system Z: .06877+j.96807
C
C    STRONG DORSEY EQUIVALENT
C
C <NODE NAMES>             <ZERO,POS SEQUNCE>
C <-BUS1<-BUS2             <----R<----------X
51EDORSADORB2A              .3068 .96807
52EDORSBDORB2B              .2116 4.3801
53EDORSCDORB2C
C
C ------------------------------------------------------------------------------
C GRADING CAPACITOR MODELS:
C
  DORC2ADORA2A                          .00508
  DORC2BDORA2B                          .00508
  DORC2CDORA2C                          .00508
C
C ------------------------------------------------------------------------------
C   -----> First Order Bus Capacitance Matrix:
C             Dorsey 230 kV bus A2 & B2
C             442.57 m of 2x1843.2 MCM ACSR dia: 1.6"
C
C                       B2                              A2
C              /--------^----------\          /---------^---------\
C
C              |<- 13' ->|<- 13' ->|<-- 22' -->|<- 13' ->|<- 13' ->|
C          --- O O       O O       O O         O O       O O       O O
C           ^   A         B         C           A         B         C
C           |
C          37'
C           |
C          ------------------------------------------------------------
C          ////////////////////////////////////////////////////////////
C
SVINTAGE,1
 1DORC2A                  1.000000000E+99 0.000000000E-01 1.023120074E-02
 2DORC2B                  0.000000000E-02 0.000000000E-01-2.876418978E-03
                          1.000000000E+99 0.000000000E-01 1.099207042E-02
 3DORC2C                  0.000000000E-02 0.000000000E-01-1.017177422E-03
                          0.000000000E-02 0.000000000E-01-2.744746208E-03
                          1.000000000E+99 0.000000000E-01 1.063613391E-02
 4DORA2A                  0.000000000E-02 0.000000000E-01-3.633450318E-04
                          0.000000000E-02 0.000000000E-01-6.251015102E-04
                          0.000000000E-02 0.000000000E-01-1.631218420E-03
                          1.000000000E+99 0.000000000E-01 1.063613391E-02
 5DORA2B                  0.000000000E-02 0.000000000E-01-2.021682956E-04
                          0.000000000E-02 0.000000000E-01-2.949899670E-04
                          0.000000000E-02 0.000000000E-01-6.251015102E-04
                          0.000000000E-02 0.000000000E-01-2.744746208E-03
                          1.000000000E+99 0.000000000E-01 1.099207042E-02
 6DORA2C                  0.000000000E-02 0.000000000E-01-1.603387903E-04
                          0.000000000E-02 0.000000000E-01-2.021682956E-04
                          0.000000000E-02 0.000000000E-01-3.633450318E-04
                          0.000000000E-02 0.000000000E-01-1.017177422E-03
                          0.000000000E-02 0.000000000E-01-2.876418978E-03
                          1.000000000E+99 0.000000000E-01 1.023120074E-02
SVINTAGE,0
C
```

```
C
C Additional stray capacitance due to bushings etc. (4000 pF)
C                            | R   || L   || C   |
  DORA2A                                    .00800
  DORA2B                                    .00800
  DORA2C                                    .00800
C
C ~~~~~~~~~~~~~~~~~~~~~~~~~~~~~~~~~~~~~~~~~~~~~~~~~~~~~~~~~~~~~~~~~~~~~~~~~~~~~~~~
C  DORSEY FILTERS CONNECTED TO B2 BUS
C  ** CONNECT F9 TO A2 BUS BY MODIFYING SWITCH NODE NAMES
C
C       i. BP1 FILTERS (350 MVAR)
C
C F1: 11th and 13th: 45.14 MVAr
C                           | R   || L   || C   |
 0DORB2A                      1.84 16.74 1.310
 0DORB2B                      1.84 16.74 1.310
 0DORB2C                      1.84 16.74 1.310
C
 0DORB2A                      2.17 16.74 .9380
 0DORB2B                      2.17 16.74 .9380
 0DORB2C                      2.17 16.74 .9380
C
C F2: 5th and 7th: 52.00 MVAr
 0DORB2A                      3.17 63.34 1.670
 0DORB2B                      3.17 63.34 1.670
 0DORB2C                      3.17 63.34 1.670
C
 0DORB2A                      4.43 63.34 .8520
 0DORB2B                      4.43 63.34 .8520
 0DORB2C                      4.43 63.34 .8520
C
C F3: HP: 80.72 MVAr
C
 0BP1DA1DORB2A                             4.040
 0BP1DB1DORB2B                             4.040
 0BP1DC1DORB2C                             4.040
 0BP1DA1                     41.0
 0BP1DB1                     41.0
 0BP1DC1                     41.0
 0BP1DA1                           1.534
 0BP1DB1                           1.534
 0BP1DC1                           1.534
C
C F4: 11th and 13th: 45.14 MVAr
C                           | R   || L   || C   |
 0DORB2A                      1.84 16.74 1.310
 0DORB2B                      1.84 16.74 1.310
 0DORB2C                      1.84 16.74 1.310
C
 0DORB2A                      2.17 16.74 .9380
 0DORB2B                      2.17 16.74 .9380
 0DORB2C                      2.17 16.74 .9380
C
C F5: 5th and 7th: 52.00 MVAr
 0DORB2A                      3.17 63.34 1.670
 0DORB2B                      3.17 63.34 1.670
 0DORB2C                      3.17 63.34 1.670
C
 0DORB2A                      4.43 63.34 .8520
 0DORB2B                      4.43 63.34 .8520
 0DORB2C                      4.43 63.34 .8520
C
C F6: HP: 80.72 MVAr
C
 0BP1DA2DORB2A                             4.040
 0BP1DB2DORB2B                             4.040
 0BP1DC2DORB2C                             4.040
 0BP1DA2                     41.0
 0BP1DB2                     41.0
 0BP1DC2                     41.0
 0BP1DA2                           1.534
```

```
 0BP1DB2                          1.534
 0BP1DC2                          1.534
C       ii. BP2 FILTERS (400 MVAR)
C
C F7: 11th and 13th: 140 MVAr
 0DORB2A                    1.08 5.391 4.1000
 0DORB2B                    1.08 5.391 4.1000
 0DORB2C                    1.08 5.391 4.1000
C
 0DORB2A                    1.27 5.391 2.9000
 0DORB2B                    1.27 5.391 2.9000
 0DORB2C                    1.27 5.391 2.9000
C
C F8: HP: 120 MVAr
 0DORB2ABP2HPA                         6.0000
 0DORB2BBP2HPB                         6.0000
 0DORB2CBP2HPC                         6.0000
 0BP2HPA                     158.
 0BP2HPB                     158.
 0BP2HPC                     158.
 0BP2HPA                         .8294
 0BP2HPB                         .8294
 0BP2HPC                         .8294
C
C F9: 11th and 13th: 140 MVAr
 0BP2F9A                    1.08 5.391 4.1000
 0BP2F9B                    1.08 5.391 4.1000
 0BP2F9C                    1.08 5.391 4.1000
C
 0BP213A                    1.27 5.391 2.9000
 0BP213B                    1.27 5.391 2.9000
 0BP213C                    1.27 5.391 2.9000
C
C ------------------------------------------------------------------------------
C TRANSFORMER MODELS:
C
C    DORSEY   230KV-115V POTENTIAL TRANSFORMER (V13F)
C    4 KVA THERMAL RATING (SINGLE PHASE)
C    TAPS: X1-X3 1200:1; X2-X3 2000:1
C    Assume Xac=148.4 H or 55951.7 ohms
C    Resistance primary winding = 7490 ohms
C    Resistance secondary winding = .0463 ohms
C    Core losses require 9.52E7 ohms (200 Watts at 115 kV)
C    Secondary Resistance=.046 or 66200 (reflected to prim)
C    Secondary inductance=0.1642 or 236500 (to prim)
C    PF=0.27
C          > REFBUS      STEA_I< FLUX   BUS  RMAG      ...IOUT(COL 80)          *
  TRANSFORMER             .00478450.38P1A PH9.52E7                              1
C         CURRENT<---        FLUX
  0.47802326E-02  0.45038324E+03
  0.58271496E-02  0.49542156E+03
  0.99568473E-02  0.53994220E+03
  0.16453655E-01  0.56272021E+03
  0.24258283E-01  0.58498053E+03
  0.34983873E-01  0.60775853E+03
  0.51536774E-01  0.63001885E+03
  0.76007830E-01  0.65279685E+03
  0.12093922E+00  0.67505717E+03
  0.21079611E+00  0.70249431E+03
  0.43580606E+02  0.34084175E+04
           9999
C
C   BUS1  BUS2            <--RK <--LK <turns           ...IOUT(COL 80)
 1TV13FA                  7490. 0.001 1200.
 2XV13FA                  .0460 .1642    1.
C             REFBUS       CUR  FLUX  BUSTOP  RMAG      ...IOUT(COL 80)          *
  TRANSFORMER P1A PH                   P1B PH                                    1
 1TV13FB
 2XV13FB
C             REFBUS       CUR  FLUX  BUSTOP  RMAG      ...IOUT(COL 80)          *
  TRANSFORMER P1A PH                   P1C PH                                    1
 1TV13FC
```

```
 2XV13FC
C
C PT BURDEN (75 VA CSA Standard) assumed: (163.2+j0.268)
C                          | R   || L   || C   |
  XV13FA                   163.2   .268
  XV13FB                   163.2   .268
  XV13FC                   163.2   .268
C
C    DORSEY   230KV-115V POTENTIAL TRANSFORMER (V33F)
C    4 KVA THERMAL RATING (SINGLE PHASE)
C    TAPS: X1-X3 1200:1; X2-X3 2000:1
C    Assume Xac=148.4 H or 55951.7 ohms
C    Resistance primary winding = 7490 ohms
C    Resistance secondary winding = .0463 ohms
C    Core losses require 9.52E7 ohms (200 Watts at 115 kV)
C    Secondary Resistance=.046 or 66200 (reflected to prim)
C    Secondary inductance=0.1642 or 236500 (to prim)
C    PF=0.27
C           > REFBUS       STEA_I< FLUX   BUS  RMAG      ...IOUT(COL 80)          *
  TRANSFORMER              .00478450.38P2A PH9.52E7                               1
C         CURRENT<---         FLUX
  0.47802326E-02  0.45038324E+03
  0.58271496E-02  0.49542156E+03
  0.99568473E-02  0.53994220E+03
  0.16453655E-01  0.56272021E+03
  0.24258283E-01  0.58498053E+03
  0.34983873E-01  0.60775853E+03
  0.51536774E-01  0.63001885E+03
  0.76007830E-01  0.65279685E+03
  0.12093922E+00  0.67505717E+03
  0.21079611E+00  0.70249431E+03
  0.43580606E+02  0.34084175E+04
           9999
C
C   BUS1  BUS2             <--RK <--LK <turns           ...IOUT(COL 80)
 1TV33FA                   7490. 0.001  1200.
 2XV33FA                   .0460 .1642     1.
C             REFBUS        CUR   FLUX  BUSTOP  RMAG      ...IOUT(COL 80)          *
  TRANSFORMER P2A PH                    P2B PH                                    1
 1TV33FB
 2XV33FB
C             REFBUS        CUR   FLUX  BUSTOP  RMAG      ...IOUT(COL 80)          *
  TRANSFORMER P2A PH                    P2C PH                                    1
 1TV33FC
 2XV33FC
C
C PT BURDEN (75 VA CSA Standard) assumed: (163.2+j0.268)
C                          | R   || L   || C   |
  XV33FA                   163.2   .268
  XV33FB                   163.2   .268
  XV33FC                   163.2   .268
C
C    DORSEY   230KV-4160V STATION SERVICE TRANSFORMER (SST2)
C    10 MVA (THREE PHASE)
C    XHL=12.20% R1=12 ohms Xac=884 ohms
C    split leakage 50-50
C    Core losses require 3.11E6 ohms (17000 Watts at 230 kV)
C
C           > REFBUS       STEA_I< FLUX   BUS< RMAG      ...IOUT(COL 80)          *
  TRANSFORMER              .02485390.04P3A PH3.11E6                               1
C         CURRENT<---         FLUX
  0.24849753E-01  0.39004167E+03
  0.64678684E-01  0.42491130E+03
  0.12967085E+00  0.45828649E+03
  0.21305588E+00  0.48319337E+03
  0.26390417E+00  0.49813752E+03
  0.42907889E+00  0.53798848E+03
  0.54855853E+00  0.55542321E+03
  0.76131575E+00  0.58282045E+03
  0.11461796E+01  0.60772742E+03
  0.62047277E+02  0.69241084E+03
  0.22137816E+03  0.10162005E+04
```

```
  0.25798675E+03  0.10959024E+04
          9999
C
C   BUS1  BUS2            <--RK <--LK <ratio           ...IOUT(COL 80)
 1TSST2A                   12.0 322.69 132.8
 2XSST2AXSST2G                .1056    2.4
C             REFBUS       CUR  FLUX  BUSTOP  RMAG     ...IOUT(COL 80)         *
  TRANSFORMER P3A PH                   P3B PH                                  1
 1TSST2B
 2XSST2BXSST2G
C             REFBUS       CUR  FLUX  BUSTOP  RMAG     ...IOUT(COL 80)         *
  TRANSFORMER P3A PH                   P3C PH                                  1
 1TSST2C
 2XSST2CXSST2G
C
C 2.4 OHM NEUTRAL GROUNDING RESISTOR
C
C                           | R  || L  || C  |
  XSST2G                    2.4
C
C    DORSEY   230KV-115V POTENTIAL TRANSFORMER (FILTER DISCHARGE)
C    4 KVA THERMAL RATING (SINGLE PHASE)
C    TAPS: X1-X3 1200:1; X2-X3 2000:1
C    Assume Xac=.08X1, where X1=.05 pu on 4 kVA base (19044 ohms or 50 H)
C    Resistance primary winding = 4654 ohms
C    Resistance secondary winding = .0225 ohms
C    Core losses require 9.52E7 ohms (200 Watts at 115 kV)
C    Assume pf=0.27
C    high knee point model
C
C           > REFBUS      STEA_I< FLUX   BUS  RMAG     ...IOUT(COL 80)         *
  TRANSFORMER             .00377389.8 P4A PH9.52E7                             1
C         CURRENT<---        FLUX
  0.37712362E-02  0.38981446E+03
  0.56310396E-02  0.42864060E+03
  0.79155467E-02  0.50681056E+03
  0.10509987E-01  0.54563670E+03
  0.14482506E-01  0.58498053E+03
  0.17894943E-01  0.62380667E+03
  0.24818348E-01  0.66263281E+03
  0.31800187E-01  0.70145895E+03
  0.42321896E-01  0.74080277E+03
        0.0600          800.00
        0.1143          873.41
        0.1511          887.14
        0.1904          898.12
        0.2650          914.59
        0.3561          925.57
       1.84463         1000.76
          9999
C
C   BUS1  BUS2            <--RK <--LK <turns           ...IOUT(COL 80)
 1TVFDFA                   4654. .0010 1200.
 2XVFDFA                   .0225 .0830    1.
C             REFBUS       CUR  FLUX  BUSTOP  RMAG     ...IOUT(COL 80)         *
  TRANSFORMER P4A PH                   P4B PH                                  1
 1TVFDFB
 2XVFDFB
C             REFBUS       CUR  FLUX  BUSTOP  RMAG     ...IOUT(COL 80)         *
  TRANSFORMER P4A PH                   P4C PH                                  1
 1TVFDFC
 2XVFDFC
C
C PT BURDEN (75 VA CSA Standard) assumed: (163.2+j0.268)
C                           | R  || L  || C  |
  XVFDFA                    163.2  .268
  XVFDFB                    163.2  .268
  XVFDFC                    163.2  .268
C
C CONNECT SYNCHRONIZING SOURCES TO GROUND
  SYNS_A                    1.0
  SYNS_B                    1.0
```

```
  SYNS_C                  1.0
C
BLANK ENDS BRANCH
C
C ------------------------------------------------------------------------------
C SWITCHING DATA
C
C 1. LAST BREAKER TO CLEAR BUS A2 (R55)
C
C CLASS 1 - (TIME-CONTROLLED SWITCH) OPENS WHEN CURRENT GOES THROUGH ZERO
C <-BUS1<-BUS2<--T CLOSE<---T OPEN<-I MARGIN                                  O
  DORC2ADORA2A      -1.0    .039444                                           3
  DORC2BDORA2B      -1.0    .039444                                           3
  DORC2CDORA2C      -1.0    .039444                                           3
C
C 2. MEASURING SWITCH TO MEASURE TOTAL PT LOAD CURRENT (IN V13F)
C <-BUS1<-BUS2<--T CLOSE<---T OPEN<-I MARGIN                                  O
  DORA2ATV13FA      -1.0     9999.                                            3
  DORA2BTV13FB      -1.0     9999.                                            3
  DORA2CTV13FC      -1.0     9999.                                            3
C
C 3. MEASURING SWITCH TO MEASURE TOTAL PT LOAD CURRENT (IN V13F)
C <-BUS1<-BUS2<--T CLOSE<---T OPEN<-I MARGIN                                  O
  DORA2ATV33FA      -1.0     9999.                                            3
  DORA2BTV33FB      -1.0     9999.                                            3
  DORA2CTV33FC      -1.0     9999.                                            3
C
C 4. MEASURING SWITCH TO MEASURE TOTAL LOAD CURRENT (IN SST2)
C <-BUS1<-BUS2<--T CLOSE<---T OPEN<-I MARGIN                                  O
  DORA2ATSST2A     9999.     9999.                                            3
  DORA2BTSST2B     9999.     9999.                                            3
  DORA2CTSST2C     9999.     9999.                                            3
C
C 5. MEASURING SWITCH TO MEASURE TOTAL PT LOAD CURRENT (IN Filter Discharge PT)
C <-BUS1<-BUS2<--T CLOSE<---T OPEN<-I MARGIN                                  O
  DORA2ATVFDFA     9999.     9999.                                            3
  DORA2BTVFDFB     9999.     9999.                                            3
  DORA2CTVFDFC     9999.     9999.                                            3
C
C Moved filters (F9) to B2 BUS
C 6. MEASURING SWITCH TO MEASURE TOTAL CURRENT (IN F9 11 th harmonic)
C <-BUS1<-BUS2<--T CLOSE<---T OPEN<-I MARGIN                                  O
  DORB2ABP2F9A      -1.0     9999.                                            3
  DORB2BBP2F9B      -1.0     9999.                                            3
  DORB2CBP2F9C      -1.0     9999.                                            3
C
C 7. MEASURING SWITCH TO MEASURE TOTAL CURRENT (IN F9 13 th harmonic)
C <-BUS1<-BUS2<--T CLOSE<---T OPEN<-I MARGIN                                  O
  DORB2ABP213A      -1.0     9999.                                            3
  DORB2BBP213B      -1.0     9999.                                            3
  DORB2CBP213C      -1.0     9999.                                            3
C
C 8. MEASURING SWITCH TO MEASURE TOTAL CURRENT FLOWING THROUGH GRADING CAPS
C    AND CIRCUIT BREAKER
C
C CLASS 1 - (TIME-CONTROLLED SWITCH) OPENS WHEN CURRENT GOES THROUGH ZERO
C <-BUS1<-BUS2<--T CLOSE<---T OPEN<-I MARGIN                                  O
  DORB2ADORC2A      -1.0     9999.                                            3
  DORB2BDORC2B      -1.0     9999.                                            3
  DORB2CDORC2C      -1.0     9999.                                            3
C
C BLANK CARD TERMINATING SWITCHES
BLANK ENDS SWITCH
C
C ------------------------------------------------------------------------------
C IDEAL SOURCE (1.045/_0) on bus B2
C          <-         <-         <-         <-         <-         <-TSTART  <-TSTOP
14EDORSA   183950.00      60.0       0.00                              -1.0
14EDORSB   183950.00      60.0    -120.00                              -1.0
14EDORSC   183950.00      60.0     120.00                              -1.0
C
BLANK ENDS SOURCE
```

```
C
C ------------------------------------------------------------------------------
C OUTPUT NODE SPECS FOLLOW
C
  DORB2A      DORB2B      DORB2C      DORA2A      DORA2B      DORA2C
  TV13FA      TV13FB      TV13FC      TV33FA      TV33FB      TV33FC
  XV13FA      XV13FB      XV13FC      XV33FA      XV33FB      XV33FC
C BLANK CARD TERMINATING THE OUTPUT NODE SPECS
BLANK ENDS OUTPUT
C BLANK CARD TERMINATING THE BATCH MODE PLOT REQUESTS
BLANK ENDS PLOT
BLANK
C
C BLANK CARD TERMINATING EMTP SOLUTION MODE
BLANK
BEGIN NEW DATA CASE
BLANK
```

B.2 LABORATORY MODEL

```
BEGIN NEW DATA CASE
C
C
C              ************************************************
C              ***                                          ***
C              ***  EMTP FERRORESONANCE MODEL               ***
C              ***                                          ***
C              ***              VERSION 1.0                 ***
C              ***                                          ***
C              ************************************************
C
C   CASE NAME: nsat_case4d.dat     --- non linear inductor model
C   DATE: June 01, 2000
C
C   DESCRIPTION: 2.3 kV / 115 V  2.5 kVa transformer
C                No hysteresis modeled
C                Benchmark case #4 5xPec
C                Time step/Iplot setup to get 64 samples/cycle
C                Added extra winding
C
C  SPECIAL REQUEST CARDS:
INITIALIZATION WITH HARMONICS
C
C  FIRST CARD
C                  ohms      uF
C DELTAT<---TMAX<---XOPT<---COPT<-EPSILN<----TOL
8.9799-6     1.00      60.       0.   1.E-10  1.E-10
C SECOND CARD
C Setup Iplot to get 64 samples/cycle:
C Default time step is 46.296 microseconds (360 samples/cycle)
C Modify time step so that 5*64=320 samples/cycle result.
C 16.667 msec/64=0.260416666 msec
C .260416666 msec/52.0833333 microsec.=5 (Iplot)
C Require finer time step for ferroresonance calculations...
C Therefore, divide timestep by 5 and multiply Iplot by 5:
C DeltaT=8.9799usec and Iplot=29
C
C   IOUT   IPLOT  IDOUBL  KSSOUT  MAXOUT    IPUN  MEMSAV    ICAT  NENERG IPRS
    9999      29       0       3       1       0       0       1       0
C  ** NEXT CARD USED IF NENERG IS NOT ZERO- STATISTICS SWITCHES USED
C     TYPICAL VALUE FOR NENERG IS 60
C STATISTICS CARD
C    ISW   ITEST   IDIST   AINCR  XMAXNX  DEGMIN  DEGMAX  STATFR  SIGMAX NSEED
C      1       0       0       0     3.0       0     360      60       0        0
C
TACS HYBRID
C
BLANK ENDS TACS
C
C ------------------------------------------------------------------------------
C
```

```
C EQUIVALENT SOURCE MODEL
C
C    EQUIVALENT IMPEDANCE of UofM 115 Volt Source
C
C                          | R  || L  || C  |
C Modified source impedance
  EDORSAIDORSA             .09296.07965
C
C ------------------------------------------------------------------------------
C
C GRADING CAPACITOR MODELS:
C
C Equivalent grading capacitance (microFarads)
C                          | R  || L  || C  |
  DORA2ATSST2A             0.18          182.3
C
C Equivalent stray capacitance  (microFarads)
C                          | R  || L  || C  |
  TSST2A                                 39.7
C
C Contact resistance
C                          | R  || L  || C  |
  TSST1ATSSTYA             0.0001
C ------------------------------------------------------------------------------
C
C TRANFORMER MODEL:
C
C    Machines Lab  115V-2300V TRANSFORMER (SST2)
C    2.5 kVA (SINGLE PHASE)
C    split leakage reactance 50-50,resistance according to DC resistance test;
C    Test 19th order polynomial with 21 points
C eddy current losses, modeled by a resistor = (115.1^2/(28.639)=461.78
C
C            > REFBUS      STEA_I< FLUX   BUS< RMAG     ...IOUT(COL 80)          *
  TRANSFORMER              0.5456.36238P3A PH461.78                              1
C         CURRENT<---        FLUX
      0.545605     0.362377
      0.591643     0.375319
      0.661367     0.388261
      0.773163     0.401203
      0.958311     0.414145
       1.26911     0.427088
       1.79166     0.44003
        2.6655     0.452972
       4.11377     0.465914
       6.48838     0.478856
       10.3375     0.491798
        16.505     0.50474
       26.2751     0.517682
       41.5814     0.530624
       65.3061     0.543566
       101.703     0.556508
       156.995     0.56945
       240.201     0.582392
       364.289     0.595334
       547.749     0.608276
       816.749     0.621218
            9999
C
C   BUS1  BUS2             <--RK <--LK <ratio           ...IOUT(COL 80)
 1TSSTYA                    .0486 .0265    1.
 2      TSSTXA              .0486 .0265    1.
 3XSST2AXSST3A             7.814 10.59   20.
C
C Dummy cap to make ground connection
C                          | R  || L  || C  |
  XSST3A                                 0.1
C try doubling core losses after switch opens
C                          | R  || L  || C  |
  P4A_PH                   461.78
  P4A_PH                   461.78
  P4A_PH                   461.78
```

```
  P4A_PH                    461.78
C CONNECT SYNCHRONIZING SOURCES TO GROUND
  SYNS_A                    1.0
C
BLANK ENDS BRANCH
C
C ------------------------------------------------------------------------------
C SWITCHING DATA
C
C TIME-CONTROLLED SWITCHES:
C
C 1. Switch for measuring total load current
C
C CLASS 1 - (TIME-CONTROLLED SWITCH) OPENS WHEN CURRENT GOES THROUGH ZERO
C <-BUS1<-BUS2<--T CLOSE<---T OPEN<-I MARGIN                                  O
  IDORSADORA2A      -1.0    9999.                                             3
  TSST2ATSST1A      -1.0    9999.                                             3
C
C Switch for triggering ferroresonance
C 2. MEASURING SWITCH TO MEASURE TOTAL LOAD CURRENT (IN SST2)
C <-BUS1<-BUS2<--T CLOSE<---T OPEN<-I MARGIN                                  O
  DORA2ATSST2A      -1.0     0.100                                            3
  P3A PHP4A_PH      0.10     999.0                                            3
C
C BLANK CARD TERMINATING SWITCHES
BLANK ENDS SWITCH
C
C         <-        <-        <-        <-        <-        <-TSTART  <-TSTOP
C
C IDEAL SOURCE (1.00pu/_0) on bus B2 -- 115 Volt -> 162.6346 Vpeak
C
14EDORSA   162.6346       60.                                  -1.0     9999.
C
BLANK ENDS SOURCE
C
C ------------------------------------------------------------------------------
C OUTPUT NODE SPECS FOLLOW
C
  IDORSA      DORA2A      TSST2A      XSST2A      TSST1A      TSSTXA
C
C BLANK CARD TERMINATING THE OUTPUT NODE SPECS
BLANK ENDS OUTPUT
C BLANK CARD TERMINATING THE BATCH MODE PLOT REQUESTS
BLANK ENDS PLOT
BLANK
C
C BLANK CARD TERMINATING EMTP SOLUTION MODE
BLANK
BEGIN NEW DATA CASE
BLANK
```

B.3 TRANSFORMER-TERMINATED DOUBLE-CIRCUIT

```
BEGIN NEW DATA CASE
C
C              ************************************************
C              ***                                          ***
C              ***  EMTP SILVER TAP FERRORESONANCE MODEL     ***
C              ***                                          ***
C              ***              VERSION 2.0                 ***
C              ***             November 1998                ***
C              ***                                          ***
C              ************************************************
C
C  SPECIAL REQUEST CARDS
C  ---------------------
C
C SOLUTIONS TO CASE CONVERGENCE PROBLEMS
C 1. DECREASE TIME STEP:
C 2. INCREASE NUMBER OF ITERATIONS (MAXZNO)
C 3. INCREASE DIVERGENCE TOLERANCE (EPSTOP) Default: BLANK=VREF/10.
```

```
C
C 1. --->DECREASING TIME STEP CAUSES LIST SEVEN TO RUN OUT OF SPACE
C NOTE: LT7-> AN RMS SENSOR REQUIRES 1/(F*DELTAT) CELLS: 17000 PER DEVICE
C       THEREFORE REMOVE THE RMS DEVICES OR INCREASE LISTSIZE 19
ABSOLUTE TACS DIMENSIONS
      50       50    2000       50       50      500    40000     3000
C
C 2. ---> CONTROL NEWTON RAPHSON ITERATIVE SOLUTION
C
C   ZINC OXIDE  <-MAXZNO<-EPSZNO<-EPWARN<-EPSTOP<ZNOLIM1<ZNOLIM2
ZINC OXIDE            20  0.1E-6  0.1E-4  0.1E-4        0        0
C
C FIRST CARD
C ----------
C                   ohms      uF
C DELTAT<---TMAX<---XOPT<---COPT<-EPSILN<----TOL
  10.E-6    0.50      60.       0.  1.E-10  1.E-10
C
C SECOND CARD
C -----------
C    IOUT    IPLOT   IDOUBL  KSSOUT  MAXOUT    IPUN  MEMSAV    ICAT  NENERG IPRS
   99999       17        0       3       1       0       0       1       0
C
C STATISTICS CARD
C ---------------
C  ** NEXT CARD USED IF NENERG IS NOT ZERO- STATISTICS SWITCHES USED
C     TYPICAL VALUE FOR NENERG IS 50
C     ISW    ITEST    IDIST    AINCR  XMAXNX  DEGMIN  DEGMAX  STATFR  SIGMAX NSEED
C       1        0        0        0     3.0       0     360      60       0        0
C
C ------------------------------------------------------------------------------
C
TACS HYBRID
C
BLANK ENDS TACS
C
C ------------------------------------------------------------------------------
C
C Thevenin Source Impedances
C
C POS. SEQ. DATA: calculated from PSSE MMTU SC Model
C ZERO SEQ. DATA: " "
C
C       i. DORSEY EQUIVALENT (83)
C
C <NODE NAMES>             <ZERO,POS SEQUNCE>
C <-BUS1<-BUS2             <----R<----------X
51EDORSADORB2A              .0741    1.0368
52EDORSBDORB2B              .2539    5.4275
53EDORSCDORB2C
C
C       ii. ROSSER (84)
C
51EROSSAROSSRA              .4814   14.0767
52EROSSBROSSRB             2.8090   23.7309
53EROSSCROSSRC
C
C       iii. RIDGEWAY (81)
C
51ERIDGA RIDGA              .5766   14.7750
52ERIDGB RIDGB             3.1423   29.4812
53ERIDGC RIDGC
C
C       iv. VERMILLION (91)
C
51EVERMA VERMA             1.6875   24.1753
52EVERMB VERMB             9.5696   49.8477
53EVERMC VERMC
C
C ------------------------------------------------------------------------------
C
C GRADING CAPACITOR MODELS:
```

```
C
C  R6/R7: ABB-ELF BREAKERS (2x1500 pF) 1500 pF total
C                            | R   || L   || C   |
  DORB2ADORASA                                .00150
  DORB2BDORASB                                .00150
  DORB2CDORASC                                .00150
C
C  R1/R3: BRBO-DCVF BREAKERS (6X130 PF) 50 pF total
C                            | R   || L   || C   |
  ASHRNAASDORA                                .00005
  ASHRNBASDORB                                .00005
  ASHRNCASDORC                                .00005
C
C  R9/R10: ABB-HPL BREAKERS (2X1600) 1600 pF total
C                            | R   || L   || C   |
  ROSASAROSSRA                 50.            .00160
  ROSASBROSSRB                 50.            .00160
  ROSASCROSSRC                 50.            .00160
C
C  NEW: ASSUME ABB-HPL BREAKERS (2X1600) 1600 pF total
C                            | R   || L   || C   |
  ROSILAROSSRA                                .00160
  ROSILBROSSRB                                .00160
  ROSILCROSSRC                                .00160
C
C  R1/R3: BRBO-DCVF BREAKERS (6X130 PF) 50 pF total
C                            | R   || L   || C   |
  ASHRNAASROSA                 50.            .00005
  ASHRNBASROSB                 50.            .00005
  ASHRNCASROSC                 50.            .00005
C
C  R2: ABB-HPL BREAKERS (2X1600) 800 pF total
C                            | R   || L   || C   |
  SILCTASILVBA                50.0            .00080
  SILCTBSILVBB                50.0            .00080
  SILCTCSILVBC                50.0            .00080
C
C  NEW: ASSUME ABB-HPL BREAKERS (2X1600) 800 pF total
C                            | R   || L   || C   |
  SIL2HASILVBA                50.0            .00080
  SIL2HBSILVBB                50.0            .00080
  SIL2HCSILVBC                50.0            .00080
C
C ------------------------------------------------------------------------------
C TRANSMISSION LINES:
C
C      *** MANITOBA HYDRO TRANSMISSION LINES: Peripheral to study area
C
C i:   D16R, D13R
C ii:  D5R
C iii: D36R, R23R
C iv:  A6V
C v:   G1A, G2A
C vi:  G31V
C vii: Future: Rosser-Silver
C
C      i. DOUBLE CCT. BETWEEN DORSEY AND ROSSER
C         D16R,D13R
C
C LINE-MODEL          CP-LINE   QREAL
C METRIC
C UNTRANSPOSED MODELLING. PARAMETERS AT F =  6.0000E+01  HZ
$VINTAGE,1
C R' IN OHMS/KM, ZC IN OHMS, TAU IN SEC, LENGTH IN KM
-1DOR16AROSSRA              4.28811E-01 1.15570E+03 9.41306E-05-1.94600E+01 2 06
-2DOR16BROSSRB              4.99597E-02 4.36928E+02 6.64163E-05-1.94600E+01 2 06
-3DOR16CROSSRC              5.32271E-02 4.20976E+02 6.66059E-05-1.94600E+01 2 06
-4DOR13CROSSRC              4.97607E-02 3.50235E+02 6.61558E-05-1.94600E+01 2 06
-5DOR13BROSSRB              5.20595E-02 3.41140E+02 6.62079E-05-1.94600E+01 2 06
-6DOR13AROSSRA              5.21800E-02 3.51354E+02 6.61918E-05-1.94600E+01 2 06
$VINTAGE,0
  0.35170500 -0.29975879  0.50649655  0.50581117  0.37534650  0.29462107
```

```
   0.00000000  0.00000000  0.00000000  0.00000000  0.00000000  0.00000000
   0.38193604 -0.52729801  0.02366887  0.01620921 -0.46361206 -0.57957532
   0.00000000  0.00000000  0.00000000  0.00000000  0.00000000  0.00000000
   0.47989880 -0.34354378 -0.49264711 -0.48417618  0.37895958  0.27780550
   0.00000000  0.00000000  0.00000000  0.00000000  0.00000000  0.00000000
   0.35170500  0.29975879  0.50649655 -0.50581117 -0.37534650  0.29462107
   0.00000000  0.00000000  0.00000000  0.00000000  0.00000000  0.00000000
   0.38193604  0.52729801  0.02366887 -0.01620921  0.46361206 -0.57957532
   0.00000000  0.00000000  0.00000000  0.00000000  0.00000000  0.00000000
   0.47989880  0.34354378 -0.49264711  0.48417618 -0.37895958  0.27780550
   0.00000000  0.00000000  0.00000000  0.00000000  0.00000000  0.00000000
C
C       ii. SINGLE CCT. BETWEEN DORSEY AND ROSSER
C           D5R
C
C LINE-MODEL          CP-LINE   QREAL
C METRIC
C UNTRANSPOSED MODELLING. PARAMETERS AT F =  6.0000E+01  HZ
SVINTAGE,1
C R' IN OHMS/KM, ZC IN OHMS, TAU IN SEC, LENGTH IN KM
-1DOR5RBROSSRB              3.26212E-01 7.56327E+02 8.96876E-05-1.94600E+01 2 03
-2DOR5RAROSSRA              8.14698E-02 3.62478E+02 6.60357E-05-1.94600E+01 2 03
-3DOR5RCROSSRC              8.19418E-02 4.13809E+02 6.65584E-05-1.94600E+01 2 03
SVINTAGE,0
   0.59088916 -0.41137023  0.70710678
   0.00000000  0.00000000  0.00000000
   0.54921623  0.81334063  0.00000000
   0.00000000  0.00000000  0.00000000
   0.59088916 -0.41137023 -0.70710678
   0.00000000  0.00000000  0.00000000
C
C       iii. DOUBLE CIRCUIT BETWEEN RIDGEWAY AND ROSSER
C            D36R,R23R
C
C LINE-MODEL          CP-LINE   QREAL
C METRIC
C UNTRANSPOSED MODELLING. PARAMETERS AT F =  6.0000E+01  HZ
SVINTAGE,1
C R' IN OHMS/KM, ZC IN OHMS, TAU IN SEC, LENGTH IN KM
-1D36R3C RIDGC              4.28811E-01 1.15570E+03 7.93773E-05-1.64100E+01 2 06
-2D36R3B RIDGB              4.99597E-02 4.36928E+02 5.60067E-05-1.64100E+01 2 06
-3D36R3A RIDGA              5.32271E-02 4.20976E+02 5.61667E-05-1.64100E+01 2 06
-4ROSSRA RIDGA              4.97607E-02 3.50235E+02 5.57871E-05-1.64100E+01 2 06
-5ROSSRB RIDGB              5.20595E-02 3.41140E+02 5.58310E-05-1.64100E+01 2 06
-6ROSSRC RIDGC              5.21800E-02 3.51354E+02 5.58174E-05-1.64100E+01 2 06
SVINTAGE,0
   0.35170500 -0.29975879  0.50649655  0.50581117  0.37534650  0.29462107
   0.00000000  0.00000000  0.00000000  0.00000000  0.00000000  0.00000000
   0.38193604 -0.52729801  0.02366887  0.01620921 -0.46361206 -0.57957532
   0.00000000  0.00000000  0.00000000  0.00000000  0.00000000  0.00000000
   0.47989880 -0.34354378 -0.49264711 -0.48417618  0.37895958  0.27780550
   0.00000000  0.00000000  0.00000000  0.00000000  0.00000000  0.00000000
   0.35170500  0.29975879  0.50649655 -0.50581117 -0.37534650  0.29462107
   0.00000000  0.00000000  0.00000000  0.00000000  0.00000000  0.00000000
   0.38193604  0.52729801  0.02366887 -0.01620921  0.46361206 -0.57957532
   0.00000000  0.00000000  0.00000000  0.00000000  0.00000000  0.00000000
   0.47989880  0.34354378 -0.49264711  0.48417618 -0.37895958  0.27780550
   0.00000000  0.00000000  0.00000000  0.00000000  0.00000000  0.00000000
C
C        iv. SINGLE CIRCUIT LINE FROM ASHERN to VERMILLION
C            A6V
C
C LINE-MODEL          CP-LINE   BALANCED
C METRIC
C BALANCED-LINE MODELLING. PARAMETERS AT F =  6.0000E+01  HZ
SVINTAGE,1
C R' IN OHMS/KM, ZC IN OHMS, TAU IN SEC, LENGTH IN KM
-1ASVERA VERMA              3.50900E-01 7.35400E+02 6.22413E-04 1.29710E+02 2 00
-2ASVERB VERMB              8.18372E-02 3.75687E+02 4.43988E-04 1.29710E+02 2 00
-3ASVERC VERMC
SVINTAGE,0
C
```

```
C         v. DOUBLE CIRCUIT LINE FROM ASHERN to GRAND RAPIDS
C              G1A,G2A
C
C LINE-MODEL          CP-LINE   QREAL
C METRIC
C UNTRANSPOSED MODELLING. PARAMETERS AT F =  6.0000E+01  HZ
SVINTAGE,1
C R' IN OHMS/KM, ZC IN OHMS, TAU IN SEC, LENGTH IN KM
-1ASG1AAGRG1AA              1.00802E+00 9.80698E+02 1.56584E-03-2.34350E+02 2 06
-2ASG1ABGRG1AB              5.24653E-02 4.49615E+02 8.58040E-04-2.34350E+02 2 06
-3ASG1ACGRG1AC              4.69970E-02 3.23598E+02 7.99722E-04-2.34350E+02 2 06
-4ASG2AAGRAPDA              4.66404E-02 3.02245E+02 7.92594E-04-2.34350E+02 2 06
-5ASG2ABGRAPDB              4.66341E-02 2.65377E+02 7.91401E-04-2.34350E+02 2 06
-6ASG2ACGRAPDC              4.65908E-02 2.61569E+02 7.91387E-04-2.34350E+02 2 06
SVINTAGE,0
  0.43687984 -0.55407055 -0.50818741  0.40620576 -0.28577772  0.24340605
  0.00000000  0.00000000  0.00000000  0.00000000  0.00000000  0.00000000
  0.38278855 -0.38828035  0.00411324 -0.22296477  0.57599350 -0.52517754
  0.00000000  0.00000000  0.00000000  0.00000000  0.00000000  0.00000000
  0.40324619 -0.20333745  0.48972727 -0.53206331 -0.29199261  0.40424047
  0.00000000  0.00000000  0.00000000  0.00000000  0.00000000  0.00000000
  0.40324619  0.20333745  0.48972727  0.53206331 -0.29199261 -0.40424047
  0.00000000  0.00000000  0.00000000  0.00000000  0.00000000  0.00000000
  0.38278855  0.38828035  0.00411324  0.22296477  0.57599350  0.52517754
  0.00000000  0.00000000  0.00000000  0.00000000  0.00000000  0.00000000
  0.43687984  0.55407055 -0.50818741 -0.40620576 -0.28577772 -0.24340605
  0.00000000  0.00000000  0.00000000  0.00000000  0.00000000  0.00000000
C
C         vi. SINGLE CIRCUIT LINE FROM GRAND RAPIDS to VERMILLION
C              G31V
C
C LINE-MODEL          CP-LINE   BALANCED
C METRIC
C UNTRANSPOSED MODELLING. PARAMETERS AT F =  6.0000E+01  HZ
SVINTAGE,1
C R' IN OHMS/KM, ZC IN OHMS, TAU IN SEC, LENGTH IN KM
-1GRVERA VERMA              5.50567E-01 8.54793E+02 1.42702E-03-2.53020E+02 2 03
-2GRVERB VERMB              1.08916E-01 3.46195E+02 8.60969E-04-2.53020E+02 2 03
-3GRVERC VERMC              1.09165E-01 3.95704E+02 8.67789E-04-2.53020E+02 2 03
SVINTAGE,0
  0.58576076 -0.41189262  0.70710678
  0.00000000  0.00000000  0.00000000
  0.56013990  0.81282444  0.00000000
  0.00000000  0.00000000  0.00000000
  0.58576076 -0.41189262 -0.70710678
  0.00000000  0.00000000  0.00000000
C
C         vii. SINGLE CIRCUIT LINE FROM Rosser to Silver
C
C LINE-MODEL          CP-LINE   QREAL
C METRIC
C UNTRANSPOSED MODELLING. PARAMETERS AT F =  6.0000E+01  HZ
SVINTAGE,1
C R' IN OHMS/KM, ZC IN OHMS, TAU IN SEC, LENGTH IN KM
-1ROSILASILROA              3.78012E-01 7.29422E+02 4.57001E-04-9.50000E+01 2 03
-2ROSILBSILROB              1.08933E-01 3.46076E+02 3.23244E-04-9.50000E+01 2 03
-3ROSILCSILROC              1.09223E-01 3.95697E+02 3.25817E-04-9.50000E+01 2 03
SVINTAGE,0
  0.58236105 -0.41517919  0.70710678
  0.00000000  0.00000000  0.00000000
  0.56719393  0.80947604  0.00000000
  0.00000000  0.00000000  0.00000000
  0.58236105 -0.41517919 -0.70710678
  0.00000000  0.00000000  0.00000000
C
C ------------------------------------------------------------------------------
C TRANSMISSION LINES:
C
C     *** MANITOBA HYDRO TRANSMISSION LINES: study area
C
C long case representation of A3R, A4D, Silver Tap
C Frequency dependent line model: 105% of base length
```

```
C optimized FD. Q is selected by AUX -> 1153/1286 Hz. Fit region increased.
C LINE-MODEL          FD-LINE   QREAL                          0.01        20         9
C METRIC
C   1 .353   .09300 4     1.0    2.54   -21.65    23.47    9.45
C   1 .353   .09300 4     1.0    2.54   -21.24    23.47    9.45
C   2 .353   .09300 4     1.0    2.54   -14.33    23.47    9.45
C   2 .353   .09300 4     1.0    2.54   -13.93    23.47    9.45
C   3 .353   .09300 4     1.0    2.54    -7.02    23.47    9.45
C   3 .353   .09300 4     1.0    2.54    -6.61    23.47    9.45
C   4 .353   .09300 4     1.0    2.54     6.61    23.47    9.45
C   4 .353   .09300 4     1.0    2.54     7.02    23.47    9.45
C   5 .353   .09300 4     1.0    2.54    13.93    23.47    9.45
C   5 .353   .09300 4     1.0    2.54    14.33    23.47    9.45
C   6 .353   .09300 4     1.0    2.54    21.24    23.47    9.45
C   6 .353   .09300 4     1.0    2.54    21.65    23.47    9.45
C   0    .5  4.6990 4     1.0   .9144   -19.21    29.57   21.73
C   0    .5  4.6990 4     1.0   .9144    -9.05    29.57   21.73
C   0    .5  4.6990 4     1.0   .9144    19.21    29.57   21.73
C   0    .5  4.6990 4     1.0   .9144     9.05    29.57   21.73
C LINE LENGTH =  3.3690E+01  KM
C TRANSFORMATION MATRIX AT F =  1.1534E+03  HZ
C *** FD Code deleted
C LINE-MODEL          FD-LINE   QREAL                          0.01        20        10
C METRIC
C same as above
C LINE LENGTH =  1.6550E+01  KM
C TRANSFORMATION MATRIX AT F =  1.1534E+03  HZ
C *** FD Code deleted
C LINE-MODEL          FD-LINE   QREAL                          0.01        20         9
C METRIC
C same as above
C LINE LENGTH =  4.7390E+01  KM
C TRANSFORMATION MATRIX AT F =  1.1534E+03  HZ
C *** FD Code deleted
C LINE-MODEL          FD-LINE   QREAL                          0.01        20         9
C METRIC
C same as above
C LINE LENGTH =  6.4340E+01  KM
C TRANSFORMATION MATRIX AT F =  1.1534E+03  HZ
C *** FD Code deleted
C LINE-MODEL          FD-LINE   QREAL                          0.01        20         9
C METRIC
C same as above
C LINE LENGTH =  2.7210E+01  KM
C TRANSFORMATION MATRIX AT F =  1.1534E+03  HZ
C *** FD Code deleted
C LINE-MODEL          FD-LINE   QREAL                          0.01        20         9
C METRIC
C   1 .392   .08050 4     1.0   2.692    -5.49    16.39    8.70
C   2 .392   .08050 4     1.0   2.692     0.00    17.46    9.77
C   3 .392   .08050 4     1.0   2.692     5.49    16.39    8.70
C   0    .5  4.6990 4     1.0   .9144    -3.05    20.11   16.54
C   0    .5  4.6990 4     1.0   .9144     3.05    20.11   16.54
C LINE LENGTH =  6.4050E+01  KM
C TRANSFORMATION MATRIX AT F =  1.2907E+03  HZ
C *** FD Code deleted
C LINE-MODEL          FD-LINE   QREAL                          0.01        20        10
C METRIC
C   1 .391   .0504  4     1.0  3.378   26.213   34.442  19.202
C   2 .391   .0504  4     1.0  3.378   23.165   28.956  13.716
C   3 .391   .0504  4     1.0  3.378   26.213   23.470   8.230
C   4 .391   .0504  4     1.0  3.378   34.747   34.442  19.202
C   5 .391   .0504  4     1.0  3.378   37.795   28.956  13.716
C   6 .391   .0504  4     1.0  3.378   34.747   23.470   8.230
C   0 .500  4.699  4     1.0   .9144   30.480   43.510  32.232
C LINE LENGTH =  1.7820E+01  KM
C TRANSFORMATION MATRIX AT F =  1.2861E+03  HZ
C *** FD Code deleted
C ~~~~~~~~~~~~~~~~~~~~~~~~~~~~~~~~~~~~~~~~~~~~~~~~~~~~~~~~~~~~~~~~~~~~~~~~~~~~~~~~
C SILVER TRANFORMER MODEL: BCTRAN WITH TYPE 96 REACTOR
C                          no ss load. Iexc=.2% 50 kw core loss. 1:3 ratio
C                          80% base flux
```

```
C
C     SILVER: 230-66.0 KV  (Bank #2)
C     HV/LV WDGS  50 MVA (3 PHASE)
C     IMPEDANCES ON  50 MVA BASE: Xh-l=8.22%
C     MODELLED USING 3 PHASE CORE 'BCTRAN'
C     SATURATION APPLIED TO DELTA WINDING
C
C Iexc=0.20%, Tap=N
SVINTAGE, 1
 1SILVHASILVNA             0.1385768360E+010.3531032820E+06
 2SILDUASILVSB             0.0000000000E+000.1754588225E+06
                           0.3423293280E+000.8720711989E+05
 3SILVHBSILVNB             0.0000000000E+00-.1759842613E+06
                           0.0000000000E+00-.8746648628E+05
                           0.1385768360E+010.3531032820E+06
 4SILDUBSILVSC             0.0000000000E+00-.8746648628E+05
                           0.0000000000E+00-.4347288011E+05
                           0.0000000000E+000.1754588225E+06
                           0.3423293280E+000.8720711989E+05
 5SILVHCSILVNC             0.0000000000E+00-.1759842613E+06
                           0.0000000000E+00-.8746648628E+05
                           0.0000000000E+00-.1759842613E+06
                           0.0000000000E+00-.8746648628E+05
                           0.1385768360E+010.3531032820E+06
 6SILDUCSILVSA             0.0000000000E+00-.8746648628E+05
                           0.0000000000E+00-.4347288011E+05
                           0.0000000000E+00-.8746648628E+05
                           0.0000000000E+00-.4347288011E+05
                           0.0000000000E+000.1754588225E+06
                           0.3423293280E+000.8720711989E+05
SVINTAGE, 0
C
C  SILVER TRANSFORMER MAGNETIZATION CURVE ON 66 KV (DELTA WINDING)
C  air core reactance not set
C 25% Hysteresis losses
C Isat=1.20, Flux=290.0
C BUS-->BUS-->BUS-->BUS-->Is--->PHIs->Ph-Re>                                *
96SILDUASILVSB          8888.          0.00                                 3
 -0.45000000E+00 -0.28317647E+03
 -0.30000000E+00 -0.28147059E+03
 -0.13500000E+00 -0.27550000E+03
 -0.60000000E-01 -0.26952941E+03
 -0.22500000E-01 -0.26441176E+03
  0.75000000E-02 -0.25417647E+03
  0.26250000E-01 -0.24223529E+03
  0.43500000E-01 -0.22176471E+03
  0.52500000E-01 -0.18764706E+03
  0.60000000E-01 -0.13647059E+03
  0.75000000E-01  0.91264706E+02
  0.82500000E-01  0.12623529E+03
  0.10500000E+00  0.17058824E+03
  0.13500000E+00  0.20470588E+03
  0.16350000E+00  0.22176471E+03
  0.21375000E+00  0.23882353E+03
  0.29250000E+00  0.25417647E+03
  0.40125000E+00  0.26611765E+03
  0.52500000E+00  0.27464706E+03
  0.75000000E+00  0.28317647E+03
  0.12000000E+01  0.29000000E+03
  0.16500000E+01  0.29170588E+03
   .99990000E+04
C
96SILDUBSILVSCSILDUASILVSB8888.        0.000                                3
96SILDUCSILVSASILDUASILVSB8888.        0.000                                3
C
C  CORE LOSSES ACROSS 66 KV WINDING (50 KW - .261E6) * set at 75%
C                         | R  || L  || C  |                                *
  SILDUASILVSB            .348E6
  SILDUBSILVSC            .348E6
  SILDUCSILVSA            .348E6
C
C  WINDING IMPEDANCE FOR NL ELEMENT ISOLATION
```

```
C                          | R  || L  || C  |                                    *
 SILDUASILVSA     4.E-2                     1
 SILDUBSILVSB     4.E-2                    1
  SILDUCSILVSC             4.E-2                                               1
C
C  STRAY CAPACITANCE: ASSUME 4000 PF
C                          | R  || L  || C  |                                    *
  SILVHA                                .00400
  SILVHB                                .00400
  SILVHC                                .00400
C
C  SILVER SECONDARY WDG Load: 500 pF - open circuit assumed capacitance
C                                      to give ground connection
C                          | R  || L  || C  |
 0SILVSA                               .00050
 0SILVSB                               .00050
 0SILVSC                               .00050
C
C  B. SILVER SECONDARY WDG Load: 3.4 MW, 0.8 MVAr (extreme min.)
C                          | R  || L  || C  |
 0SILVLA                  1214. 285.6
 0SILVLB                  1214. 285.6
 0SILVLC                  1214. 285.6
C
C ------------------------------------------------------------------------------
C    SILVER: 230-66.0 KV  (Bank #2 - hot standby)
C    HV/LV WDGS  50 MVA (3 PHASE)
C    IMPEDANCES ON  50 MVA BASE: Xh-l=8.22%
C    MODELLED USING 3 PHASE CORE 'BCTRAN'
C    SATURATION APPLIED TO DELTA WINDING
C
C Iexc=0.20%, Tap=N
SVINTAGE, 1
 1SIL2HA                  0.1357731361E+010.3531030368E+06
 2SI2DUASIL2SB            0.0000000000E+000.1754588225E+06
                          0.3354032880E+000.8720711987E+05
 3SIL2HB                  0.0000000000E+00-.1759838731E+06
                          0.0000000000E+00-.8746648632E+05
                          0.1357731361E+010.3531030368E+06
 4SI2DUBSIL2SC            0.0000000000E+00-.8746648632E+05
                          0.0000000000E+00-.4347288013E+05
                          0.0000000000E+000.1754588225E+06
                          0.3354032880E+000.8720711987E+05
 5SIL2HC                  0.0000000000E+00-.1759838731E+06
                          0.0000000000E+00-.8746648632E+05
                          0.0000000000E+00-.1759838731E+06
                          0.0000000000E+00-.8746648632E+05
                          0.1357731361E+010.3531030368E+06
 6SI2DUCSIL2SA            0.0000000000E+00-.8746648632E+05
                          0.0000000000E+00-.4347288013E+05
                          0.0000000000E+00-.8746648632E+05
                          0.0000000000E+00-.4347288013E+05
                          0.0000000000E+000.1754588225E+06
                          0.3354032880E+000.8720711987E+05
SVINTAGE, 0
C
C  SILVER TRANSFORMER MAGNETIZATION CURVE ON 66 KV (DELTA WINDING)
C  air core reactance not set
C  25% Hysteresis losses
C  same as bank #2
C BUS-->BUS-->BUS-->BUS-->Is--->PHIs->Ph-Re>                                    *
96SI2DUASIL2SB            8888.          0.00                                   1
 -0.45000000E+00 -0.28317647E+03
 -0.30000000E+00 -0.28147059E+03
 -0.13500000E+00 -0.27550000E+03
 -0.60000000E-01 -0.26952941E+03
 -0.22500000E-01 -0.26441176E+03
  0.75000000E-02 -0.25417647E+03
  0.26250000E-01 -0.24223529E+03
  0.43500000E-01 -0.22176471E+03
  0.52500000E-01 -0.18764706E+03
  0.60000000E-01 -0.13647059E+03
```

```
   0.75000000E-01  0.91264706E+02
   0.82500000E-01  0.12623529E+03
   0.10500000E+00  0.17058824E+03
   0.13500000E+00  0.20470588E+03
   0.16350000E+00  0.22176471E+03
   0.21375000E+00  0.23882353E+03
   0.29250000E+00  0.25417647E+03
   0.40125000E+00  0.26611765E+03
   0.52500000E+00  0.27464706E+03
   0.75000000E+00  0.28317647E+03
   0.12000000E+01  0.29000000E+03
   0.16500000E+01  0.29170588E+03
    .99990000E+04
C
96SI2DUBSIL2SCSI2DUASIL2SB8888.         0.000                                  1
96SI2DUCSIL2SASI2DUASIL2SB8888.         0.000                                  1
C
C  CORE LOSSES ACROSS 66 KV WINDING (50 KW - .261E6) * set at 75%
C                           | R  || L  || C  |                                  *
  SI2DUASIL2SB              .348E6
  SI2DUBSIL2SC              .348E6
  SI2DUCSIL2SA              .348E6
C
C  WINDING IMPEDANCE FOR NL ELEMENT ISOLATION
C                           | R  || L  || C  |                                  *
 SI2DUASIL2SA      4.E-2                    1
 SI2DUBSIL2SB      4.E-2                   1
  SI2DUCSIL2SC             4.E-2                                              1
C
C  STRAY CAPACITANCE: ASSUME 4000 PF
C                           | R  || L  || C  |                                  *
  SIL2HA                                .00400
  SIL2HB                                .00400
  SIL2HC                                .00400
C
C  SILVER SECONDARY WDG Load: 500 pF - open circuit assumed capacitance
C                           | R  || L  || C  |
 0SIL2SA                                .00050
 0SIL2SB                                .00050
 0SIL2SC                                .00050
C
C ------------------------------------------------------------------------------
C ADDITIONAL TRANFORMER MODELS:
C
C    Grand Rapids   230KV-13.8 KV generator transformer
C    4*90 MVA RATING (Three PHASE ONAN, 4 PARALLEL TRANSFORMERS)
C    TAPS: +2.5%
C    No saturation modelled, ONLY LINEAR MAGNETIZING IMPEDANCE
C    impedance Zxl = .26%+j7.26%
C    Core losses ignored
C
C <----------> REFBUS       STEA_I<-FLUX<--BUS<-RMAG      ...IOUT(COL 80)       *
  TRANSFORMER               4.677 498.12P1MAPH
C <------CURRENT<-----------FLUX
           4.677  0.49812800E+03
            9999
C Transformer Characteristics
C
C   BUS1  BUS2              <--RK <--LK <turns            ...IOUT(COL 80)       *
 1GRAPDA                   .1910 5.334 9.8631
 2EGRAPAEGRAPB             .00207.0577     1.
C              REFBUS       CUR   FLUX  BUSTOP  RMAG      ...IOUT(COL 80)       *
  TRANSFORMER P1MAPH                    P1MBPH
 1GRAPDB
 2EGRAPBEGRAPC
C              REFBUS       CUR   FLUX  BUSTOP  RMAG      ...IOUT(COL 80)       *
  TRANSFORMER P1MAPH                    P1MCPH
 1GRAPDC
 2EGRAPCEGRAPA
C
C ------------------------------------------------------------------------------
C    Current Transformer model (150:5)
```

```
C
C <----------> REFBUS       STEA_I<-FLUX<--BUS<-RMAG      ...IOUT(COL 80)          *
  TRANSFORMER               .08485 .0075PCTAPH  1.E3
C <------CURRENT<-----------FLUX
  0.84852814E-01  0.75026360E-02
  0.14848176E+00  0.11253954E-01
  0.35528741E+00  0.14255008E-01
  0.67630573E+00  0.15005272E-01
  0.15777295E+02  0.41264498E-01
          9999
C Transformer Characteristics
C used 0.5 ohm, 0.5 mH leakage from McLaren IEEE paper
C    data was from a 1600:5 CT with 10 L 800 accuracy (CSA?)
C
C   BUS1  BUS2              <--RK <--LK <turns           ...IOUT(COL 80)          *
 1SICTSA                   .0005 .0002    30.
 2SILCTASILVHA             .01   .01       1.                                    1
C              REFBUS        CUR   FLUX  BUSTOP  RMAG      ...IOUT(COL 80)          *
  TRANSFORMER PCTAPH                  PCTBPH  1.E3
 1SICTSB
 2SILCTBSILVHB                                                                   1
C              REFBUS        CUR   FLUX  BUSTOP  RMAG      ...IOUT(COL 80)          *
  TRANSFORMER PCTAPH                  PCTCPH  1.E3
 1SICTSC
 2SILCTCSILVHC                                                                   1
C
C  CT BURDEN (IEEE C57.13-1993) B-8 Burden (8 ohm)
C                           | R   || L   || C   |                                 *
  SICTLA                  8.00   6.937
  SICTLB                  8.00   6.937
  SICTLC                 8.00   6.937
C
C ------------------------------------------------------------------------------
C ASHERN REACTOR MODEL:
C
C  Ashern 50 MVAr reactor (DETAILED MODEL FROM DATA SHEETS)
C  Three legged core model. X1/R1=400, assume X0/R0=23 (from IEEE paper)
C Install on A4D: CHANGE C/S LOCATION (ASDORA) on line A3R: (ASROSA)
C
C
C <NODE NAMES>            <ZERO,POS SEQUNCE>
C <-BUS1<-BUS2            <----R<----------X                                      *
51ASREDAASNEUT             16.04    368.92
52ASREDBASNEUT             2.814   1065.51
53ASREDCASNEUT
C
C Static Arc Resistance: Using EMTP Rule Book eqn. 2.23
C                          | R   || L   || C   |
 0ASREDAASNEUT             3.77E6
 0ASREDBASNEUT             3.77E6
 0ASREDCASNEUT             3.77E6
C
C Stray Capacitance: Using typical value from EMTP appli. guide p. 3-44
C                         | R   || L   || C   |
 0ASREAAASNEUT                        .00150
 0ASREABASNEUT                        .00150
 0ASREACASNEUT                        .00150
C
C ------------------------------------------------------------------------------
C ARRESTER MODELS:
C
C    Silver 230 KV LINE ARRESTER MODEL ASSUMING A SINGLE COLUMN ARRESTER
C    A MINIMUM VI CHARACTERISTIC IS USED TO MAXIMIZE ENERGY
C
C RATING =258000.00  V-MULT =  0.10000E+01  I-MULT =  0.10000E+01  GAPLESS
92SILVBA MOSAA                        5555.                                     4
C              VREFERENCE              VFLASHOVER
    0.516000000000000E+06   -0.100000000000000E+03
C              MULTIPLIER                EXPONENT                        VMIN
    0.383018778929996E+09    0.554185403154591E+02    0.617997266717781E+00
    0.265741563699778E+07    0.396422132092866E+02    0.729733972369103E+00
    0.503026019385050E+06    0.338499816858101E+02    0.750240062677929E+00
```

```
     0.583908413271788E+05    0.254018602689520E+02    0.774988792360988E+00
     0.674585424953417E+04    0.156449465157678E+02    0.801556221723850E+00
     0.601240880220415E+04    0.136520668585089E+02    0.943879323303920E+00
                    9999
92SILVBB MOSABSILVBA MOSAA              5555.                                  4
92SILVBC MOSACSILVBA MOSAA              5555.                                  4
C
C   ARRESTER GROUND JUMPERS
 0 MOSAAMOSAGA             .005                                                 1
 0 MOSABMOSAGB             .005                                                 1
 0 MOSACMOSAGC             .005                                                 1
 0MOSAGA                   .005
 0MOSAGB                   .005
 0MOSAGC                   .005
C
C ------------------------------------------------------------------------------
C MISC ELEMENTS:
C
C Local loads:
C
C  Grand Rapids local load model (To Overflowing River and William's River)
C  45.1+j66.5 MVA
C                          | R  || L  || C  |
 0GRAPDA                   369.53544.87
 0GRAPDB                   369.53544.87
 0GRAPDC                   369.53544.87
C
C  Ashern local load model (To 66 kV)
C  9.8+j2.3 MVA
C                          | R  || L  || C  |
 0ASHRNA                   5116.21200.7
 0ASHRNB                   5116.21200.7
 0ASHRNC                   5116.21200.7
C
C ------------------------------------------------------------------------------
C Parallel resistors to aid in damping numerical oscillations
C                          | R  || L  || C  |
 0SILVSASILVLA             1.E12
 0SILVSBSILVLB             1.E12
 0SILVSCSILVLC             1.E12
C
C DUMMY resistors to allow parallel breaker connection at Rosser 230 kV
 0ROSDUAROSASA             0.01
 0ROSDUBROSASB             0.01
 0ROSDUCROSASC             0.01
C
C FAULT RESISTANCE: Primary arc resistance .01 < R < .1
C For 230 kV faults: 0.05 ohms is reasonable
C For 66 kV faults: the resistance needs to be decreased in order for breaker
C                   to open successfully.
  FAULPA                   0.01
  FAULPB                   0.01
  FAULPC                   0.01
C FAULT RESISTANCE: Secondary arc resistance
  FAULSA                   100.
  FAULSB                   100.
  FAULSC                   100.
C
C ------------------------------------------------------------------------------
BLANK ENDS BRANCH
C
C TIME-CONTROLLED SWITCHES: For monitoring the peripheral system
C
C 1. DORSEY-RIDGEWAY 230 TLINE BREAKERS                    (CLOSED AT TIME=0)
C
C CLASS 1 - (TIME-CONTROLLED SWITCH) OPENS WHEN CURRENT GOES THROUGH ZERO
C <-BUS1<-BUS2<--T CLOSE<---T OPEN<-I MARGIN                                   O
  DORB2ADORRIA      -1.0      99.9
  DORB2BDORRIB      -1.0      99.9
  DORB2CDORRIC      -1.0      99.9
C
C 2. DORSEY-ROSSER 230 TLINE BREAKERS  (CCT 1)             (CLOSED AT TIME=0)
```

```
C
C CLASS 1 - (TIME-CONTROLLED SWITCH) OPENS WHEN CURRENT GOES THROUGH ZERO
C <-BUS1<-BUS2<--T CLOSE<---T OPEN<-I MARGIN                                    O
  DORB2ADOR16A       -1.0      99.9
  DORB2BDOR16B       -1.0      99.9
  DORB2CDOR16C       -1.0      99.9
C
C 3. DORSEY-ROSSER 230 TLINE BREAKERS  (CCT 2)              (CLOSED AT TIME=0)
C
C CLASS 1 - (TIME-CONTROLLED SWITCH) OPENS WHEN CURRENT GOES THROUGH ZERO
C <-BUS1<-BUS2<--T CLOSE<---T OPEN<-I MARGIN                                    O
  DORB2ADOR13A       -1.0      99.9
  DORB2BDOR13B       -1.0      99.9
  DORB2CDOR13C       -1.0      99.9
C
C 4. DORSEY-ROSSER 230 TLINE BREAKERS  (CCT 3)              (CLOSED AT TIME=0)
C
C CLASS 1 - (TIME-CONTROLLED SWITCH) OPENS WHEN CURRENT GOES THROUGH ZERO
C <-BUS1<-BUS2<--T CLOSE<---T OPEN<-I MARGIN                                    O
  DORB2ADOR5RA       -1.0      99.9
  DORB2BDOR5RB       -1.0      99.9
  DORB2CDOR5RC       -1.0      99.9
C
C
C 5. ASHERN-VERMILLION 230 TLINE BREAKERS                   (CLOSED AT TIME=0)
C
C CLASS 1 - (TIME-CONTROLLED SWITCH) OPENS WHEN CURRENT GOES THROUGH ZERO
C <-BUS1<-BUS2<--T CLOSE<---T OPEN<-I MARGIN                                    O
  ASHRNAASVERA       -1.0      99.9
  ASHRNBASVERB       -1.0      99.9
  ASHRNCASVERC       -1.0      99.9
C
C 6. ASHERN-GRAND RAPIDS 230 TLINE BREAKERS                 (CLOSED AT TIME=0)
C
C CLASS 1 - (TIME-CONTROLLED SWITCH) OPENS WHEN CURRENT GOES THROUGH ZERO
C <-BUS1<-BUS2<--T CLOSE<---T OPEN<-I MARGIN                                    O
  ASHRNAASG1AA       -1.0      99.90
  ASHRNBASG1AB       -1.0      99.90
  ASHRNCASG1AC       -1.0      99.90
C
C 7. ASHERN-GRAND RAPIDS 230 TLINE BREAKERS                 (CLOSED AT TIME=0)
C
C CLASS 1 - (TIME-CONTROLLED SWITCH) OPENS WHEN CURRENT GOES THROUGH ZERO
C <-BUS1<-BUS2<--T CLOSE<---T OPEN<-I MARGIN                                    O
  ASHRNAASG2AA       -1.0      99.9
  ASHRNBASG2AB       -1.0      99.9
  ASHRNCASG2AC       -1.0      99.9
C
C 8. GRAND RAPIDS-VERMILLION 230 TLINE BREAKERS             (CLOSED AT TIME=0)
C
C CLASS 1 - (TIME-CONTROLLED SWITCH) OPENS WHEN CURRENT GOES THROUGH ZERO
C <-BUS1<-BUS2<--T CLOSE<---T OPEN<-I MARGIN                                    O
  GRAPDAGRVERA       -1.0      99.9
  GRAPDBGRVERB       -1.0      99.9
  GRAPDCGRVERC       -1.0      99.9
C
C NEW TRANSMISSION LINE:
C 9. SILVER - ROSSER CIRCUIT BREAKER            (CLOSED AT TIME=0)
C
C CLASS 1 - (TIME-CONTROLLED SWITCH) OPENS WHEN CURRENT GOES THROUGH ZERO
C <-BUS1<-BUS2<--T CLOSE<---T OPEN<-I MARGIN                                    O
  SILVBASILROA      9999.     99.9
  SILVBBSILROB      9999.     99.9
  SILVBCSILROC      9999.     99.9
C
C NEW TRANSMISSION LINE:
C 10. ROSSER - SILVER CIRCUIT BREAKER            (CLOSED AT TIME=0)
C
C CLASS 1 - (TIME-CONTROLLED SWITCH) OPENS WHEN CURRENT GOES THROUGH ZERO
C <-BUS1<-BUS2<--T CLOSE<---T OPEN<-I MARGIN                                    O
  ROSSRAROSILA      9999.     99.9
  ROSSRBROSILB      9999.     99.9
```

```
  ROSSRCROSILC     9999.     99.9
C
C 11. GRAND RAPIDS 'G1A' BREAKER          (CLOSED AT TIME=0)
C
C CLASS 1 - (TIME-CONTROLLED SWITCH) OPENS WHEN CURRENT GOES THROUGH ZERO
C <-BUS1<-BUS2<--T CLOSE<---T OPEN<-I MARGIN                                  O
  GRAPDAGRG1AA    -9999.     99.90
  GRAPDBGRG1AB    -9999.     99.90
  GRAPDCGRG1AC    -9999.     99.90
C
C 12. SILVER TAP 230 TLINE DISCONNECT           (CLOSED AT TIME=0)
C
C CLASS 1 - (TIME-CONTROLLED SWITCH) OPENS WHEN CURRENT GOES THROUGH ZERO
C <-BUS1<-BUS2<--T CLOSE<---T OPEN<-I MARGIN                                  O
  A3R_1AA3R02A    -999.0     99.9
  A3R_1BA3R02B    -999.0     99.9
  A3R_1CA3R02C    -999.0     99.9
C
C 13. SILVER-BANK #1 CURRENT TRANSFORMER (Load)          (CLOSED AT TIME=0)
C
C CLASS 1 - (TIME-CONTROLLED SWITCH) OPENS WHEN CURRENT GOES THROUGH ZERO
C <-BUS1<-BUS2<--T CLOSE<---T OPEN<-I MARGIN                                  O
  SICTSASICTLA    -9999.     99.90                                            1
  SICTSBSICTLB    -9999.     99.90                                            1
  SICTSCSICTLC    -9999.     99.90                                            1
C
C 14. SILVER BANK #1 NEUTRAL CURRENT            (CLOSED AT TIME=0)
C
C CLASS 1 - (TIME-CONTROLLED SWITCH) OPENS WHEN CURRENT GOES THROUGH ZERO
C <-BUS1<-BUS2<--T CLOSE<---T OPEN<-I MARGIN                                  O
  SILVNT           -1.0     99.9                                             1
C
C 15. SILVER current measurement                (CLOSED AT TIME=0)
C
C CLASS 1 - (TIME-CONTROLLED SWITCH) OPENS WHEN CURRENT GOES THROUGH ZERO
C <-BUS1<-BUS2<--T CLOSE<---T OPEN<-I MARGIN                                  O
  SILVNASILVNT    -9999.     99.9                                             1
  SILVNBSILVNT    -9999.     99.9                                             1
  SILVNCSILVNT    -9999.     99.9                                             1
C
C ------------------------------------------------------------------------------
C SWITCHING DATA: setup to bench mark test #4
C    DESCRIPTION: Line A3R open. Trip reactor. 2 transformers connected
C ------------------------------------------------------------------------------
C A4D: closed
C A4D: DORSEY-ASHERN 230 TLINE BREAKERS                    (CLOSED AT TIME=0)
C
C CLASS 1 - (TIME-CONTROLLED SWITCH) OPENS WHEN CURRENT GOES THROUGH ZERO
C <-BUS1<-BUS2<--T CLOSE<---T OPEN<-I MARGIN                                  O
  DORB2ADORASA     -1.0     99.9                                             3
  DORB2BDORASB     -1.0     99.9                                             3
  DORB2CDORASC     -1.0     99.9                                             3
C
C A4D: ASHERN-DORSEY 230 TLINE BREAKERS                    (CLOSED AT TIME=0)
C    request power flow output
C CLASS 1 - (TIME-CONTROLLED SWITCH) OPENS WHEN CURRENT GOES THROUGH ZERO
C <-BUS1<-BUS2<--T CLOSE<---T OPEN<-I MARGIN                                  O
  ASHRNAASDORA     -1.0     99.9                                             3
  ASHRNBASDORB     -1.0     99.9                                             3
  ASHRNCASDORC     -1.0     99.9                                             3
C
C ------------------------------------------------------------------------------
C A3R: open at t=0-
C A3R: ASHERN-ROSSER 230 TLINE BREAKERS                    (CLOSED AT TIME=0)
C    request power flow output
C CLASS 1 - (TIME-CONTROLLED SWITCH) OPENS WHEN CURRENT GOES THROUGH ZERO
C <-BUS1<-BUS2<--T CLOSE<---T OPEN<-I MARGIN                                  O
  ASHRNAASROSA     99.0    99.900                                            3
  ASHRNBASROSB     99.0    99.900                                            3
  ASHRNCASROSC     99.0    99.900                                            3
C
C A3R: ROSSER-ASHERN 230 TLINE BREAKERS                    (CLOSED AT TIME=0)
```

```
C 250 msec Zone 2 delay. 1 sec. neutral
C CLASS 1 - (TIME-CONTROLLED SWITCH) OPENS WHEN CURRENT GOES THROUGH ZERO
C <-BUS1<-BUS2<--T CLOSE<---T OPEN<-I MARGIN                                    O
  ROSSRAROSASA      99.0     99.900                                             3
  ROSSRBROSASB      99.0     99.900                                             3
  ROSSRCROSASC      99.0     99.900                                             3
C
C A3R: ROSSER-ASHERN "reclose" 230 TLINE BREAKERS            (CLOSED AT TIME=0)
C
C CLASS 1 - (TIME-CONTROLLED SWITCH) OPENS WHEN CURRENT GOES THROUGH ZERO
C <-BUS1<-BUS2<--T CLOSE<---T OPEN<-I MARGIN                                    O
  ROSSRAROSDUA      99.0     99.000                                             3
  ROSSRBROSDUB      99.0     99.000                                             3
  ROSSRCROSDUC      99.0     99.000                                             3
C
C ------------------------------------------------------------------------------
C SILVER TRANSFORMER BANK #1: connected with no load
C
C SILVER-BANK #1 TRANSFORMER 230 kv BREAKERS           (CLOSED AT TIME=0)
C
C CLASS 1 - (TIME-CONTROLLED SWITCH) OPENS WHEN CURRENT GOES THROUGH ZERO
C <-BUS1<-BUS2<--T CLOSE<---T OPEN<-I MARGIN                                    O
  SILVBASILCTA     -1.000    99.000                                             3
  SILVBBSILCTB     -1.000    99.000                                             3
  SILVBCSILCTC     -1.000    99.000                                             3
C
C SILVER-BANK #1 TRANSFORMER 66 kv BREAKERS (Load)     (OPEN AT TIME=0)
C
C CLASS 1 - (TIME-CONTROLLED SWITCH) OPENS WHEN CURRENT GOES THROUGH ZERO
C <-BUS1<-BUS2<--T CLOSE<---T OPEN<-I MARGIN                                    O
  SILVSASILVLA      9999.     99.00                                              3
  SILVSBSILVLB      9999.     99.00                                              3
  SILVSCSILVLC      9999.     99.00                                              3
C
C SILVER-BANK #1 DELTA CURRENT MEASUREMENT          (CLOSED AT TIME=0)
C
C CLASS 1 - (TIME-CONTROLLED SWITCH) OPENS WHEN CURRENT GOES THROUGH ZERO
C <-BUS1<-BUS2<--T CLOSE<---T OPEN<-I MARGIN                                    O
C ** replaced by isolation resistors to allow type 92 reactor connection
C
C ------------------------------------------------------------------------------
C SILVER TRANSFORMER BANK #2: connected with no load
C
C CLASS 1 - (TIME-CONTROLLED SWITCH) OPENS WHEN CURRENT GOES THROUGH ZERO
C <-BUS1<-BUS2<--T CLOSE<---T OPEN<-I MARGIN                                    O
  SILVBASIL2HA      -1.00    99.90                                              3
  SILVBBSIL2HB      -1.00    99.90                                              3
  SILVBCSIL2HC      -1.00    99.90                                              3
C
C SILVER-BANK #2 TRANSFORMER 66 kv BREAKERS DON'T EXIST YET: HOT STANDBY
C
C SILVER-BANK #2 DELTA CURRENT MEASUREMENT          (CLOSED AT TIME=0)
C ** replaced by isolation resistors to allow type 92 reactor connection
C
C ------------------------------------------------------------------------------
C ASHERN REACTOR: switched off
C 1. ASHERN REACTOR CIRCUIT SWITCHER            (CLOSED AT TIME=0)
C ** reactor connected to A3R
C CLASS 1 - (TIME-CONTROLLED SWITCH) OPENS WHEN CURRENT GOES THROUGH ZERO
C <-BUS1<-BUS2<--T CLOSE<---T OPEN<-I MARGIN                                    O
  ASROSAASRMAA     -9999.     0.04                                              3
  ASROSBASRMAB     -9999.     .048                                              3
  ASROSCASRMAC     -9999.     0.04                                              3
C
C 2. ASHERN REACTOR current measurement            (CLOSED AT TIME=0)
C
C CLASS 1 - (TIME-CONTROLLED SWITCH) OPENS WHEN CURRENT GOES THROUGH ZERO
C <-BUS1<-BUS2<--T CLOSE<---T OPEN<-I MARGIN                                    O
  ASRMAAASREAA     -9999.    99.90                                              3
  ASRMABASREAB     -9999.    99.90                                              3
  ASRMACASREAC     -9999.    99.90                                              3
C
```

```
C 3. ASHERN REACTOR current measurement                (CLOSED AT TIME=0)
C
C CLASS 1 - (TIME-CONTROLLED SWITCH) OPENS WHEN CURRENT GOES THROUGH ZERO
C <-BUS1<-BUS2<--T CLOSE<---T OPEN<-I MARGIN                                  O
  ASREAAASREDA     -9999.      99.9                                           1
  ASREABASREDB     -9999.      99.9                                           1
  ASREACASREDC     -9999.      99.9                                           1
C
C 4. ASHERN REACTOR NEUTRAL CURRENT              (CLOSED AT TIME=0)
C
C CLASS 1 - (TIME-CONTROLLED SWITCH) OPENS WHEN CURRENT GOES THROUGH ZERO
C <-BUS1<-BUS2<--T CLOSE<---T OPEN<-I MARGIN                                  O
  ASNEUT             -1.0     99.9                                           1
C
C ------------------------------------------------------------------------------
C FAULT SWITCH: no fault
C
C PSEUDO-DYNAMIC FAULT RESISTANCE MODEL
C
C CLASS 1 - (TIME-CONTROLLED SWITCH) OPENS WHEN CURRENT GOES THROUGH ZERO
C <-BUS1<-BUS2<--T CLOSE<---T OPEN<-I MARGIN                                  O
  SILVBBFAULTA       -1.0     99.90                                          3
  FAULTAFAULPA      9999.     9999.
  FAULTAFAULSA      9999.     9999.
C
C ------------------------------------------------------------------------------
C
BLANK ENDS SWITCH
C
C BUS--><I<AMPLITUDE<FREQUENCY<--TO|PHI0<---0=PHI0<-IGNORE-><---TSTART<----TSTOP
14EVERMA  184629.662       60.    79.0299        0.                  -1.     9999.
14EVERMB  184629.662       60.   -40.9701        0.                  -1.     9999.
14EVERMC  184629.662       60.   199.0299        0.                  -1.     9999.
C
14EROSSA  204937.080       60.    76.3223        0.                  -1.     9999.
14EROSSB  204937.080       60.   -43.6777        0.                  -1.     9999.
14EROSSC  204937.080       60.   196.3223        0.                  -1.     9999.
C
14ERIDGA  203690.636       60.    73.5250        0.                  -1.     9999.
14ERIDGB  203690.636       60.   -46.4750        0.                  -1.     9999.
14ERIDGC  203690.636       60.   193.5250        0.                  -1.     9999.
C
14EDORSA  193198.699       60.    84.5124        0.                  -1.     9999.
14EDORSB  193198.699       60.   -35.4876        0.                  -1.     9999.
14EDORSC  193198.699       60.   204.5124        0.                  -1.     9999.
C
C ------------------------------------------------------------------------------
C Model of Grand Rapids: aggregate of four parallel units 4(115)=460 MVA
C Terminal connections for phase A, (PHASE B & C: LEAVE COLUMN 1/2 BLANK)
C BUS-->  <-----VOLT<-----FREQ<----ANGLE
59EGRAPA   11262.503     60.00      73.6
  EGRAPB
  EGRAPC
C
C Machine Parameter Cards (optional)
C        1         2         3         4         5         6         7         8
C 345678901234567890123456789012345678901234567890123456789012345678901234567890
C --------------key word<-----FM
PARAMETER FITTING            1.0
C
C 1. tolerances special request
C 2. parameter fitting special request: parameter optimization used
C 3. delta connection special request
C
C Note: 115 MVA/machine
C Electrical Parameters of Machine
C <-<-<-NP<---SMOUTP<---SMOUTQ<-----RMVA<------RKV<---AGLINE<-------S1<-------S2
 1 1    64         1.         1.       460.       13.8    -2660.0    2952.6     4788.
C
C Col: (1-2) Number Mass units, Col (3-4): Kmachine, Col (4-5): Kexciter
C 1 connected mass (generator rotor, given mass number 1)
C synch. speed 112.5 rpm : P=60*2*60/112.5
```

```
C If AGLINE < 0, saturation is included: (volt,current) - (AD1,S1), (AD2,S2)
C          <------AD1<------AD2
                   1.0       1.2
C Machine parameters: manufacturers supplied data (no parameter fitting)
C assume: X'q=Xq, X''q=X''d
C <-----Ra<-------Xl<-------Xd<-------Xq<------X'd<------X'q<-----X''d<-----X''q
   0.00586    0.0983    0.6960    0.2980    0.2010    0.2980    0.1510    0.1510
C assume: T'q0=0.0, ungrounded wye connected, use default caney reactance
C <---T'd0<-----T'q0<----T''d0<----T''q0<-------X0<-------Rn<-------Xn<-------Xc
      6.21        0.0     0.0440    0.0380    0.1110                100.0
C
C Mechanical Parameters
C moment of inertia: assume 4*(270 million lb/ft**2)
C It appears rule book data units are incorrect.
C <------><----ExTrs<-----HICO<------DSR<------DSM<------HSP<------DSD
 1                1.0     1080.
C
BLANK ends MASS data
C
C Output Requests
C
C GA<-->N1<---N2<---N3<---N4<---N5<---N6<---N7<---N8<---N9<--N10<--N11<--N12
  10          1     2     3     4     11
  21
  31
C Col(3): Group, Col(4): 0-selective outputs, 1-all
C Group 1: voltages and currents
C Group 2: mechanical angles (degrees)
C Group 3: Mech. speed deviations (rad/sec)
C
BLANK ends machine output requests
C
C TACS interface cards
C Assume exciter is regulating to 1 pu.
C Bus--><----><KI
  FINISH
C
BLANK ENDS SOURCE
C
C ~~~~~~~~~~~~~~~~~~~~~~~~~~~~~~~~~~~~~~~~~~~~~~~~~~~~~~~~~~~~~~~~~~~~~~~~~~~~~~~~
C OUTPUT NODE VOLTAGES FOR PLOTTING:
C
C        1         2         3         4         5         6         7         8
C 345678901234567890123456789012345678901234567890123456789012345678901234567890
  DORB2A    DORB2B    DORB2C    DORASA    DORASB    DORASC
  A4D02A    A4D02B    A4D02C    ASDORA    ASDORB    ASDORC
  ASHRNA    ASHRNB    ASHRNC    A3R02A    A3R02B    A3R02C
  SILVHA    SILVHB    SILVHC    ROSSRA    ROSSRB    ROSSRC
   RIDGA     RIDGB     RIDGC    SILVSA    SILVSB    SILVSC
  GRAPDA    GRAPDB    GRAPDC     VERMA     VERMB     VERMC
  EGRAPA    EGRAPB    EGRAPC    SILVBA    SILVBB    SILVBC
  ASROSA    ASROSB    ASROSC    ROSASA    ROSASB    ROSASC
  A3R02A    A3R02B    A3R02C    A3R04A    A3R04B    A3R04C
  ASREAA    ASREAB    ASREAC
C BLANK CARD TERMINATING THE OUTPUT NODE VOLTAGE SPECS
BLANK ENDS OUTPUT
C BLANK CARD TERMINATING THE BATCH MODE PLOT REQUESTS
BLANK ENDS PLOT
BLANK
C
C BLANK CARD TERMINATING EMTP SOLUTION MODE
BLANK
BEGIN NEW DATA CASE
BLANK
```